

Aus dem Institut für Pharmakologie und Toxikologie
Geschäftsführender Direktor: Prof. Dr. Frank Czubayko
des Fachbereichs Medizin der Philipps-Universität Marburg

Localization and Functional Analysis of the Calcium Permeable Melastatin-like Channel TRPM3

Inaugural-Dissertation zur Erlangung
des Doktorgrades der Humanbiologie
dem Fachbereich Medizin der Philipps-Universität Marburg



vorgelegt von

CHEN, XIAODI

aus Shanghai, China

Marburg/Lahn 2009

Angenommen vom Fachbereich Medizin der Philipps-Universität Marburg
am: 10.12.2009
Gedruckt mit Genehmigung des Fachbereichs.

Dekan: Prof. Dr. Matthias Rothmund

Referent: Prof. Dr. Tim Plant

Korreferent: Prof. Dr. Dr. Jürgen Daut

To my wife and daughter

Acknowledgement

I would like to acknowledge all those very helpful people who have assisted me in my work.

First and foremost, I would like to sincerely thank my mentor, Dr. Thomas Hofmann, for his guidance, understanding, insightful criticisms, patience, and most importantly, his friendship during my doctoral thesis at Philipps–University Marburg. He encouraged me to develop independent thinking and research skills, and helped me in the final stage of writing the thesis.

I wish to express my sincere gratitude to Prof. Dr. Tim Plant for his kindness, support and suggestions throughout all stages of the thesis. I would also like to thank Dr. Vladimir Chubanov for his assistance and guidance in various molecular biologic approaches.

My thanks go to all of the members of the Dr. Thomas Hofmann research group, especially, Fatma Aktuna, Anna Dietz, for helping me in the experiments and giving some needed humor and entertainment in a somewhat stressful laboratory environment. Thanks to Prof. Dr. Alexander Dietrich, Prof. Dr. Achim Aigner, and Prof. Dr. Frank Czubayko, whose advice, guidance and wisdom aided the writing of this thesis. My thanks also go to Daniel Schulze, Meike Fahlbusch, Tim Mayer, Sabrina Höbel, Ahmed Ibrahim, Winfried Lorenz, Susanne Ziegler, with whom I worked efficiently and solved many of the same problems.

I am deeply grateful to the Department of Pharmacology and Toxicology at Philipps–University Marburg, especially to those members who gave me their valuable input and advice.

Philipps University
Marburg
December 11, 2009

Table of Contents

<i>Acknowledgement</i>	iv
<i>List of Figures</i>	xi
<i>List of Tables</i>	xiii
<i>List of Abbreviations</i>	xiv
1 Introduction	1
1.1 Ca ²⁺ signaling and phospholipase C-mediated signaling pathways	1
1.2 TRP channels	3
1.2.1 The molecular structure of mammalian TRP channels	3
1.2.1.1 Transmembrane domains, N- and C-termini of TRP channels	3
1.2.1.2 Multimerization of mammalian TRP channel subunits . . .	5
1.2.2 Tissue expression and biological functions of mammalian TRP channels	5
1.2.3 TRPM channels	6
1.3 TRPM3	9
1.3.1 Structural features of TRPM3	9
1.3.1.1 Genomic regions and transcript variants	9
1.3.1.2 Protein structure	10
1.3.2 Tissue distribution of TRPM3	10
1.3.3 Channel properties of TRPM3	11
1.3.4 Inhibition, blockage and activation of TRPM3	12
1.3.5 Biological role and relevance of TRPM3	13
1.4 Objectives of this thesis	13

TABLE OF CONTENTS

2	Materials and Methods	14
2.1	Materials	14
2.1.1	Animals, bacteria, cell lines and yeast cells	14
2.1.2	Antibodies	14
2.1.3	Cell culture materials	15
2.1.4	Chemicals	15
2.1.5	Consumables and laboratory equipment	17
2.1.6	Enzymes and peptides	18
2.1.7	Molecular biology reagent systems	18
2.1.8	Nucleic acids and plasmids	19
2.1.9	Bioinformatic tools and online databases	19
2.1.10	Oligonucleotides	20
2.2	Methods	21
2.2.1	DNA analysis and preparation	21
2.2.1.1	General DNA methods	21
2.2.1.2	Polymerase chain reaction (PCR)	21
2.2.1.3	Preparation of chemocompetent DH5 α <i>E.coli</i> cells	22
2.2.1.4	DNA transfection	23
2.2.1.5	Rapid amplification of cDNA ends (RACE)	23
2.2.1.6	Site-directed mutagenesis	25
2.2.1.7	TOPO [®] -cloning	25
2.2.2	RNA analysis and preparation	26
2.2.2.1	Isolation of total RNA from eukaryotic cells and tissues	26
2.2.2.2	Selection of <i>Poly(A)</i> ⁺ RNA from total RNA	26
2.2.2.3	Electrophoresis of RNA with agarose-formaldehyde gels	27
2.2.2.4	Northern blotting	27
2.2.2.5	Random-primed radioactive DNA labeling	28
2.2.2.6	Northern hybridization	29
2.2.3	Protein biochemical analysis	29
2.2.3.1	Membrane protein extraction from mouse tissues	30
2.2.3.2	SDS-PAGE	30
2.2.3.3	Western blot	30
2.2.3.4	Co-immunoprecipitation	31

TABLE OF CONTENTS

2.2.3.5	Fluorescence resonance energy transfer (FRET)	32
2.2.4	Yeast genetics	33
2.2.4.1	Yeast two hybrid screening	33
2.2.4.2	Transformation of DNA into competent yeast cells	37
2.2.4.3	Preparation of yeast total DNA using glass beads	37
2.2.4.4	Yeast protein extraction	38
2.2.4.5	Yeast colony-PCR	39
2.2.4.6	Colony-lift filter assay	39
2.2.5	Cell culture	39
2.2.5.1	General cell culture techniques	39
2.2.5.2	Primary cell culture: melanocyte isolation from the mouse dermis	39
2.2.5.3	Generation of stable mammalian cell lines using the GeneSwitch™ system	40
2.2.6	Methods for histology and immunohistochemistry	42
2.2.6.1	General histological techniques	42
2.2.6.2	β -galactosidase (<i>lacZ</i>) assay	42
2.2.6.3	Immunofluorescent labeling of adherent cells	44
2.2.6.4	Confocal and fluorescence microscopy	44
2.2.6.5	Antigen design and antibody production	44
2.2.7	Measurement of the intracellular free Ca^{2+} concentration	45
2.2.7.1	Fura-2	45
2.2.7.2	Aequorin	46
2.2.8	<i>LacZ</i> transgenic TRPM3 mouse, mouse genotyping and phenotyping	48
2.2.8.1	<i>LacZ</i> transgenic TRPM3 mouse	48
2.2.8.2	Genotyping of <i>lacZ</i> transgenic TRPM3 mice	48
2.2.8.3	Phenotypic analysis of TRPM3 ^{-/-} mice	50
3	Results	52
3.1	Molecular cloning and functional analysis of mTRPM3	52
3.1.1	Molecular cloning of mM3 ₁₇₁₉ and mM3 ₁₃₃₇	52
3.1.2	Analysis of mM3 ₁₇₁₉ and mM3 ₁₃₃₇ protein expression	53
3.1.3	Functional analysis of mM3 ₁₇₁₉	56

TABLE OF CONTENTS

3.1.3.1	Quantification of intracellular Ca^{2+} concentration increase in HEK-293 cells expressing mM3 ₁₇₁₉ and mM3 ₁₃₃₇	57
3.1.3.2	Effects of divalent cations on Ca^{2+} entry in HEK-293 cells expressing mM3 ₁₇₁₉	59
3.2	Identification of functional domains in mM3 ₁₇₁₉	61
3.2.1	Structure of the pore and C-terminus of mM3 ₁₇₁₉	61
3.2.1.1	Site-directed mutagenesis of amino acid residues relevant to Ca^{2+} entry in the mM3 ₁₇₁₉ pore	61
3.2.1.2	Characterization of the mM3 ₁₇₁₉ C-terminus	64
3.2.2	Analysis of mM3 ₁₇₁₉ homomer formation	69
3.2.3	Identification of putative interaction partners of mM3 ₁₇₁₉	74
3.2.3.1	Identification of putative interaction partners of mM3 ₁₇₁₉ using the yeast two hybrid system	74
3.2.3.2	Analysis of protein kinase inhibitor- γ as an interaction partner for mM3 ₁₇₁₉	77
3.3	Tissue distribution of mouse TRPM3	79
3.3.1	Northern blot analysis of mouse TRPM3 tissue distribution	79
3.3.2	Western blot analysis of mouse TRPM3 expression	80
3.3.2.1	Characterization of mouse TRPM3 antibodies	80
3.3.2.2	Analysis of the TRPM3 protein expression in the adult mouse eye	82
3.3.3	Histochemical and immunohistochemical analysis of TRPM3 expression using a <i>lacZ</i> transgenic mouse model	83
3.3.3.1	<i>LacZ</i> gene expression in <i>lacZ</i> transgenic TRPM3 ^{-/-} adult mice	83
3.3.3.2	Tissue distribution of TRPM3 during mouse development	90
3.4	Phenotypic analysis of a TRPM3 ^{-/-} mouse model	96
3.4.1	Genotyping and genetic background correction	96
3.4.2	The viability of TRPM3 ^{-/-} mice	98
3.4.3	Morphological observations on TRPM3 ^{-/-} mice	99
3.4.4	Behavioral analyses of the visual ability of TRPM3 ^{-/-} mice	99
4	Discussion	101
4.1	Molecular cloning and functional analysis of mM3 ₁₇₁₉ and mM3 ₁₃₃₇	101

TABLE OF CONTENTS

4.1.1	Cloning and characterization of mM3 ₁₇₁₉ and mM3 ₁₃₃₇	101
4.1.2	Mutagenesis analysis of the pore	104
4.2	Molecular structure and functional relevance of the C-terminus	106
4.2.1	C-terminus of mM3 ₁₇₁₉ and palmitoylation	106
4.2.2	C-terminus of mM3 ₁₇₁₉ and homomultimerization	108
4.2.3	C-terminus of mM3 ₁₇₁₉ and its putative interaction partners	109
4.3	Expression pattern of mouse TRPM3	110
4.3.1	Expression analysis of TRPM3 in mouse tissues using Northern blot, antibodies and <i>lacZ</i> staining	110
4.3.2	Mouse TRPM3 and subcellular localization	111
4.3.3	Mouse TRPM3 expression and its biological roles	112
4.4	Phenotype of the TRPM3 knockout mice	113
5	Conclusions	115
	References	139
	Curriculum Vitae	141
	Declaration	143

List of Figures

1.1	Ca ²⁺ signaling and phospholipase C-mediated signaling pathways	2
1.2	Phylogenetic tree of mammalian TRP channels	3
1.3	Molecular structure of TRP channels	4
1.4	Phylogenetic relationship and domain comparison of the TRPM subfamily	7
1.5	Putative pore structure	11
2.1	General principle of FRET	32
2.2	Principle of yeast two hybrid library screening	34
2.3	Flow chart of yeast two hybrid screening and verification of putative protein interactions in yeast cells	36
2.4	Mechanism of the GeneSwitch™ system	41
2.5	Mechanism of the β -galactosidase (<i>lacZ</i>) assay	43
2.6	Introduction of fura-2 into the cytoplasm and excitation spectrum of fura-2 under different Ca ²⁺ -concentrations	46
2.7	Ca ²⁺ -induced bioluminescence of aequorin	47
2.8	Gene trap strategy for generating TRPM3 mutations and primer selection for genotyping	49
2.9	Visual Cliff Apparatus	51
3.1	Sequence of TRPM3	53
3.2	Localization of mM3 ₁₇₁₉ and mM3 ₁₃₃₇ in HEK-293 cells and/or MDCK cells	55
3.3	Quantification of intracellular Ca ²⁺ concentration increases caused by extracellular Ca ²⁺ and PS applications in HEK-293 cells expressing mM3 ₁₇₁₉ and mM3 ₁₃₃₇	58
3.4	Analysis of the effects of extracellular Ni ²⁺ on Ca ²⁺ entry in mM3 ₁₇₁₉	59

LIST OF FIGURES

3.5	Effects of divalent ions on Ca ²⁺ entry through mM3 ₁₇₁₉	60
3.6	Ca ²⁺ entry through mM3 ₁₇₁₉ with <i>P1060R</i> and <i>G1066V</i> pore mutations . .	62
3.7	Ca ²⁺ entry through mM3 ₁₇₁₉ with the <i>D1074A</i> pore mutation	64
3.8	Protein expression of the mM3 ₁₇₁₉ C-terminus in HEK-293 cells and the putative role of PH-domain in the plasma membrane attachment of the mM3 ₁₇₁₉ C-terminus	66
3.9	Effects of cysteine residues on the plasma membrane attachment of M3TC .	67
3.10	Effects of palmitoylation on the function and subcellular localization of mM3 ₁₇₁₉	68
3.11	Analysis of mM3 ₁₇₁₉ homomultimerization using the FRET technique . . .	71
3.12	Analysis of mM3 ₁₇₁₉ homomultimerization using co-immunoprecipitation . .	72
3.13	Analysis of the mM3 ₁₇₁₉ and mM3 ₁₃₃₇ subunit interactions using the yeast two hybrid system	73
3.14	Subunit interaction analysis between mTRPM3 and PKIG	77
3.15	Effects of db-cAMP on Ca ²⁺ entry through mTRPM3	78
3.16	Northern blot analysis of mouse TRPM3 expression	80
3.17	Immunofluorescence with mouse TRPM3 antibodies	81
3.18	Analysis of TRPM3 protein expression in the adult mouse eye	82
3.19	<i>LacZ</i> gene expression of mouse TRPM3 in the CNS	84
3.20	<i>LacZ</i> gene expression of mouse TRPM3 in the retina	85
3.21	<i>LacZ</i> gene expression of mouse TRPM3 in the gastrointestinal tract	86
3.22	<i>LacZ</i> gene expression of mouse TRPM3 in the liver and pancreas	87
3.23	<i>LacZ</i> gene expression of mouse TRPM3 in the reproductive system	88
3.24	<i>LacZ</i> gene expression of mouse TRPM3 in the skin, heart, kidney, conducting airways and spleen	89
3.25	<i>LacZ</i> staining of whole TRPM3 ^{-/-} mouse embryos	90
3.26	TRPM3- <i>lacZ</i> expression in frozen cranial sections at stage 13	91
3.27	TRPM3- <i>lacZ</i> expression in frozen cranial and cervical sections at stage 13 .	92
3.28	TRPM3- <i>lacZ</i> expression in frozen thoracic sections at stage 13	93
3.29	TRPM3- <i>lacZ</i> expression in frozen caudal sections at stage 13	94
3.30	Generation of homozygous <i>Agouti</i> and <i>non-albino</i> TRPM3 ^{-/-} mouse . . .	97
3.31	Generation of homozygous <i>Agouti</i> and <i>non-albino</i> TRPM3 ^{-/-} mice using genotyping and DNA sequencing	98
3.32	Phenotype of TRPM3 ^{-/-} mice and visual testing	100

LIST OF FIGURES

4.1	TRPM3 protein isoforms	102
4.2	Pore model of mM3 ₁₇₁₉	105

List of Tables

2.1	Animals, bacteria, cell lines and yeast cells	14
2.2	Antibodies	14
2.3	Cell culture materials	15
2.4	Chemicals	15
2.5	Consumables and laboratory equipment	17
2.6	Enzymes and peptides	18
2.7	Molecular biology reagent systems	18
2.8	Nucleic acids and plasmids	19
2.9	Bioinformatic tools and online databases	19
2.10	Oligonucleotides	20
2.11	Standard PCR components	21
2.12	Standard PCR conditions	22
2.13	Buffer and medium for chemocompetent DH5 α <i>E.coli</i> cells preparation	22
2.14	Transfection conditions	23
2.15	PCR components for first and nested reaction	24
2.16	PCR conditions for first and nested reaction	25
2.17	Thermal cycling parameters for site-directed mutagenesis	26
2.18	Total RNA isolation from HEK293 cells and mouse tissues	27
2.19	Touchdown PCR conditions for mouse genotyping	50
3.1	Putative interaction partners of mM3 ₁₇₁₉ identified by high stringency selection	75
3.2	Putative interaction partners of mM3 ₁₇₁₉ identified by medium stringency selection	76
3.3	<i>LacZ</i> gene expression in the <i>lacZ</i> transgenic TRPM3 ^{-/-} mouse	95

LIST OF TABLES

4.1 Domain composition of mM3 ₁₇₁₉	108
---	-----

List of Abbreviations

3-AT	3-amino-1,2,4-triazole
AER	apical ectodermal ridge
ANKTM1	ankyrin-like with transmembrane domains 1
APS	ammonium persulfate
BSA	bovine serum albumin
CP	choroid plexus
CSF	cerebrospinal fluid
DAG	diacylglycerol
DAPI	4', 6-diamidino-2-phenylindole
DEPC	diethyl pyrocarbonate
DMF	N,N-dimethylformamide
DMSO	dimethyl sulfoxide
DTT	dithiothreitol
EDTA	ethylene-diamine-tetraacetic acid
EGTA	ethylene-glycol-tetraacetic acid
FCS	fetal calf serum
Fura-2AM	fura-2-acetoxymethyl ester
GFP	green fluorescent protein
HA	hemagglutinin
HEPES	4-(2-hydroxyethyl)-1-piperazineethanesulfonic acid
HRP	horseradish peroxidase
IPTG	isopropyl- β -D-thiogalacto-pyranoside
LiAc	lithium acetate
MDCK	Madin-Darby canine kidney
mM3-S	mouse TRPM3 short splice variant

LIST OF ABBREVIATIONS

mM3-T	mouse TRPM3-T splice variant
MOPS	3-(<i>N</i> -morpholino)propanesulfonic acid
NCC	neural crest cells
NOMP-C	no mechanoreceptor potential-C
NP-40	nonylphenyl polyethylene glycol
NUDT9	human nucleoside diphosphate-linked moiety X-type motif 9
PAGE	polyacrylamide gel electrophoresis
PEG	polyethylene glycol
PET	polyester
PFA	paraformaldehyde
PIC	pancreatic islet cells
PIP ₂	phosphatidylinositol(4,5)-biphosphate
PIPES	piperazine- <i>N,N'</i> -bis(2-ethanesulfonic acid)
PKIG	protein kinase inhibitor gamma
PLC γ	phospholipase C γ
PMSF	phenylmethanesulphonyl fluoride
PS	pregnenolone sulfate
pS	picosiemens
RIPA	radio-immuno-precipitation assay
RLM-RACE	RNA ligase-mediated rapid amplification of 5' and 3' cDNA ends
SAP	shrimp alkaline phosphatase
SDS	sodium dodecyl sulfate
SSC	sodium chloride/sodium citrate
TAE	tris acetate EDTA
TCA	trichloroacetic acid
TEMED	<i>N,N,N',N'</i> -tetramethyl-ethylendiamine
Tris base	2-amino-2-hydroxymethyl-propane-1,3-diol
UAS	upstream activating sequence
X-gal	5-bromo-4-chloro-3-indolyl- β -D-galactopyranoside

1

Introduction

1.1 Ca^{2+} signaling and phospholipase C-mediated signaling pathways

Calcium (Ca^{2+}) is a universal second messenger that is responsible for fundamental biological processes such as excitation–contraction coupling of muscle cells, signaling in the nervous system and embryonic development [16, 207, 237]. The spatial Ca^{2+} distribution between cellular compartments (cytosol: $\sim 10^{-7}$ M, intracellular Ca^{2+} stores: 10^{-4} – 10^{-3} M) and extracellular fluid ($\sim 10^{-3}$ M) plays a decisive role in Ca^{2+} signaling, and is strictly controlled by several mechanisms including Ca^{2+} permeable channels, Ca^{2+} pumps and Ca^{2+} – Na^{+} exchangers [208]. The large Ca^{2+} concentration ($[\text{Ca}^{2+}]$) gradient between intracellular and extracellular compartments permits a rapid intracellular Ca^{2+} concentration ($[\text{Ca}^{2+}]_i$) change and therefore gives Ca^{2+} a signal character. Opening of Ca^{2+} permeable channels caused by ligand binding, mechanical stretch, membrane depolarization [108], or by depletion of intracellular Ca^{2+} stores [32] results in an increase of intracellular Ca^{2+} coming either from the lumen of endoplasmic reticulum/sarcoplasmic reticulum (ER/SR) or from the cell exterior across the plasma membrane. The increased cytosolic free Ca^{2+} triggers Ca^{2+} –dependent signal cascades that are mediated either directly by Ca^{2+} –binding molecules such as calmodulin and troponin C that *e.g.*, initiate muscle cell contraction, or indirectly by Ca^{2+} /calmodulin–dependent protein kinases (CaM–kinases) that result in serine or threonine phosphorylation of target proteins.

Many non–excitable cells can be stimulated by neurotransmitters, hormones or growth factors that cause $[\text{Ca}^{2+}]_i$ increases through phospholipase C (PLC)–mediated signaling

pathway. The activated PLC cleaves phosphatidylinositol 4,5-bisphosphate (PIP_2), a membrane-bound inositol phospholipid, into two second messengers: diacylglycerol (DAG) and inositol 1,4,5-trisphosphate (IP_3). Whereas DAG remains within the plasma membrane and activates PKC or some non-voltage-dependent Ca^{2+} channels (e.g., TRPC3/6/7 cation channels [14, 77]), IP_3 diffuses into the cytosol and binds to the IP_3 receptor resulting in Ca^{2+} release from the lumen of ER (Figure: 1.1). It is well known that the PLC-mediated signaling pathway is involved in the physiological functions of various membrane receptors and ion channels such as transient receptor potential (TRP) channels.

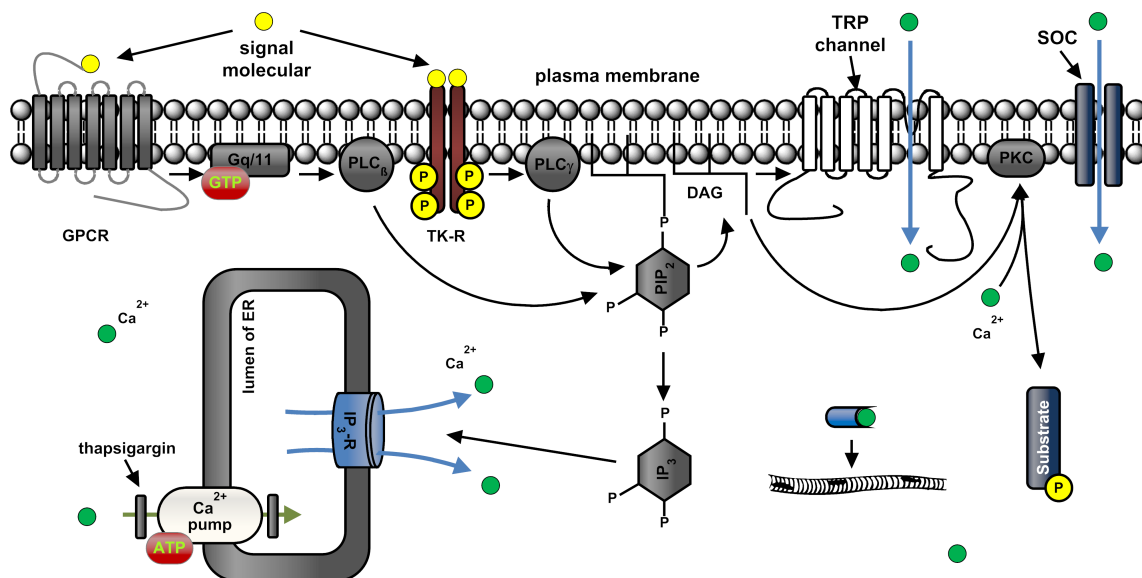


Figure 1.1: Ca^{2+} signaling and phospholipase C-mediated signaling pathways

PLC(β or γ) can be activated by active G-proteins or receptor tyrosine kinases and in turn hydrolyzes PIP_2 into DAG and IP_3 . Apart from PLC-mediated signaling pathways (s. text for detail), a Ca^{2+} influx from cell exterior into cytosol can also be induced by store-operated channels (SOCs) which are activated by the depletion of intracellular Ca^{2+} stores (e.g., thapsigargin treatment) [5, 85, 144, 164]. **Abbreviations:** GPCR, G protein-coupled receptor; PLC β , phospholipase C β ; PLC γ , phospholipase C γ ; PIP_2 , phosphatidylinositol 4,5-bisphosphate; IP_3 , inositol 1,4,5-trisphosphate; IP_3 -R, inositol triphosphate receptor; DAG, diacylglycerol; PKC, protein kinase C; TK-R, tyrosine kinase receptor; TRP channel, transient receptor potential channel; SOC, store-operated channel.

1.2 TRP channels

Transient receptor potential (TRP) channels were first described in *Drosophila*, where they play a critical role in PLC-mediated visual transduction [38, 126, 131]. In *Drosophila*, the *trp* mutant has a transient voltage response to light and exhibits a visual defect caused by a significant decrease in light-induced Ca^{2+} influx into photoreceptors [67, 124, 125]. TRP channels are highly conserved throughout evolution [123] and have been classified into seven subfamilies. With the exception of TRPN (NOMP-C) which is only found in zebrafish [200] and invertebrates [233], TRPC (Classical or Canonical), TRPA (ANKTM1), TRPV (Vanilloid), TRPM (Melastatin), TRPP (Polycystin) and TRPML (Mucolipin) channels are widely expressed in both vertebrates and invertebrates [132] (Figure: 1.2).

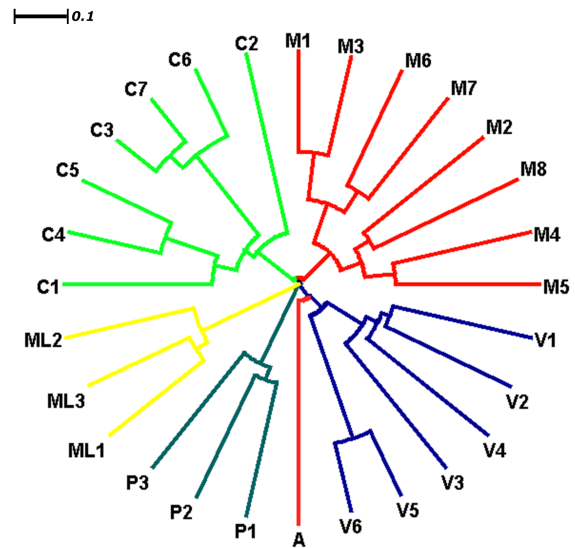


Figure 1.2: Phylogenetic tree of mammalian TRP channels The dendrogram showing the evolutionary relationship among mammalian TRP channels was produced by using *ClustalW2* for multiple sequence alignments and *Dendroscope 2* for a graphical representation [83]. The evolutionary distance is expressed as the number of amino acid substitutions per residue.

1.2.1 The molecular structure of mammalian TRP channels

TRP channels constitute a complex group of cation channels and demonstrate their biological diversity not only in ion selectivities and physiological functions, but also in activation and regulation mechanisms [66]. However, TRP channels have several structural similarities such as six putative transmembrane domains with a pore region between the fifth and sixth transmembrane (TM5 and TM6) domains, and cytoplasmic N- and C-termini.

1.2.1.1 Transmembrane domains, N- and C-termini of TRP channels

The precise molecular structure of the six transmembrane (6TM) domains of TRP channels is unknown, but the TM5 and TM6 domains are thought to be analogous to the 2TM

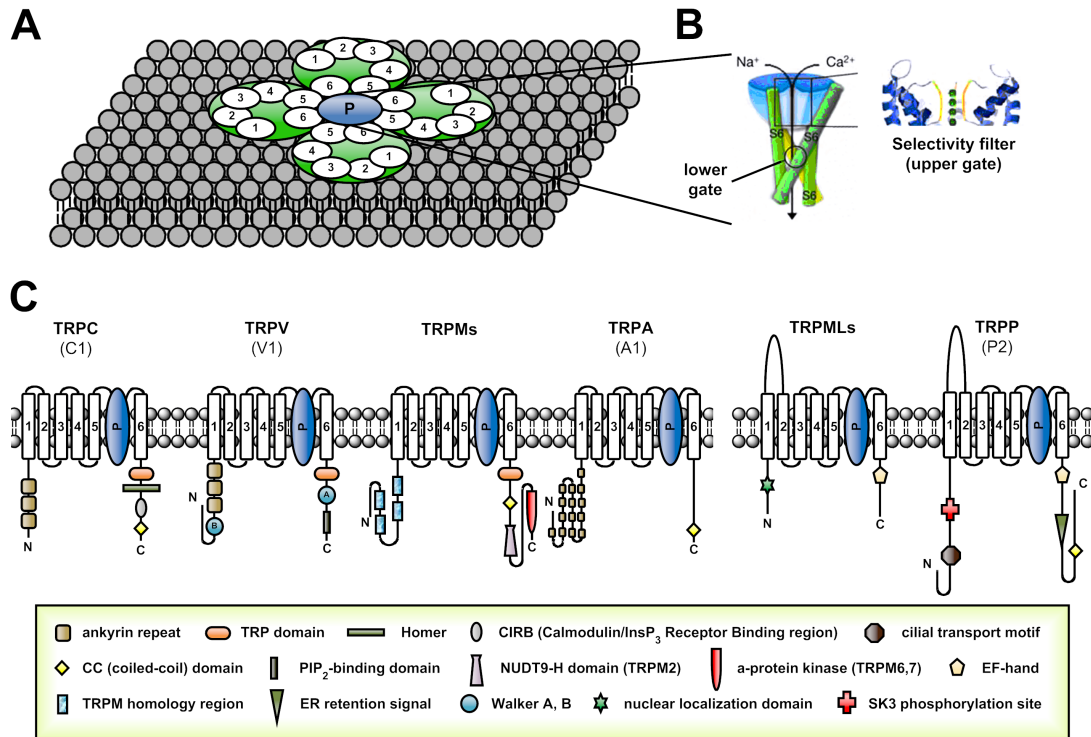


Figure 1.3: Molecular structure of TRP channels

A: Tetrameric assembly of TRP channels. 4×TM5–loop–TM6 units form a cation permeable channel. **B:** Cations diffusing into the cytosol are mainly controlled by selectivity filter and lower gate. The photo was adapted from Clapham, 2003 [32]. **C:** Structural topology of mammalian TRP channels. Ankyrin repeats are found in TRPC, TRPV (3–4 in number) and TRPA1 (14 in number). The TRP domain in TRPC is more conserved than it in TRPV and TRPM channels. Homer, an adaptor protein, regulates protein interaction between TRPC1 and IP₃R1, thus affecting Ca²⁺ influx [251]. CIRB is conserved in all seven TRPC channels and may be crucial to the channel activity [159, 210, 239]. Walker A and B domains binding with ATP regulate the biological function of TRPV1 [90]. PDZ-binding sites in TRPC4 and TRPC5; and PH (pleckstrin homology) domain in TRPC3 [221] and TRPM4 [145] are not shown.

of voltage-dependent KcsA channels [42, 249]. The 6TM domains assemble to form a tetramer [95] in which the TM5 domain faces the lipid membrane and the TM6 domain lines the pore region [33]. Four “TM5–pore–TM6” units construct a special cation-permeable channel that contains a selectivity filter (upper gate) and a lower gate (Figure: 1.3). The selectivity filter, which is located near the outer face of the membrane and formed by amino acids of the four selectivity loop units, selects cations to diffuse into cytosol. The lower gate formed by cytoplasmic ends of TM6 domains regulates the cation influx through the channel [32]. The detailed structure of the TM1–4 domains remains unclear; even so,

the deficiency of positively charged arginines in TM4 domain probably explains the weak voltage dependence of TRP channels [26]. Compared to other TRP channels, the TRPP and TRPML superfamilies have a large extracellular loop between TM1–2 domains and share a low sequence similarity in the transmembrane domains. They are classified as Group 2 TRP channels, while the TRPC, TRPV, TRPM, TRPA and TRPN channels belong to Group 1 TRP channels [132, 226].

Protein motifs in the cytoplasmic N- and C-termini are the basic structural features of the TRP channels. TRPC and some TRPV channels contain multiple ankyrin repeats in the N terminus which probably play an essential role in specific protein–protein interactions [192]. In the TRPC, TRPM and TRPN channels, a highly conserved amino acid region – the TRP domain – is located C-terminally of the TM6 helix [132]. The TRP domain contains a TRP box (WKFQR) which is followed by proline-rich sequences in some TRP channels. Rohács and colleagues found that the TRP domain may function as a interaction site for PI(4,5)P₂ to regulate TRPM8 channel activity [178]. Some other important motifs are shown in Figure 1.3.

1.2.1.2 Multimerization of mammalian TRP channel subunits

Except for voltage dependent Ca²⁺ and Na⁺ channels, all hexahelical cation channels require a functional pore structure assembled by four subunits [187]. Due to analogy with the more distantly related KcsA channels [42] and cyclic-nucleotide-gated channels [94], TRP channels are presumed to be expressed as oligomeric complexes composed of two or more highly phylogenetically related TRP subunits [132, 187]. However, the mechanisms and biological functions of the channel multimerization are still poorly understood. Several TRP channels have been confirmed to form homomeric and/or heteromeric channel complexes such as TRPC3/6/7 [56] and TRPM6/7 [31]. The N-terminus [8, 49] and C-terminus [54] of TRPs may be responsible for the channel subunit–subunit interactions.

1.2.2 Tissue expression and biological functions of mammalian TRP channels

The TRP channels constitute one of the largest ion channel families known [162]. The gene expression of the TRP channels can be found in various tissues and organs where they fulfill their specific physiological functions [177]. For example, TRPC5 is widely expressed in the

brain and plays a role in the neurite outgrowth and axonal pathfinding [57]. TRPV5–6 channels are enriched in intestinal tract and kidney where they are involved in Ca^{2+} reabsorption [49]. Due to the localization in both kino- and stereocilia, TRPP channels are thought to be able to detect signal changes in the extracellular environment such as osmolarity in fluid flow and mechanical stress [132]. TRPML3 is found in hair cells and has effects on hearing [41].

Almost all TRP channels are non-selective cation channels (with the exception of the Ca^{2+} impermeable TRPM4 and TRPM5 channels [104, 110], and the highly Ca^{2+} permeable TRPV5 and TRPV6 channels [161]), and the activation mechanisms of them are largely unknown. However, the TRP channels are thought to be mainly activated or modulated by PLC–signal transduction pathways [32, 133]. The biological functions of the TRP channels are considered to be closely related to their specific tissue expressions [34, 132]. For example, “loss-” or “gain-of-function” of TRP channels can induce the pathophysiological changes in tissues [153]. Besides the PLC-mediated signaling pathways, the cAMP/PKA-dependent signaling is also involved in the regulation of TRP channel activities. For example, PKA plays a role in the phosphorylation and sensitization of TRPV1 [172] and in the channel activity up-regulation of TRPM7 [209].

1.2.3 TRPM channels

The TRPM subfamily is named after its founding member, melastatin (TRPM1). In vertebrates, the TRPM subfamily consists of eight members which have been classified into four groups: TRPM1/3, TRPM2/8, TRPM4/5 and TRPM6/7 based on the sequence similarity (Figure: 1.2).

In comparison with TRPC and TRPV channels, the N-termini of TRPM channels are longer (~ 750 residues) and do not contain ankyrin repeats but have a large “TRPM homology region” whose functions are still elusive [132]. The six transmembrane domains (6TM) of TRPM channels constitute a cation permeable channel in a functional multimeric form [31, 109, 171, 187]. The 6TM and pore structures among the members of TRPM subfamily are highly conserved. The C-termini of TRPM channels can be divided into two regions [113]: a conserved region containing TRP and Coiled-Coil (C-C) domains, and a variable region whose molecular structure are little known (Figure: 1.4). The TRP domain is C-terminally close to the TM6 and probably serves as a binding site for $\text{PI}(4,5)\text{P}_2$ in the TRPM8 channel [178]. The C-C domain may be associated with channel subunit

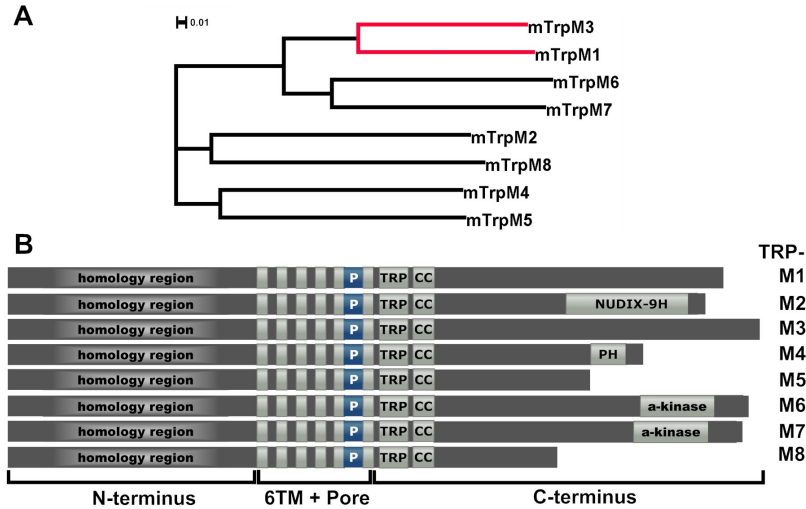


Figure 1.4: Phylogenetic relationship and domain comparison of the TRPM subfamily

The dendrogram was generated using *ClustalW2* for multiple sequence alignments and *Dendroscope 2* for a graphical representation [83]. The evolutionary distance was expressed as the number of amino acid substitutions per residue (A). See text for the detail description of the important structural domains of TRPM subfamily.

multimerization and probably has regulatory function on the channel activities [47, 48, 88, 118, 218]. The TRPM2, TRPM6 and TRPM7 channels were referred as “chanzymes” because of the C-terminal fusion with enzymatic domains. The NUDIX box domain of TRPM2 channel is highly homologous to NUDT9 which is a NUDIX enzyme with ADP-ribose hydrolase activity [169, 185, 193]. The NUDIX domain probably plays an important role in TRPM channel evolution. During evolution, a loss of NUDIX domain-coding exons causes TRPM3-like channels (TRPM1, TRPM3, TRPM6, TRPM7) in bilateral animals [117]. The Ser/Thr protein kinase domains of TRPM6 and TRPM7 [139, 181] belong to the atypical α -kinase family [182] which includes elongation factor-2 kinase [183] and myosin heavy chain kinase A [53]. While the functions of the TRPM6 kinase domain remain unknown, the kinase activity of TRPM7 was thought to modulate channel sensitivity for Mg^{2+} inhibition [190] and intracellular cAMP regulation [209]. TRPM6 and TRPM7 form a multimeric complex which is required for TRPM6 plasma membrane localization [29, 31]. TRPM8 and TRPM2 belong to the same subgroup, but TRPM8 does not contain an enzymatic domain. Phelps *et al.* found that the N- and C-termini were critical for TRPM8 physiological function, and the six transmembrane domains were sufficient for TRPM8

tetramerization [171]. TRPM4 possesses a C-terminal pleckstrin homology (PH) domain, a putative PIP₂ binding domain, which modulates the Ca²⁺ sensitivity of the channel [66, 110, 145]. Besides the typical TRPM channel structures: four homology domains in the N-termini, six transmembrane domains, TRP domains followed by C-C domains in the C-termini, no enzymatic or other functional domains have been described in the TRPM1 and TRPM3 channels until now.

The members of the TRPM subfamily have individual characteristics in their expression patterns, ion selectivities and gating mechanisms, which are directly involved in the channel biological functions such as controlling cation entry and cell growth. TRPM1 was isolated from mouse melanoma cell lines and supposed to be a constitutively open Ca²⁺ entry channel [247]. TRPM2 is a voltage-independent non-selective cation channel. TRPM2 is permeable not only to monovalent cations such as Na⁺, K⁺ and Cs⁺, but also to divalent cations such as Ca²⁺ [72, 169]. TRPM2 expression can be detected in many cell types, especially in brain and immune cells [140, 185], and its channel activity is regulated by a variety of factors including warm temperature (>35°C), oxidative stress and TNF α [65, 121, 214, 240]. TRPM3 is the last identified member of the TRPM subfamily and is structurally most related to TRPM1 (Section: 1.3) [106, 156]. TRPM4 is expressed as three isoforms in man (TRPM4a, TRPM4b and TRPM4c [137, 148]) and found in various tissues and cell types including excitable and non-excitable cells. TRPM4b is reported to be a monovalent cation selective channel that is impermeable to Ca²⁺. However, TRPM4b can be directly activated by increased [Ca²⁺]_i [104] and is regulated by PIP₂, PKC phosphorylation and the presence of calmodulin [145, 148, 151, 152]. TRPM5, like TRPM4, is a Ca²⁺-activated non-selective cation channel (CAN) impermeable to divalent cations, but non-selective for monovalent cations [76]. TRPM5 is broadly distributed in different tissues, especially in the taste receptor cells where it is essential for the signal transduction of sweet, umami, and bitter tastes [168, 174, 254]. By desensitizing and re-sensitizing the TRPM5 channel respectively, intracellular Ca²⁺ and PIP₂ regulate the taste transduction in the taste receptor cells [110]. TRPM6 is highly expressed in the kidney and intestine, and plays an important role in renal and intestinal Mg²⁺ homeostasis and reabsorption [230]. TRPM6 is mainly permeable to divalent cations (Mg²⁺>Ca²⁺) [109]. TRPM7 is a divalent specific cation channel permeable not only to Mg²⁺ and Ca²⁺ but also to many trace metal ions, with a permeability sequence of Zn²⁺ \approx Ni²⁺ \gg Ba²⁺ > Co²⁺ > Mg²⁺ \geq Mn²⁺ \geq Sr²⁺ \geq Cd²⁺ \geq Ca²⁺ [130]. The tissue expression of TRPM7 is ubiquitous and the channel activity of TRPM7 can be stimulated by

intracellular alkalinization, by protons and by fluid flow [89, 98, 139, 154]. TRPM8 is found in the prostate and dorsal root and trigeminal ganglia where it executes functions in the thermosensation and nociception [99, 167, 217]. TRPM8 is also one of the “thermoTRPs” because it can be activated by cool temperature ($<26^{\circ}\text{C}$) [115] and cooling agents such as icilin and menthol [142, 167, 227].

1.3 TRPM3

TRPM3 is most phylogenetically related to TRPM1 which is the founding member of the TRPM subfamily. In comparison to other TRPM channels (*e.g.*, TRPM4, TRPM6 and TRPM7), TRPM1 and TRPM3 lack functional elements such as an enzyme domain in their C-termini. Because TRPM1 and TRPM3 are highly conserved throughout evolution, they are considered as archetypal channels in the TRPM subfamily [117]. Whereas the expression of TRPM1 is restricted to melanocytes and pigmented melanoma cell lines [43, 44, 81] and can be transcriptionally regulated by microphthalmia-associated transcription factor (MITF) [120], the tissue distribution and regulation mechanisms of TRPM3 remain elusive.

1.3.1 Structural features of TRPM3

1.3.1.1 Genomic regions and transcript variants

The TRPM3 gene is highly conserved across mammalian species. The mouse TRPM3 (mTRPM3) gene is more than 850 kb and contains 28 exons located on the chromosome 19qB [157], while the human TRPM3 (hTRPM3) gene is more than 910 kb and consists of 24 exons mapped to the chromosome 9q21.11–q21.12 [106].

Due to alternative splicing, the TRPM3 gene encodes many different transcript variants. Oberwinkler *et al.* (2005) cloned five different TRPM3 cDNAs (mTRPM3 α 1-5) from mouse brain, whose protein coding sequences range from 1699 to 1721 amino acid residues [157]. The second exon (exon 2) of mTRPM3 α 1-5 cDNAs is not transcriptionally expressed. However, exon 2 is the first encoded exon of a human splice variant, hTRPM3₁₃₂₅. This hTRPM3₁₃₂₅ transcript variant isolated by Grimm *et al.* (2003) from human kidney has a shorter C-terminus and contains only 1325 amino acid residues [58, 156, 157]. About 350 amino acid residues and part of the untranslated region at its C-terminus are removed by splicing within exon 28, that also introduces a frameshift resulting in seven alternative amino acid residues at the C-terminal end [58, 156]. According to the start codon present in

exon 4 predicted by using sequence alignment, Lee *et al.* (2003) cloned six human TRPM3 cDNAs (hTRPM3a–f) from a human kidney cDNA library [106]. Because the exon 1 and exon 2 were overlooked, the N–termini of hTRPM3a–f variants are 155 amino acid residues shorter than the N–termini of mTRPM3 α 1–5 variants [156]. As a result of alternative splicing, the TRPM3 transcript variants differ also by the presence or absence of four short amino acid fragments (10–25 in length) encoded by exons 8, 15, 17 and 24. The divergent pictures of TRPM3 function in the literature may reflect the diversity of cDNAs used in these studies.

1.3.1.2 Protein structure

Almost all TRPM3 isoforms share the typical TRP channel structural features: six trans-membrane domains (6TM) with a pore region between TM5 and TM6, and cytoplasmatic N– and C–termini.

In the N–terminus, a large TRPM homology region is present. The start sequence of this homology region, (W/F)IX₃-(F/L/I)CK(R/K)EC(V/I/S)X_{12–24}CXCG [58], only exists in the mTRPM3-a/b/c/d/e/f, hTRPM3-k and hTRPM3₁₃₂₅ isoforms. In contrast to the N–terminus, the structural characteristics of TRPM3 C–terminus remains elusive. Except for the TRP domain and Coiled–Coil domain (C–C domain), no other functional elements have been found so far. Whereas the sequences of 6TM are identical among the TRPM3 isoforms, the sequences of pore region vary in thirteen amino acid residues, RKQVYDSHTPKSA, that are only present in mTRPM3-a and hTRPM3c isoforms (Figure: 4.1). The presence or absence of this short amino acid stretch probably has an effect on the ion selectivity [157] (Section: 1.3.3). Moreover, a hydrophobic pore helix conserved in all TRPM channels and a putative ion selectivity loop domain are detected within the TRPM3 pore region [149, 161, 215, 244], although, how they influence the ion permeation and selectivity is poorly understood.

1.3.2 Tissue distribution of TRPM3

Using different molecular techniques including RT–PCR, in situ hybridization, immunocytochemistry, Northern and Western blots, TRPM3 expression was detected in some human and/or mouse tissues such as human kidney and mouse brain [58, 106, 157]. Nevertheless, its expression could not be proved in a given tissue and cell type due to the sensitivity of the methods and the amplification of parts of the transcripts [156]. The expression pattern of

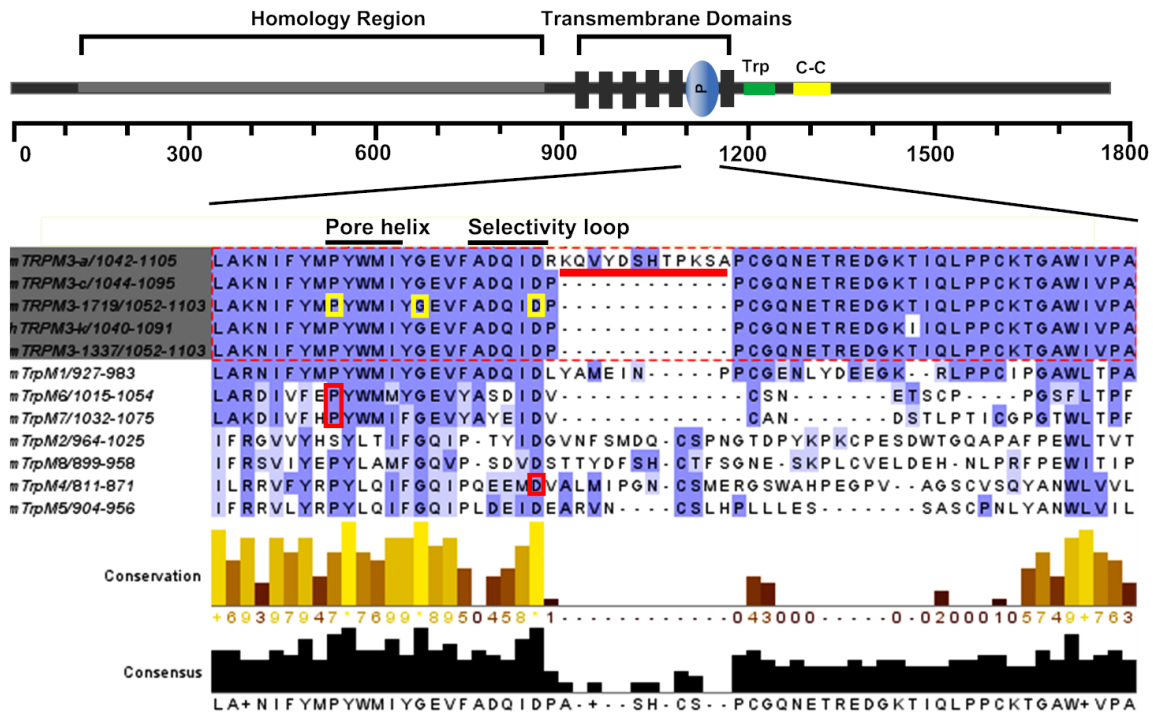


Figure 1.5: Putative pore structure

Pore regions of some TRPM3 isoforms compared to the corresponding sequences of other TRPM channels. *ClustalW2* and *Jalview 2.4* were used for multiple sequence alignments and a graphical representation, respectively. *BLOSUM62* score matrix was used to calculate pairs of aligned residues based on alignments with identity of at least 62%. Within the TRPM3 subfamily, the hTRPM3c (not shown) and mTRPM3-a isoforms possess an additional 12 amino acids in the pore region. The localizations of the conserved hydrophobic pore helix and putative selectivity loop are shown. The two red-boxed proline residues in the TRPM6 and TRPM7 and one aspartate residue in the TRPM4 are highly conserved and were mutated to generate dominant negative mutants [30, 117, 149]. Pro¹⁰⁶⁰, Gly¹⁰⁶⁶ and Asp¹⁰⁷⁴ boxed in yellow are identical in all TRPM subfamily. Their functional relevance were tested by site-directed mutagenesis (P→R, G→V, D→A, respectively).

TRPM3 is still not conclusively resolved, *e.g.*, TRPM3 was mostly found in human kidney, but not in mouse kidney [58, 106, 157].

1.3.3 Channel properties of TRPM3

Although several TRPM3 splice variants have been reported, functional data for them are only limited to four isoforms, mTRPM3-a [157], mTRPM3-c [157], hTRPM3a [106] and hTRPM3₁₃₂₅ [58, 59, 246]. The biophysical properties, like selectivity and conductance,

are highly dependent upon the TRPM3 splice variant and the experimental conditions [58, 59, 157].

The mTRPM3-c and hTRPM3₁₃₂₅ channels had a significantly higher divalent to monovalent permeability ratio than the mTRPM3-a channel. Contrarily, mTRPM3-a showed a lower permeability to divalent cations based on the experimental results that no significant inward currents through the channel were observed [157]. TRPM3 has also been reported to have constitutive activity when expressed in a heterologous system [58, 106, 157]. The cells expressing TRPM3 have a higher $[Ca^{2+}]_i$ than the control cells, even in the absence of any stimuli [58, 106, 157]. In electrophysiological experiments, Grimm *et al.* (2003) and Oberwinkler *et al.* (2005) observed decrease and increase in $[Ca^{2+}]_i$ occurred on removal and readmission of extracellular $[Ca^{2+}]_o$, respectively.

1.3.4 Inhibition, blockage and activation of TRPM3

TM3E3, a polyclonal antibody, raised against the third extracellular (E3) loop of TRPM3 was reported to partially inhibit Ca^{2+} entry in cells expressing human TRPM3 in a peptide-specific manner [141]. Oberwinkler and co-workers (2005) reported that the constitutive activities of heterologously expressed mTRPM3-a and mTRPM3-c channels were similarly inhibited by millimolar $[Mg^{2+}]_i$. It was suggested that the selectivity filters of both isoforms did not have effects on the intracellular Mg^{2+} -induced channel inhibition [157].

2-aminoethoxydiphenyl borate (2-APB, 100 μ M) has been reported to block the channel activity of TRPM3 expressed in HEK-293 cells from the extracellular face of the membrane [246]. Some ions such as Gd^{3+} (100 μ M) and La^{3+} (100 μ M) can block Ca^{2+} entry through TRPM3 channels [58, 106]. The mechanisms by which these ions inhibit Ca^{2+} entry are not fully understood. However, all these substances are not specific for TRPM3 channels and can block a number of other TRP channels and other Ca^{2+} -permeable channels [164, 175].

Lee *et al.* (2003) treated hTRPM3-a-transfected cells with thapsigargin and carbachol to empty Ca^{2+} stores. Then, they added Ca^{2+} at different concentrations to HEK-293 cells and found that the $[Ca^{2+}]_i$ increase in hTRPM3-a-transfected cells was larger than in control cells [106]. However, Grimm *et al.* (2005) performed similar experiments using hTRPM3₁₃₂₅ variant, and did not find any increase in Mn^{2+} - or Ca^{2+} -entry after thapsigargin treatment [58, 59]. Hence, it is still controversial whether store depletion is able to activate TRPM3 channel activity. TRPM3 has also been suggested to be a cation channel activated by extracellular hypotonicity [68]. Compared to control cells, $[Ca^{2+}]_i$ in HEK 293

cells expressing hTRPM3₁₃₂₅ was increased when the extracellular osmolarity was decreased to 200 mosmol/L [58]. Some pharmacological substances such as nifedipine (a dihydropyridine Ca²⁺ channel blocker) and pregnenolone sulphate (PS) have been shown to enhance TRPM3 channel activity [231]. However, their physiological importance of TRPM3 channel function need to be investigated further.

1.3.5 Biological role and relevance of TRPM3

It has been suggested that TRPM3 might be involved in renal Ca²⁺ homeostasis and osmoregulation, because it is permeable to divalent cations, sensitive to extracellular hypo-osmolarity changes and present in human renal tubules [58, 106]. Recently, Wagner *et al.* (2008) found that TRPM3 was present in pancreatic β cells. Insulin secretion was enhanced when TRPM3 was activated by 50 μ M pregnenolone sulfate [231]. This indicates that TRPM3 might have an endocrine function and play a role in insulin release from pancreatic islets. TRPM3 is also a candidate gene for some diseases, *e.g.*, haemophagocytic lymphohistiocytosis, infantile nephronophthisis, amyotrophic lateral sclerosis with frontotemporal dementia, and early-onset pulverent cataract [106, 146]. However, convincing evidence for a functional relevance in these diseases is missing so far.

1.4 Objectives of this thesis

Throughout evolution, TRPM3 is one of the most highly conserved members of the TRPM subfamily. The phenotypes of mutation in the TRPM3 gene are unknown and the available data concerning its expression patterns and functions are still controversial. Therefore, the goals of this work are to:

1. clone a new cDNA of mouse TRPM3 and study its biological function *in vitro*;
2. raise antibodies against mouse TRPM3 in order to determine its expression profiles;
3. obtain a mouse with a TRPM3 knockout allele, and investigate its phenotype.

2

Materials and Methods

2.1 Materials

2.1.1 Animals, bacteria, cell lines and yeast cells

Table 2.1: Animals, bacteria, cell lines and yeast cells

Name	Provider
Competent yeast cells AH109 and Y187	Clontech
<i>E.coli</i> DH5 α	Invitrogen
GeneSwitch TM -293 cell line	Invitrogen
GeneSwitch TM -MDCK cell line	Invitrogen
<i>LacZ</i> transgenic TRPM3 knockout mice	Lexicon Genetics

2.1.2 Antibodies

Table 2.2: Antibodies

Antibodies	Dilution	Animal	Manufacturer
Anti-GFP antibody polyclonal	1:1000 (IF)	rabbit	Clontech
Anti-HA antibody polyclonal	1:1000 (IF)	rabbit	Sigma-Aldrich
Anti-TRPM3 antibodies polyclonal	1:2000 (IF)	rabbit	Eurogentec
Anti-rabbit-IgG Alexa Fluor 488	1:2000 (IF)	goat	Eugene
Anti-rabbit-IgG peroxidase	1:2000 (IF)	goat	Sigma-Aldrich
Anti-rabbit-MAP2 polyclonal	1:200 (IF)	rabbit	Abcam

2.1.3 Cell culture materials

Table 2.3: Cell culture materials

Name	Manufacturer
Bovine pituitary extract	Invitrogen
Cell culture dishes, flasks and scrapers	SARSTEDT AG & Co
Dulbecco's modified eagle medium (DMEM), high Glucose (4,5 g/l)	PAA Laboratories
DMSO	Carl Roth
Fetal calf serum	Gibco-BRL
Glutamine	Invitrogen
Goat serum	PAA Laboratories
Ham's F-10 medium	Invitrogen
Minimal essential medium eagle (MEM)	PAA Laboratories
Newborn calf serum	Invitrogen
Opti-MEM [®] I reduced serum medium	Invitrogen
Transwell [®] PET membrane insert (0.4 μ M)	Corning Life Sciences
Penicillin/Streptomycin (100x)	PAA Laboratories
Penicillin/Streptomycin/fungizone (100x)	VWR International GmbH
Trypsin/EDTA (10x)	PAA Laboratories

2.1.4 Chemicals

Table 2.4: Chemicals

Name	Manufacturer
3-AT	Sigma-Aldrich
12- <i>O</i> -tetradecanoylphorbol-13-acetate	Sigma-Aldrich
[α - ³² P]-dCTP	GE Healthcare
Adenine hemisulfate	Sigma-Aldrich
Bacto [™] -agar	Becton Dickinson
2-Bromopalmitate	Sigma-Aldrich
Coelenterazine	Biaffin
Coomassie-Brilliant Blue G-250	Merck
DAPI	Sigma-Aldrich
Deoxycholate	Sigma-Aldrich
D- <i>erythro</i> -Sphingosine	Calbiochem
Dibutryl adenosine cyclic 3',5'-monophosphate	Sigma-Aldrich
dNTP Mix (10mM)	Fermentas

2.1. Materials

EDTA, EGTA	Carl Roth
Fluorescence mounting medium	DaKo
Forskolin	Sigma-Aldrich
FuGENE [®] HD transfection reagent	Roche Diagnostics
Fura-2AM	Fluka
Geneticin (G418 sulphate)	PAA Laboratories
Glutaraldehyde	Sigma-Aldrich
Glycogen	Fermentas
HEPES	Carl Roth
Hygromycin B	PAA Laboratories
Isobutylmethylxanthine	Sigma-Aldrich
Isoflurane	Baxter
L-Histidine HCl monohydrate	Sigma-Aldrich
L-Leucine	Sigma-Aldrich
L-Tryptophan	Sigma-Aldrich
Lipofectamine [™] 2000	Invitrogen
Lithium acetate	Sigma-Aldrich
2-Mercaptoethanol	Sigma-Aldrich
Mifepristone	Invitrogen
NP-40	Calbiochem
PEG 3350	Sigma-Aldrich
Phenol:Chloroform:Isoamyl Alcohol 25:24:1	Carl Roth
PIPES	Sigma-Aldrich
PMSF	Sigma-Aldrich
Potassium acetate	Carl Roth
Potassium ferrocyanide	Sigma-Aldrich
Potassium ferricyanide	Sigma-Aldrich
Pregnenolone sulfate	Sigma-Aldrich
Protease inhibitor cocktail tablets	Roche Diagnostics
Protein A-Sepharose [®] from <i>Staphylococcus aureus</i>	Sigma-Aldrich
Roti phenol	Carl Roth
RotiPhores [®] Gel 40	Carl Roth
SD/-Ade/-His/-Leu/-Trp supplement	Clontech
SD/-Leu/-Trp supplement	Clontech
Silver nitrate (AgNO ₃)	Merck
Streptomycin	PAA Laboratories
TEMED	Sigma-Aldrich
Trichloroacetic acid (TCA)	Sigma-Aldrich
Triton X-100	Calbiochem
TRIzol [®] reagent	Sigma-Aldrich
Tryptone	Carl Roth

2.1. Materials

Tween 20	Sigma-Aldrich
Urea	Carl Roth
Yeast extract	Carl Roth
Yeast nitrogen base without amino acids	Sigma-Aldrich
X- α -gal	Carl Roth
X-gal	Sigma-Aldrich
Zeocin™	Invitrogen

2.1.5 Consumables and laboratory equipment

Table 2.5: Consumables and laboratory equipment

Names	Manufacturer
Axiovert 200M inverted microscope	Carl Zeiss
Beckman LS 6000IC liquid scintillation counter	Beckman Coulter
BioMax MS and X-OMAT™ films	Kodak
Biomax TranScreen LE	Kodak
BioPhotometer 6131	Eppendorf AG
Bio-Spin® 6 columns	Bio-Rad
Centrifuge Bio-, Megafuge	Heraeus Instruments
Cryocut 1850 cryomicrotome	Leica MICROSYSTEMS
Exposition chamber hypercassette™	Amersham Bioscience
FLUOstar OPTIMA	BMG LABTECH
Glass beads	Sigma-Aldrich
Hybond™-N membrane	Amersham Bioscience
Hybridization oven	Robbins Scientific
Laser scanning microscope (LSM 510 META)	Carl Zeiss
MiniVE system blot module	Amersham Bioscience
MiniVE vertical electrophoresis system	Amersham Bioscience
Nitrocellulose membrane	Schleicher&Schuell BioScience
Olympus IX70 inverted microscope	Olympus America, Inc.
PCR machine T3 thermal cycler	Biometra
Superfrost® plus microscope slides	Thermo SCIENTIFIC
TILLvisION highest speed imaging system	TILL Photonics GmbH
Video documentation system (INFINITY Model)	PEQLAB Biotechnology
VWR grade 410 paper filters	VWR International
Whatman paper	Whatman International

2.1.6 Enzymes and peptides

Table 2.6: Enzymes and peptides

Name	Manufacturer
GeneRuler™ DNA Ladder Plus (100 bp, 1k bp)	Fermentas
PageRuler™ Prestained Protein Ladder	Fermentas
Proteinase K, recombinant	Roche Diagnostics
Restriction enzymes (10-20 U/μl)	Fermentas
Ribonuclease A	Sigma-Aldrich
ssRNA ladder	New England Biolabs
SuperScript™ III reverse transcriptase	Invitrogen
Taq-Polymerase (500 U/μl)	Fermentas
T ₄ DNA ligase (200-1000 U/μl)	Fermentas

2.1.7 Molecular biology reagent systems

Table 2.7: Molecular biology reagent systems

Name	Manufacturer
Expand High Fidelity ^{PLUS} PCR System	Roche Diagnostics
Expand Long Template PCR System	Roche Diagnostics
GeneJET™ Plasmid Miniprep Kit	Fermentas
GeneRacer™ Kit	Invitrogen
HexaLabel™ DNA Labeling Kit	Fermentas
NUCLEOBOND Midi-prep Kit	Macherey-Nagel
Oligotex Direct mRNA Mini Kit	QIAGEN
pcDNA3.1/V5-His [©] TOPO [®] TA Expression Kit	Invitrogen
peqGOLD Gel Extraction Kit	PEQLAB Biotechnology
peqGOLD Plasmid Miniprep Kit II	PEQLAB Biotechnology
Pretransformed Human Kidney Matchmaker™ cDNA Library	Clontech
QuikChange [®] XL Site-Directed Mutagenesis Kit	Stratagene
SuperSignal West Pico Chemiluminescent Substrate	Pierce Biotechnology
SuperSignal West Femto Maximum Sensitivity Substrate	Pierce Biotechnology
Topo TA Cloning [®] Kit for Sequencing	Invitrogen

2.1.8 Nucleic acids and plasmids

Table 2.8: Nucleic acids and plasmids

Name	Provider
DNA sodium salt from herring testes Type XIV	Sigma-Aldrich
pACT2 AD vector	Clontech
pEGFP-C1 and pEGFP-N1 vectors	Clontech
pGAD424 AD vector	Clontech
pGADT7-T control vector	Clontech
pGBKT7 DNA-BD vector	Clontech
pGBKT7-53 control vector	Clontech
pGene/V5-His A, B, C vector	Invitrogen
pSwitch vector	Invitrogen

2.1.9 Bioinformatic tools and online databases

Table 2.9: Bioinformatic tools and online databases

Tools and Databases	URL or Manufacturer
Axio vision 3.1	Carl Zeiss Vision GmbH
Blast	http://www.ncbi.nlm.nih.gov/blast/Blast.cgi
ClustalW2	EMBL-European Bioinformatics Institute
Dendroscope 2	Center for Bioinformatics Tübingen (ZBIT)
DNA Sequencing	MWG Biotech AG
ENSEMBL	http://www.ensembl.org/index.html
ExPASy Proteomics Server	http://www.expasy.org/
Mouse Gene Expression Database (GXD)	http://www.informatics.jax.org/mgihome
Human Protein Reference Database	http://www.hprd.org/
ImageJ	National Institutes of Health
Jalview 2.4	The Barton Group, University of Dundee
JAX Mice Database	http://jaxmice.jax.org/
LaserGene	DNASTAR, Inc.
Mammalian Protein Localization Database	http://locate.imb.uq.edu.au/
Mouse Genome Informatics (MGI)	http://www.informatics.jax.org
National Center for Biotechnology Information (NCBI)	http://www.ncbi.nlm.nih.gov/
SOSUI Server	Mitaku Group, Nagoya University
TILLvisION 3.0	TILL Photonics GmbH
Worldwide Protein Data Bank	http://www.wwpdb.org/

2.1.10 Oligonucleotides

Table 2.10: Oligonucleotides

Applications	Primers (5'→3')
5'-RACE	GeneRacer™ 5' primer: <i>CGACTGGAGCACGAGGACACTGA</i>
	GeneRacer™ 5' nested primer: <i>GGACTGACATGGACTGAAGGAGTA</i>
	GSP primer 1: <i>AGTTTCACCTCTGCTCCGTATTTTC</i>
	GSP primer 2: <i>ATCAAAAAGATACTCGGACATACATAG</i> GSP primer 3: <i>CTATGAGGCGTCCACAGCAACAC</i>
Mutagenesis	<i>Rey</i> Forward: <i>GGTCAGGGATGTCAAAAAGGGAAACCTGCCCCC</i> Reverse: <i>GGGGCAGGTTTCCCTTTTTGACATCCCTGACC</i>
	<i>T1088I</i> Forward: <i>CGAGAGGATGGCAAGATAATCCAGCTGCCCCC</i> Reverse: <i>GGGGCAGCTGGATTATCTTGCCATCCTCTCG</i>
	<i>P1060R</i> Forward: <i>GCCAAGAATATCTTCTACATGCGTTATTGGATGATTTATGGGG</i> Reverse: <i>CCCATAAATCATCCAATAACGCATGTAGAAGATATTCTTGGC</i>
	<i>G1066V</i> Forward: <i>GCCTTATTGGATGATTTATGTGGAAGTGTTTGCTGACC</i> Reverse: <i>GGTCAGCAAACACTTCCACATAAATCATCCAATAAGGC</i>
	<i>D1074A</i> Forward: <i>GCTGACCAGATAGCCCCCTCCCTGTGGAC</i> Reverse: <i>GTCCACAGGGAGGGGCTATCTGGTCAGC</i>
	<i>C1301S</i> Forward: <i>AGGACCTCCTCAGACAGCACAGATGCAGCC</i> Reverse: <i>GGCTGCATCTGTGCTGTCTGAGGAGGTCTT</i>
	<i>C1210S</i> Forward: <i>GTACACGATTTTGAAGAGCAGAGCATAGAGGAATATTTCCGA</i> Reverse: <i>TCGGAAATATTCCCTCTATGCTCTGCTCTTCAAATCGTGTAC</i>
	<i>CC1174SS</i> Forward: <i>ATCTTCCAGCATGTGTCTCCCGGTGGAGGAAGCAT</i> Reverse: <i>ATGCTTCTCCACCGGGAGGACACATGCTGGAAGTA</i>
Mouse Genotyping	TRPM3– WT Forward: <i>CTGTGGCTGCCAAGCACCGTGAC</i> Reverse: <i>CCTCAAGACTCCCAATCCAAG</i>
	TRPM3– Neo Forward: <i>CCTCAAGACTCCCAATCCAAG</i> Reverse: <i>GCAGCGCATCGCCTTCTATC</i>
	Non–Agouti (a) Forward: <i>GGAGAGGCGTGGGTGGCTGAATGG</i> Reverse: <i>TTACAAGAAGAAGTGGGGAATGAAGA</i>
	Tyrosinase (C) Forward: <i>GCTGTTTTGTATTGCCTTCTGTGGAGTTTC</i> Reverse: <i>AAGGATGCTGGGCTGAGTAAGTTAGGATTTTC</i>
M3TC Cloning	Forward: <i>ACCGCCATGACCATGATCTTCCAGC</i> Reverse: <i>TTACGCGTAATCAGGAACATCATATGG</i> Forward: <i>ACCGCCATGACCATGATCTTCCAGC</i> Reverse: <i>GAATTCCTTGTACAGCTCGTCCATGCC</i>
	Y2H Constructs
Y2H Constructs	N–Termi Forward: <i>CAATTGCCAGGGCCGTGGGGGACC</i> Reverse: <i>GTCGACCTACTCATAGATTTTTTCGGCCCACG</i>
	C–Termi Forward: <i>GAATTCTCGATATCCAACCAAGTATGG</i> Reverse: <i>GTCGACTTAGTTGTGCTTGCTTTCAAAGC</i>
Y2H	C–Termi(S) Forward: <i>GAATTCTCGATATCCAACCAAGTATGG</i> Reverse: <i>GTCGACTTATACTGAATAAAAAGGATGTTCTGCAGGGTC</i>

2.2 Methods

2.2.1 DNA analysis and preparation

2.2.1.1 General DNA methods

The standard molecular biological methods for DNA analysis such as agarose gel electrophoresis, DNA digestion and ligation, DNA isolation from agarose gel, DNA purification by phenol extraction and ethanol/isopropanol precipitation, DNA transformation into competent *E.coli*, and mini-, midi- and maxi-preparations of plasmid DNA were carried out according to Sambrook *et.al* [2000] [184] and Ausubel *et.al* [2001] [10], and are not described here in detail. All experiments and centrifugations were performed at room temperature unless otherwise stated.

2.2.1.2 Polymerase chain reaction (PCR)

The polymerase chain reaction (PCR) was used to amplify specific DNA sequences. The components and conditions of standard PCR are shown in the following tables. Some variations on the standard PCR, such as PCR in mutagenesis, touchdown PCR, nested PCR and colony PCR, are described in the corresponding sections.

Table 2.11: Standard PCR components

Components	Amount
DNA (template)	~ 0.5 µg
10x reaction buffer (Mg ²⁺ final concentration: 1.5–2.5 mM)	2.5 µl
dNTP (10 mM)	0.5 µl
Forward primer (50 µM)	0.25 µl
Reverse primer (50 µM)	0.25 µl
Polymerase	0.25 µl
ddH ₂ O	Add to 25 µl

Samples were handled on ice, and enzymes were always added last. The annealing temperature was selected according to different primer pairs. The PCR products were directly analyzed by means of agarose gel electrophoresis and visualized by ethidium bromide.

Table 2.12: Standard PCR conditions

Steps	Temp.	Time	Note
1	94°C	3 min	
2	94°C	1 min	
3	58°C	1 min	
4	68°C	1 min/kb amplified DNA	Go to 2, 30 cycles
5	68°C	5 min	
6	4°C	hold	

2.2.1.3 Preparation of chemocompetent DH5 α *E.coli* cells

Chemocompetent DH5 α cells were prepared according to a Mn²⁺-based method that yield 1x 10⁸ to 3x 10⁸ transformed colonies/mg of plasmid DNA [84]. Transformation buffer and SOB bacterial medium were as fresh as possible when used (Table: 2.13).

Table 2.13: Buffer and medium for chemocompetent DH5 α *E.coli* cells preparation

Buffer/Medium	Composition
Transformation buffer:	PIPES 10 mM
	CaCl ₂ 15 mM
	KCl 250 mM
	MnCl ₂ 55 mM
	ddH ₂ O ad 500 ml
	Adjusted to pH 6.7. Add MnCl ₂ only after the titration and sterilize the buffer by filtration (0.45 μ m).
SOB medium:	KCl 2.5 mM
	NaCl 8.55 mM
	MgCl ₂ 10 mM
	Tryptone 20 g/L
	Yeast extract 5 g/L
	Adjusted to pH 7.0 with HCl. Autoclave the medium.

A strain of *E.coli* was streaked on an antibiotic-free LB plate and incubated at 37°C overnight. A single colony (3-5 mm in diameter) was cut out of the agar and transferred into 400 ml of SOB medium in a flask. The culture was incubated at 18°C with shaking until an OD₆₀₀ of 0.4–0.6 was reached. The flask was cooled on ice for 10 min, and the pellet was collected by centrifugation at 2500g at 4°C for 10 min. The cells were gently resuspended in >100 ml of ice-cold transformation buffer and harvested again as above. The pellet was

resuspended in 20 ml of ice-cold transformation buffer, and 7% DMSO was added slowly with gentle shaking. After additional 10 min incubation on ice, the bacterial suspension was aliquoted into 0.5 ml Eppendorf tubes (110 μ l each). The aliquots were immediately shock-frozen in a bath of liquid nitrogen and stored at -80°C . To test transformation efficiency (with 10 pg DNA), a non-transformation aliquot as negative control and a commercial competent cell (like “OneShots” from *Invitrogen*) as positive control were tested.

2.2.1.4 DNA transfection

At the time of transfection, the cells were 70-90% confluent in the proper growth medium. The DNA transfection progress is described in Table 2.14:

Table 2.14: Transfection conditions

Cell lines	Reagents	Transfection solution per well in a 6-well plate	Transfection protocol
HEK-293 (Attached; Human Epithelial)	FuGENE-HD	~ 2 μ g DNA + 4 μ l FuGENE-HD in 100 μ l Opti-MEM [®] I reduced serum medium	Incubate the transfection solution at room temperature for 15 min; vortex briefly and add to the well containing cells.
MDCK (Attached; Dog Epithelial)	Lipofectamine [™] 2000	Solution A: 4 μ g DNA + 50 μ l Opti-MEM [®] I reduced serum medium; Solution B: 10 μ l lipofectamine [™] 2000 + 50 μ l Opti-MEM [®] I reduced serum medium	Incubate solution A and B at room temperature for 5 min, and mix the solutions gently; incubate the complex at room temperature for another 20 min, then add the complex to the well containing cells.

2.2.1.5 Rapid amplification of cDNA ends (RACE)

RACE is a PCR-based cloning technique particularly applied to obtain full length cDNA ends and to identify unknown terminal sequences. RACE amplifies the transcripts of interest through reverse transcription and anchored PCR using gene-specific primers (GSP) and adapter primers that anneal with defined internal sites of exon and target unknown sequences at either the 5' or 3' end of the mRNA, respectively. In this thesis, GeneRacer[™] kit (*Invitrogen*) 5'-RACE was used to clone cDNA variants of mTRPM3.

Treatment of 5' end of $Poly(A)^+$ mRNA for 5'-RACE To dephosphorylate non-mRNA or truncated mRNA, 1 μ g of mouse kidney $Poly(A)^+$ mRNA (Section: 2.2.2.2) was

treated with 1 μ l of calf intestinal phosphatase (CIP, 10 U/ μ l) in a 10 μ l reaction in DEPC H₂O containing 1 μ l of CIP buffer and 1 μ l of RNaseOut™ (40 U/ μ l). After 1 hr incubation at 50°C, the dephosphorylated mRNA and the intact full length mRNA were extracted with phenol:chloroform and precipitated with 100% ethanol (Section: 2.18). To ligate with the GeneRacer™ RNA Oligo (5'-CGACUGGAGCACGAGGACACUGACAUGGACUGAAGGAGUAGAA), the 5' phosphate of the full-length mRNA was exposed through treating the precipitated mRNA (7 μ l) with 1 μ l of tobacco acid pyrophosphatase (TAP, 0.5 U/ μ l) in a 10 μ l decapping reaction containing 1 μ l of 10 \times TAP buffer and 1 μ l of RNaseOut™ (40 U/ μ l). The mixture was incubated at 37°C for 1 hr, and the decapped full-length mRNA was phenol:chloroform extracted and ethanol precipitated.

First strand cDNA synthesis The first strand cDNA was synthesized by SuperScript™ III reverse transcriptase (Invitrogen). The mixture containing 10 μ l of ligated RNA, 0.5 μ l of GeneRacer™ 5' primer, 0.5 μ l of GSP primer 1 (Table: 2.10), 1 μ l of dNTP and 1 μ l of ddH₂O was incubated at 65°C for 5 min and then chilled on ice for 1 min. After adding 4 μ l of 5x first strand buffer, 1 μ l of 0.1 M DTT, 1 μ l of RNaseOut™ (40 U/ μ l) and 1 μ l of SuperScript™ III reverse transcriptase (200 U/ μ l), the reaction mix was incubated at 50°C for 60 min and at 55°C for 5 min. The reaction was deactivated at 70°C for 15 min, and the reaction mix chilled on ice followed by incubation with 1 μ l of RNase H (2 U) at 37°C for 30 min.

Table 2.15: PCR components for first and nested reaction

First reaction	Nested reaction	Amount
DNA (first strand cDNA)	DNA (from first reaction, 1:50 dilution)	1 μ l
10x reaction buffer	10 \times reaction buffer	2.5 μ l
dNTP (10 mM)	dNTP (10 mM)	1.25 μ l
10 μ M GSP primer 1 (or GSP primer 2)	10 μ M GSP primer 2 (or GSP primer 3)	1 μ l
GeneRacer™ 5' primer	GeneRacer™ 5' nested primer	1 μ l
Expand long template polymerase	Expand long template polymerase	0.5 μ l
ddH ₂ O	ddH ₂ O	Add to 25 μ l

Amplification of 5' end of mTRPM3 cDNA The 5' cDNA end of mTRPM3 was amplified by touchdown PCR and nested PCR using GeneRacer™ 5' primer /nested primer and GSP primers 1/2/3 (Table: 2.10) derived from the core mRNA sequence of mTRPM3

(GenBank™ accession number: NM_001035240). The amplified PCR product was cloned into the pCR®4-TOPO® vector for sequence analysis.

Table 2.16: PCR conditions for first and nested reaction

Steps	First reaction			Nested reaction		
	Temp.	Time	Note	Temp.	Time	Note
1	94°C	2 min		94°C	2 min	
2	94°C	1 min		94°C	1 min	
3	65°C	1 min		60°C	1 min	
4	68°C	1 min/kb	Go to 2, 10 cycles	68°C	1 min/kb	Go to 2, 10 cycles
5	94°C	1 min		94°C	1 min	
6	65°C	1 min		60°C	1 min	
7	68°C	1 min/kb	Go to 5, 30 cycles, dt(s):10 sec	68°C	1 min/kb	Go to 5, 20 cycles, dt(s):10 sec
8	68°C	10 min		68°C	10 min	
9	4°C	hold		4°C	hold	

2.2.1.6 Site-directed mutagenesis

Point mutations, frameshift mutations, deletion/insertion of amino acid(s) were performed by using QuikChange® XL Site-Directed Mutagenesis Kit. Once the specific primers were synthesized, 1 µl of template DNA (10 ng) was amplified by 0.3 µl of *Pfu Turbo* polymerase (2.5 U/µl) in a final volume of 12.5 µl reaction solution containing 1.25 µl of 10× reaction buffer, 0.5 µl of each primer (0.5 mM), 0.25 µl of dNTP (10 mM), 0.75 µl of QuikSolution and 8.25 µl of ddH₂O. The thermal cycling parameters were described in Table 2.17. Finally, the amplification product was thoroughly mixed with 1 µl of *Dpn* I restriction enzyme (10 U/µl) which digests the *dam*-methylated parental template DNA. After incubation at 37°C for 1–2 hr, the reaction complex was transformed into the chemocompetent DH5α cells as described in Section 2.2.1.3.

2.2.1.7 TOPO®-cloning

TOPO® cloning was performed using a linearized pcDNA3.1/V5-His-TOPO® vector (Invitrogen) which is engineered with 3' thymidine (T) overhangs and covalently bound to Topoisomerase I. Before the TOPO® cloning, the blunt-ended PCR fragments (10 µl) which were amplified by some proofreading polymerases like *pfu* polymerase were first incubated with 0.5 µl of dNTP and 0.5 µl of *Taq* polymerase (72°C, 30 min) in order to add

a 3'-single-stranded poly(A)-tail. The sticky-ended PCR fragments (2 μ l) were directly ligated with 0.5 μ l of pcDNA3.1/V5-His-TOPO[®] vector combined with 0.5 μ l of salt solution. After incubation for 15 min at room temperature, the TOPO cloning products were transformed into the chemocompetent DH5 α cells, and the correct orientation of the PCR fragments was analyzed using the endonuclease restriction method.

Table 2.17: Thermal cycling parameters for site-directed mutagenesis

Steps	Temp.	Time	Note
1	95°C	1 min	
2	95°C	50 sec	
3	58°C	50 sec	
4	68°C	1 min/kb amplified DNA	Go to 2, 18 cycles
5	68°C	7 min	
6	4°C	hold	

2.2.2 RNA analysis and preparation

RNA handling was carried out under RNase-free conditions. Sterile disposable plasticware was used throughout the laboratory procedures. Non-disposable plasticware and glassware were thoroughly rinsed with 0.1 M NaOH for 1 hr followed by DEPC-treated ddH₂O (0.1%, v/v). Lab bench and electrophoresis tanks were cleaned with 10% SDS to maintain an RNase-free environment. The buffers and solutions for RNA analysis were prepared according to Sambrook *et.al* [2000] [184] and Ausubel *et.al* [2001] [10].

2.2.2.1 Isolation of total RNA from eukaryotic cells and tissues

The total RNA isolation from eukaryotic cells grown in monolayer and from animal tissue samples are indicated in Table 2.18.

2.2.2.2 Selection of *Poly(A)*⁺ RNA from total RNA

The *Poly(A)*⁺ RNA which is enriched for mRNA was purified from total RNA by using *Oligotex Direct mRNA Mini Kit* (Qiagen). The *Poly(A)*⁺ RNA was bound to 'Oligotex' resin through the *Poly(A)*⁺ tails which were exposed by denaturing the total RNA. The remainder of total RNA was washed away and the *Poly(A)*⁺ RNA was eluted with warm salt-free elution buffer.

Table 2.18: Total RNA isolation from HEK293 cells and mouse tissues

Procedures	Materials	
	HEK293 cells	Mouse tissues
Tissue lysis	Wash cells once with ice-cold PBS (2 ml per 100 mm dish). Lyse cells in TRIzol [®] reagent (1 ml per 100 mm dish). Transfer the cell lysates into a fresh 1.5 ml Eppendorf tube.	Place the isolated tissues directly into liquid nitrogen. Pulverize the frozen tissues (~ 1 g) with a pestle in a mortar containing liquid nitrogen. Transfer the powder to a 15 ml Falcon tube containing 10 ml of TRIzol [®] reagent.
Homogenization	Homogenize the samples with a polytron homogenizer for 15-30 seconds.	
RNA extraction	Incubate the samples at room temperature for 5 min. Add 0.1 ml of 2 M sodium acetate (pH 4.0), 1 ml of equilibrated phenol, and 0.2 ml of chloroform-isoamyl alcohol per ml of TRIzol [®] reagent used. Vortex the mixture vigorously for 15 sec and incubate it for an additional 15 min. Centrifuge the mixture at 13,000 rpm for 30 min at 4°C and then transfer the upper aqueous phase to a fresh Eppendorf-tube.	
RNA precipitation	Add 0.5 ml of isopropanol to the RNA extract, mix it well, and incubate it at -80°C for 1 hr. Centrifuge the solution at 13,000 rpm at 4°C, wash the pellet with 75% ethanol. Air-dry the RNA pellet at room temperature (10–15 min). Dissolve the pellet with 100 µl of DEPC-treated ddH ₂ O and store the RNA solution at -80°C .	

2.2.2.3 Electrophoresis of RNA with agarose–formaldehyde gels

Under denaturing conditions, RNA is fully denatured and can be separated according to its size (\log_{10} of molecular weight). RNA gel loading mix was incubated at 65°C for 15 min prior to being loaded onto an agarose–formaldehyde gel. RNA samples and RNA marker were co-electrophoresed at 4 V/cm for 1–2 hr until the bromophenol blue dye reached approximately 3/4 the gel length. To calculate the sizes of RNA samples after Northern-Hybridization (Section: 2.2.2.6), the gel slice containing the RNA marker was cut out and visualized by ethidium bromide staining (0.5 µg/ml in 0.1 M ammonium acetate, 45 min). The RNA samples were transferred from the gel onto a nitrocellulose membrane as described in Section 2.2.2.4.

2.2.2.4 Northern blotting

Following electrophoresis, the denatured gel containing RNA of interest was successively soaked briefly in DEPC–treated water, in 0.05 N NaOH for 20 min, briefly in DEPC–treated water, and in 20× SSC for 45 min. The capillary blotting apparatus for Northern analysis was assembled according to Sambrook *et al.* (2000). After RNA transfer (6–18 hr), the nitrocellulose membrane was removed to a tray containing 6× SSC for 5 min incubation

with slight shaking. The membrane was air-dried on a paper towel for at least 30 min. The dried membrane was placed between two pieces of Whatman paper and baked at 80°C for 2 hr in a vacuum oven. The efficiency of RNA transfer was analyzed by staining the gel with ethidium bromide (0.5 µg/ml in 0.1 M ammonium acetate) for 45 min and visualized by UV illumination.

2.2.2.5 Random-primed radioactive DNA labeling

Template DNA preparation for radioactive labeling 5 µg of plasmid was digested by restriction enzymes (*BcuI*, *MluI*, *XbaII*, *XmaII*) which only cut the recipient vector (pcDNA3.1) so that the insert fragment (mTRPM3) could be separated from the recipient vector by agarose gel electrophoresis and then purified with a *gel extraction kit*. Subsequently, the purified TRPM3 insert was digested by *BauI*, *BglIII*, *PstI* restriction enzymes so that the template DNA was between 400–800 bp in size. While 5 µl of the digested DNA fragments were loaded into agarose gel to check the quality of the restriction process, the rest was directly radiolabeled for Northern hybridization (Section: 2.2.2.5).

DNA labeling by random oligonucleotide extension DNA template (mTRPM3) was labeled with [α -³²P]-dCTP by using the *HexaLabel™ DNA Labeling Kit* according to the manufacturer's instruction. The complementary radiolabeled DNA sequences were synthesized by Klenow fragment in the presence of random hexanucleotide primers and radiolabeled dNTP. Briefly, 10 ng of DNA template, 10 µl of 5× *reaction buffer* and ddH₂O were added to a final volume of 40 µl in a microcentrifuge tube. To denature the DNA template, the mixture was boiled for 10 min and then cooled quickly on ice. In the same tube 3 µl of *Mix C*, 5 µl of [α -³²P]-dCTP (50 µCi) and 1 µl of *Klenow Fragment* (exo⁻, 5 U) were added. The tube was shaken briefly and centrifuged for 3–5 sec followed by 30 min incubation at 37°C. After adding 4 µl of dNTP, the sample was incubated at 37°C for a further 5 min. The reaction was stopped by adding 1 µl of EDTA (0.5 M, pH 8.0).

Purification of radioactively labelled DNA Prior to Northern hybridization (Section: 2.2.2.6), the unincorporated dNTPs were removed by *Bio-Spin® columns* following the manufacturer's instruction. 250 µl of the reaction mixture was obtained after the purification.

Determination of the degree of radioactive labeling 2 μ l of the purified reaction mixture was spotted onto two pieces of Whatman paper and air-dried. One piece of Whatman paper was then successively washed three times for 5 min in 100 ml of sodium phosphate (0.5 M, pH 6.8), once in ddH₂O for 1 min and once in 70% ethanol for 2 min, then air-dried. The incorporated radioactivity (washed Whatman paper) and the total radioactivity (unwashed Whatman paper) were measured with a liquid scintillation counter (Beckmann). The specific activity of the radiolabeled probe was calculated to be 2.4×10^9 cpm/ μ g based on the following formula (simplified):

$$\frac{\text{incorporated radioactivity (cpm)} \times \text{total reaction volume}}{\text{input DNA (ng)} \times 0.001 (\mu\text{g/ng})} = \text{specific activity (cpm}/\mu\text{g)} \quad (2.1)$$

2.2.2.6 Northern hybridization

The nitrocellulose membrane was incubated at 68°C for 2 hr in a hybridization tube containing 20 ml of prehybridization solution. Radiolabeled DNA template (mTRPM3) was boiled for 5 min and chilled quickly on ice. The denatured radiolabeled probe was directly added to the prehybridization solution and hybridized with RNA transferred to the membrane overnight (12–16 hr) at 42°C. After hybridization, the membrane was removed from the hybridization tube and rinsed with $2 \times$ SSC for 30 min at room temperature. Subsequently, the membrane was washed with three prewarmed wash buffers (55°C) in succession: $2 \times$ SSC, $0.5 \times$ SSC with 0.1% SDS, and $0.1 \times$ SSC with 0.1% SDS. Each washing step was carried out for 20 min with gentle shaking. The membrane was air-dried and then exposed to X-ray film (BioMax MS) at -80°C with an intensifying screen (Biomax TranScreen LE) for 3–4 weeks. After exposure, the film was developed in the dark-room until the cassette came to room temperature thus avoiding black dots or stripes on the autoradiogram resulting from static discharge.

2.2.3 Protein biochemical analysis

The buffers and solutions for protein analysis such as SDS-PAGE and Western blot were prepared according to Sambrook *et.al* [2000] [184] and Ausubel *et.al* [2001] [10].

2.2.3.1 Membrane protein extraction from mouse tissues

Tissues (eyes) isolated from TRPM3^{-/-} and TRPM3^{+/+} mice were washed in ice-cold PBS and frozen in liquid nitrogen. The tissues were ground in a mortar. The powdered tissues were transferred into 10 ml of lysis buffer (5 mM Tris-HCl (pH 7.4), 2 mM EDTA and protease inhibitor cocktail (1 tablet)) and homogenized by using a polytron 5 times (20 sec bursts/20 sec cooling/200–300 Watt). After centrifugation for 15 min at 500g at 4°C, the supernatant of the samples was kept and the pellet was homogenized again with an additional 1 ml of lysis buffer (5× 20 sec bursts/20 sec cooling/200–300 Watt). The samples were centrifuged again for 15 min at 500g at 4°C. Both supernatants were pooled and centrifuged at 45.000g at 4°C for 15 min. The pellets were washed twice with lysis buffer, and resuspended in resuspension buffer (75 mM Tris-HCl (pH 7.4), 12.5 mM MgCl₂ and 5 mM EDTA). The samples were stored at -80°C or directly used for western blot analysis.

2.2.3.2 SDS-PAGE

SDS-polyacrylamide gel electrophoresis (SDS-PAGE) was used to separate proteins according to their molecular weights. After assembling the electrophoresis apparatus and casting polyacrylamide gels, the proteins to be analyzed were mixed with 1× Laemmli buffer and subsequently boiled for 5 min. The mixture was directly placed on ice and then centrifuged briefly. 20 µl of the denatured proteins and 5 µl protein-ladder were loaded into the wells formed in the polyacrylamide gel submerged in 1× SDS-running buffer. A constant current of 10–15 mA per gel was applied for 2–4 hr causing the negatively-charged proteins to migrate towards the positive electrode. Finally, proteins were visualized by either Western blot, Coomassie blue or silver staining.

2.2.3.3 Western blot

Following SDS-PAGE, the polyacrylamide gel containing the separated proteins was carefully removed from the electrophoresis apparatus with a gel knife. The gel/blot sandwich was assembled in a *MiniVE System Blot Module* following the manufacturer's instruction. The separated proteins were transferred onto a nitrocellulose membrane (0.45 µm pore size) by electroelution performed with a constant current of 30mA in 1× SDS transfer buffer

supplemented with 20% methanol overnight. After transfer, the membrane was gently separated from the polyacrylamide gel and immediately washed with $1\times$ TBST for 5 min in a Petri dish. To prevent nonspecific binding of antibodies, the membrane was blocked in blocking buffer (1% BSA in $1\times$ TBST, w/v) for 1 hr and afterwards rinsed with $1\times$ TBST three times for 5 min. To detect proteins, the membrane was incubated with the primary antibody at 4°C for 2 hr. Unbound antibodies were removed by washing three times. The membrane was then incubated for 1 hr with the secondary antibody. Finally, the membrane was washed for 5 min three times with $1\times$ TBST to remove unbound secondary antibody. The proteins were visualized using a chemiluminescence substrate (Pierce) prepared according to manufacturer's instructions. X-ray film was exposed in the dark-room and several different duration of exposure were tried.

2.2.3.4 Co-immunoprecipitation

The following procedure was used for co-immunoprecipitation (Co-IP) using adherent cells. The plasmids containing the DNA sequences of the proteins of interest were co-transfected into the cells in a 6 cm culture dish (Table: 2.14). Following 24–48 hr incubation, the culture dish was placed on ice and the growth medium was removed by aspiration. After washing cells with ice-cold PBS and lysing them with ice-cold lysis buffer (10 ml of RIPA buffer (NaCl (150 mM), Nonidet P-40 (1% (v/v)), SDS (0.1% (v/v)), sodium deoxycholate (0.5% (v/v)) and Tris-HCl (pH 8.0, 50 mM)) and one tablet of protease inhibitor cocktail), the cell suspension was gently transferred into a pre-cooled microfuge tube and centrifuged at $9,000g$ for 15 min at 4°C . The supernatant was carefully transferred into a fresh pre-cooled microfuge tube and centrifuged at $50,000g$ for 2 hr at 4°C . 50 μl of supernatant (lysate) was kept as a control sample at 4°C . 2 μg of the appropriate antibody were added to 400 μl of lysate. The supernatant-antibody mixture was rocked at 4°C overnight. 10 mg of protein A-Sepharose powder was incubated with 50–100 μl of lysis buffer in a microfuge tube and washed for ~ 30 min to allow it to swell. The protein A-Sepharose slurry was centrifuged at 2,000 rpm for 1–2 min and rinsed with 1 ml RIPA buffer three times as above. 10 μl of the protein A-Sepharose beads were added to the reaction mixture. Following 2 hr incubation of the immunoprecipitate-bead mixture at 4°C under rotary agitation, the mixture was centrifuged at 3,000 rpm for 2 min and subsequently washed with 1 ml RIPA buffer three times. The immunoprecipitate-bead pellet and lysate were mixed with $2\times$ Laemmli buffer, then boiled for 5–10 min and cooled on ice. The samples (ca. 25 μl) were directly loaded

onto the SDS–PAGE gradient gel for further analysis.

2.2.3.5 Fluorescence resonance energy transfer (FRET)

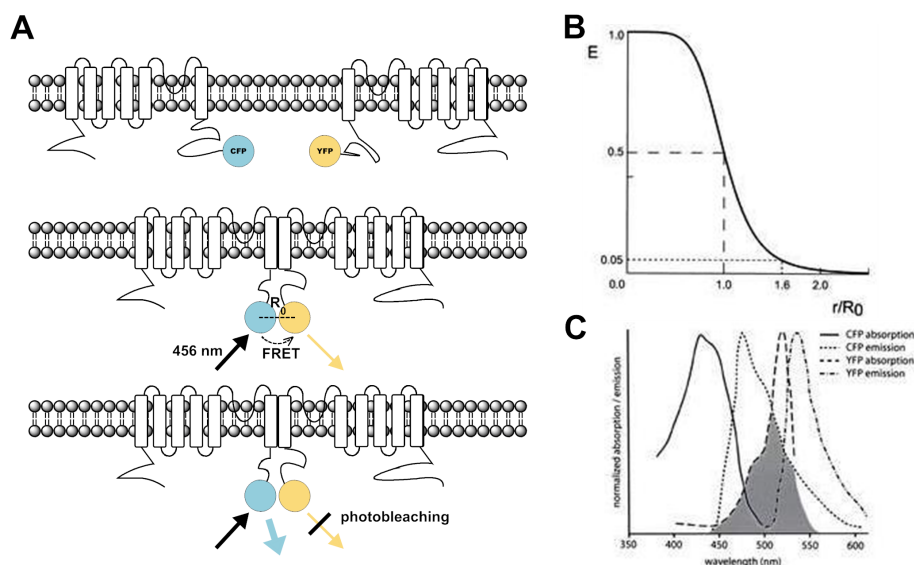


Figure 2.1: General principle of FRET

A: Two membrane proteins tagged with CFP (donor) and YFP (acceptor) were excited at 456 nm wavelength. Due to the spectral overlap between CFP emission and YFP absorption, the FRET occurs when both proteins are extremely adjacent to each other (≤ 100 Å). The FRET efficiency can be measured with acceptor photobleaching method by comparing donor emission intensity before and after bleaching the acceptor. **B:** r/R_0 indicates FRET efficiency (E) to be a function of the actual distance between the fluorophores (r) in units of R_0 . R_0 is the Förster distance at which 50% energy from donor was transferred to acceptor. **C:** The shaded area shows the spectral overlap between CFP emission and YFP absorption. Figure B and C were adapted from *Protein–Protein Interactions: A Molecular Cloning Manual* 2nd Ed., © 2005 by Cold Spring Harbor Laboratory Press.

FRET is widely used to detect protein–protein interactions [40, 96], to image cellular processes [242] and to analyze protein localization [248]. FRET occurs between a donor fluorophore and an acceptor fluorophore. When both are in close proximity (typically ≤ 100 Å) [35, 243] and the spectra of donor emission and acceptor absorption overlap [180, 220], the energy is non–radiatively transferred from the excited donor fluorophore to the acceptor fluorophore. The cyan fluorescent protein (CFP) – yellow fluorescent protein (YFP) pair is a frequently used FRET fluorophore pair in which CFP can be excited at a wavelength 420–460 nm and YFP has a peak excitation wavelength at 514 nm [63]. To measure static FRET,

acceptor photobleaching is an effective method whereby the donor emission is increased after photobleaching of the acceptor through quenching. Under these conditions, the FRET efficiency (E) is proportional to the intensity of increased donor emission:

$$E = 1 - \left(\frac{I_i}{I_a} \right) \quad (2.2)$$

where I_i and I_a represent the donor emission intensity in the presence and absence of FRET, respectively [63].

C-terminally CFP- and YFP-fused TRPM3 cDNAs were transiently co-transfected into HEK-293 cells at a molar ratio of 1:3 (CFP:YFP) [78]. The intensities of several regions of interests (ROIs) were measured and quantified by using the *TILLvisION imaging system* (TILL Photonics). The detailed protocols for fluorescence videoimaging and acceptor photobleaching are available in Amiri *et al.* [6] and Hofmann *et al.* [78]. The FRET efficiency was obtained by linear regression analysis whereby the CFP fluorescence intensities measured at various time points before and after photobleaching were plotted against fractional YFP fluorescence intensities. Data were presented as the means \pm SEM from a minimum of three independent experiments, and Student's *t*-test was used for statistical analysis.

2.2.4 Yeast genetics

The buffers and solutions for all yeast experiments were prepared according to the manual of the *Matchmaker™ GAL4 Two-Hybrid System 3 & Libraries* (Clontech).

2.2.4.1 Yeast two hybrid screening

The yeast two hybrid (Y2H) system is a standard approach to detect protein-protein interactions and protein-DNA interactions [27, 51, 82, 250]. This assay is based on the fact that the eukaryotic transcriptional activator (such as GAL4) consists of two individual domains, the DNA binding domain (DNA-BD) and the transcriptional activation domain (AD) [21, 80]. The DNA-BD recognizes the binding site in the UAS region, and the AD coordinates the transcriptional machinery and enables RNA polymerase II to transcribe a specific reporter gene downstream of the promoter sequence. The protein fused to the DNA-BD (“bait”) and the protein fused to the AD (“prey”) are either co-expressed in yeast cells to determine whether the two proteins interact, or separately expressed in two different haploid yeast strains of opposite mating type for yeast mating [15]. The prey can be either a

single known protein or a library of known or unknown proteins from a particular organism or tissue. After mating or co-transformation, the proteins interact. The interaction between “bait” and “prey” allows AD to come in the proximity of DNA–BD constituting an active transcription activator so that the reporter gene is activated (Figure: 2.2).

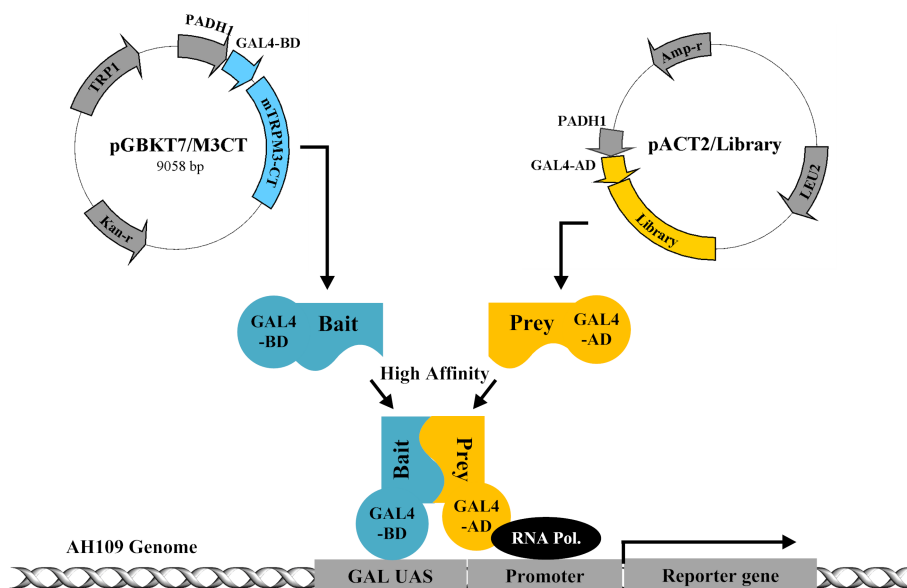


Figure 2.2: Principle of yeast two hybrid library screening

The transcriptional activator GAL4 is divided into two parts: DNA binding domain (DNA–BD) and activation domain (AD). The bait, C–terminus of mM3₁₇₁₉ (M3CT), was fused to GAL–BD in the pGBKT7 vector, while the preys, human kidney cDNA library, were constructed in the pACT2 vector. When a given prey has a high affinity with the bait, AD comes into proximity of DNA–BD constituting an active transcription activator that enables RNA polymerase II to transcribe reporter genes of the yeast strain AH109.

To study the multimerization of mM3₁₇₁₉ and to identify its putative interacting partners, the *Matchmaker*TM GAL4 Two–Hybrid System (Clontech) was used. In response to two–hybrid interactions, yeast strain AH109 stably expresses four reporter genes (*HIS3*, *ADE2*, *MEL1* and *lacZ*) under the control of distinct Gal4–responsive UASs and TATA boxes, whereby the false positives are virtually eliminated. The *HIS3* and *ADE2* reporter genes provide a strong nutritional selection, whereas the *MEL1* and *lacZ* reporter genes which encode α -galactosidase and β -galactosidase, respectively, are used for the X-gal assay.

For the analysis of mM3₁₇₁₉ homomultimerization, the cDNAs of baits and preys were

amplified by using primers specific for the N-terminus of mM3₁₇₁₉ cDNA and C-termini of mM3₁₇₁₉ and mM3₁₃₃₇ cDNAs (Table: 2.10). The amplified PCR products were sub-cloned into both pGBKT7 and pGAD424 vectors. Before the two hybrid assay, control experiments like auto-activation and toxicity test of bait/prey were performed according to the manufacturer's instructions. Transformation of baits/preys cDNA constructs into yeast cells and interaction confirmation of two known proteins using high-, or medium-stringency selection are described in Section 2.2.4.2 and in Figure 2.3, respectively.

For the identification of new proteins that interact with mM3₁₇₁₉, the *Matchmaker*TM *pretransformed cDNA library of human kidney* was used. The key screening procedures are shown in Figure 2.3. The C-terminus of mM3₁₇₁₉ (bait) was cloned into pGBKT7. Before screening the library, the autonomous activation and toxicity of bait were tested, and the library was titered by using the protocols from *Clontech*. The library titer (colony forming units per milliliter (cfu/ml)) was calculated according to following formula:

$$\text{cfu/ml} = \frac{\text{number of colonies on a SD/-Leu plate}}{\text{plating volume (ml)} \times \text{dilution factor}} \quad (2.3)$$

Two-hybrid library screening was performed using the yeast mating method (Section: 2.2.4.1) according to the manufacturer's instructions. The mating efficiency which should be more than 1% was determined as described below:

$$\text{Mating efficiency} = \frac{\text{Viability of diploid}}{\text{Viability of prey library}} = \frac{\text{No. of cfu/ml on a SD/-Leu/-Trp plate}}{\text{No. of cfu/ml on a SD/-Leu plate}} \quad (2.4)$$

200 μ l of mated culture was plated on SD/-Ade/-His/-Leu/-Trp/X- α -Gal (QDO/X- α -Gal) agar plates (150 mm in diameter) and incubated at 37°C for 3–8 days. The plasmids pGBKT7-53 and pGADT7-T encoding DNA-BD/murine p53 fusion protein and AD/SV40 large T antigen fusion protein, respectively, were used as positive controls. Compared to the positive control, blue colonies (≥ 2 mm) were picked and restreaked on QDO/X- α -Gal agar plates (100 mm in diameter) in order to confirm the correct phenotype based on the fact that the initial library co-transformants contain more than one AD/prey plasmid. After 2–4 days of incubation at 37°C, single blue colonies (≥ 2 mm) grown on QDO/X- α -Gal plates were picked for colony PCR which eliminates duplicates containing the same AD/prey and reduces false positives of which the AD/prey plasmid does not exist (Section: 2.2.4.5). The

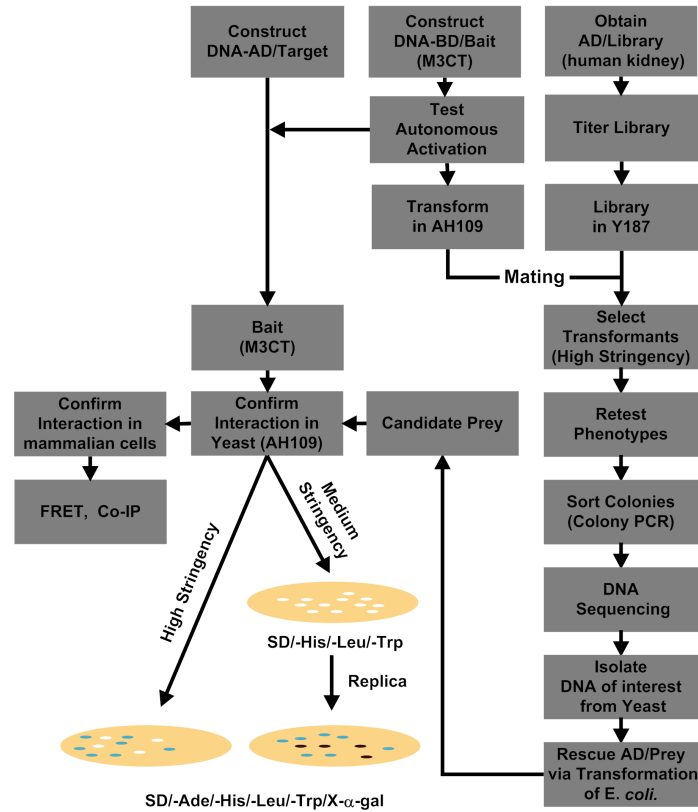


Figure 2.3: Flowchart of yeast two hybrid screen and verification of putative protein interactions in yeast cells

The procedures for yeast two hybrid screening are shown (*gray*). The protein interaction between bait and candidate prey was retested in yeast by co-transformation (*yellow*). Selection with medium stringency was also used for screening interacting proteins because weak and transient protein interaction may be missed by high stringency selection. The positive control (pG-BKT7-53/pGADT7-T) and negative controls (pGBKT7-bait/pGAD424-empty and pGBKT7-empty/pACT2-prey) were always done in the experiments (not shown).

PCR products were separated using agarose gel electrophoresis and isolated by using a gel extraction kit. After DNA sequencing, the AD/prey plasmid of interest was rescued from yeast through two steps: first step, total nucleic acids in yeast (bait plasmid, prey plasmid and yeast genomic DNA) were directly prepared from yeast (Section: 2.2.4.3); second step, the prepared total yeast nucleic acids were transformed into *E.coli* and the AD/prey plasmid of interest was isolated by ampicillin selection followed by standard plasmid preparation procedure.

In some cases, the AD/prey can activate reporter genes in the absence of BD/bait.

To reduce these false positives and verify genuine positive interactions between BD/bait and AD/prey, the isolated AD/prey plasmid candidate was separately co-transformed with BD/bait and BD/empty plasmids into AH109 yeast cells. The co-transformants were either directly plated on a QDO/X- α -Gal agar plate for high stringency selection, or first plated on a SD/-His/-Leu/-Trp/X- α -Gal (TDO/X- α -Gal) agar plate, then replicated on a QDO/X- α -Gal agar plate for medium stringency selection (Figure: 2.3). The high stringency selection reduces the number of false positives, but weak and transient interactions will be missed. Once the genuine positive interactions that require both BD/bait and AD/prey to activate reporter genes were identified, the prey cDNAs of interest were fused with HA- and YFP-tags and subcloned into the mammalian expression vector pcDNA3.1/V5-His for Co-IP and/or FRET assays.

2.2.4.2 Transformation of DNA into competent yeast cells

A single colony (1–3 week-old, 2–3 mm) was picked from a YPDA plate and inoculated in 1 ml of YPDA medium. The cell clumps were dispersed by vortexing and transferred to a flask containing 50 ml of YPDA medium for cultivating overnight at 30°C with shaking. The overnight cell culture ($OD_{600} \geq 1.5$) was centrifuged at 1000g for 5 min to collect the cell pellet. The cell pellet was successively washed with 10 ml of ddH₂O and 5 ml of freshly prepared 1× TE/LiAc solution. The cell pellet was recollected as above. After resuspending the cell pellet in 1 ml of 1× TE/LiAc solution, 100 μ l of the competent cells were mixed with 1 μ g of plasmid DNA, 50 μ g of denatured herring testes DNA (95°C, 20 min) and 500 μ l of freshly prepared PEG/LiAc solution in a clean 1.5 ml Eppendorf tube. The complexes were vigorously vortexed and incubated at 30°C for 30 min with shaking. After the addition of 50 μ l of DMSO, the gently mixed complexes were heat-shocked at 42°C for 15 min. The cells were pelleted at 3000 rpm for 30 sec and resuspended in 100 μ l of 1× TE buffer. 10–30 μ l of cell suspension was plated on the appropriate SD selection plate.

2.2.4.3 Preparation of yeast total DNA using glass beads

15 ml of cell culture in SD selective medium were incubated at 30°C overnight with shaking until an OD_{600} of 1.5 was reached. The cell pellet was collected by centrifugation at 1000g for 5 min and suspended in 1 ml of ddH₂O. The cell suspension was transferred to a fresh Eppendorf tube and spun down again as above. The cell pellet was resuspended in 150 μ l of breaking buffer, and then mixed with 150 μ l of phenol-chloroform-isoamylalcohol and

150 μ l of glass beads. The mixture was vigorously vortexed for 8 \times 30 sec with 30 sec on ice between the pulses, and subsequently centrifuged for 15 min at 13000 rpm at 4°C. DNA precipitation was achieved by adding 1/10 volume of 3 M NaAc (pH 5.2) and 2.5 volume of 100% ethanol. The sample was incubated at -80°C for 30 min followed by centrifugation as above. After rinsing the precipitate with 400 μ l of 75% ethanol, the pellet was air-dried and resuspended in 100 μ l of 1x TE buffer.

2.2.4.4 Yeast protein extraction

Yeast culture preparation Yeast cultures for protein extraction were prepared according to the *Yeast Protocols Handbook* (Clontech). Before storing the cells at -70°C, the cell pellet was washed with ice-cold 20% TCA (see below), recovered by centrifugation at 1000g for 5 min at 4°C, and immediately frozen in liquid nitrogen.

Yeast whole cell protein extraction using the TCA method Trichloroacetic acid (TCA) is used for precipitating proteins because the dissociated chloride ions of TCA compete with water for hydrogen bonds of protein and the dissociated acetate ions strongly change the pH value in solution [202]. For Western blot analysis, the protocol for yeast whole cell protein extraction was adapted from the *Keogh Lab* [97], and all steps were performed at 4°C unless otherwise noted. Briefly, the cell pellet was thawed on ice (10–20 min) and suspended in 250 μ l of ice-cold 20% TCA. The suspension was incubated with 250 μ l of glass beads on ice for 5 min, and then vortexed at maximum speed for 4 \times 1 min with 1 min on ice between. The Eppendorf tube containing the suspension and the glass beads was pierced at the bottom with a 21G needle (B. Braun Melsungen), and immediately placed into another fresh, prechilled Eppendorf tube. The first cell extract was collected by centrifugation at 6000 rpm for 2 min. The glass beads were washed with 300 μ l of ice-cold 5% TCA, and centrifuged as above. The resulting cell extract containing the first spin was mixed with 700 μ l of 5% ice-cold TCA by pipetting, and centrifuged at 14000 rpm for 10 min. The pellet was washed with 750 μ l of 100% ethanol (-20°C), and resuspended in 40 μ l of Tris-HCl (pH 8.0) and 80 μ l of 2 \times SDS-PAGE loading buffer (60 mM Tris-HCl, pH 6.8, 2% SDS, 10% glycerol, 0.2% bromophenol blue, 100 mM DTT). After 5 min of boiling, the insoluble material was removed by centrifugation at 14000 rpm for 5 min at room temperature, and 15 μ l of the supernatant was directly loaded on an SDS-PAGE gel (Section: 2.2.3.2) to further analysis.

2.2.4.5 Yeast colony-PCR

A fresh yeast colony (2–3 mm) was touched with a sterile pipet tip (10 μ l), and directly transferred to a PCR mix containing 1.25 μ l of 10 \times reaction buffer (15 mM Mg²⁺), 0.25 μ l of dNTP (10 mM), 0.5 μ l of forward primer (50 μ M), 0.5 μ l of reverse primer (50 μ M), 0.15 μ l of *Expand High Fidelity Enzyme* and 10 μ l of ddH₂O. The cell clumps were dispersed by gently pipetting up and down. With the help of the primers (5' \rightarrow 3': CTATTCGATGATGAAGATACCCCAACCAACCC, GTGAACTTGCGGGTTTTTCAGTATCTACGAT), the insert was amplified by PCR under the conditions described in Table 2.12 and analyzed using agarose gel electrophoresis.

2.2.4.6 Colony-lift filter assay

The β -galactosidase colony-lift filter assay was used to detect an interaction between two known proteins in the GAL4 two-hybrid system. The assay was carried out according to the *Yeast Protocols Handbook* (Clontech).

2.2.5 Cell culture

2.2.5.1 General cell culture techniques

All cell culture experiments were performed under a laminar flow hood under sterile conditions. Cells were incubated in a humidified 37°C, 5% CO₂ incubator unless otherwise stated. Antibiotics penicillin/streptomycin solution and FCS were added to the media at a final concentration of 100 U/ml, 100 μ g/ml and 10%, respectively. Media, trypsin/EDTA, and PBS were pre-warmed to 37°C before use. The cell freezing, thawing and passaging were carried out according to the manufacture's instruction or Sambrook *et.al* [2000] [184].

2.2.5.2 Primary cell culture: melanocyte isolation from the mouse dermis

Melanocytes were isolated from dorsal skin of 1 day old mice (B6(Cg)-*Tyr*^{c-2J}/J mice). The dissected skin was rinsed immediately with 70% ethanol twice and with PBS twice in quick succession. The skin was individually incubated in 3 ml of 0.25% trypsin in MEM at 4°C overnight. The epidermis was carefully removed and the dermis cut into small pieces and transferred into 3 ml of melanocyte growth medium (MGM) consisting of Ham's F-10 medium

supplemented with 10% fetal bovine serum, 10% newborn calf serum, 0.1 mM isobutylmethylxanthine, 10 µg/ml bovine pituitary extract, 48 nM 12-*O*-tetradecanoylphorbol-13-acetate, 1% Penicillin/Streptomycin/fungizone and 1 mM glutamine. The tissues were incubated in a humidified 37°C, 5% CO₂ incubator. After 2 days, tissue debris was removed by suction and the cells treated with MGM supplemented with 100 µg/ml geneticin (G418 sulphate) until no fibroblasts and keratinocytes persisted. Once pure melanocyte colonies appeared, the medium was changed to the melanocyte maintenance medium (MMM) containing Ham's F-10 medium supplemented with 20% fetal bovine serum, 0.1 mM dibutyryl adenosine cyclic 3',5'-monophosphate, 10 µg/ml bovine pituitary extract, 48 nM 12-*O*-tetradecanoylphorbol-13-acetate, 1% Penicillin/Streptomycin/fungizone and 1 mM glutamine. The isolated melanocytes were cultured using MMM during the experiments.

2.2.5.3 Generation of stable mammalian cell lines using the GeneSwitch™ system

The stable MDCK cell line in which HA-tagged mTRPM3₁₇₁₉ (mM3₁₇₁₉) expression can be induced by mifepristone [234] were established using the GeneSwitch™ System (Invitrogen).

The GeneSwitch™ System consists of a combination of an inducible expression plasmid (pGene/V5-His) and a regulatory plasmid (pSwitch). The pGene/V5-His plasmid carrying a zeocin resistance expresses the gene of interest, whereas the pSwitch plasmid with hygromycin resistance expresses a regulatory fusion protein (/GAL4-DBD/hPR-LBD/p65-AD) under the control of the GAL4 UAS promoter. In the absence of mifepristone, a synthetic 19-norsteroid, the pSwitch regulatory protein is minimally expressed and predominantly localized in the cell nucleus in an inactive form [13]. Upon addition, mifepristone binds to the truncated hPR-LBD (human progesterone receptor ligand binding domain) with high affinity (K_d : $\sim 3 \times 10^{-9}$ M) [223]. Mifepristone binding causes a conformational change in the hPR-LBD so that the expressed pSwitch regulatory protein dimerizes to an active form. This ligand-bound homodimer interacts with GAL4 binding sites in the GAL4 UAS of pGene/V5-His, initiating expression of the gene of interest. Moreover, the expression is further amplified by an auto-regulatory feedback loop whereby the active regulatory protein up-regulates its own gene expression via binding to GAL4 binding sites in the GAL4 UAS of pSwitch plasmid (Figure: 2.4).

The HA-tagged mM3₁₇₁₉ cDNA was subcloned into the pGene/V5-His A expression

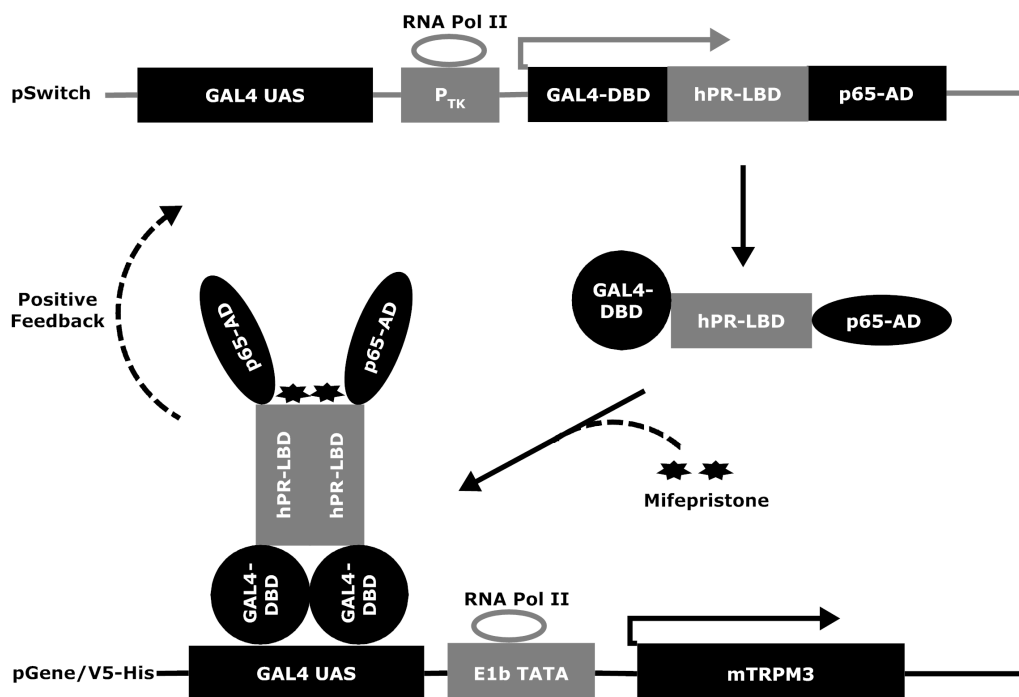


Figure 2.4: Mechanism of the GeneSwitch™ system

In the GeneSwitch™ System, the mifepriston-bound dimerized pSwitch regulatory fusion protein (GAL4-DBD/hPR-LBD/p65-AD) binds to GAL4 site within GAL4 UAS promoter resulting in expression of both the gene of interest and its own gene (positive feedback). Abbreviations: E1b, adenovirus major late E1b gene; TK, thymidine kinase from herpes simplex virus; DBD, DNA binding domain; hPR, human progesterone receptor; LBD, ligand binding domain; p65, human p65 subunit of NF- κ B; AD, activation domain. This figure is modified from “GeneSwitch™ System: A Mifepristone-Regulated Expression System for Mammalian Cells” (Invitrogen).

vector and transfected into the GeneSwitch™-MDCK cell lines engineered with pSwitch regulatory plasmid (Section: 2.14). After 24–48 hrs of transfection, the medium was changed to D-MEM medium supplemented with 50 μ g/ml of hygromycin and 400 μ g/ml of Zeocin™. The medium was exchanged three times a week, and the dual selection was maintained for 2 weeks. Thereafter, the cells were trypsinized and resuspended in a 15 ml falcon tube. One or two serial dilutions were made and the concentration of the cell dilution was determined with a cytometer. A sufficient amount of a 10–15 cells/ml cell dilution was prepared in hygromycin- and Zeocin™-supplemented D-MEM medium. 100 μ l of this cell solution was distributed to each well of a 96-well plate. The cells were grown in the wells for 2 weeks and the selection medium was exchanged 3 times a week. Once monoclonal colonies were visible

(about 1/4 of the well diameter), they were trypsinized and transferred to a 6-well plate filled with selection medium. The selected cell clones were tested for mifepristone-induced mM3₁₇₁₉ expression (1×10^{-8} M) in Western blots (Section: 2.2.3.3) or immunofluorescent labeling (Section: 2.2.6.3) using a polyclonal anti-HA antibody. The GeneSwitchTM-MDCK cells stably expressing HA-tagged mM3₁₇₁₉ (M3^{pGene} cells) were polarized on a semipermeable Polyester Transwell membrane filter (Corning Life Sciences) with 0.4 μ m pore size. The expression of mM3₁₇₁₉ induced by mifepristone was tested by immunofluorescent labeling using a polyclonal anti-HA antibody, and fluorescent images were captured using a confocal microscope (Section: 2.2.6.4).

2.2.6 Methods for histology and immunohistochemistry

2.2.6.1 General histological techniques

General histological techniques such as paraformaldehyde fixation, embedding and sectioning of frozen mouse tissues and embryos were performed according to Ausubel *et.al* [10]. For paraformaldehyde fixation, the dissected tissues and embryos were fixed with freshly prepared 4% paraformaldehyde (PFA) in labeled vials at 4°C. The fixation time varied depending on the age and size of the samples (15 min to 4 hr). For embedding and sectioning, the dissected tissues and embryos were quickly frozen in dry ice, embedded on cryostat chucks and sectioned (10 μ m in thickness) by a cryomicrotome. The frozen sections were collected on microscope slides and stored at -80°C.

2.2.6.2 β -galactosidase (*lacZ*) assay

The β -galactosidase encoded by the *lacZ* gene hydrolyzes β -galactosides into mono-saccharides. The X-gal is a chromogenic substance consisting of a galactoside and an indole ring. In the presence of β -galactosidase, X-gal is cleaved into galactose and 5-bromo-4-chloro-3-hydroxyindole, which is oxidized to an insoluble blue product, 5,5'-dibromo-4,4'-dichloro-indigo (Figure: 2.5). The X-gal staining method has particularly been used to distinguish functional *lacZ* gene in the β -geo cassette. The protocol for the X-gal staining buffer was adapted from the homepage of the *The Wellcome Trust Sanger Institute*. In order to prevent precipitation of X-Gal, staining buffer was pre-warmed to 37°C before adding X-Gal and filtered through a 0.45 micron syringe filter.

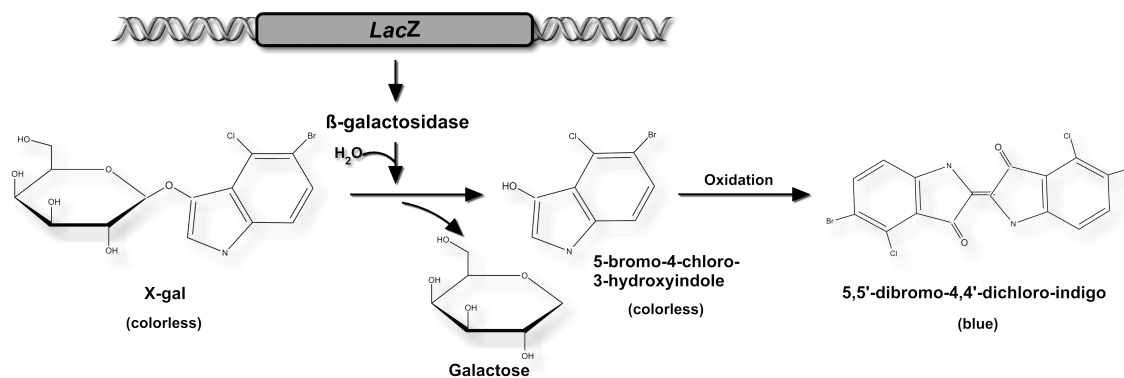


Figure 2.5: Mechanism of the β -galactosidase (*lacZ*) assay

As a substrate of β -galactosidase, colorless X-gal is hydrolyzed to 5-bromo-4-chloro-3-hydroxyindole which is quickly oxidized to an insoluble blue 5,5'-dibromo-4,4'-dichloro-indigo. Adapted and modified from Joung *et al.* [91].

X-gal staining of frozen cryostat sections The frozen cryostat sections were air-dried for 15 min and directly fixed for 15 min in fixation buffer containing 0.2% glutaraldehyde. The fixed sections were washed in wash buffer (3 \times 5 min) and then stained in staining buffer containing X-gal (1 mg/ml). The slides were transferred to a humidified chamber and incubated overnight at 37°C. After rinsing the slides in wash buffer (2 \times 5 min), the sections were counter-stained with 50 ng/ml DAPI in wash buffer for 30 min and mounted with fluorescence mounting medium (DaKo) for visualizing under an Axiovert 200M inverted microscope (Zeiss).

X-gal staining of whole mouse embryos Whole mouse embryos (up to 14 days post coitum (dpc)) were carefully dissected away from their extraembryonic membranes and transferred to a 24-well tissue culture dish filled with PBS solution. The embryos were fixed in fixation buffer for 15–30 min, washed three times for 5–15 min in wash buffer, and incubated in staining buffer at 37°C in the dark until the color was maximally developed. After staining, the embryos were dehydrated successively with 70%, 90%, 95%, and 100% ethanol prepared in xylene, and visualized using a microscope, or cryosectioned for further analysis.

2.2.6.3 Immunofluorescent labeling of adherent cells

The cells to be analyzed were grown to confluence on glass cover slips in 6-well culture dishes. The cells were washed for 5 min in PBS followed by fixation for 10 min in 0.15 M sodium phosphate buffer containing 4% PFA. After the sodium phosphate buffer washes (3×10 min), the cells were permeabilized by incubation with 0.15 mM sodium phosphate buffer supplemented with Triton X-100 (0.1%, v/v) and goat serum (1%, v/v) for 1 hr. Subsequently, the cells were incubated with the primary antibodies (1 µg/ml) for 1 hr, washed three times (10 min/wash) and incubated with the Alexa 488 secondary antibody (1 µg/ml) for 1 hr. The primary and secondary antibodies were prepared in 0.15 mM sodium phosphate buffer containing Triton X-100 (0.1%, v/v) and goat serum (1%, v/v). Finally, the glass cover slips were mounted with mounting medium and inverted on the microscope slides for observation using either an inverted or a confocal microscope.

2.2.6.4 Confocal and fluorescence microscopy

Application of confocal microscopy For confocal microscopy, living cells were visualized with a laser scanning microscope (LSM 510 META, Carl Zeiss) by using a Plan-Apochromat 63×1.4 NA objective. The images of cells expressing HA-, CFP- and YFP-tagged TRPM3 channels were obtained using an argon laser with an excitation wavelength of 488-nm. Emission filters BP 460–500 and LP 505 were used for CFP and YFP, respectively. The pinhole size was adjusted to 0.8 Airy units in order to get the best signal:noise ratio (optical slices ≤ 0.8 µm). To study the localization of the HA-tagged TRPM3 channel in the polarized MDCK cell line, images were collected using the *Z-Sectioning* module. The optimal *Z*-interval depended on the objective used, and the pinhole setting was determined (0.3–0.7 µm) using *Optical Slice Option*.

Application of fluorescence microscopy Images of cryostat sections were captured with an Axiovert 200M inverted microscope (Carl Zeiss). DAPI fluorescence was excited by a mercury-arc lamp at 330–385 nm with a 420 nm emission filter.

2.2.6.5 Antigen design and antibody production

Before the antibodies were raised, specific peptide sequences of mM3₁₇₁₉ were selected by means of analysis algorithms incorporated in the commercial software package DNASTM [165, 166]. The appropriate sequences (M3-7; M3-8) were accepted when they passed the

following selection criteria: 1) the antigenic epitopes of the peptide sequences must be hydrophilic, surface orientated and flexible [219]; 2) the sequences should contain highly hydrophilic and antigenic regions, which were calculated by *Kyte–Doolittle* and *Jameson–Wolf* methods, respectively; 3) the sequences were chosen in the C-terminus of mM3₁₇₁₉, because the C-terminus is more variable than the N-terminus which is homologous in the TRPM channel subfamily; 4) the length of the selected peptide sequences ranged between 10–20 residues. The anti-peptide rabbit antibodies (M3-7 and M3-8) were generated and affinity-purified by *Eurogentec*. The purified antibodies were characterized by immunohistochemical staining as well as by Western blot (Section: 3.3.2.1).

2.2.7 Measurement of the intracellular free Ca²⁺ concentration

2.2.7.1 Fura-2

Fura-2 is a UV-excitable fluorescent calcium indicator. Upon binding of Ca²⁺, the fluorescent excitation maximum of fura-2 shifts from 380 nm (Ca²⁺-free) to 340 nm (Ca²⁺-saturated), while the fluorescent emission maximum remains basically unchanged at 500 nm. Normally, hydrophilic fura-2 is introduced into the cells by means of its lipophilic derivative – fura-2-acetoxymethyl ester (fura-2AM). Once inside the cell, the acetoxymethyl ester group of fura-2-AM is cleaved by esterases releasing fura-2 to bind with Ca²⁺ (Figure: 2.6).

HEK 293 cells transfected with the cDNAs to be analyzed were grown on a glass coverslip in a 35 mm cell culture dish. The cells were washed once with HBS/Ca²⁺ buffer (10 mM HEPES, 1 mM MgCl₂, 140 mM NaCl, 5 mM KCl, 2 mM CaCl₂, 5 mM glucose, 0.1% BSA, pH 7.4) and loaded with fura-2AM (5 μM) prepared in 1 ml of HBS/Ca²⁺ buffer at room temperature in the dark. After 30 min incubation, the cells were rinsed with 1 ml of HBS/Ca²⁺ buffer. The glass coverslip was removed from the culture dish, mounted in a perfusion chamber, and covered with HBS/Ca²⁺ buffer. Ca²⁺ imaging was performed using an Olympus IX70 inverted microscope and controlled by a computer running the *TILLvisION 3.0* software. The cells were alternately excited at wavelengths of 340 nm (Ca²⁺-saturated) and 380 nm (Ca²⁺-free) [60], ROIs (region of interest) and backgrounds were marked at each wavelength. After 60 sec, the agonists at different concentrations were carefully pipetted onto the cells. The experiment was stopped after about 600 sec. The 340/380 nm fluorescence quotient is a measure of the absolute [Ca²⁺]_i regardless of fura-2 loading efficiency, illumination intensity, and optical path length [11]. The background values were subtracted and the [Ca²⁺]_i was calculated using following equation [60, 238]:

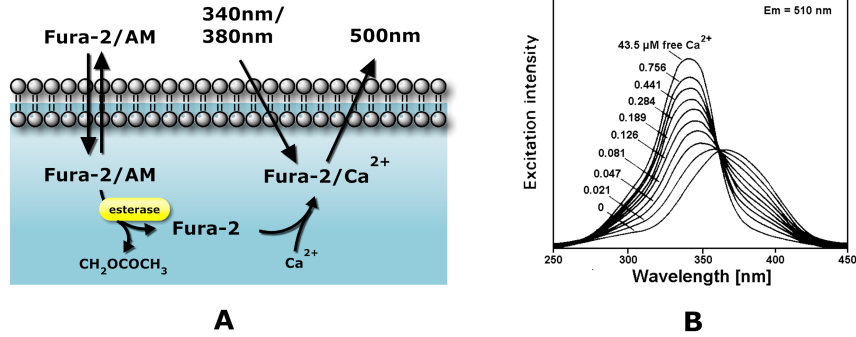


Figure 2.6: Introduction of fura-2 into the cytoplasm and excitation spectrum of fura-2 under different Ca^{2+} -concentrations:

A: Fura-2AM, a lipophilic derivative of fura-2, permeates into the cell and is de-esterified by cellular esterases to fura-2 free acid. The cells loaded with fura-2 are alternatively excited at 340 and 380 nm wavelength, and the fluorescence emission (500 nm) can be quantitatively analyzed for $[\text{Ca}^{2+}]_i$. **B:** The excitation spectrum of fura-2 in the presence of different concentrations of Ca^{2+} . The fluorescence intensities were measured at 510 nm emission wavelength using excitation wavelengths between 250 nm and 450 nm. [After Richard P. I Jaugland, and Karen D. Larison, *Handbook of Fluorescent Probes and Research Chemicals* (5th Edition 1992-1994).]

$$[\text{Ca}^{2+}]_i = K_d \times \frac{R - R_{min}}{R_{max} - R} \times \frac{F380_{min}}{F380_{max}} \quad (2.5)$$

where K_d is the dissociation constant of fura-2 (264 nM at 22°C), R is fura-2 340/380 nm ratio, R_{max} and R_{min} are the 340/380 nm ratios in the presence of a saturating $[\text{Ca}^{2+}]$ or in the absence of Ca^{2+} respectively, $F380_{min}$ is the fluorescence of Ca^{2+} -free fura-2 sample, and $F380_{max}$ is the fluorescence of Ca^{2+} -saturated fura-2 sample.

2.2.7.2 Aequorin

Aequorin, a Ca^{2+} -binding photoprotein, was originally isolated from the jellyfish *A. victoria* [195, 197] and is composed of the apoprotein apoaequorin and the prosthetic group coelenterazine [194]. In the presence of molecular oxygen, aequorin reconstitutes spontaneously from apoaequorin and coelenterazine [196]. Binding of three Ca^{2+} to aequorin triggers an intramolecular oxidation by which coelenterazine is oxidized to coelenteramide [158]. When the excited coelenteramide returns to its ground state, blue light ($\lambda_{max} = 469$ nm) is emitted. Because aequorin and other bioluminescent molecules have a low quantum light yield of a few photons per molecule, the bioluminescent signals are difficult to measure [12]. On

the other hand, photoproteins like aequorin can be easily transfected as a cDNA into cultured cells. The stability of aequorin can be increased by a GFP–aequorin fusion [12, 128]. GFP absorbs the blue light emitted from aequorin and gives off green fluorescence with a maximum wavelength of 509 nm (Figure: 2.7). Ward and Cormier studied photoproteins in *Renilla* and concluded that such radiationless energy transfer increased the quantum light yield and gain measured in the bioluminescent processes [235, 236]. Baubet and colleagues constructed numerous GFP–apoaequorin fusion proteins with linker sequences of different sizes (5 aa to 55 aa) between GFP and apoaequorin, and found that the Ca^{2+} –triggered bioluminescence and quantum yield of all these fusion proteins were better than aequorin alone. GFP probably stabilizes apoaequorin in the recombinant chimaera, and therefore the light–emitting activity is increased [12]. Based on these mechanisms, aequorin has been extensively used as a Ca^{2+} indicator to measure changes in $[\text{Ca}^{2+}]_i$. Using regular coelenterazine, 0.1–1 μM was the useful sensitivity range [119].

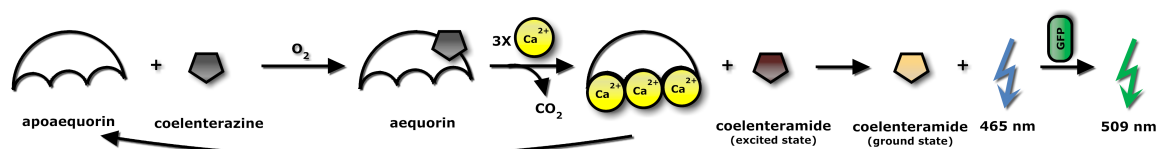


Figure 2.7: Ca^{2+} –induced bioluminescence of aequorin, which is composed of apoaequorin and coelenterazine.

Two microgram of the cDNAs to be analyzed were co-transfected with 0.2 μg of pG5A into HEK 293 cells using FuGENE-HD (Table: 2.14). pG5A is the pEGFP-C1 vector containing a fusion construct of GFP–apoaequorin with 5 added linker sequences [12]. 24 hrs after transfection, the cells were trypsinized and collected by centrifugation at 2000 rpm for 2 min. The cells were washed once with HBS/ Ca^{2+} buffer and then incubated with coelenterazine (5 μM) for 15 min in the dark. After washing twice with HBS/ Ca^{2+} buffer, 50–100 μl of cells were transferred to a luminometer microplate. Aequorin light emission was recorded every second using a *FLUOstar OPTIMA* (BMG LABTECH) when Ca^{2+} (10 mM) and pregnenolone sulfate (50 μM) were applied into extracellular compartments of the cells. Finally, an equal volume of HBS/ Ca^{2+} buffer supplemented with 0.5% Triton X-100 was injected to the sample to quench all aequorin [127]. Because the speed of aequorin consumption is dependent on the Ca^{2+} concentration [208], $[\text{Ca}^{2+}]_i$ can be calculated by a

rate constant (κ) using following equation [24]:

$$\text{pCa}^{2+} = 0.332588 \times (-\log \kappa) + 5.5593 \quad (2.6)$$

$$\kappa = \frac{\text{luminescence at a given point (photon counts/s)}}{\text{total luminescence counts}} \quad (2.7)$$

where pCa^{2+} is the negative decadic logarithm of the $[\text{Ca}^{2+}]$.

2.2.8 *LacZ* transgenic TRPM3 mouse, mouse genotyping and phenotyping

2.2.8.1 *LacZ* transgenic TRPM3 mouse

Due to the support by the National Institutes of Health (NIH), we could purchase TRPM3 mice which are heterozygous for the TRPM3 knockout allele and have 129S5Ev^{Brd} and $\text{B6(Cg)-Tyr}^{c-2J}/\text{J}$ genetic background generated by *Lexicon Pharmaceuticals* using a gene trap approach in 129S5Ev^{Brd} -derived embryonic stem (ES) cells. Compared to gene targeting which targets a specific gene sequence by homologous recombination, the gene trapping randomly inserts a gene cassette into an intron of the targeted gene with gene trap vectors. To generate a TRPM3 mutation, the gene trap vector (pKOS-55) that is composed of a promoterless gene trap cassette (β -geo) flanked by an upstream splice acceptor sequence (SA) and a downstream polyadenylation sequence (PA) (Figure: 2.8) was integrated into the intron between exons 1–2 resulting in incorrect splicing and disruption of the protein expression. Only β -geo and exon(s) upstream of the insertion site are transcribed in the form of a fusion protein. β -geo is a fusion of neomycin phosphotransferase and β -galactosidase genes, the former is used as a neomycin resistance gene and the latter is applied for *in vivo* expression studies such as immunohistochemistry or *lacZ* staining assay (Section: 2.2.6.2).

2.2.8.2 Genotyping of *lacZ* transgenic TRPM3 mice

The mouse genotypes were determined by PCR analysis using genomic DNA isolated from tail tissue. The primer pairs for identifying the wild-type, heterozygous and homozygous TRPM3 mutant mice are shown in the Table 2.10 and Figure 2.8. To confirm the gene trap insertion, a primer in *Neo* (P_{Neo}) was combined with a primer (P6) in the intron upstream of the 5' end of exon 2. A primer in the intron at position 17 (P3) was used in

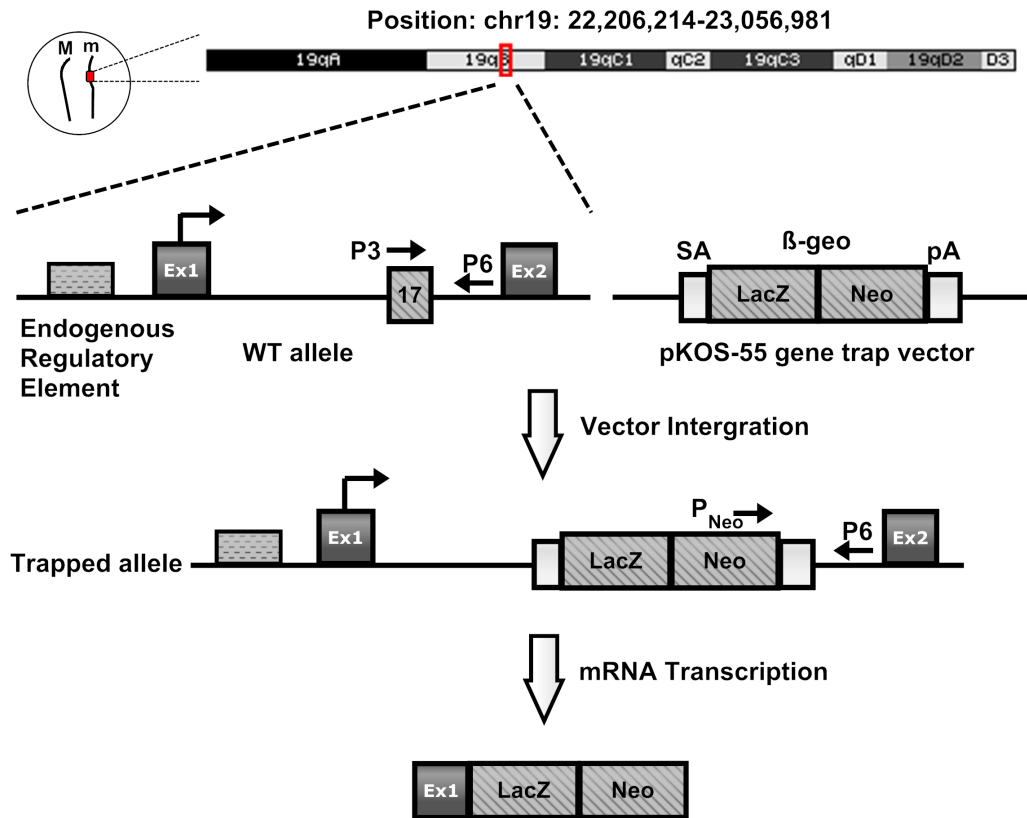


Figure 2.8: Gene trap strategy for generating TRPM3 mutation and primer selection for genotyping

The mTRPM3 gene is located on chromosome 19qB. The pKOS-55 gene trap vector contains a β -geo cassette and is integrated into the intron at position 17 between exon 1 and exon 2 of mTRPM3. Only β -geo and its upstream exon were transcribed in the form of a fusion protein. The *lacZ* gene in the β -geo cassette can be used for immunohistochemical staining. The primer pairs P3/P6 and P_{Neo} /P6 were used for detecting wild-type allele and gene trap insertion, respectively. **Abbreviations:** SA, splice acceptor sequence; PA, polyadenylation sequence.

combination with P6 to detect the wild-type allele. The primers for the selection of the homozygous *Agouti* and *non-albino* (A/A; C/C) mice were chosen based on the sequence of the viral insert resulting in a *non-agouti* allele (GenBank: NC_000068) and *tyrosinase* sequence (GeneBank: NM.011661), respectively (Section: 2.2.8.2).

Genomic DNA isolation from mouse tissues The genomic DNA isolation from mouse tissues, such as mouse tail and ear, was performed by using the protease K method [79]. Under anesthesia, 6–10 mm of mouse tail (from mice of approx. three weeks of age) or

100 mg of mouse tissues were removed and transferred to a 1.5 ml microcentrifuge tube. The sample was mixed with 300 μ l of Tail Buffer (25 mM EDTA, pH 8.0, 75 mM NaCl), 30 μ l of 10% SDS and protease K (1 μ g/ μ l), and incubated at 55°C overnight. Following additional incubation with 1.2 μ l of RNase A (5 mg/mL) at 37°C for 1 hr, proteins and other contaminants were precipitated by adding 100 μ l of saturated sodium chloride. The precipitates were removed by centrifugation (13000 rpm, 30 min), and the DNA recovered by precipitation with 800 μ l of 100% ethanol. The DNA pellet was washed with 75% ethanol, air-dried and resuspended in 100 μ l of ddH₂O.

Mouse genotyping using touchdown PCR The mouse genotype was determined by using touchdown PCR. In 25 μ l of PCR reaction mix, 1 μ l of mouse tail DNA was mixed with 0.5 μ l of dNTP, 4 μ l of 10x buffer ($[Mg^{2+}]_{Fin}$: 1.5 mM), 0.5 μ l of each forward and reverse primers (50 μ M) and 0.2 μ l of polymerase. The touchdown PCR conditions, the primers and the polymerases used for genotyping are listed in Tables 2.10 and 2.19.

Table 2.19: Touchdown PCR conditions for mouse genotyping

Steps	Temp.	Time	Note
1	94°C	2 min	
2	94°C	30 sec	
3	65°C	30 sec	-1°C/cycle
4	72°C	1 min/kb amplified DNA	Go to 2, 10 cycles
5	94°C	30 sec	
6	55°C	30 sec	
7	72°C	1 min/kb amplified DNA	Go to 5, 35 cycles
8	4°C	hold	

2.2.8.3 Phenotypic analysis of TRPM3^{-/-} mice

General observations To detect overt and serious dysfunctions, the TRPM3 wild-type and knock-out mice were routinely observed, especially in the following areas: color of the body hair, thickness of the whiskers, grooming behavior, body size, posture and gait (in the open field).

Visual placing test Mouse vision was tested by using the visual placing test [39, 75, 173]. When the tail of the mouse was held at height of ca. 15 cm above a table surface, its limbs were held close to the body. Then, the mouse was gradually lowered towards the table

surface. The wild-type mouse sees the approaching table surface and extends its forepaws for landing, whereas the blind mouse does not extend its forepaws until its whiskers or nose touch the table.

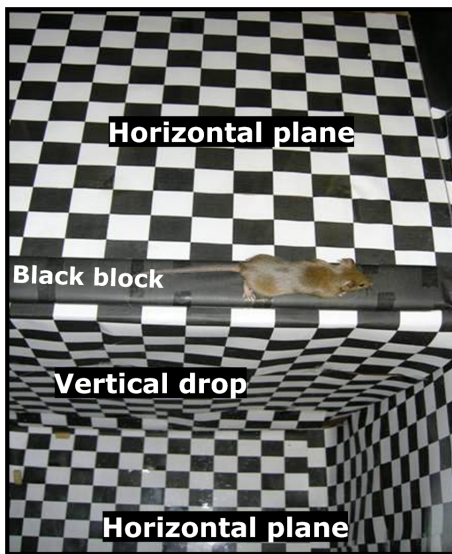


Figure 2.9: Visual cliff apparatus

A sheet of clear Plexiglas was placed across the top horizontal plane extending across the cliff. Each mouse was tested for 10 consecutive trials. The trial was measured as positive when the mouse moved off the center block with all 4 paws placed one side of the block. Between trials, the Plexiglas, box walls and block were cleaned using diluted ethanol on a fresh paper towel. The percentage of the time taken for the mouse to walk over the “safe” side as opposed to over the “unsafe” side was recorded (percent correct (%)).

Visual cliff test The gross visual ability, including visual acuity and depth perception, of TRPM3 wild-type and knock-out mice was studied in a visual cliff test [2, 52, 62]. The procedures were performed according to Crawley *et al.* [39, 71, 101]. Briefly, the mouse to be tested was placed on a black block (38 cm length×3.8 cm width×2 cm height) at the center of an open-top box (70 cm length×40 cm width×65 cm height) (Figure: 2.9). This box is composed of a horizontal plane (“safe” side), a vertical drop (0.5 meter) and a second horizontal plane at a lower level (“unsafe” side). The inside surfaces of the box were covered by a black and white checkerboard pattern of 2 cm squares to accentuate the vertical drop-off. A

3

Results

3.1 Molecular cloning and functional analysis of mTRPM3

In order to assess TRPM3 function, we need a valid TRPM3 cDNA which is expressible in HEK-293 cells and should preferably correspond to the major splice variant in most tissues. Therefore, we cloned new mouse TRPM3 cDNAs and tested their protein expression level in heterologous systems. Subsequently, the functions of splice variants were analyzed by using aequorin- and/or fura-2-based intracellular Ca^{2+} assays.

3.1.1 Molecular cloning of mM3₁₇₁₉ and mM3₁₃₃₇

Because the 3'-end cDNA sequences of TRPM members are identical, the 5'-RACE system was used to generate 5'-end partial mouse TRPM3 (mTRPM3) cDNA clones. 1 μg of mouse kidney *Poly(A)*⁺ mRNA was sequentially pre-treated with dephosphorylation, decapping and GeneRacerTM RNA-Oligo ligation procedures (Section: 2.2.1.5). The 5' cDNA end of mTRPM3 was amplified by PCRs between the RACE anchor primer and the GSP-RT primer directly against the known core sequence of mTRPM3. The resulting products were subcloned and sequenced, and showed a valid transcription start and first coding exon of mTRPM3. Subsequently, we performed a PCR against the whole sequence of mTRPM3 from the starting exon previously found by 5'-RACE to the final exon, covering the whole coding sequence. The 3' reverse primers for mTRPM3 cDNA amplification were used with the known 3' UTR of TRPM3 under the GenBankTM accession numbers AJ544534 [157] and AJ505026 [59]. Both cDNA clones (mM3₁₇₁₉ and mM3₁₃₃₇) were TOPO-cloned into pcDNA3.1 vector for sequencing and further analyses (Section: 2.2.1.7).

and Western blot.

Because no specific mTRPM3 antibodies were available when I began this work (the purchased commercially available antibodies proved to be useless after testing), the cDNA constructions of C-terminally hemagglutinin (HA)- and yellow fluorescent protein (YFP)-tagged mM3₁₇₁₉ and mM3₁₃₃₇ were generated. The stop codons of mM3₁₇₁₉ and mM3₁₃₃₇ cDNAs were replaced by *SalI* restriction sites using PCR. The HA and YFP cDNAs were added to the C-termini of both mM3₁₇₁₉ and mM3₁₃₃₇ cDNAs by means of in-frame fusion. The physiological properties of mM3₁₇₁₉ and mM3₁₃₃₇ such as channel activities and subcellular localization were not influenced by the HA and YFP tags according to the intracellular Ca²⁺ assay with aequorin and immunocytochemical staining, respectively (data not shown).

The protein expression of HA- and YFP-tagged mM3₁₇₁₉ and mM3₁₃₃₇ was confirmed in Western blots by using anti-HA and anti-GFP antibodies (Figure: 3.2 and 3.12). The observed molecular weights (mM3₁₇₁₉: ca. 180 kDa, mM3₁₃₃₇: ca. 140 kDa) match with the data calculated by bioinformatic tools (*e.g.*, *DNAstar*). This result implies that both cDNAs are expressed as proteins in the heterologous system, and no truncated and post-translationally modified forms of both expressed proteins exist under these conditions.

Furthermore, we tested in which subcellular compartments of HEK-293 cells the cDNAs of mM3₁₇₁₉ and mM3₁₃₃₇ were expressed. Using immunocytochemical staining (Alexa-488 was used as a secondary antibody) and confocal microscopy, mM3₁₇₁₉ and mM3₁₃₃₇ were predominantly to be localized in intracellular compartments (Figure: 3.2). Occasionally, the immunofluorescence signals of mM3₁₇₁₉ and mM3₁₃₃₇ were observed at the plasma membrane of HEK-293 cells. In summary, either splice variant of mTRPM3 was expressible in HEK-293 cells, and appears to be able to reach the plasma membrane. However, we wanted to test whether mTRPM3 is expressed at the plasma membrane under more physiological conditions, like in differentiated epithelia.

Protein expression of mM3₁₇₁₉ and mM3₁₃₃₇ in MDCK cells The predominantly intracellular localization of mM3₁₇₁₉ and mM3₁₃₃₇ in HEK-293 cells could either indicate that TRPM3 functions as an intracellular channel, or reflect a channel overexpression artifact. In order to address this question, we studied the protein expression and subcellular localization of both newly cloned mTRPM3 cDNAs in Madin-Darby canine kidney (MDCK) cells. MDCK cells derived from the dog kidney collecting duct are an established cell model for studying epithelial differentiation [25, 64]. When grown on semipermeable filters in

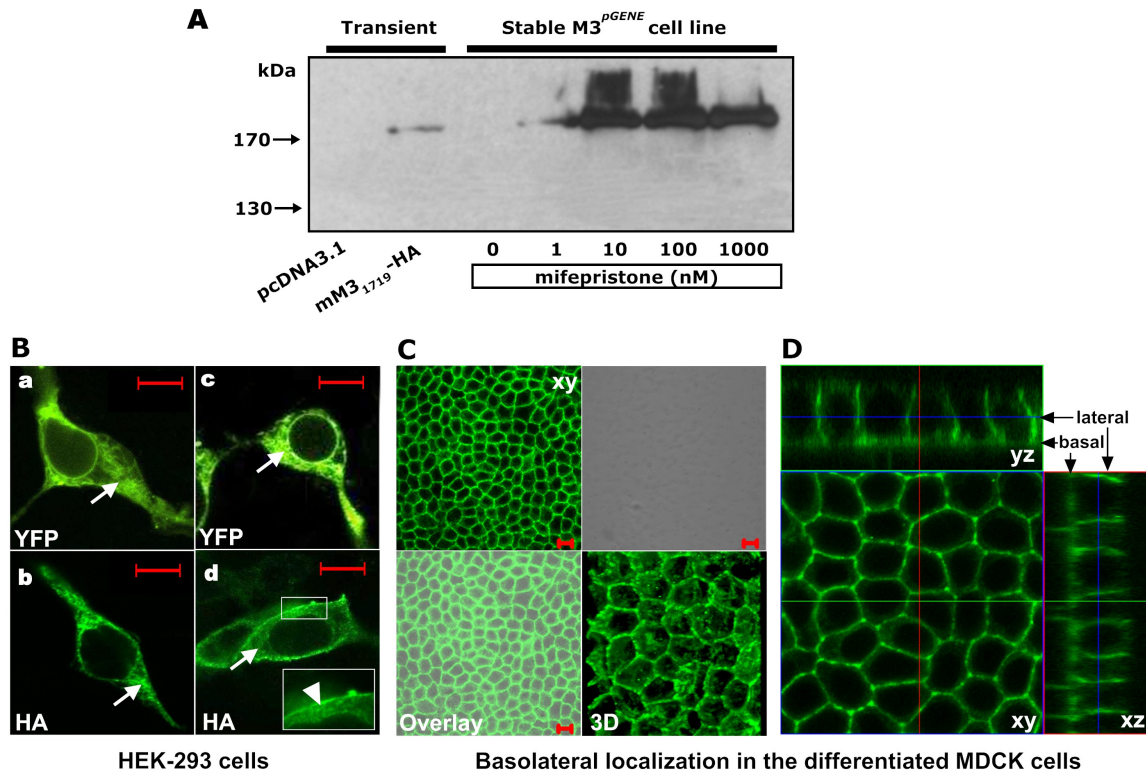


Figure 3.2: Cellular localization of mM3₁₇₁₉ in transiently transfected HEK-293 cells and differentiated MDCK cells

A: Western blot shows the dose-dependent mifepristone-induced mM3₁₇₁₉-HA expression in the M3^{Gene} cells. The immuno-reactive bands with the predicted molecular weight (>170 kDa) were detected by an anti-HA antibody and first observed when the cell lines were treated with the lowest tested mifepristone concentration of 1 nM. Compared with HEK-293 cells transiently transfected with pcDNA3.1 and mM3₁₇₁₉ (1 µg, respectively), the mM3₁₇₁₉-HA expression induced by mifepristone (≥10 nM) showed strong immunoreactive signals. **B:** The localization of HA- and YFP-tagged mM3₁₇₁₉ (a, b) and mM3₁₃₃₇ (c, d) was primarily found in the intracellular compartments of HEK-293 cells (arrows). The expression of TRPM3 was also occasionally found in the plasma membrane region (d, inset, arrowhead). **C:** The MDCK cells stably expressing HA-tagged mM3₁₇₁₉ were grown and polarized on a semi-permeable filter. **C:** Basolateral localization of mM3₁₇₁₉ in the polarized MDCK cells was shown by horizontal (xy plane) and vertical (xz and yz planes) confocal scans (0.7 µm). Cells were immuno-stained with an anti-HA antibody, and observed with a confocal microscope with a detector pinhole diameter of 0.8 Airy units. Each bar represents 10 µm.

cell culture, these cells differentiate to form polarized monolayers and retain most of the properties of *in vivo* epithelia [37, 103].

Because transiently transfected MDCK cells showed a predominantly intracellular localization (data not shown), a stable MDCK cell line inducibly expressing HA-tagged mM3₁₇₁₉ (M3^{pGene} cell line) was generated in order to characterize the steady-state distribution of mM3₁₇₁₉. The HA-tagged mM3₁₇₁₉ cDNA was subcloned into the pGene/V5-His A expression vector and transfected into the GeneSwitchTM-MDCK cell lines engineered with the pSwitch regulatory plasmid. The cells were grown under double-antibiotic selection (hygromycin (50 µg/mL) and ZeocinTM (400 µg/mL)) for ≥2 weeks. Once monoclonal colonies were visible, they were tested for mifepristone-induced mM3₁₇₁₉ expression by Western blots and immunofluorescent labeling (Section: 2.2.5.3). The expression of mM3₁₇₁₉ was induced by mifepristone with the induction concentration adjusted to 10 nM according to the Western blot analysis (Figure:3.2A). It was found that the protein expression of mM3₁₇₁₉-HA in the undifferentiated M3^{pGene} cells remained in the intracellular compartment (data not shown). However, when the M3^{pGene} cells were grown on a Transwell[®] PET membrane for ≥2 weeks, and differentiated to a polarized monolayer, the protein expression of mM3₁₇₁₉-HA was observed at the basolateral side of the differentiated MDCK cells (Figure: 3.2C). These data indicate that mM3₁₇₁₉ is expressible in the MDCK cells and primarily localized at the basolateral plasma membrane of epithelial cells.

3.1.3 Functional analysis of mM3₁₇₁₉

To study Ca²⁺ entry through mM3₁₇₁₉ and mM3₁₃₃₇, we used HEK-293 cells instead of MDCK cells as a cell model, because MDCK differentiation is extensively time consuming and the transient transfection efficiency of HEK-293 cells is much higher. Since a different TRPM3 splice variant with the same pore splicing configuration has been reported to be Ca²⁺-permeable when expressed in a heterologous system [58, 106, 157], calcium indicators aequorin and fura-2 were applied to measure changes in [Ca²⁺]_i upon extracellular application of different chemicals in HEK-293 cells. Compared to patch clamp, these aequorin- and fura-2-based [Ca²⁺]_i measurements provide simple and sensitive analytical approaches to characterize physiological functions of ion channels that are Ca²⁺ permeable at an appreciable rate [163].

3.1.3.1 Quantification of intracellular Ca^{2+} concentration increase in HEK-293 cells expressing mM3₁₇₁₉ and mM3₁₃₃₇

To measure Ca^{2+} entry through mM3₁₇₁₉ and mM3₁₃₃₇, the aequorin-based method was preferred, because 1) aequorin measurement in a cuvette can be safely calibrated; 2) this method has high signal-to-noise ratio; 3) aequorin is nearly insensitive to the buffer conditions such as pH value and changes in $[\text{Mg}^{2+}]$ [22]; 4) single cell measurement is not important under these experimental conditions. The $[\text{Ca}^{2+}]$ in HBS buffer solution was adjusted to 2 mM (data not shown) before the experiments.

It is disputed whether TRPM3 is either a SOC [58, 106], osmolality-regulated [68, 70], or a lipid-activated channel [59]. Firstly, we examined the responses of HEK-293 cells expressing mM3₁₇₁₉ and mM3₁₃₃₇ to an application of thapsigargin (1 μM) which depletes intracellular Ca^{2+} stores by specific inhibition of the endoplasmic reticulum Ca^{2+} -ATPase [211]. However, no responses were observed during the experiments. We also used 200 Osm and D-erythro-sphingosine (20 μM) to respectively test whether mM3₁₇₁₉ and mM3₁₃₃₇ are activated by hypo-osmolality and lipid. Like the result from the thapsigargin experiment, neither of the new mTRPM3 splice variants was activated by 200 Osm and D-erythro-sphingosine (data not shown). It has also been reported that TRPM3 can be activated by pregnenolone sulfate (PS) [231]. Therefore, we applied PS (50 μM) to the cells expressing mM3₁₇₁₉ and mM3₁₃₃₇. Both groups of cells showed a strong $[\text{Ca}^{2+}]_i$ increase. Because TRPM3 is thought to be constitutively active, we increased the Ca^{2+} driving force across the plasma membrane by Ca^{2+} steps (extracellular $[\text{Ca}^{2+}]$ was increased from 2 mM to 12 mM) in order to amplify the constitutive channel activity. The Ca^{2+} influx was highly increased in the cells expressing mM3₁₇₁₉ and mM3₁₃₃₇ compared to the control cells (Figure: 3.3C-E).

The Ca^{2+} steps-induced Ca^{2+} influx through mM3₁₇₁₉ was also observed in the fura-2 measurement. We observed the changes of the 340/380 nm fluorescence ratio in response to Ca^{2+} steps. Whereas no major changes occurred in pcDNA3.1-transfected cells, addition of Ca^{2+} resulted in large increase in $[\text{Ca}^{2+}]_i$ in mM3₁₇₁₉-transfected cells (Figure: 3.3A, B).

Thus, in summary, our findings show that 1) mM3₁₇₁₉ and mM3₁₃₃₇ are not store-operated channels and cannot be activated by hypo-osmolality and D-erythro-sphingosine; 2) mM3₁₇₁₉ and mM3₁₃₃₇ can be activated by extracellular application of PS (50 μM), however, it is still questionable whether PS is a physiological activator of TRPM3 because the physiological concentration of PS is in the nanomolar range; 3) mM3₁₇₁₉ and mM3₁₃₃₇ are constitutively active and functional Ca^{2+} permeable channels. Based on the results

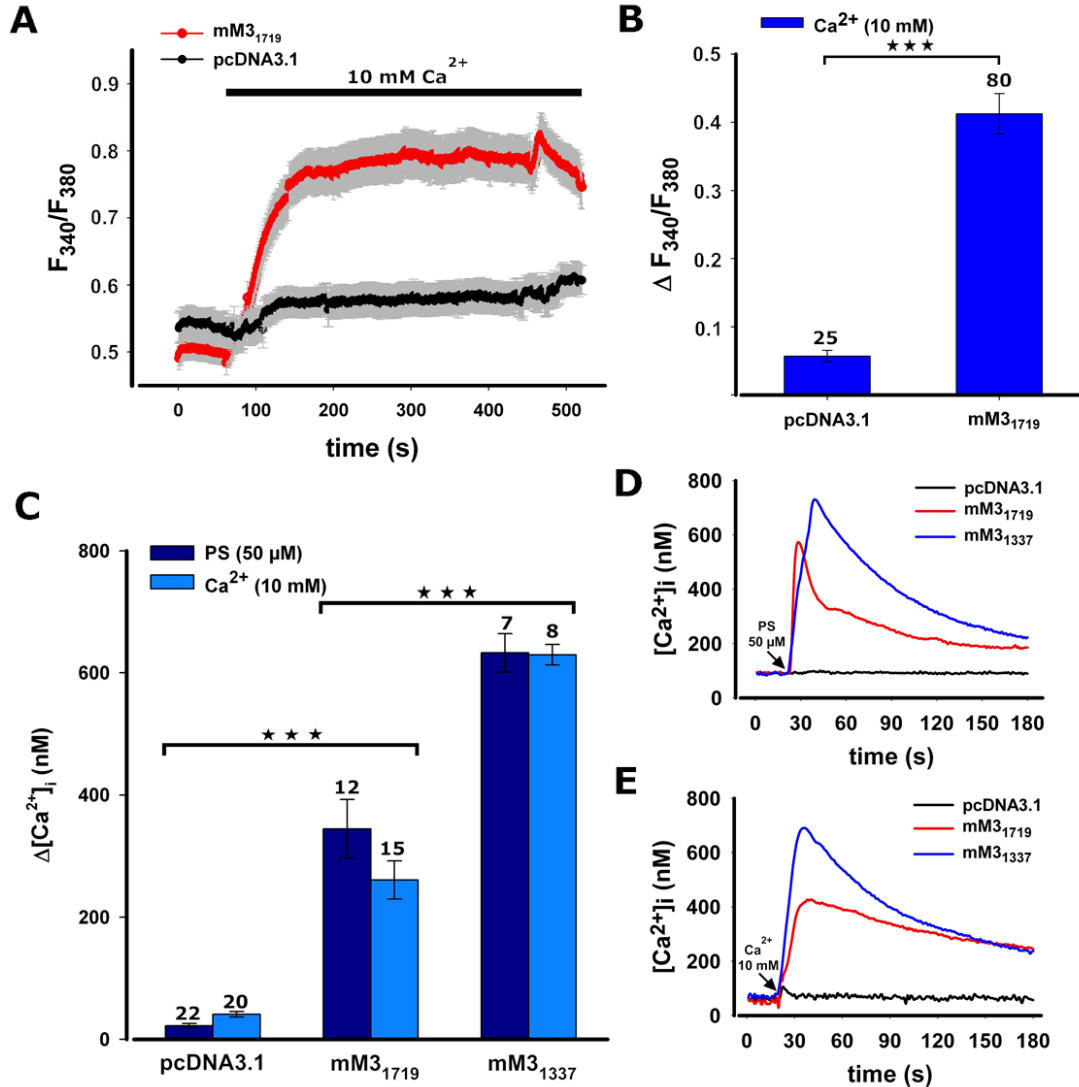


Figure 3.3: Quantification of $[Ca^{2+}]_i$ increases caused by extracellular Ca^{2+} and PS applications in HEK-293 cells expressing mM3₁₇₁₉ and mM3₁₃₃₇

A-B: Ca^{2+} influx through mM3₁₇₁₉ was detected in fura-2-loaded HEK-293 cells expressing mM3₁₇₁₉ in response to changes in $[Ca^{2+}]$ in the buffer solution. Data are mean \pm SEM of $n=5$ independent transfection experiments containing data from a total number of 25 (pcDNA3.1) and 80 cells (mM3₁₇₁₉). **C-E:** Intracellular Ca^{2+} measurement with aequorin showed that cells expressing either mM3₁₇₁₉ or mM3₁₃₃₇ respond to changes in the extracellular Ca^{2+} or PS. Moreover, the induced responses in cells expressing mM3₁₃₃₇ is stronger than that in cells expressing mM3₁₇₁₉. For statistical analysis, unpaired Student's *t*-test ($n=5, 6$) was used to calculate the *P*-value. Numbers above the bars indicate the total number of experiments performed. *** = $P < 0.001$. **Abbreviation:** PS, pregnenolone sulfate.

described above, Ca^{2+} steps and PS application combined with aequorin bioluminescence were used as standard approaches to score modulation of the TRPM3 activity.

3.1.3.2 Effects of divalent cations on Ca^{2+} entry in HEK-293 cells expressing *mM3*₁₇₁₉

The Ca^{2+} permeability of TRPM3 raises the possibilities that TRPM3 might be influenced or inhibited by other divalent cations.

Ni^{2+} was first chosen to investigate cation selectivity for *mM3*₁₇₁₉, because: 1) some TRPM channels such as TRPM6 [230] and TRPM7 [130] have been reported to conduct Ni^{2+} (20 mM and 1 mM $[\text{Ni}^{2+}]$, respectively); 2) Ni^{2+} has been shown to selectively block t-type calcium channels [105] and SOCE pathway [114].

After 18 hr transfection with 2 μg of *mM3*₁₇₁₉ or pcDNA3.1 (as negative control), the transfected HEK-293 cells were prepared in a series of HBS/ Ca^{2+} solutions containing 0 μM , 1 μM , 3 μM , 10 μM , 30 μM , 100 μM , 300 μM , 1 mM, 3 mM, 10 mM and 30 mM NiCl_2 for 10–15 min. Upon the application of PS (50 μM) and Ca^{2+} (10 mM), the changes of $[\text{Ca}^{2+}]_i$ were recorded by an aequorin-based intracellular Ca^{2+} measurement.

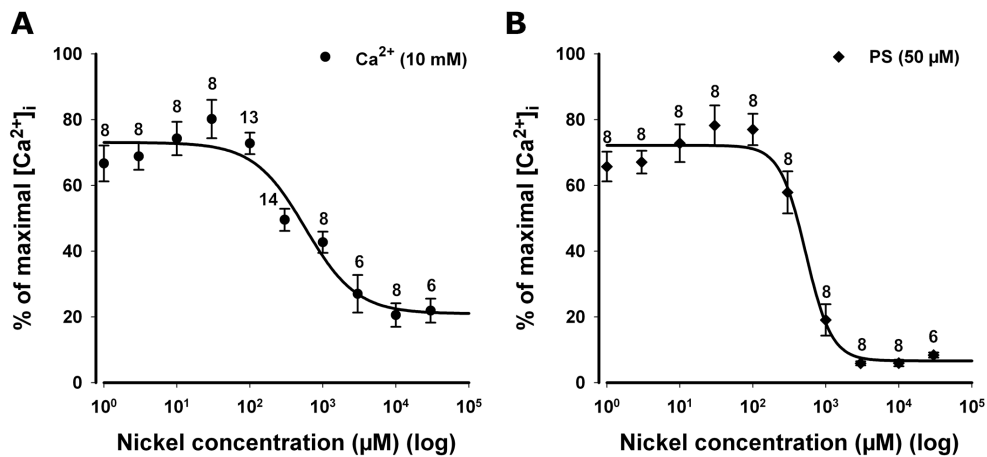


Figure 3.4: Analysis of the effects of extracellular Ni^{2+} on Ca^{2+} entry in *mM3*₁₇₁₉
A-B: Dose response curves were plotted from maximal $[\text{Ca}^{2+}]_i$. Extracellular Ni^{2+} decreased Ca^{2+} - and PS-induced $[\text{Ca}^{2+}]_i$ increase in a concentration-dependent manner, with an IC_{50} of $575 \pm 224.7 \mu\text{M}$ ($P < 0.05$) and $531.1 \pm 88.9 \mu\text{M}$ ($P < 0.001$), respectively. Both IC_{50} values are in a similar range. Data represent the average responses from five independent transfection experiments (Mean \pm SEM, $n=5$). For statistics, unpaired Student's t-test was performed. The total number of experiments was shown as numbers above the bars. **Abbreviation:** PS, pregnenolone sulfate.

Figure 3.4 shows that the channel activities of *mM3₁₇₁₉* were not affected when the extracellular Ni^{2+} concentration was lower than 100 μM . However, the Ca^{2+} influx through *mM3₁₇₁₉* was extensively reduced when the extracellular Ni^{2+} concentration reached 1 mM. Dose–response analysis indicates that Ni^{2+} reduced Ca^{2+} – and PS–induced Ca^{2+} influx through *mM3₁₇₁₉* in a concentration–dependent manner, with an IC_{50} of $575 \pm 224.7 \mu\text{M}$ ($P < 0.05$) and $531.1 \pm 88.9 \mu\text{M}$ ($P < 0.001$), respectively. Both IC_{50} values are in a similar range.

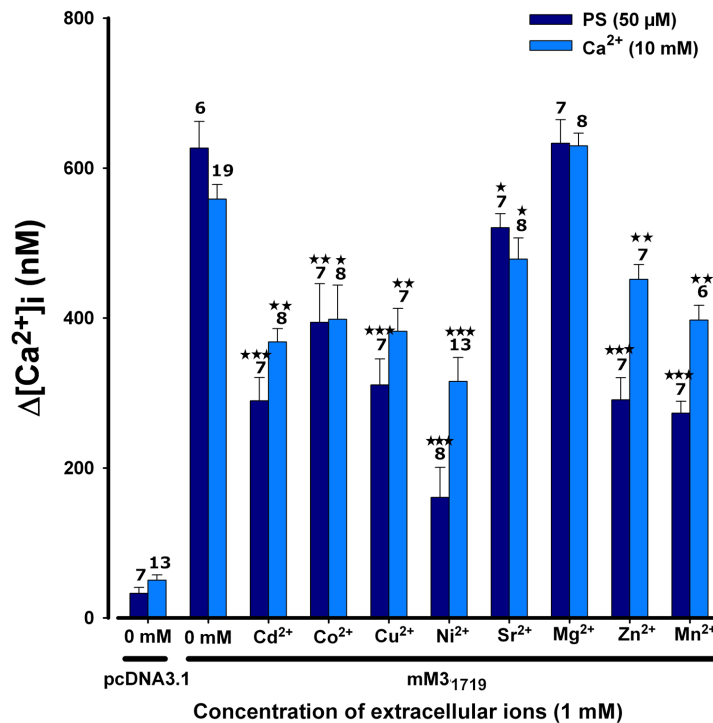


Figure 3.5: Effects of divalent ions on Ca^{2+} entry through *mM3₁₇₁₉*
 Aequorin–based intracellular Ca^{2+} measurement indicated that PS– and Ca^{2+} –induced $[\text{Ca}^{2+}]_i$ increases in the cells expressing *mM3₁₇₁₉* were inhibited by extracellular application of 1 mM Cd^{2+} , Co^{2+} , Cu^{2+} , Ni^{2+} , Sr^{2+} , Zn^{2+} and Mn^{2+} . Mg^{2+} (1 mM) did not have any inhibitory effects on the Ca^{2+} entry through *mM3₁₇₁₉*. Bar graphs represent mean \pm SEM, $n=4$. Numbers above the bars indicate the total number of experiments. $\star = 0.01 < P < 0.05$, $\star\star = 0.001 < P < 0.01$, $\star\star\star = P < 0.001$. **Abbreviation:** PS, pregnenolone sulfate.

To test whether other divalent ions have effects on the Ca^{2+} permeability of *mM3₁₇₁₉*, several trace divalent ions such as cadmium (Cd^{2+}), cobalt (Co^{2+}), copper (Cu^{2+}), strontium (Sr^{2+}), magnesium (Mg^{2+}), zinc (Zn^{2+}) and manganese (Mn^{2+}), were examined. This

is because these trace divalent ions are known to permeate TRPM7 which is phylogenetically related to TRPM3 (Figure: 1.4). These divalent ions might also be meaningful for the TRPM7's function and phenotype [130]. Based on the results from Ni²⁺ experiment above, the cells expressing mM3₁₇₁₉ and pcDNA3.1 were placed in the HBS/Ca²⁺ solution containing such divalent ions (1 mM). Ca²⁺ influxes were induced by PS (50 μM) and Ca²⁺ (10 mM) applications. The [Ca²⁺]_i change was measured with aequorin. The results show that 1 mM of all divalent ions tested with the notable exception of Mg²⁺ reduced Ca²⁺ influx through mM3₁₇₁₉ (Figure: 3.5).

In summary, the experimental data indicate that many divalent cations probably have inhibitory effects on the mM3₁₇₁₉ Ca²⁺ entry at millimolar concentration; and that Mg²⁺, at the physiological concentration, does not inhibit mM3₁₇₁₉ Ca²⁺ entry.

3.2 Identification of functional domains in mM3₁₇₁₉

Based on the studies with TRPM4, TRPM6 and TRPM7, we can predict which residues in the pore might be involved in Ca²⁺ permeation, channel inhibition by other divalent ions, and possibly channel gating. We therefore introduced the analogous mutations into the pore of mM3₁₇₁₉. Additionally, because the N-terminus of TRPM3 is highly conserved among the members of TRPM subfamily (Figure: 1.4), we focused on the C-terminus of mM3₁₇₁₉ to analyze features of its molecular structure and to elucidate its biological roles in the channel properties and functions.

3.2.1 Structure of the pore and C-terminus of mM3₁₇₁₉

3.2.1.1 Site-directed mutagenesis of amino acid residues relevant to Ca²⁺ entry in the mM3₁₇₁₉ pore

Comparisons of the cDNA sequences of the TRPM subfamily establish that the pore region of all such proteins shares some common structures, namely, pore helix and selectivity loop [149, 244] (Figure: 4.1). Here, the effects of the pore region on the biophysical properties of the mM3₁₇₁₉ channel were investigated by using various molecular biological methods (*e.g.*, site-directed mutagenesis) and pharmacological approaches.

Analysis of mutations in *Pro*¹⁰⁶⁰ and *Gly*¹⁰⁶⁶ in the mM3₁₇₁₉ pore region *Pro*¹⁰⁶⁰ in the pore helix and *Gly*¹⁰⁶⁶ in the linker between pore helix and selectivity loop are highly

consistent and conserved in the TRPM subfamily (Figure: 1.5). Studies in other TRPM showed that the mutations of *Pro*¹⁰⁶⁰ and *Gly*¹⁰⁶⁶ in the TRPM6 and TRPM7 channels generate dominant-negative mutants [30, 117, 149]. In mM3₁₇₁₉, *Pro*¹⁰⁶⁰ was mutated to *Arg*¹⁰⁶⁰ (*P1060R* mutation, mM3-RYW mutant) because both amino acids contain 3 carbon atoms in the side-chain group. Arginine (Arg) has a positively charged guanidino group, whereas proline (Pro) has a nonpolar side chain. *Gly*¹⁰⁶⁶ was mutated to *Val*¹⁰⁶⁶ (*G1066V* mutation, mM3-VEV mutant) because valine (Val) is not only an analog of glycine (Gly) but also has less conformational flexibility due to its isopropyl side chain.

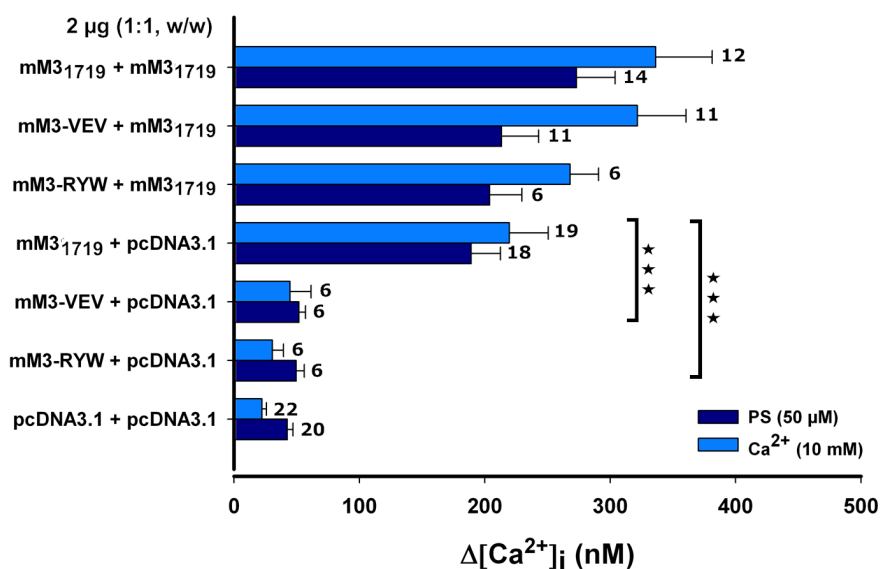


Figure 3.6: Ca²⁺ entry through mM3₁₇₁₉ with *P1060R* and *G1066V* pore mutations

Ca²⁺ entry in mM3₁₇₁₉ with *P1060R* and *G1066V* pore mutations were analyzed by using aequorin-based intracellular Ca²⁺ measurements. HEK-293 cells were co-transfected with different cDNA combinations. The cells expressing mM3-RYW or mM3-VEV did not show Ca²⁺ influx in response to application of extracellular Ca²⁺ (10 mM) and PS (50 µM). Bar graphs represent the average of transfection experiments (n=4); error bars represent ± SEM. Numbers next to the bars indicate the total number of experiments performed. *** = P < 0.001. **Abbreviation:** PS, pregnenolone sulfate.

To test whether *Pro*¹⁰⁶⁰ and *Gly*¹⁰⁶⁶ are essential for the channel activities of mM3₁₇₁₉, and whether mM3-RYW and mM3-VEV are dominant-negative mutants, different cDNA combinations (2 µg) of pcDNA3.1/pcDNA3.1, mM3₁₇₁₉/pcDNA3.1, mM3-RYW/pcDNA3.1, mM3-VEV/pcDNA3.1, mM3₁₇₁₉/mM3-RYW, mM3₁₇₁₉/mM3-VEV, mM3₁₇₁₉/mM3₁₇₁₉,

were co-transfected into HEK-293 cells (cDNA ratio, 1:1). In comparison with the cells expressing mM3₁₇₁₉ wild-type, no Ca²⁺ influx was detected in the cells expressing mM3-RYW or mM3-VEV mutants (Figure: 3.6). This result indicates that the *P1060R* and *G1066V* mutations probably cause loss of Ca²⁺ conduction through the channel. However, the mM3-RYW and mM3-VEV mutants did not show any inhibitory effects on the function of mM3₁₇₁₉ wild-type, because all cells expressing mM3₁₇₁₉/mM3₁₇₁₉, mM3-RYW/mM3₁₇₁₉ and mM3-VEV/mM3₁₇₁₉ exhibited similar responses to the extracellular Ca²⁺ and PS applications. Theoretically, we would have expected a less than 50% response of mM3-RYW/mM3₁₇₁₉ and mM3-VEV/mM3₁₇₁₉ compared to mM3₁₇₁₉/mM3₁₇₁₉ if one of these mutants had a dominant-negative effect. Thus, the mM3-RYW and mM3-VEV mutants are not dominant-negative mutants for mM3₁₇₁₉, although they disrupt mM3₁₇₁₉ function.

Analysis of mutations in Asp¹⁰⁷⁴ in the mM3₁₇₁₉ selectivity loop The Asp¹⁰⁷⁴ amino acid residue is highly conserved and identical in the TRPM subfamily (Figure: 1.5). The neutralization of this Asp amino acid residue in TRPM4 yielded a non-functional channel with a dominant-negative mutation [150]. To analyze its effects on the channel activity and ion selectivity of mM3₁₇₁₉, Asp¹⁰⁷⁴ of mM3₁₇₁₉ was mutated to Ala¹⁰⁷⁴ (*D1074A* mutation, mM3-AP mutant) by site-directed mutagenesis. 2 µg of cDNA combinations of pcDNA3.1/pcDNA3.1, mM3-AP/pcDNA3.1, mM3₁₇₁₉/pcDNA3.1, mM3₁₇₁₉/mM3-AP, and mM3₁₇₁₉/mM3₁₇₁₉, were co-transfected into HEK-293 cells (cDNA ratio, 1:1). Upon the application of extracellular Ca²⁺ (10 mM) and PS (50 µM), a [Ca²⁺]_i increase was observed in the cells expressing mM3-AP/pcDNA3.1, although the measured Ca²⁺ influx was less than in the cells expressing mM3₁₇₁₉/pcDNA3.1. Since the expression level between them can be expected to be the same, our results indicate a partial reduction in Ca²⁺ entry. This is either due to a reduced channel activity, or, more likely, due to a decrease in Ca²⁺ permeability. Like the mM3-RYW and mM3-VEV mutants, the mM3-AP mutant did not inhibit the channel function of mM3₁₇₁₉ by 50% under this experimental condition, and thus it could not function as a dominant-negative mutant (Figure: 3.7).

In summary, we identified three amino acid residues, Pro¹⁰⁶⁰, Gly¹⁰⁶⁶ and Asp¹⁰⁷⁴ which may play a role in the Ca²⁺ entry through mM3₁₇₁₉, and thus may be critical for the function of mM3₁₇₁₉.

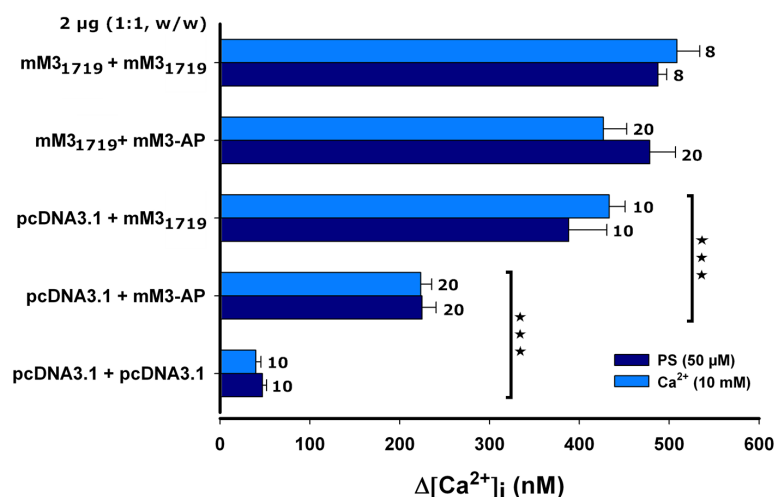


Figure 3.7: Ca²⁺ entry through mM3₁₇₁₉ with *D1074A* pore mutation

The Ca²⁺ entry in mM3₁₇₁₉ with *D1074A* pore mutation were analyzed using aequorin-based intracellular Ca²⁺ measurements. The cells expressing the mM3-AP mutant showed increased Ca²⁺ influx upon the extracellular Ca²⁺ (10 mM) and PS (50 µM) applications. However, the [Ca²⁺]_i increase in the mM3-AP transfected cells was less than it was in the mM3₁₇₁₉ transfected cells. When mM3-AP and mM3₁₇₁₉ were co-expressed, the mM3-AP mutant did not inhibit the channel activity of mM3₁₇₁₉. Therefore, mM3-AP is a functional channel without dominant-negative properties. For statistics, unpaired Student's t-test and independent transfection experiments (Mean ± SEM, n=4) were performed. Numbers next to the bars indicate the total number of performed experiments. *** = P < 0.001. **Abbreviation:** PS, pregnenolone sulfate.

3.2.1.2 Characterization of the mM3₁₇₁₉ C-terminus

Little is known about the structure and function of the C-terminus of TRPM3. Firstly, the molecular structure of C-terminus is variable among the TRPM channels, but conserved in the TRPM3-like channels. Besides a TRP domain and a coiled-coil (C-C) domain which are close to the 6 transmembrane segments (6TM), the C-terminal protein sequence lacks predicted domains such as enzymatic domains. Secondly, PS- and Ca²⁺-induced Ca²⁺ entry through the short splice variant mM3₁₃₃₇ was significantly larger than that through the long splice variant mM3₁₇₁₉. This indicates that the protein structure of the C-terminus probably plays an important role in the specific regulation of the TRPM3 channel. Hence, to investigate the biological roles of the mTRPM3 C-terminus, we studied its molecular structure and function using subcellular localization studies and Ca²⁺ entry measurements

with C-terminal mM3₁₇₁₉ mutants.

Subcellular localization of the soluble mM3₁₇₁₉ C-terminus protein The cDNA sequence of the mM3₁₇₁₉ C-terminus (M3TC, amino acid residues 1166–1719) was amplified by PCR using specific primers with a Kozak consensus sequence (Section: 2.10). The amplified cDNA fragment was cloned into the pcDNA3.1/V5-His-TOPO[®] vector, and afterwards C-terminally fused with YFP-, and HA-tags by using in-frame fusion. To test whether the cloned C-terminal sequence of mM3₁₇₁₉ is expressible in HEK cells and to study its subcellular localization, the C-terminally HA-, YFP-tagged M3TC were transfected into HEK-293 cells and the protein expression checked with immunocytochemical staining and confocal microscopy. Whereas the full length mM3₁₇₁₉ immunoreactivity is primarily observed in intracellular compartments (Figure: 3.8A-B), the immunoreactivity of M3TC was entirely found at the plasma membrane (Figure: 3.8C-D), indicating a binding of M3TC to the plasma membrane.

A number of TRP channels have been shown to bear PH domains or similar phospholipid binding motifs (*e.g.*, TRPM4 [145]). Therefore, we manipulated the membrane lipid content to document the possible changes in the mM3₁₇₁₉ C-terminus subcellular localization. Since the protein-lipid interaction through PH domain can be broken by activated PLC β which catalyzes the hydrolysis of PIP₂ to form DAG and IP₃, some agonists such as histamine, carbachol (CCh) [50], PGE2 [136], thrombin [189], and UTP [4, 213] which can activate PLC β via a protein-coupled receptor were used to investigate the putative role of PH domain in M3TC plasma membrane attachment. Figure 3.8E-H was obtained by using an Olympus IX70 inverted microscope, and shows HEK-293 cells co-expressing a YFP-tagged M3TC and the histamine H₁ receptor (M3TC-H1) and the HEK-293 cells co-expressing a YFP-tagged PH domain (from PLC γ) and the histamine H₁ receptor (PH-H1). The PH-H1 was used as a positive control (molar ratio, 1:1). After treatment with histamine for 10 min, the PH domain was released from the plasma membrane (Figure: 3.8E-F), but the M3TC was still bound to the plasma membrane (Figure 3.8G-H). The experiments were repeated using carbachol (100 μ M), PGE2 (1 μ M), thrombin (4 units/ml) and UTP (100 μ M), however, no disassociation of M3TC from the plasma membrane was detected (data not shown). Thus, the binding of the mM3₁₇₁₉ C-terminus to the plasma membrane is not mediated by a PH domain or other PIP₂ binding motifs.

M3TC could also be anchored to the cytosolic face of the membrane either through *N*-myristoylation on a NH₂-terminal glycine residue via an amide bond [216] or through

3.2. Identification of functional domains in mM3₁₇₁₉

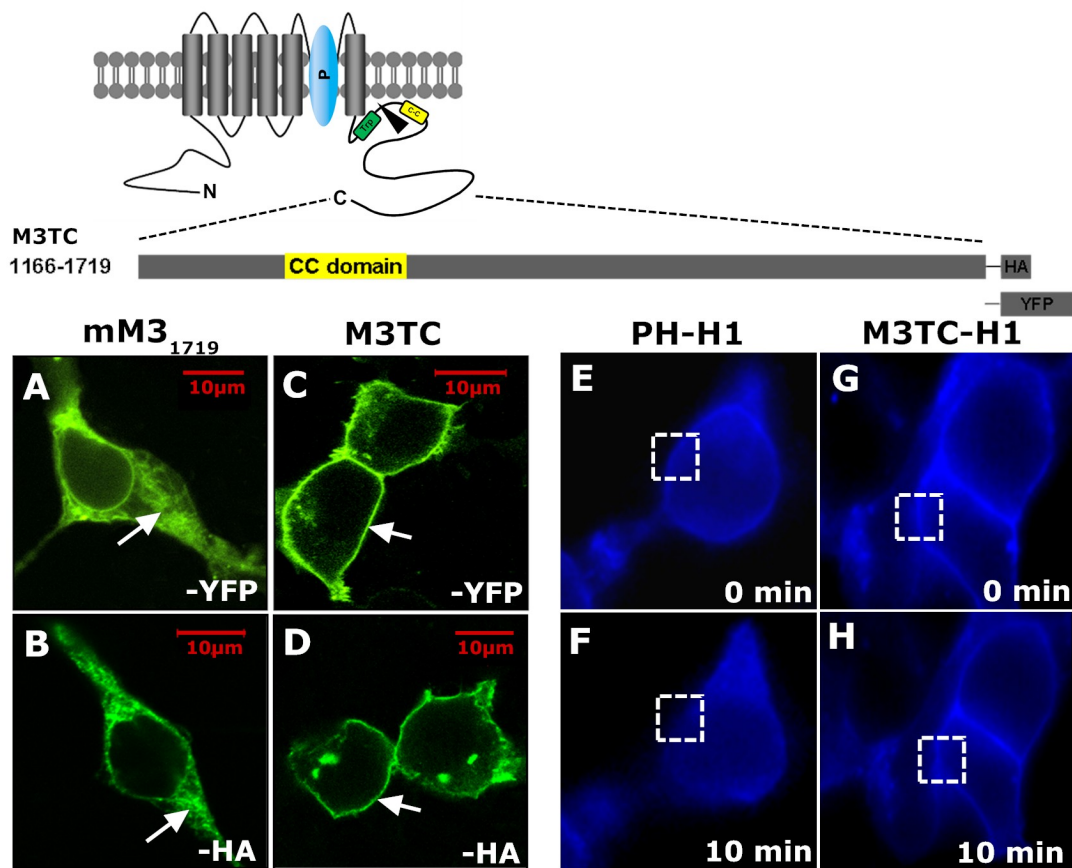


Figure 3.8: Protein expression of the mM3₁₇₁₉ C-terminus in HEK-293 cells and the putative role of PH-domain in the plasma membrane attachment of the mM3₁₇₁₉ C-terminus

Schematic of the C-terminal region of mM3₁₇₁₉ that begins at residue 1169. HA- or YFP-tagged M3TC were transfected into HEK-293 cells and visualized by immunocytochemical staining and confocal microscopy. **A-B:** YFP- and HA-tagged mM3₁₇₁₉ were localized in intracellular compartments (arrow). **C-D:** plasma membrane localization of YFP- and HA-tagged M3TC was observed (arrow). **E-F:** HEK-293 cells were cotransfected with the YFP-tagged M3TC and the histamine H₁ receptor (M3TC-H1). The histamine H₁ receptor was activated with 100 μM histamine, and the images were obtained by illumination with 475 nm light using an Olympus IX70 inverted microscope with a 40× oil objective. As a positive control, YFP-tagged PH domain co-expressed with H1 receptor (PH-H1) in HEK-293 cells showed a plasma membrane localization (E). After 10 min histamine stimulation, the PH domain was disassociated from the plasma membrane (broken square, F). **G-H:** YFP-tagged M3TC was still observed in the plasma membrane (broken square, H) after the co-expressed H1 receptor was activated for 10 min with histamine. **Abbreviations:** H1, histamine H₁ receptor; M3TC, C-terminus of mM3₁₇₁₉; PH domain, pleckstrin homology domain.

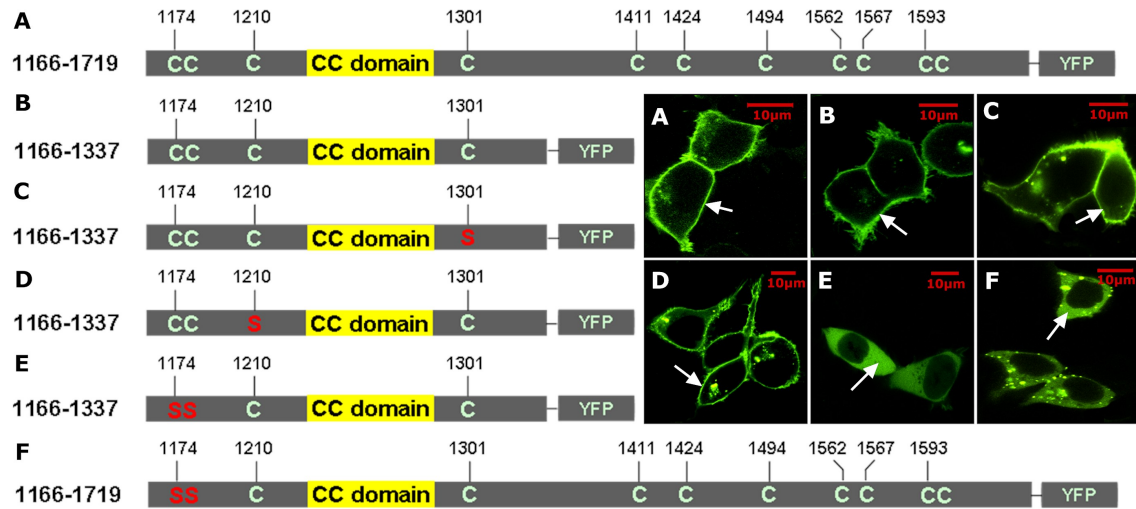


Figure 3.9: Effects of cysteine residues on the plasma membrane attachment of M3TC

M3TC and mutants of the C-termini were fused with YFP tags. Photos were taken using a confocal microscope. **A:** Cysteine residues in M3TC are indicated, M3TC is bound to the plasma membrane (arrow). **B:** The C-terminus of mM3₁₃₃₇ was generated by PCR (residues 1166–1337). This short C-terminus is also attached to the plasma membrane (arrow). **C–D:** Cys¹³⁰¹ and Cys¹²¹⁰ were mutated to Ser¹³⁰¹ and Ser¹²¹⁰ in the C-terminus of mM3₁₃₃₇. However both mutants showed high levels of membrane localization (arrows). **E–F:** Cytosolic localizations of the C-termini of either M3₁₃₃₇ or M3₁₇₁₉ were observed when their amino acid residues Cys¹¹⁷⁴–Cys¹¹⁷⁵ were both substituted by serine.

farnesylation and *S*-acylation (palmitoylation) via an ester linkage to the thiol group of a cysteine residue [203]. Because *N*-myristoylation is a stable co-translational lipid modification process and its typical recognition motif (Met-Gly-X-X-X-Ser/Thr) [176, 253] is missing in the M3TC, we focused on the analysis of the cysteine residues in M3TC with site-directed mutagenesis and confocal microscopy methods. To more precisely map the protein–lipid binding sites, a series of mutations in which the cysteine residues were step-wise mutated to the corresponding serine (S) were performed, because the side chains of serine and cysteine are most similar. All of the mutants were fused with YFP-tags as described above. Mutations of Cys¹³⁰¹ or Cys¹²¹⁰ alone (*C1301S*, *C1210S*) did not have an impact on M3TC binding to the plasma membrane (Figure: 3.9C-D), while the mutations of Cys¹¹⁷⁴–Cys¹¹⁷⁵ (*CC1174SS*) in the M3TC protein of either mM3₁₇₁₉ or mM3₁₃₃₇ caused protein release from the plasma membrane into the cytosol (Figure:3.9E-F). These

3.2. Identification of functional domains in mM3₁₇₁₉

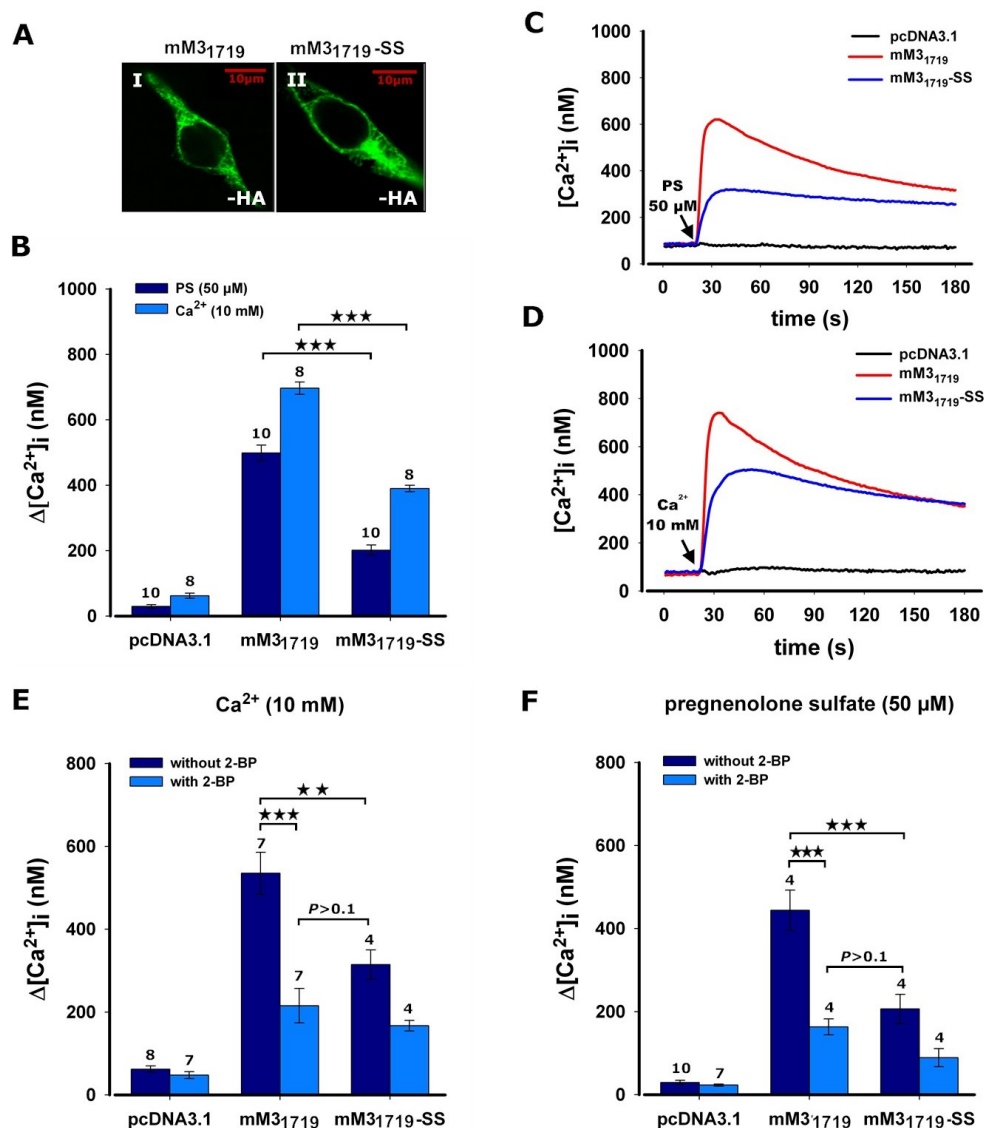


Figure 3.10: Effects of palmitoylation on the function and subcellular localization of mM3₁₇₁₉

The role of palmitoylation in mM3₁₇₁₉ was analyzed by using immunocytochemical staining and an aequorin-based functional assay with and without 2-bromopalmitate (2-BP) treatment. **A:** The HA-tagged mM3₁₇₁₉-SS mutant was still found in the intracellular compartment. The subcellular localization of the mM3₁₇₁₉ was unchanged by palmitoylation. The images were obtained by confocal microscope. **B-D:** Compared to mM3₁₇₁₉, the Ca²⁺ influx through mM3₁₇₁₉-SS upon the extracellular application of 10 mM Ca²⁺ and 50 μM PS was reduced. **E-F:** The decreased Ca²⁺ entry through mM3₁₇₁₉-SS mutant without 2-BP treatment was nearly equal to the decreased Ca²⁺ entry through mM3₁₇₁₉ wild-type with 2-BP treatment (100 μM). The data indicate mean ± SEM, n ≥ 3. For statistics, unpaired Student's t-test was used. The total number of performed experiments was shown as numbers above the bars. ** = P < 0.01, *** = P < 0.001. **Abbreviations:** 2-BP, 2-bromopalmitate; PS, pregnenolone sulfate.

data demonstrate that the Cys¹¹⁷⁴–Cys¹¹⁷⁵ residues, but not other cysteine residues in the C-terminus of mM3₁₇₁₉, disrupted the plasma membrane localization of M3TC.

The M3TC attachment to the plasma membrane is most likely mediated by palmitoylation via cysteine residues (Section: 4.2.1). In order to investigate the effects of this lipid modification, we introduced two point mutations in the full-length mM3₁₇₁₉ (mM3₁₇₁₉-SS mutant, Cys¹¹⁷⁴–Cys¹¹⁷⁵→Ser¹¹⁷⁴–Ser¹¹⁷⁵). 2-bromopalmitate (2-BP) which blocks palmitoyl acyltransferases and functions as a palmitoylation inhibitor [107, 255] was applied to learn whether Cys¹¹⁷⁴–Cys¹¹⁷⁵ residues are involved in the mM3₁₇₁₉ palmitoylation and channel function. The Ca²⁺ entry of mM3₁₇₁₉ wild-type and mM3₁₇₁₉-SS mutant were assessed with an aequorin-based functional assay in the presence and absence of 2-BP. For immunocytochemical staining, HA-tags were fused to both mM3₁₇₁₉ and mM3₁₇₁₉-SS as described above. HEK-293 cells expressing mM3₁₇₁₉ and mM3₁₇₁₉-SS were pre-incubated with HBS/Ca²⁺ solution supplemented with or without 100 μM 2-BP for 30 min before the application with extracellular 10 mM Ca²⁺ and 50 μM PS. We found that the subcellular expression pattern of mM3₁₇₁₉ was not changed by the Cys¹¹⁷⁴–Cys¹¹⁷⁵ mutations, because HA-tagged mM3₁₇₁₉-SS was still observed in the intracellular compartment of HEK-293 cells (Figure: 3.10A). Moreover, these Cys¹¹⁷⁴–Cys¹¹⁷⁵ mutations probably have effects on mM3₁₇₁₉ channel function, because upon the application of extracellular Ca²⁺ or PS, the [Ca²⁺]_i increase in HEK-293 cells expressing mM3₁₇₁₉-SS mutant was less than it was in the cells expressing mM3₁₇₁₉ wild-type (Figure: 3.10B-D). We also found that 2-BP reduced the Ca²⁺ entry through mM3₁₇₁₉ wild-type. This decreased Ca²⁺ entry was not statistically significant between the mM3₁₇₁₉ wild-type with 2-BP treatment and the mM3₁₇₁₉-SS mutant without 2-BP treatment (Figure: 3.10E-F). This means that a 2-BP-inhibitable palmitoylation may be responsible for the reduced Ca²⁺ entry through mM3₁₇₁₉.

Taken together, palmitoylation attaches the soluble C-terminus of mM3₁₇₁₉ to the plasma membrane. In the absence of palmitoylation in the C-terminus, mM3₁₇₁₉ Ca²⁺ entry is reduced, despite the unchanged subcellular localization pattern. Thus, palmitoylation of the Cys¹¹⁷⁴–Cys¹¹⁷⁵ mediates this part of the channel function of mM3₁₇₁₉.

3.2.2 Analysis of mM3₁₇₁₉ homomer formation

TRP channels require a tetrameric assembly of pore-forming subunits to fulfill their physiological functions [132, 187]. Some members of TRPM subfamily have been reported to be expressed as oligomeric complexes such as TRPM4 [137] and TRPM6 [109], but the

direct experimental evidence of TRPM3 multimerization has not been described. To study homomultimerization of mM3₁₇₁₉ and its subunit association in living cells, fluorescence resonance energy transfer (FRET), co-immunoprecipitation (Co-IP) and yeast two hybrid (Y2H) techniques were applied.

As an indication of subunit assembly, the proximity of C-terminally CFP- and YFP-tagged mM3₁₇₁₉ was measured by the FRET technique [8, 73]. The expression levels were adjusted so that most cells had a molar ratio of YFP-tagged mM3₁₇₁₉ (acceptor) and CFP-tagged mM3₁₇₁₉ (donor) to a 1.5–3-fold molar ratio to ensure comparable relative CFP and YFP fluorescence intensities [6, 8]. Co-transfection experiments with mM3₁₇₁₉-CFP/TRPML1-YFP and with TRPML1-CFP/TRPML1-YFP (ML1) [225] were performed as negative and positive controls, respectively. FRET signals were obtained by measuring the donor (CFP) fluorescence recovery during selective photobleaching of the acceptor (YFP). The acceptor was selectively photobleached at 515 nm (5 second illumination per frame) [6], and the donor fluorescence recovery monitored at 440 nm. The FRET efficiency was obtained by the extrapolated intersection of the linear regression line with the y axis at $F_{YFP}/F_{YFP,0}=0$ [78]. Figure 3.11(D-E) shows that mM3₁₇₁₉ displayed a significant FRET (12.14 ± 0.08 increase in CFP fluorescence) compared with negative control (1.15 ± 0.22 increase in CFP fluorescence). But the FRET efficiency of mM3₁₇₁₉ was lower than it observed in the ML1 group (39.56 ± 0.23 increase in CFP fluorescence). Our FRET results indicate that the mM3₁₇₁₉ subunits interact with each other in living cells.

Co-immunoprecipitation (Co-IP) was used as an independent approach to test whether mM3₁₇₁₉ multimerizes. Co-IP was also used to determine whether the C-terminus and the residues Cys¹¹⁷⁴-Cys¹¹⁷⁵ play a role in the homomultimerization of mM3₁₇₁₉. Various TRPM3 cDNA constructs (mM3₁₇₁₉, mM3₁₃₃₇, mM3₁₇₁₉-SS, mM3₁₃₃₇-SS) and mouse TRPC4 cDNA (mC4) were tagged with HA or YFP at their C-termini, and co-transfected into HEK-293 cells in different combinations. The combinations, mC4/mC4 [188], mC4/mM3₁₇₁₉ and mC4/mM3₁₃₃₇ were used as positive and negative controls, respectively. After a 36-hr incubation, the cells were solubilized and immunoprecipitated with a rabbit anti-GFP antibody. Both cell lysates (upper panels) and immunoprecipitates (lower panels) were subjected to SDS-PAGE and immunoblotted with an anti-HA antibody. Anti-HA immunoreactivities were detected in the anti-GFP immunoprecipitates for mC4/mC4, mM3₁₇₁₉/mM3₁₇₁₉, mM3₁₇₁₉/mM3₁₇₁₉-SS, mM3₁₃₃₇/mM3₁₃₃₇ and mM3₁₃₃₇/mM3₁₃₃₇-SS cDNA combinations (Figure: 3.12A and B, lower right panel). Co-IP experiments not only

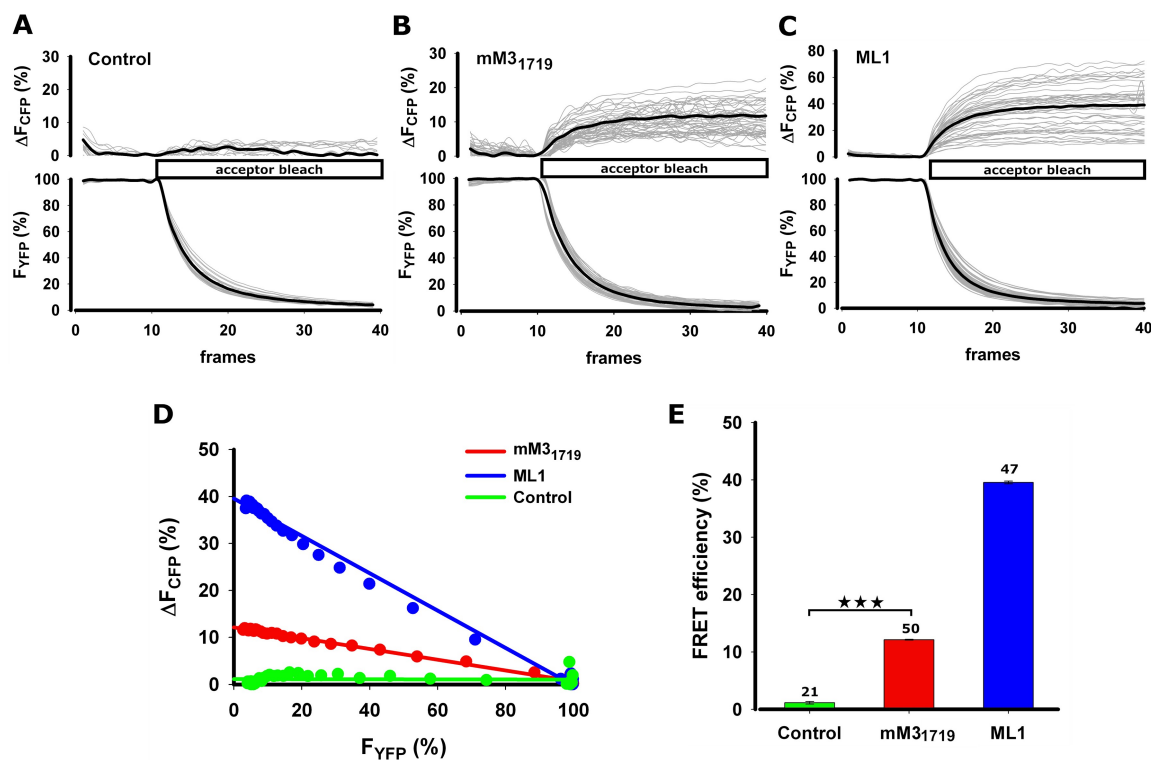


Figure 3.11: Analysis of mM3₁₇₁₉ homomultimerization using the FRET technique
A-C: Representative traces for FRET between control (negative), mM3₁₇₁₉ and ML1 (positive) groups are shown. Gray and black lines represent the single cell traces and means, respectively. Changes in the relative fluorescence intensities of CFP (ΔF_{CFP} %) and YFP (F_{YFP} %) emissions are plotted against frames (5 second illumination per frame). **D:** Linear regression analysis of relative donor fluorescence recovery (ΔF_{CFP} %) against fractional acceptor photobleaching (F_{YFP} %) is shown. **E:** FRET efficiency for homomeric analysis is statistically different between negative control and mM3₁₇₁₉ (1.15 ± 0.22 and 12.14 ± 0.08 , respectively). The data were obtained from 20–50 single cells from four independent transfections ($n=4$) and indicate mean \pm SEM of 12–15 photobleaching experiments. Unpaired Student’s t-test was used for statistical analysis. Numbers above the bars indicate the total number of recorded cells. *** = $P < 0.001$. **Abbreviation:** ML1, TRPML1.

confirm the protein interaction between mM3₁₇₁₉ subunits, but also indicate that the amino acid sequences from residues 1338 to 1719 and the residues Cys¹¹⁷⁴–Cys¹¹⁷⁵ do not play a role in the homomultimerization of mM3₁₇₁₉.

To further study the binding sites which determine the mM3₁₇₁₉ subunit interaction, the yeast two hybrid system (Y2H) was used as an *in vitro* approach. The N-terminal (N-Term, residues 1–876) and C-terminal (C-Term, residues 1133–1719, and C-Term(S), residues

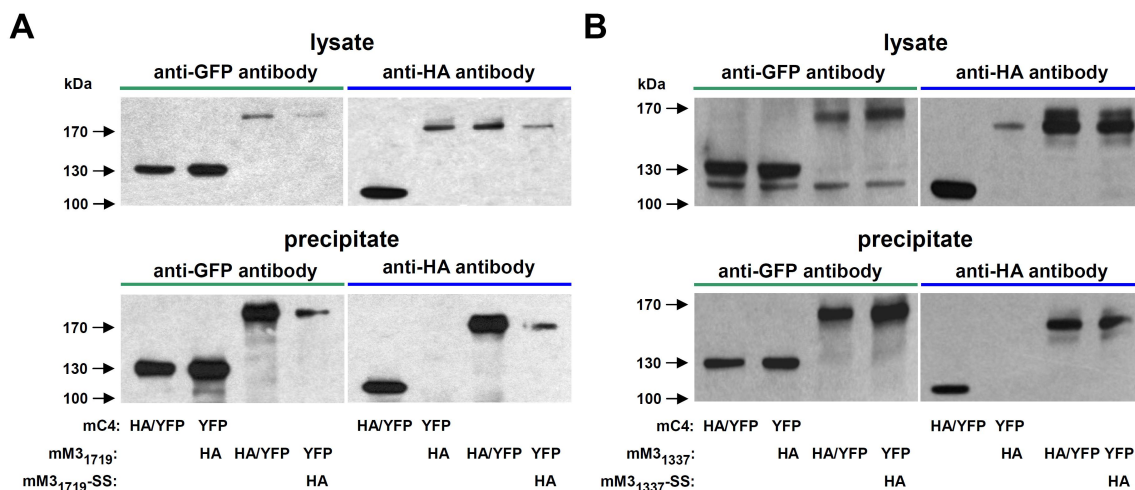


Figure 3.12: Analysis of mM3₁₇₁₉ homomultimerization using co-immunoprecipitation

Different combinations of mTRPM3 cDNAs tagged with HA or YFP were co-expressed in the HEK-293 cells. HA⁻, and YFP-tagged mouse TRPC4 (mC4) were used as a control. Co-IPs were performed with an anti-GFP antibody and Western blots were probed with an anti-HA antibody. **A:** The detected HA immunoreactivities of mM3₁₇₁₉ and mM3₁₇₁₉-SS immunoprecipitated by an anti-GFP antibody revealed the protein interactions between mM3₁₇₁₉/mM3₁₇₁₉ and between mM3₁₇₁₉/mM3₁₇₁₉-SS (lower right panel). **B:** Protein interactions were also found between mM3₁₃₃₇/mM3₁₃₃₇ and mM3₁₃₃₇/mM3₁₃₃₇-SS. The bands for mM3₁₃₃₇ and mM3₁₃₃₇-SS were detected by an anti-HA antibody in the anti-GFP immunoprecipitates (lower right panel). **Abbreviations:** mC4, mouse TRPC4; mM3₁₃₃₇, short variant of mM3₁₇₁₉; mM3₁₇₁₉-SS, mM3₁₇₁₉ with *CC1174SS* mutation; mM3₁₃₃₇-SS, mM3₁₃₃₇ with *CC1174SS* mutation.

1133–1337) fragments were PCR-amplified from mM3₁₇₁₉ and mM3₁₃₃₇ by using primers containing the desired enzyme restriction sites (Table: 2.10). The amplified PCR products were subcloned into the pGBKT7/BD and pGAD424/AD vectors, respectively. Various pGBKT7/BD and pGAD424/AD combinations with Y2H constructs were co-transformed into the yeast strain AH109, and subsequently plated on synthetic dropout (SD) plates using the medium-stringency screening method¹ (Section: 2.2.4.1). Blue colored colonies on SD/-Ade/-His/-Leu/-Trp/X-α-gal plates were used as indicators of protein interaction.

Figure 3.13 shows that the protein-protein interactions occur between C-terminal fragments of mM3₁₇₁₉ and mM3₁₃₃₇ including C-Term/C-Term, C-Term/C-Term(S), C-Term

¹All experiments were first performed using the high-stringency screening method, but no blue colonies were obtained (data not shown).

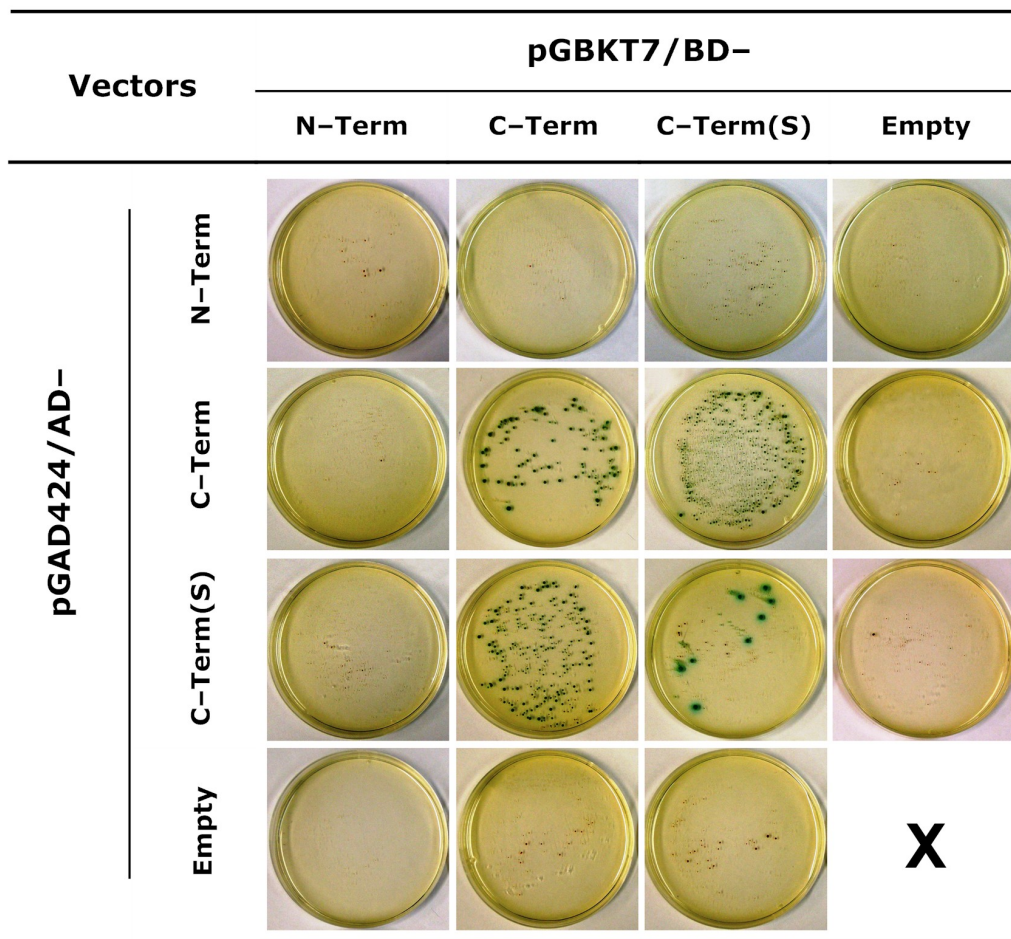


Figure 3.13: Analysis of the mM3₁₇₁₉ and mM3₁₃₃₇ subunit interactions using the yeast two hybrid system

The N-terminus and C-terminus of mM3₁₇₁₉ and the C-terminus of mM3₁₃₃₇ were constructed into the pGBKT7/BD vector expressing the GAL4 DNA binding domain and the pGAD424/AD vector expressing the GAL4 transactivation domain. For control experiments, empty pGBKT7/BD and pGAD424/AD vectors were used. Various combinations of Y2H constructs were co-transformed into AH109 yeast cells. The co-transformed cell cultures were first plated on SD/-His/-Leu/-Trp plates to select for transformants, then the transformants were replicated to SD/-Ade/-His/-Leu/-Trp plates containing 20 mg/L of X- α -gal. Colony growth and blue color indicate a protein interaction within the following two-hybrid proteins: C-Term and C-Term, C-Term and C-Term(S), C-Term(S) and C-Term(S). Interactions between N-Term and N-Term, N-Term and C-Term, N-Term and C-Term(S) were not found. **Abbreviations:** C-Term, C-terminus of mM3₁₇₁₉ (residues 1133-1719); C-Term(S), C-terminus of mM3₁₃₃₇ (residues 1133-1337); N-Term, N-terminus of mM3₁₇₁₉ (residues 1-876).

(S)/C–Term(S). No protein interactions of N–term with N–term, C–Term or C–Term(S) were observed. These results strongly suggest that the mM3₁₇₁₉ subunits involved in channel homomultimerization are determined by their C–terminal protein sequences. The binding sites for the protein–protein interaction may be located in the amino acid sequence from residues 1133 to 1337.

Thus, we could show with three independent methods that TRPM3, like other TRPs, is built from subunits. Furthermore, we can localize the multimerization sequence with Y2H to the C–terminus (probably C-C domain, Section: 4.2.2). It is unlikely that palmitoylation is involved in mM3₁₇₁₉ homomultimerization.

3.2.3 Identification of putative interaction partners of mM3₁₇₁₉

3.2.3.1 Identification of putative interaction partners of mM3₁₇₁₉ using the yeast two hybrid system

Evidence presented above shows that mTRPM3 displays constitutive activity and can be activated by PS at high concentration (50 μ M). This indicates that mTRPM3 may be implicated in Ca²⁺ signaling or other signal transduction pathways. However, little is known about the molecules that interact with mTRPM3 and mediate the physiological functions of mTRPM3 in cellular signaling.

Because the mTRPM3 N–termini are common and highly conserved among different TRPM channels, and we wanted to identify melastatin–specific determinants of function, we chose the C–terminal 587 aa of mM3₁₇₁₉ (M3CT, residues 1133–1719) as a “bait” to screen a human kidney cDNA library with the aid of the yeast two hybrid (Y2H) system. The “Bait” fusion plasmid (pGBKT7/BD-M3CT) was constructed and Y2H was performed with a high-stringency scale procedure as described in Section 2.2.4.1. Before starting Y2H screening, no auto–activation or toxicity of pGBKT7/BD-M3CT was detected (data not shown), the library titer and mating efficiency were calculated to 6×10^6 (cfu/ml) and 1.67%, respectively. The interactions between “bait” and “prey” candidates were verified in the AH109 yeast strain under high or medium stringency conditions (Figure: 2.3).

Since the C–terminus of mM3₁₇₁₉ is cytoplasmic, valid binding partners should be: 1) co-localized in same cellular compartment *in vivo*, nuclear and extracellular proteins were therefore not considered; 2) expressed in the same cells or tissues; 3) typical frequently existed hits were not considered (*e.g.*, ribosomal proteins). To meet these criteria, the amino acid sequences of “prey” candidates were “filtered” by using various online database tools

Table 3.1: Putative interaction partners of mM3₁₇₁₉ identified by high stringency selection

Candidates	Sequence	Number in GenBank	Biological Functions	Cellular localization ^a
Pre-B-cell leukemia homeobox interacting protein 1	131 AS, C-terminal	NM_020524	Cell differentiation, multicellular organismal development, negative regulation of transcription	Cytoplasm, cytoskeleton, cytosol, microtubule, nucleus
Glutaredoxin	106 AS	NP_002055	Cell redox homeostasis, electron transport chain	Cytoplasm, cytosol
Potassium channel tetramerisation domain containing 1	111 AS, C-terminal	EAX01226	Potassium ion transport	Voltage-gated potassium channel complex, membrane
Metallothionein 1F	61 AS	NP_005940	Metal ion binding	Cytoplasm
Actin related protein 2/3 complex, subunit 5	139 AS, C-terminal	NP_112240	Regulation of actin filament polymerization	Cytoplasm, cytoskeleton
cAMP-dependent protein kinase inhibitor gamma	76 AS	NP_008997	cAMP-dependent protein kinase inhibitor activity, protein binding	Cytoplasm
COP9 complex subunit 7α	112 AS, C-terminal	NP_057403	Transcription regulator activity	Cytoplasm, nucleus, signalosome
Bardet-Biedl syndrome 1	222 AS	NP_078925	Photoreceptor cell maintenance, response to stimulus, retina homeostasis, sensory cilium biogenesis	Cytoplasm
Methionine sulfoxide reductase A	130 AS, C-terminal	NP_036463	Methionine metabolic process, protein modification, response to oxidative stress	Cytoplasm, mitochondrion
EF1α-like protein	297 AS, N-terminal	BAD96750	Translational elongation	Cytoplasm, cytosol
Brain expressed X-linked 2	128 AS	NP_116010	Unknown	Cytoplasm, nucleus
TNSI tensin 1	243 AS, N-terminal	NP_072174	Actin binding, protein binding	Cell junction, cytoplasm, cytoskeleton

^aOnline database: Entrez Gene, Human Protein Reference Database, LOCATE Subcellular Localization Database

Table 3.2: Putative interaction partners of mM3₁₇₁₉ identified by medium stringency selection

Candidates	Sequence	Number in GenBank	Biological Functions	Cellular localization ^e
Crystallin, alpha B	175 AS	NP_001876	Structural constituent of eye lens, unfolded protein binding	Cytoplasm
Aldolase B, fructose-bisphosphate	351 AS, N-terminal	NP_000026	ATPase binding, protein binding, fructose binding, fructose-bisphosphate aldolase activity, lyase activity	Cytoplasm, nucleus, microtubule organizing center
DAZ associated protein 2	168 AS	NP_055579	WW domain binding, protein binding	Cytoplasm, nucleus
Lactate dehydrogenase A	104 AS, C-terminal	NP_005557	L-lactate dehydrogenase activity, oxidoreductase activity	Cytoplasm, cytosol
SRY (sex determining region Y)-box 13	177 AS	BC106038	Transcription factor activity	Cytoplasm, nucleus
Tumor protein, translationally controlled 1	138 AS	CAH72035	Calcium ion binding, protein binding	Cytoplasm, co-localized with tubulin complex
Translation elongation factor 1 alpha 1-like 14	204 AS, C-terminal	AF397403	GTP binding, GTPase activity, nucleotide binding, translation elongation factor activity	Cytoplasm, cytosol
Phosphatidylethanolamine binding protein 1	92 AS, C-terminal	AAH31102	ATP binding, lipid binding, nucleotide binding, phosphatidylethanolamine binding, serine-type endopeptidase inhibitor activity	Cytoplasm
Phytanoyl-CoA 2-hydroxylase interacting protein-like	141 AS, N-terminal	NP_115815	Unknown	Cytoplasm
Alanyl amino-peptidase (membrane)	87 AS, C-terminal	BAD93155	Amino-peptidase activity, metalloproteinase activity, peptide binding, metal ion binding, zinc ion binding	ER-Golgi, plasma membrane, cytoplasm
DEAH (Asp-Glu-Ala-His) box polypeptide 36	278 AS, N-terminal	AAH36035	ATP-dependent helicase activity, helicase activity, hydrolase activity, nucleotide binding	Cytoplasm, nucleus
TP53-induced glycolysis and apoptosis regulator	187 AS, C-terminal	NP_065108	Fructose-2,6-bisphosphate 2-phosphatase activity, hydrolase activity	Intracellular
Insulin-like growth factor II receptor	229 AS	AAK56918	Insulin-like growth factor receptor activity, glycoprotein binding, mannose binding, transporter activity	Trans-Golgi network transport vesicle, cytoplasm, integral to plasma membrane

^eOnline database: Entrez Gene, Human Protein Reference Database, LOCATE Subcellular Localization Database

such as *Entrez Gene*, *Human Protein Reference Database*, *LOCATE Subcellular Localization Database*. The putative binding partners for M3CT identified by high or medium stringency selection were listed in Table 3.1 and Table 3.2, respectively.

3.2.3.2 Analysis of protein kinase inhibitor–gamma as an interaction partner for mM3₁₇₁₉

According to the interaction partner lists above, mM3₁₇₁₉ may take part in a variety of cell biological activities, *e.g.*, protein translation, cellular homeostasis and ion binding. Protein kinase inhibitor–gamma (PKIG) was chosen as a candidate for studying the putative role of mM3₁₇₁₉ in cellular signal transduction, because PKIG is a competitive inhibitor of cAMP–dependent protein kinase (PKA) and plays a crucial role in the PKA–dependent signal transduction pathway [36]. Additionally, mTRPM3 activity could be regulated by protein signal transduction pathways. The interaction between PKIG and mM3₁₇₁₉ (or mM3₁₃₃₇) was analyzed by using Y2H (*in vitro*).

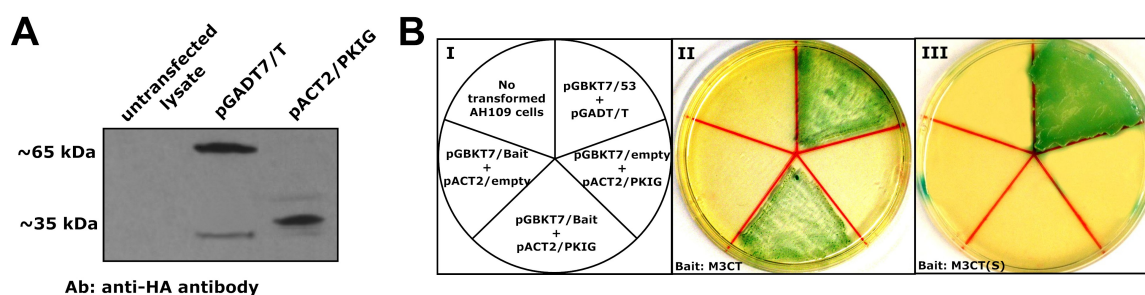


Figure 3.14: Subunit interaction analysis between mTRPM3 and PKIG

A: PKIG expression in AH109 cells was detected by Western blot with an anti–HA antibody. **B:** The protein interaction between the C–terminus of mM3₁₇₁₉ and PKIG was confirmed by Y2H method with a high–stringency scale procedure (II). No interaction between the C–terminus of mM3₁₃₃₇ and PKIG was observed. **Abbreviations:** M3CT, C–terminus of mM3₁₇₁₉ (residues 1133–1719); M3CT(S), C–terminus of mM3₁₃₃₇ (residues 1133–1337); PKIG, protein kinase inhibitor–gamma.

In Y2H experiments, vectors containing “bait” (M3CT or M3CT(S)²) and “prey” (PKIG) were co–transformed into the AH109 yeast strain and induced to grow on high stringency (QDO) plates. Protein–protein interactions were observed between the protein pairs pG–BKT7/53 and pGADT/T (positive control), and pGBKT7/M3CT and pACT2/PKIG, but

²M3CT(S) is the C–terminus of mM3₁₃₃₇ (residues 1133–1337)

not in the protein pairs of pGBKT7/M3CT(S) and pACT2/PKIG (Figure 3.14B). Figure 3.14A shows that PKIG constructed in the pACT2/AD vector was expressed in the AH109 yeast strain³.

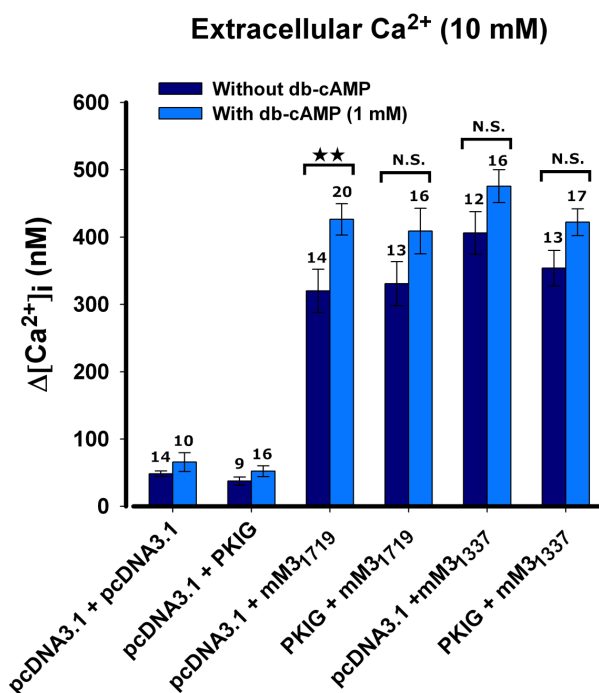


Figure 3.15: Effects of db-cAMP on Ca²⁺ entry through mM3₁₇₁₉ and mM3₁₃₃₇

Aequorin-based intracellular Ca²⁺ measurements were performed to study the biological role of PKIG in mTRPM3 channels. HEK-293 cells were transfected with different cDNA combinations (molar ratio 1:1). Treatment with db-cAMP increased Ca²⁺ influx through mM3₁₇₁₉, but not through mM3₁₃₃₇. No differences in the [Ca²⁺]_i increase were observed between the cells pre-treated with and without db-cAMP in the cells co-expressing PKIG and mM3₁₇₁₉. Db-cAMP treatment did not have any effects on the cells expressing pcDNA3.1/pcDNA3.1, pcDNA3.1/PKIG, pcDNA3.1/mM3₁₃₃₇ and PKIG/mM3₁₃₃₇. Bar graphs represent mean±SEM, n=5 transfection experiments. Numbers above the bars indicate the total number of experiments performed. Unpaired Student's t-test was used for statistics, ** = 0.001 < P < 0.05, n.s. = not significant. **Abbreviation:** PKIG, protein kinase inhibitor-γ.

To better understand a possible role of PKIG in mTRPM3 regulation, Ca²⁺ influx

³Predicted band size is 24 kDa: 0.11 × a fusion of the GAL4-AD (amino acids 768–881), an HA epitope tag (9 aa), and amino acid residues of PKIG (76 aa). The observed band size is about 34 kDa. This may be due to post-translational modification, post-translation cleavage, or multimerization.

through mM3₁₇₁₉ and mM3₁₃₃₇ were studied with or without co-expression of PKIG using a membrane-permeable cAMP-dependent protein kinase (PKA) activator, db-cAMP [199]. Various cDNA combinations (2 µg) of mTRPM3 and PKIG were transiently transfected into HEK-293 cells at a molar ratio of 1:1 as follows: 1) pcDNA3.1/pcDNA3.1; 2) pcDNA3.1/ PKIG; 3) pcDNA3.1/mM3₁₇₁₉; 4) PKIG/mM3₁₇₁₉; 5) pcDNA3.1/mM3₁₃₃₇; 6) PKIG/mM3₁₃₃₇. The cells expressing these cDNA combinations were pre-treated for 2 hr in HBS/Ca²⁺ buffer either without or supplemented with db-cAMP (1 mM). The Ca²⁺ entry was induced by Ca²⁺ steps, and the increased [Ca²⁺]_i was measured with aequorin. Figure 3.15 shows that 1) db-cAMP did not induce any Ca²⁺ influx in the control groups in which the cells only express pcDNA3.1/pcDNA3.1 or pcDNA3.1/PKIG; 2) PKIG did not have any effects on the channel activities of mM3₁₇₁₉ and mM3₁₃₃₇; 3) in the cells expressing pcDNA3.1/mM3₁₇₁₉, the Ca²⁺ influx in the cells with db-cAMP treatment was larger than it was in the cells without db-cAMP treatment; 4) db-cAMP treatment did not influence Ca²⁺ influx in the cells expressing PKIG/mM3₁₇₁₉, pcDNA3.1/mM3₁₃₃₇ and PKIG/mM3₁₃₃₇. These data indicate that db-cAMP activates PKA which probably in turn increases Ca²⁺ influx through mM3₁₇₁₉. However, the role of PKIG in mTRPM3 regulation needs further investigation.

In summary, we found a protein (PKIG) that interacts with the C-terminus of mM3₁₇₁₉ at residues 1338–1719. PKIG might play a role in the TRPM3 function, but so far, with the test performed to assess mM3₁₇₁₉ activity, we cannot definitely delineate a biological role of it in this process.

3.3 Tissue distribution of mouse TRPM3

Mouse TRPM3 expression was studied at the RNA (Northern blot) and protein (Western blot with specific antibodies) levels, and by a *lacZ* assay of the TRPM3 mice with the knockout allele.

3.3.1 Northern blot analysis of mouse TRPM3 tissue distribution

The Northern blot technique was first applied to identify mTRPM3 gene expression patterns at the RNA level. About 1 µg of *Poly(A)*⁺ RNA of various tissues were analyzed. The blot was hybridized with a ³²P-labeled mM3₁₇₁₉ cDNA, and re-probed with β-actin cDNA as a control. As shown in Figure 3.16, mM3₁₇₁₉ expression with transcripts of >9.0 kb was

observed in both the brain and eye.

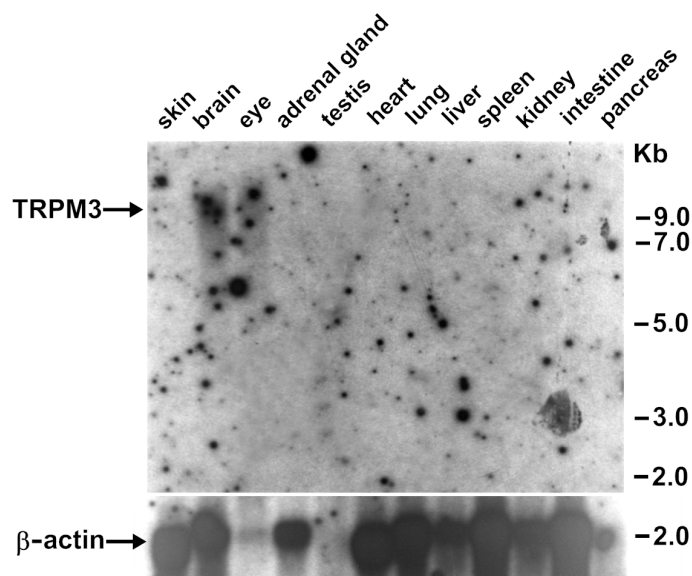


Figure 3.16: Northern blot analysis of mTRPM3 expression

Ca. 1 μg of *Poly(A)*⁺ RNA of various tissues were used for Northern blot analysis. Blots were hybridized with cDNA probes for mM3₁₇₁₉ to analyze mTRPM3 expression and for β -actin as a control. TRPM3 transcripts were detected in the mouse brain and eye.

3.3.2 Western blot analysis of mouse TRPM3 expression

3.3.2.1 Characterization of mouse TRPM3 antibodies

Two antibodies (anti-M3-7: *CLSRTSAFHSFESKH*; anti-M3-8: *CNEKNESRLSRNDIQS*) against specific peptide sequences in the C-terminus of mM3₁₇₁₉ were raised and affinity-purified (Section: 2.2.6.5). The specificity and affinity of the antibodies to the mM3₁₇₁₉ sequences were characterized by using immunocytochemical staining (Section: 2.2.6.3). 2 μg of C-terminally HA-tagged mM3₁₇₁₉ were transiently transfected into HEK-293 cells, which were then immuno-stained with anti-HA (positive control), anti-M3-7 and anti-M3-8 antibodies. C-terminally HA-tagged mTRPM1 served as a negative control and Alexa-488 as the secondary antibody. For either antiserum, we observed strong immunofluorescence signals with a pattern indistinguishable from the anti-HA staining. No cross-reactions were observed in the mTRPM1 (mM1) control groups (lanes II, IV). The results indicate that

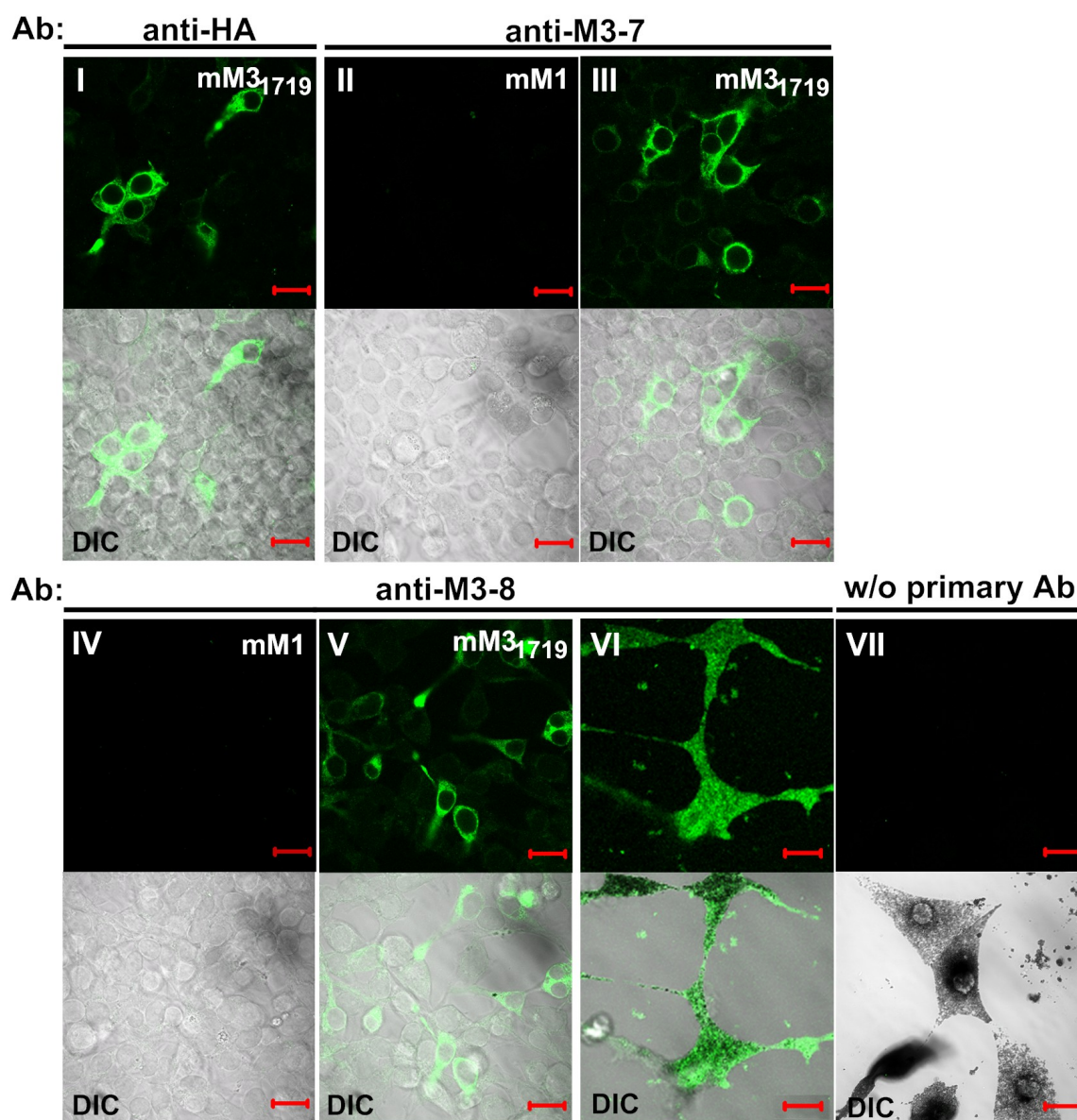


Figure 3.17: Immunofluorescence with mouse TRPM3 antibodies

The cells were imaged with a laser scanning confocal microscope. **Lanes I-V:** 2 μ g of HA-tagged mM3₁₇₁₉ or mM1 were transfected into HEK-293 cells. Anti-HA, anti-M3-7 and anti-M3-8 antibodies were tested for their ability to detect mM3₁₇₁₉ or mM1 expression. Compared to the anti-HA antibody (lane I), anti-M3-7 and anti-M3-8 antibodies displayed specificity and affinity to the mM3₁₇₁₉ (lanes III and V) and did not cross-react with mM1 (lanes II, IV). **Lanes VI-VII:** The anti-M3-8 antibody was used to detect mouse TRPM3 expression in melanocytes. The melanocytes were directly isolated from TRPM3^{+/+} mice, and stained with and without anti-M3-8 antibody (lane VI, VII). Alexa-488 was used as the secondary antibody. Bars represent 20 μ m.

both antibodies have enough specificity and affinity for mM3₁₇₁₉ (lanes III and V) compared to the positive control (lane I) (Figure 3.17).

3.3.2.2 Analysis of the TRPM3 protein expression in the adult mouse eye

We purchased TRPM3 knockout mice which were generated by *Lexicon genetics Corp.* using a GeneTrap strategy, in which a β -geo fusion construct was inserted into the intron between exon 1 and exon 2 of the mTRPM3 gene by homologous recombination. In order to make sure that the TRPM3^{-/-} mouse to be used for experiments as described below is a complete TRPM3 null allele mouse, we performed Western blots to test whether a mTRPM3 protein is still present in the TRPM3^{-/-} mouse. According to the results from the Northern blot (Section: 3.3.1), mouse eyes were chosen for the Western blot. Total membrane protein extracted from TRPM3^{+/+} and TRPM3^{-/-} mouse eyes was electrophoresed, blotted, and probed with an anti-M3-8 polyclonal antibody to detect TRPM3 protein expression. As a positive control, 2 μ g of HA-tagged mM3₁₇₁₉ (mM3₁₇₁₉-HA) were transiently transfected into HEK-293 cells. The over-expressed mM3₁₇₁₉-HA in HEK-293 cells was detected with an anti-HA antibody (Figure: 3.18, lane 2) and an anti-M3-8 antibody (Figure: 3.18, lane 4). In HEK-293 cells, 2 μ g of empty pcDNA3.1 vector was used as a negative control (Figure: 3.18, lanes 1 and 3). TRPM3 protein expression was observed in the eyes of TRPM3^{+/+} mice (Figure: 3.18, lane 6), but not in TRPM3^{-/-} mice (Figure: 3.18, lane 5). These data indicate that TRPM3 is expressed in the TRPM3^{+/+} mouse eye as a protein of the expected size of the long TRPM3 splice variants, *e.g.*, mM3₁₇₁₉. TRPM3 protein expression was not detectable in the TRPM3^{-/-} mice.

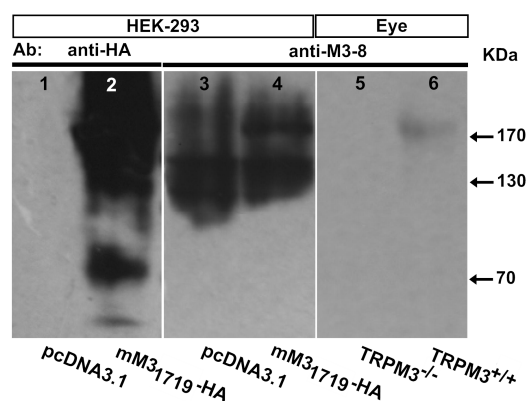


Figure 3.18: Analysis of TRPM3 protein expression in the adult mouse eye

In HEK-293 cells, TRPM3 protein expression was detected using anti-HA (lane 2) and anti-M3-8 antibodies (lane 4). Membrane proteins extracted from TRPM3^{+/+} and TRPM3^{-/-} mouse eyes were blotted with the anti-M3-8 antibody. No TRPM3 protein expression was observed in TRPM3^{-/-} mouse eyes (lane 5), but TRPM3 protein expression was detected in the TRPM3^{+/+} mouse eye (lane 6).

We also performed immunofluorescence experiments on eye cryosections with anti-TRPM3 antibodies. However, specific mTRPM3-immunoreactive signals were undetectable against the background (data not shown).

In summary, the Western blot analysis confirms that mTRPM3 is expressed in the mouse eye and no mTRPM3 protein expression is present in the TRPM3^{-/-} mouse. However, the anti-TRPM3 antibodies are not sensitive enough for cryosection staining. Thus we carried out *lacZ* staining using a *lacZ* transgenic mouse model (s. below).

3.3.3 Histochemical and immunohistochemical analysis of TRPM3 expression using a *lacZ* transgenic mouse model

Because of the low Northern signals and the high background immunofluorescence in tissue cryosections stained with anti-TRPM3 antibodies (s. above), we resorted to a genetically based method taking advantage of a *lacZ* transgenic mouse model (Figure: 2.8). We utilized the *lacZ* gene expression driven by the TRPM3 promoter(s) to detect TRPM3 tissue localization via *lacZ* histochemical staining (Section: 2.2.8.1). *LacZ* staining is an enzyme-based assay and provides a good signal-to-noise ratio with a high sensitivity.

Whole embryos (embryonic day (E) 9, 9.5, 11.5, 13, 14) and the frozen sections of tissues harvested from developing (E13) and mature TRPM3^{-/-} mice were histochemically stained with X-Gal. As a negative control, the *lacZ* staining was always performed for the whole embryos and frozen sections obtained from TRPM3^{+/+} mice (data not shown).

3.3.3.1 *LacZ* gene expression in *lacZ* transgenic TRPM3^{-/-} adult mice

Although the gross expression of mTRPM3 has been described in some tissues and organs [106, 157], the expression profile of mTRPM3 has not yet been established at the cellular level. Hence, a large number of tissues and organs (*e.g.*, CNS (brain and retina), digestive system (stomach, small intestine, pancreas and liver), reproductive system (testis, uterine tubes), spleen, kidney, skin and lung) of *lacZ* transgenic TRPM3^{-/-} adult mice were used to study *lacZ* gene expression under the control of the TRPM3 promoter(s).

The samples subjected to *lacZ* staining were obtained from adult (6-month) TRPM3^{+/+} and TRPM3^{-/-} mice. Tissues were dissected, embedded on cryostat chucks, and sectioned as described in Section 2.2.6. X-Gal staining was performed overnight⁴ at 37°C, and the

⁴Initially, *lacZ* staining of frozen sections was performed 1 hr, 3 hr, *etc.*. However, no obvious blue precipitates or sparse blue precipitates were seen. According to the low expression pattern of *lacZ* gene

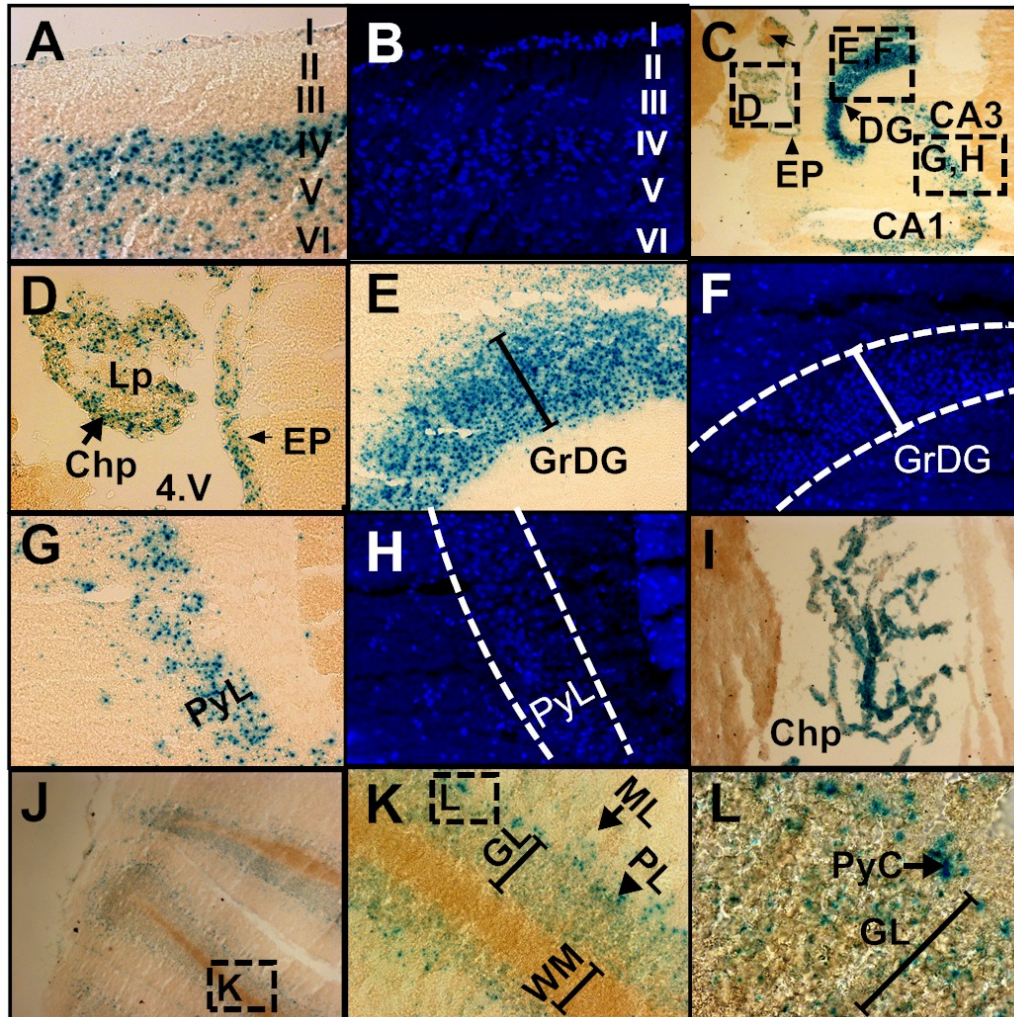


Figure 3.19: *LacZ* gene expression of mTRPM3 in the CNS

Frozen brain sections of adult *lacZ* transgenic mice were stained with X-Gal for β -galactosidase activity. **A:** Intense staining was visible in the layers I, IV, V and VI of the cerebral cortex. **B:** DAPI counterstaining was used to show different layers of cerebral cortex. **C-D:** The choroid plexus is covered by an X-Gal-stained epithelium projecting into the brain ventricle. X-Gal staining was also present in the ependyma, dentate gyrus and hippocampus. **E-H:** Intense *lacZ* signals were primarily present in the granular layer of the dentate gyrus and pyramidal cell layer of the hippocampus proper. **I:** X-Gal stained choroid plexus was observed in the brain ventricle. **J-L:** The cerebellum displays a strong *lacZ* staining in the Purkinje cell layer and granule cell layer. Brains from *TRPM3*^{+/+} mice didn't show any β -galactosidase activity (data not shown). **Abbreviations:** CA, Cornu Ammonis; Chp, choroid plexus; DG, dentate gyrus; EP, ependyma; GL, granule cell layer; GrDG, granule cell layer of the dentate gyrus; HP, hippocampus; Lp, lamina propria; ML, molecular layer; MoDG, molecular layer of the dentate gyrus; PL, Purkinje cell layer; PoDG: polymorph layer of the detate gyrus; PyL: pyramidal cell layer; PyC: Purkinje cells; WM, white matter.

images were taken using an Axiovert 200M inverted microscope (Section: 2.2.6.2).

In brain cryosections, strong β -galactosidase activity was seen in the cerebral cortex (layers I, IV, V and VI, Figure: 3.19A-B), dentate gyrus (granule cell layer, Figure: 3.19C, E-F), hippocampus proper CA1-CA3 (pyramidal cell layer, Figure: 3.19C-H), choroid plexus epithelium (Figure: 3.19C, D, I, J), ependyma (Figure: 3.19C, D) and cerebellum (Purkinje and granule cell layers, Figure: 3.19K, L).

The adult mouse retina exhibited strong *lacZ* signals in the ganglion cell layer and inner nuclear layer. Weak β -galactosidase activity was also present in the outer plexiform layer (Figure: 3.20).

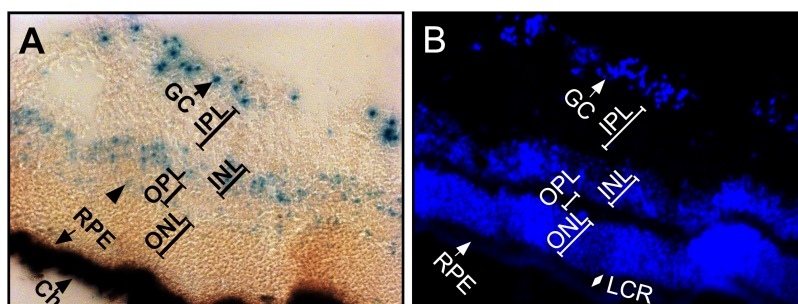


Figure 3.20: *LacZ* gene expression of mTRPM3 in the retina

Histochemical analysis of the retina of adult *lacZ* transgenic mice with X-Gal. **A:** *LacZ* staining was located in the ganglion cell, inner nuclear and outer plexiform layers (arrowhead). **B:** The arrangement of retinal layers was shown using DAPI counterstaining. Retina from WT mice did not show any β -galactosidase activity (data not shown). **Abbreviations:** Ch, choroid; GC, ganglion cell layer; INL, inner nuclear layer; IPL, inner plexiform layer, LCR, layers of rods and cones; ONL, outer nuclear layer; OPL, outer plexiform layer; RPE, retinal pigment epithelium.

Cryosections of the stomach, duodenum, jejunum, ileum and colon were investigated to assess the *lacZ* gene expression in the gastrointestinal tract. Histochemical analysis revealed that *lacZ* staining is restricted to the structure which lies between the circular and longitudinal layers of the muscularis externa (Figure: 3.21). In order to confirm whether it is neurogenic, a neuronal marker anti-MAP2 antibody [198] was applied. In double-labeling experiments, X-Gal positive cells and MAP2 stained cells colocalized (Figure: 3.21K, L). Therefore, it is likely that TRPM3 is expressed in the myenteric plexus in the gastrointestinal tract. Using the β -galactosidase assay, the *lacZ* gene expression was also detected in the

observed in HEK-293 cells (data not shown) and the low amounts of TRPM3 expression detected in Northern and Western blots, these sparse blue precipitates imply a low TRPM3 expression. Therefore, sections were routinely incubated with X-Gal for 24 hr.

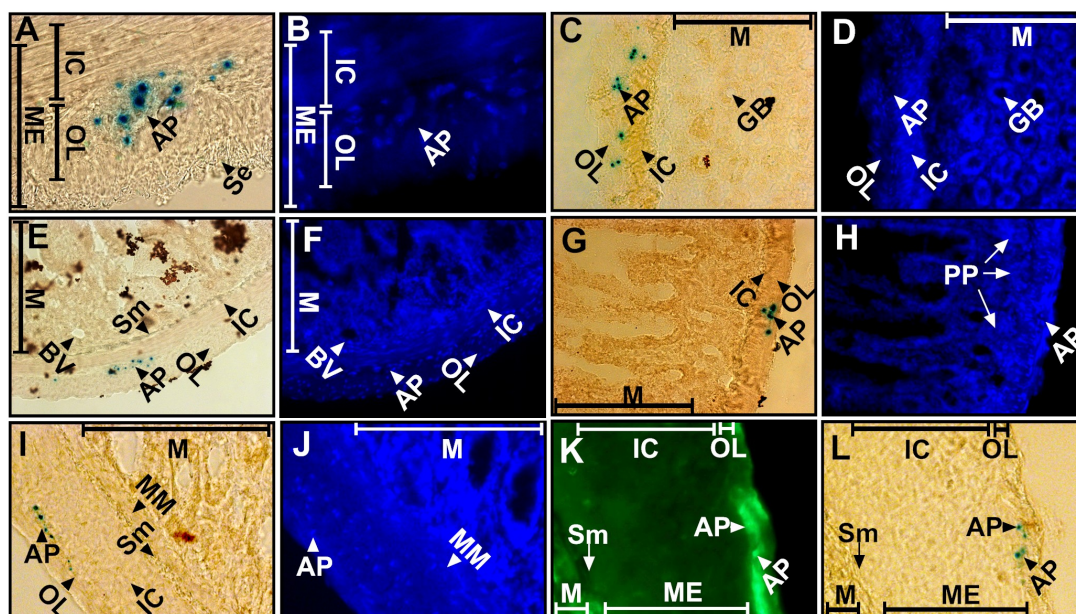


Figure 3.21: *LacZ* gene expression of mTRPM3 in the gastrointestinal tract
 Cryosections of the stomach (A-B), duodenum (C-D), jejunum (E-F), ileum (G-H) and colon (I-J) from adult *TRPM3*^{-/-} and *TRPM3*^{+/+} mice (data not shown) were histochemically stained with X-Gal, and counterstained with DAPI. Auerbach's plexus between the circular and longitudinal components of the muscularis externa showed intense *lacZ* staining. K-L: Cryosection of a part of intestinal tract was double-stained with X-Gal and anti-MAP2 antibody. Colocalization of X-Gal staining and MAP2 immunostaining was observed (arrowhead). **Abbreviations:** AP, Auerbach's plexus; BV, blood vessels; IC, inner circular muscle; GB, Brunner's glands; M, mucosa; ME, muscularis externa; MM, muscularis mucosae; OL, outer longitudinal muscle; PP, Peyer's patch; Se, serosa; Sm, submucosa.

islet of Langerhans, but not in the cells and tissues of liver of adult *lacZ* transgenic mice (Figure: 3.22).

In the reproductive system, *lacZ* positive cells were observed in the testis (Figure: 3.23A-D) and uterine tubes (Figure: 3.23M-P), but not in the uterus (Figure: 3.23I-L) and ovary (Figure: 3.23E-H). In the testis, β -galactosidase activity was found in the cells of the seminiferous tubules, but not in the Leydig cells in the interstitial tissue. In addition, X-Gal-stained cells were also not present in the tunica vaginalis (data not shown). In the uterine tubes, *lacZ* stainings are present in the mucosal layer composed of ciliated cells and secretory (peg) cells.

The *lacZ* staining analysis revealed *lacZ* gene expression in the skin, heart, kidney, lung

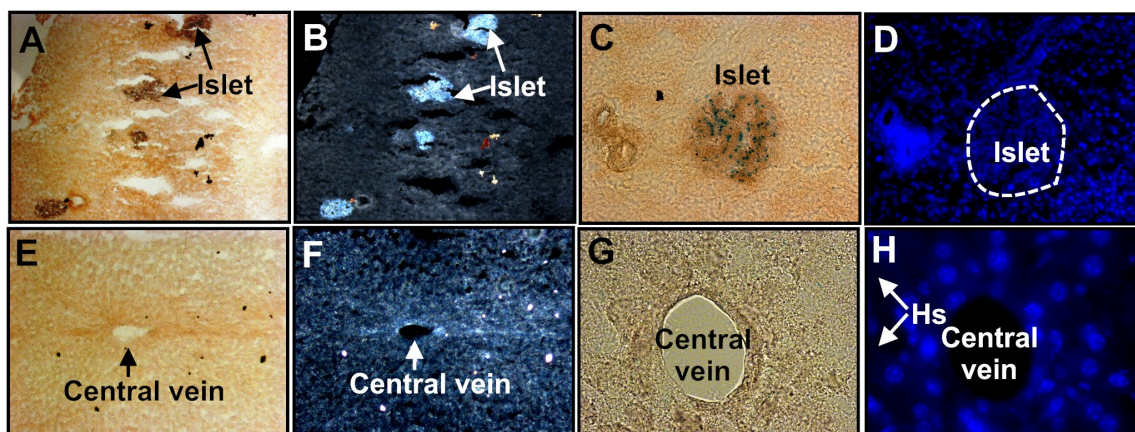


Figure 3.22: *LacZ* gene expression of mTRPM3 in the liver and pancreas

Cryosections of pancreas and liver from adult TRPM3 knock-out and wild-type mice (data not shown) were histochemically stained with X-Gal, and counterstained with DAPI. **A-D:** *LacZ* positive cells in islets of Langerhans are shown (A, C). The islets of Langerhans are shown by darkfield microscopy (B) and DAPI counterstaining (D). **E-H:** No β -galactosidase activity was observed in the liver. **Abbreviation:** Hs, hepatic sinusoids.

and spleen. Single X-Gal-stained cells were detected in the epidermis. However, X-Gal stained cells were not present in the sebaceous gland in the dermis (Figure: 3.24A-D). In the heart, sparse *lacZ* signals were found in a specific structure localized between myocardial tissues (Figure: 3.24E-H). In the kidney cortex, positive staining was observed in the renal tubules and glomerulus (Figure: 3.24I-L, arrowhead). In the conducting airways, sparse positive *lacZ* signals were detected between the two bronchial cartilage plates (Figure: 3.24M-P, arrowhead) or two tracheal cartilage plates (data not shown), but was not found in the other cell types or tissues (such as bronchioles and alveoli, data not shown). An X-Gal-stained cryosection through the spleen shows that the positive *lacZ* staining was mainly present in the fibrous trabeculae, but not in the other splenic cells and tissues including trabecular vessels which ramify in the trabeculae throughout the organ (Figure: 3.24Q-T, arrowhead).

In summary, in the adult mouse, TRPM3 is predominantly found in the nervous system such as cortex, choroid plexus, cerebellum, hippocampal formation, myenteric (Auerbach's) plexus, and retina. In order to investigate the origin of the TRPM3 expression profiles, we did similar staining with mouse embryos at different embryonic stages.

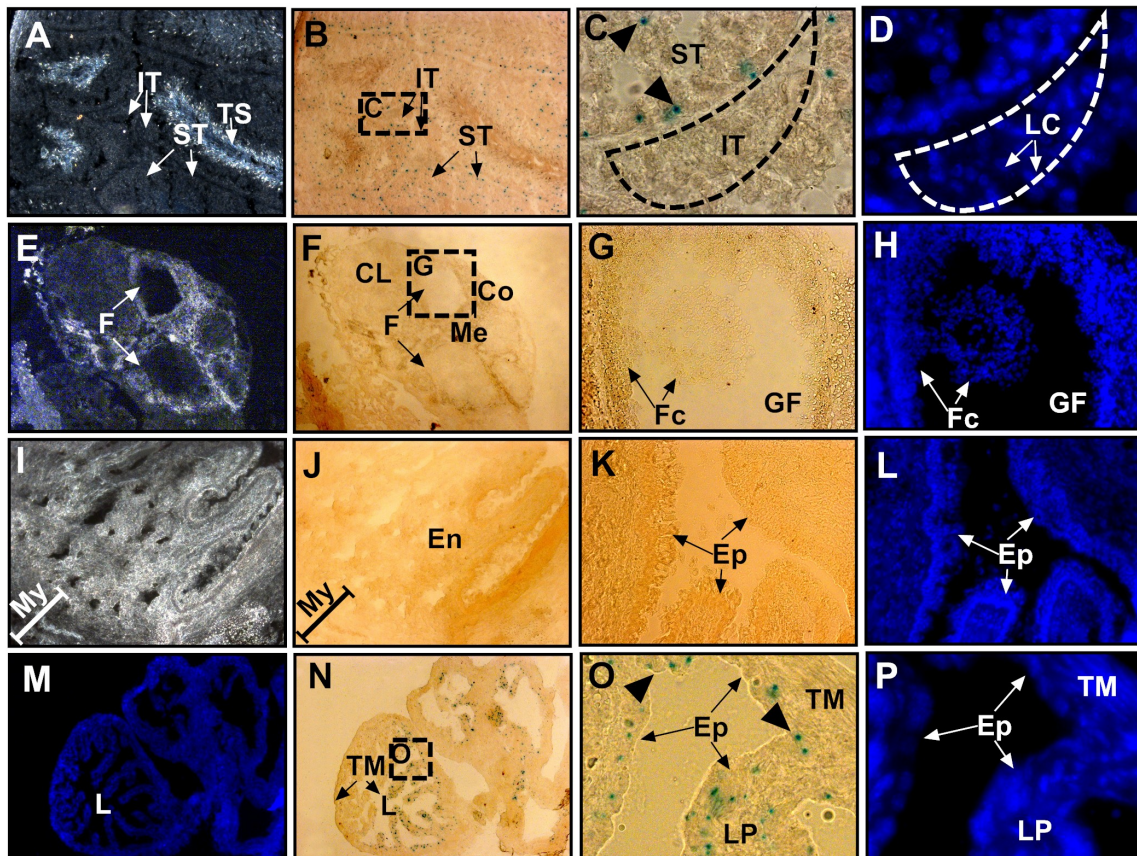


Figure 3.23: *LacZ* gene expression of mTRPM3 in the reproductive system

Adult TRPM3 wild-type mice served as a negative control (data not shown). Darkfield microscopy (A, E, I) and DAPI counterstaining (D, H, L, M, P) were applied to demonstrate to the cytoarchitecture of the corresponding tissues. **A-D:** X-Gal positive cells were found in the seminiferous tubules, but not in the interstitial tissue of testis. **E-H:** No positive X-Gal stained cells were observed in the ovary. **I-L:** No positive X-Gal stained cells were observed in the uterus. **M-P:** *LacZ* positive staining was observed in the tunica mucosa layer of the uterine tubes. **Abbreviations:** CL, corpus luteum; Co, cortex; En, endometrium; Ep, epithelium; F, follicle; Fc, follicle cells; GF, Graafian follicle; IT, interstitial tissue; L, lumen; LC, Leydig cells; LP, lamina propria; Me, medulla; My, myometrium; ST, seminiferous tubules; TM, tunica mucosa; TS, tails of spermatozoa.

3.3. Tissue distribution of mouse TRPM3

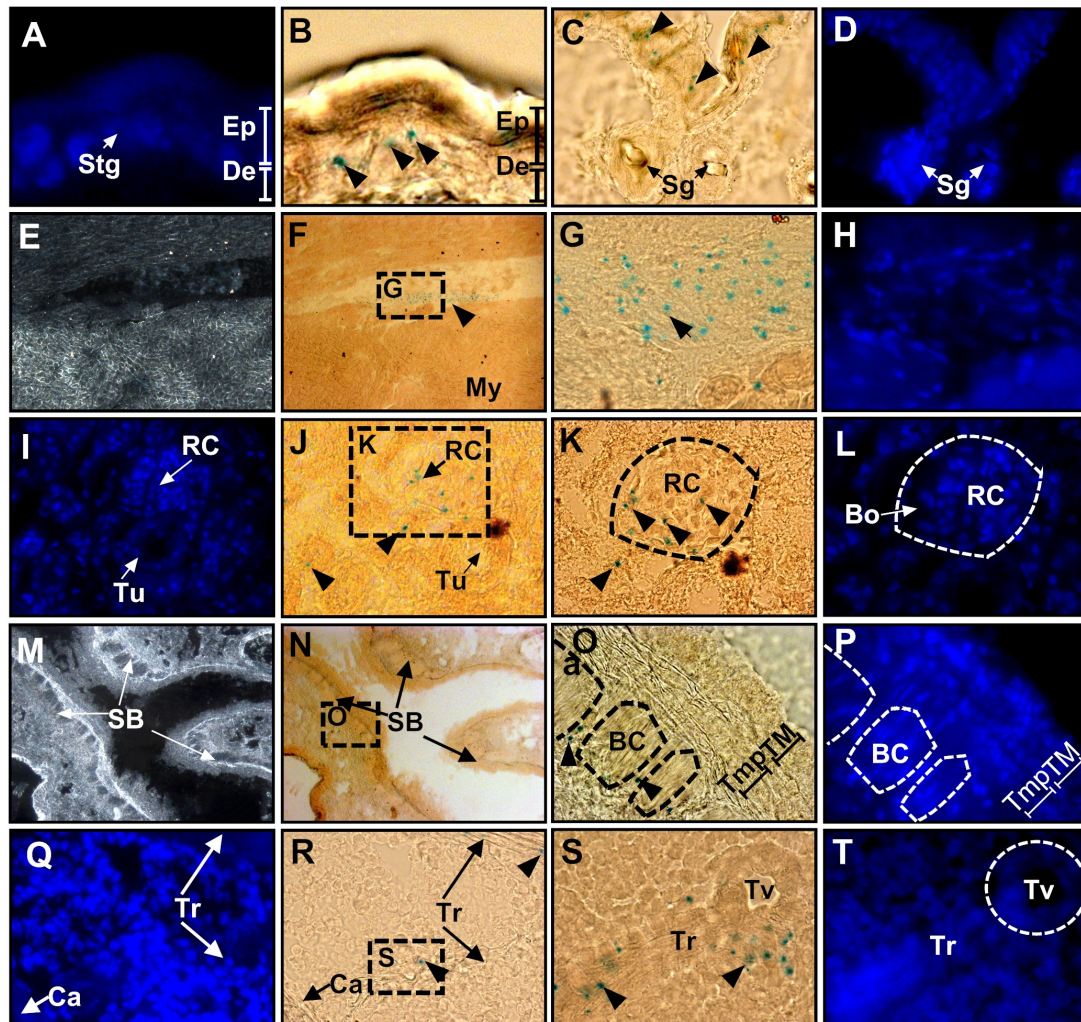


Figure 3.24: *LacZ* gene expression of mTRPM3 in the skin, heart, kidney, conducting airways and spleen

The microanatomical structures of each tissue were shown by means of a darkfield microscopy (Figs E, M) and DAPI counterstaining (Figs A, D, H, I, L, P, Q, T). *LacZ* staining was observed in the epidermis (strata spinosum and basale) (Figs B, C), heart (Figs F, G), kidney (Figs J, K), bronchi (Figs N, O), and spleen (Figs R, S). **Abbreviations:** BC, bronchial cartilages; Bo, Bowman's capsulae; BR, bronchus; Ca, capsule; De, dermis; Ep, epidermis; My, myocardium; RC: renal corpuscle; SB, secondary bronchi; Sg, sebaceous gland; Stg, strata spinosum and basale; TM, tunica mucosa; Tmp, tunica muscularis propria; Tr, trabeculae; Tu, tubules; Tv, trabecular vessel.

3.3.3.2 Tissue distribution of *TRPM3* during mouse development

Mouse embryos were used to further study m*TRPM3* tissue distribution. The embryo *lacZ* staining identifies tissues in which the gene of *TRPM3* is expressed.

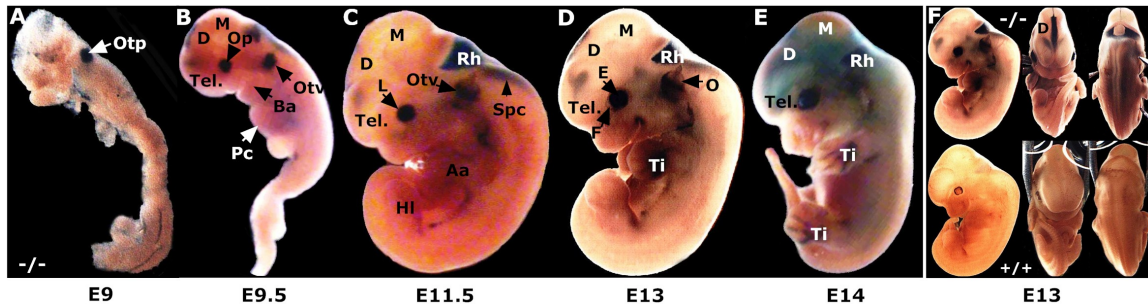


Figure 3.25: *LacZ* staining of whole *TRPM3*^{-/-} mouse embryos

LacZ staining in whole mouse *TRPM3*^{-/-} embryos (E9, 9.5, 11.5, 13, 14). **A:** At E9, staining was found in otic pit. **B-C:** Besides otic vesicle, *lacZ* expression was also present in the regions of optic vesicle, diencephalic roof and rhombencephalon. **D:** The X-Gal-stained digits of footplates are clearly seen. The pinnae were developed, and the intense staining was detected in the eye, diencephalic roof, dorsocaudal telencephalon, rhombencephalon and indented anterior footplate. **E:** Except for mesencephalon, strong staining was found throughout the brain. Stained separated toes were clearly observed in this stage. **F:** In contrast to the wild-type mouse embryo (bottom), the *TRPM3*^{-/-} mouse embryo (E13) showed significant *lacZ* gene expression. But no evident morphological changes were observed between *TRPM3*^{+/+} and *TRPM3*^{-/-} mice. **Abbreviations:** Aa, forelimb bud; Ba, branchial arch; D, diencephalon; Ey, eye; F, choroid fissure; HI, hindlimb bud; L, lens vesicle (just closed); M, mesencephalon; Nc, neopallial cortex; O, pinna; Op, optic vesicle; Otp, otic pit; Otv, otic vesicle; Pc, pericardial region; Rh, rhombencephalon; Spc, spinal cord; Tel, telencephalon; Ti, separated toes.

Whole embryo *lacZ* staining We started out doing whole embryo staining by dissecting embryos at stage E9 (embryonic day 9) from pregnant *TRPM3* mutant mouse mothers. The embryos were fixed with glutareldahyde (0.2% (v/v)), stained with X-Gal (1 mg/ml), and visualized using an Axiovert 200M inverted microscope (Carl Zeiss). The β -Galactosidase activities in embryonic *TRPM3*^{-/-} mice were observed in the otic pit region at E9 (Figure: 3.25A). Besides the otic pit/vesicle (Figure: 3.25A-C), intense *lacZ* staining was also found in the region of the ear (Figure: 3.25D, E), eye (Figure: 3.25B-E), rhombencephalon (Figure: 3.25B-E), diencephalic roof and dorsocaudal telencephalon (Figure: 3.25B-D), and the limb buds (Figure: 3.25D, E). Weak staining was also seen in the region of the telencephalon and spinal cord (Figure: 3.25C-D). At stage E14, *lacZ* staining was detected in the brain with the exception of the mesencephalon (Figure: 3.25E). Compared to wild-type

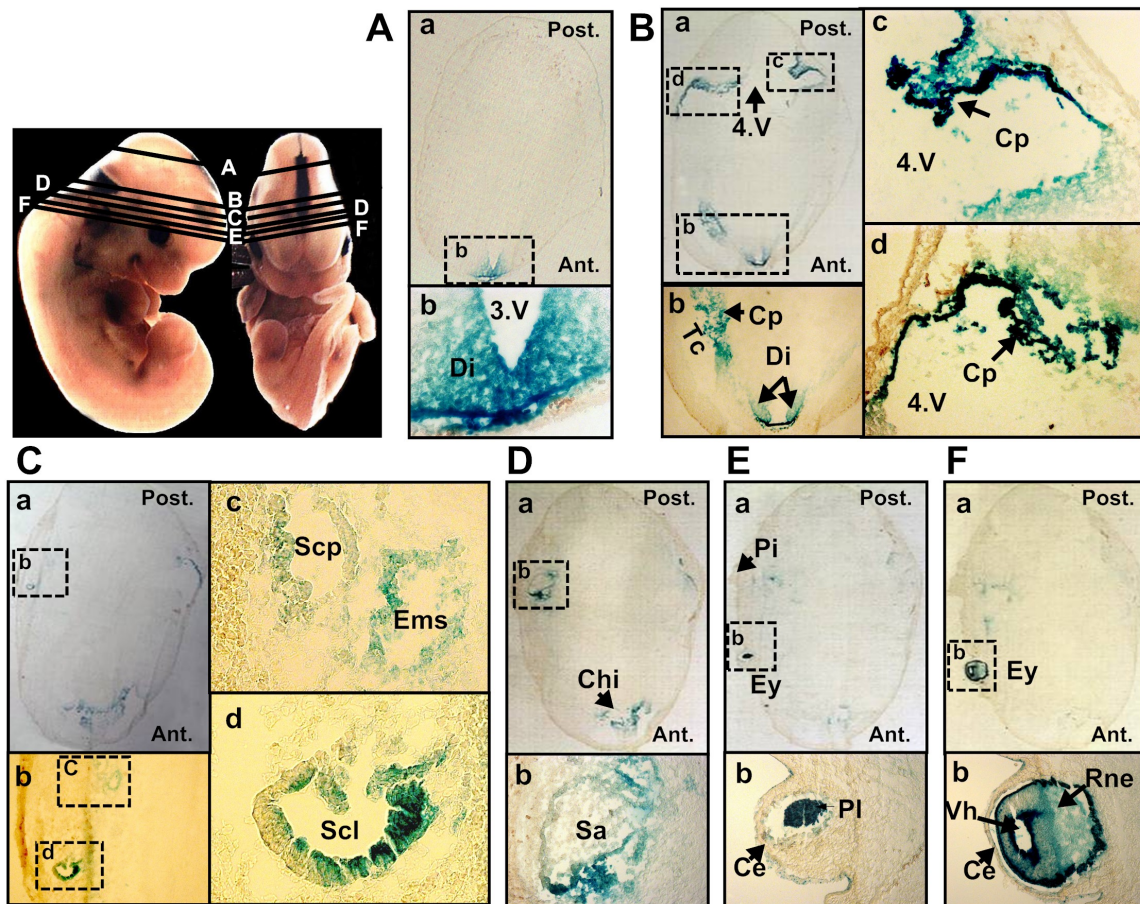


Figure 3.26: *TRPM3-lacZ* expression in frozen cranial sections at stage 13

The level of each cross-section is represented in the embryo (E13) at the *top left*. **A:** At the level of the diencephalon and mesencephalon, *lacZ* expression was mostly present in the dorsocaudal telencephalon and the roof of the diencephalon (A-b). **B:** *LacZ* staining was observed in the choroid plexus which projects into the 4th ventricle forming finger-like evagination (B-c and B-d), and originates from the medial wall of the lateral ventricle (B-b). **C-D:** X-Gal positive cells were detected in the inner ear tissues such as the endolymphatic sac, posterior semicircular canal (C-c), lateral semicircular canal (C-d), saccule (D-b). **E-F:** The pinna was formed (E-a), and intense staining was found in the pigment (E-b) and neural layers of retina (F-b), and corneal ectoderm (E-b, F-b). **Abbreviations:** 3.V, third ventricle; 4.V, fourth ventricle; Ce, corneal ectoderm; Chi, choroid invagination; Cp, choroid plexus; Di, diencephalon; Ey, eye; Ems, endolymphatic sac; Pi, pinna; Pl, pigment layer of retina; Rne, neural layer of retina; Sa, saccule; Scl, lateral semicircular canal; Scp, posterior semicircular canal; Tc, telencephalic vesicle.

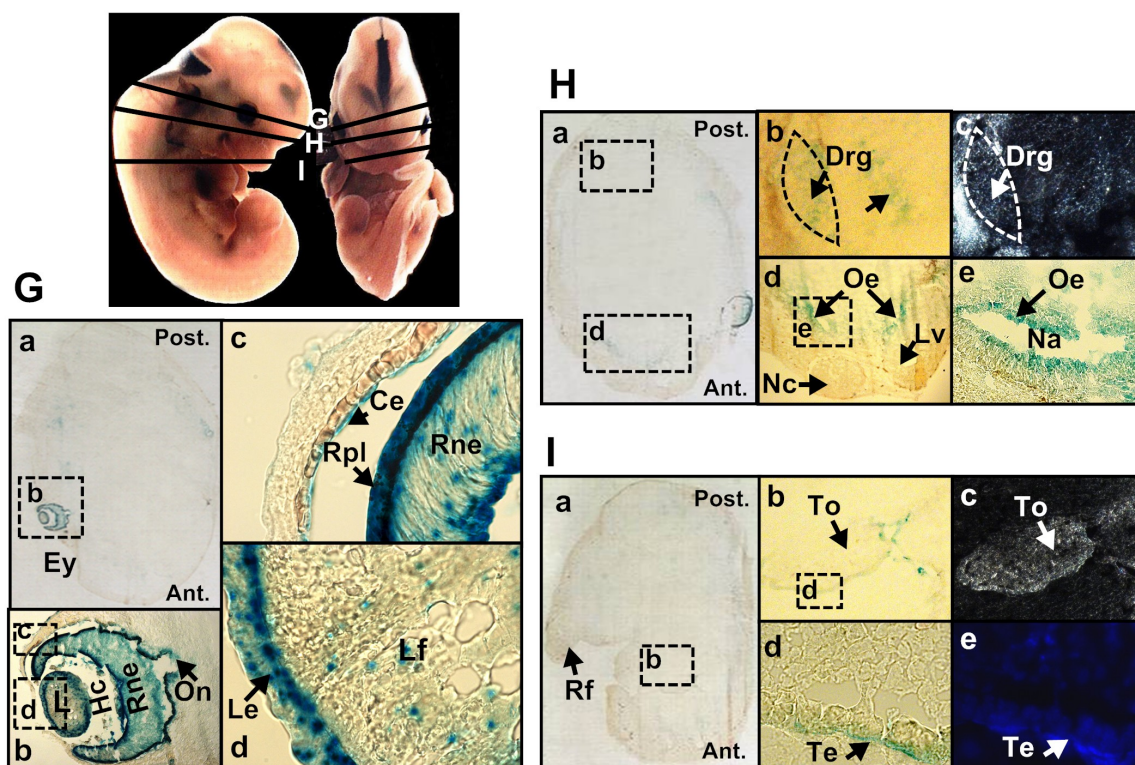


Figure 3.27: *TRPM3-lacZ* expression in frozen cranial and cervical sections at stage 13

The level of each cross-section is represented in the embryo (E13) at the *top left*. **G:** At the level of the eye, high level of β -galactosidase activity was observed in the lens and retina. The lumen of the lens vesicle has disappeared owing to the elongation of the lens fibers (d). The lens epithelial and fibril cells, the retina (pigment and neural layers) were intensively stained by X-Gal (b-d). **H:** Using X-Gal staining, intense expression of *TRPM3* was observed in the olfactory epithelium in the lumen of the primitive nasal cavity, and the low expression of *TRPM3* was found in the dorsal root ganglion and spinal cord (arrow). Darkfield microscopy clearly showed the dorsal root ganglions (c). **I:** Low expression of *TRPM3* in the epithelium of the tongue was revealed by X-Gal staining. Darkfield microscopy (c) and counterstaining with DAPI (e) showed the tongue structure and the epithelium of the tongue, respectively. **Abbreviations:** Ce, corneal ectoderm; Cp, choroid plexus in roof of fourth ventricle; Drg, dorsal root ganglion; Ey, eye; En, external naris; Hc, hyaloid cavity; L, lens; Le, lens epithelium; Lf, lens fibers; Lv, lateral ventricle; Na, lumen of primitive nasal cavity; Nc, neopallial cortex; Oe, olfactory epithelium; On, unmyelinated nerve fibers within optic stalk; Rf, right forelimb; Rne, neural layer of retina; Rpl, pigment layer of retina; Te, epithelium of tongue; To, tongue; Vh, vitreous humour.

embryos (Figure: 3.25F, bottom), *TRPM3*^{-/-} embryos (E13) displayed a significant *lacZ* expression pattern. However, there were no evident morphological changes between them. This result indicates that *TRPM3* gene expression in mouse embryos is restricted only to some specific regions such as the brain, eye and ear.

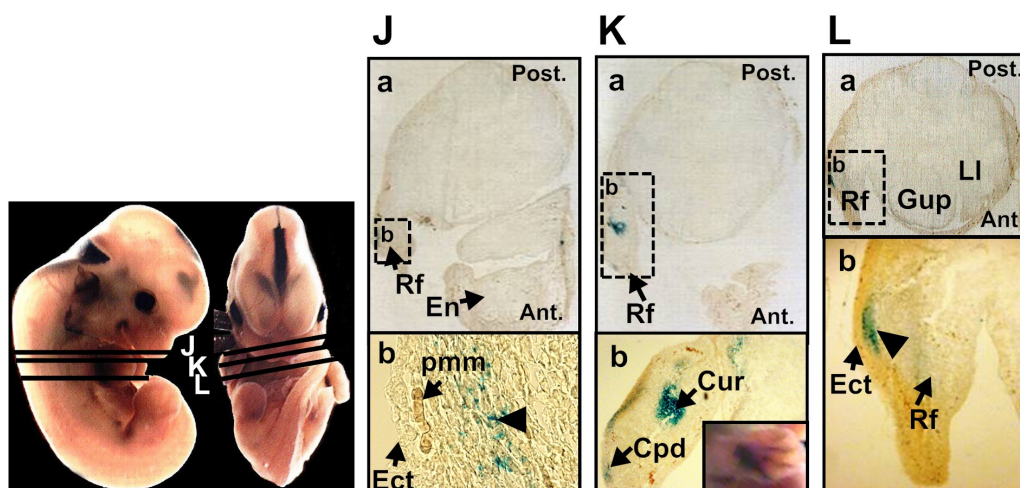


Figure 3.28: *TRPM3*–*LacZ* expression in frozen thoracic sections at stage 13

The cross-section levels of the forelimb in the embryo (E13) are represented at the left. The blue staining indicates β -galactosidase catalysis of the X-Gal substrate. **Section J–L:** Intense X-Gal staining was present in the regions beneath the outer ectoderm (arrowhead, J-b and L-b) and cartilage primordia of the ulna/radius and digital bones (K-b). No X-Gal-stained cells of premuscle mass were detected (arrow, J-b). **Abbreviations:** Cur, cartilage primordium of the right ulna/radius; Cpd, cartilage primordium of the digital bones; Ect, ectoderm; En, external naris; Gup, primitive gut; Ll, left lobe of liver; Pmm, premuscle mass of proximal extensor group of muscles; Rf, right forelimb.

Histological analysis of *lacZ* activity distribution in frozen mouse embryonic sections (E13) Based on the *lacZ* expression observed in the whole mouse embryos (Section: 3.3.3.2), frozen cryostat sections which include the regions showing intense *lacZ* signals were made (10 μ m thickness). According to the tissue distribution of m*TRPM3* previously reported [1, 92, 157], *TRPM3*^{-/-} mouse embryos at stage E13 was studied because this stage of mouse development is characterized by the appearance of the choroid plexus and the disappearance of the lens lumen [93]. Sectioned embryo stained for X-Gal activity (blue) revealed that *TRPM3* was highly expressed in the choroid plexus (Figure: 3.26A-B), inner ear (Figure: 3.26C-D), eye (retina and lens, Figure: 3.26E-F, 3.27G), olfactory epithelium

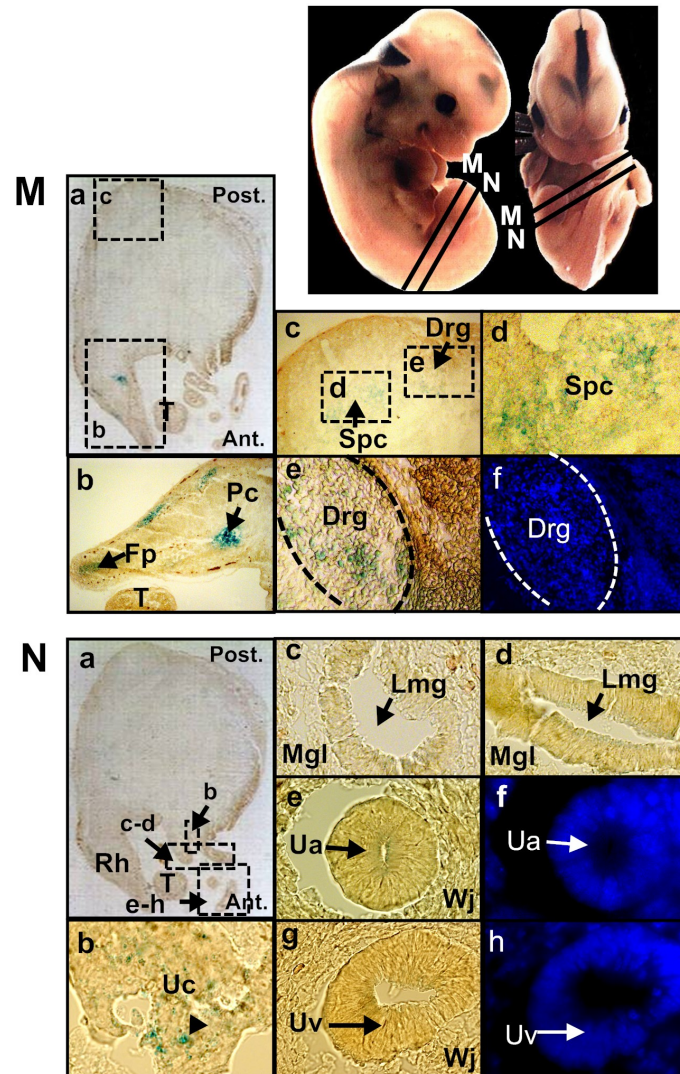


Figure 3.29: TRPM3–*LacZ* expression in frozen Caudal sections at stage 13

The cross-section levels of the hindlimb in the embryo (E13) are represented at the *top right*.

Section M: TRPM3 expression was evident in the hindlimb (b). Weak *lacZ* signals were also found in the dorsal root ganglia and spinal cord (c-f). Dapi was used for counterstaining (f).

Section N: Paired umbilical arteries and one umbilical vein embedded in Wharton’s jelly within the umbilical cord are shown (a). β -galactosidase activity was present in the umbilical ligament (arrowhead, b), but not in the endothelia of the midgut (c-d) and endothelia of umbilical vessels (e-h). Dapi was used for counterstaining. **Abbreviations:** Drg, dorsal root ganglion; Fp, foot plate; Lmg, lumen of midgut; Mgl, mitgut loop; Pc, precartilag condensation within hindlimb; Rh, right hindlimb; Spc, spinal cord; T, tail; Ua, umbilical artery; Uc, umbilical ligament; Uv, umbilical vein; Wj, Wharton’s jelly.

3.3. Tissue distribution of mouse TRPM3

(Figure: 3.27H) and cartilage primordium of developing limb buds (Figure: 3.28, 3.29M). A low level TRPM3 expression was also observed in the dorsal root ganglia (Figure: 3.27H), the epithelium of tongue (Figure: 3.27I), the spinal cord (Figure: 3.29M) and the umbilical ligament (Figure: 3.29N).

Table 3.3: *LacZ* gene expression in the *lacZ* transgenic TRPM3^{-/-} mouse

Channel	Tissue distribution	Embryonic origin ^a
Neural	Cerebral cortex: layers I, IV, V and VI	Neural tube, P84
	Cerebellum: Purkinje and granule cell layers	Neural tube, P84
	Hippocampal formation: granular layer of the dentate gyrus, pyramidal layer of the hippocampus proper	Neural tube, P7
	Ependyma	Neural tube, E12
	Choroid plexus epithelium	Neural tube, E8.5
	Spinal cord	Neural tube
	Dorsal root ganglia	Neural crest
	Myenteric (Auerbach's) plexus	Neural crest, E9.5-14.5
others	Epidermis: melanocytes or Merkel cells	Neural crest, E13
	Heart: autonomic nervous tissues, connective tissues, or constitutive/ectopic cardiac skeletal elements	Neural crest, E8.5
	Eye (retina): neural layer (ganglion cell and inner nuclear layers), pigment layer	Neural tube, E9.5
Sensory	Eye (lens): epithelium and fibers	Surface epithelium, E10
	Eye: corneal epithelium	Surface epithelium, E11.5
	Inner ear: endolymphatic sac	Surface epithelium, E10
	Inner ear: semicircular canals	Surface epithelium, E13
	Olfactory epithelium	Surface epithelium, E10.5
Epithelial	Uterine tubes: mucosa epithelium	Coelomic wall epithelium
	Islets of Langerhans	Endoderm epithelium, P70
	Limb buds: precartilaginous primordia	Mesenchymal-epithelial transformation, E12
	Testis: spermatogenic cells or Sertoli cells	Seminiferous epithelia, E14
Others ^b	kidney, lung, spleen, and umbilical ligament	

^a<http://www.mouseatlas.org/data/mouse/devstages>. E: embryonic day; P: postnatal day.

^bThe cell types have not been determined

In summary, like the tissue expression observed in the adult mouse, TRPM3 was primarily detected in the nervous and sensory systems of the mouse embryos such as choroid plexus epithelium, neural and pigment layers of retina, inner ear, and olfactory epithelia. Based on the expression pattern observed, the main role of mTRPM3 is likely to be in the nervous and sensory systems. Therefore, after a general analysis of the phenotype, we briefly looked in more detail at an aspect of sensory and nervous function of TRPM3.

3.4 Phenotypic analysis of a TRPM3^{-/-} mouse model

A major goal of this work was to investigate the phenotype of TRPM3 by preparing a knockout allele. After characterizing TRPM3 knock-out mouse model, we focused on the following questions: 1) is the TRPM3^{-/-} mouse viable?; 2) what is its general appearance such as coat color, posture and gait?; 3) does the TRPM3^{-/-} mouse have physiological defects, especially neuronal and/or sensory defects?

3.4.1 Genotyping and genetic background correction

Before performing a phenotypic analysis, the TRPM3 mutant mice were to be genotyped and tested for the presence of the mTRPM3 gene, mRNA and protein. Due to the mTRPM3 knockout procedure, the original lines carried a number of genetic backgrounds. For example, they have 129S5Ev^{Brd} (A/A) and B6(Cg)-Tyr^{c-2J}/J (a/a; c/c) genetic background (Section: 2.2.8.1). It is known that the Agouti gene is involved in controlling melanocytic differentiation in the skin in a paracrine manner [201] and mediating α -melanocyte-stimulating hormone signaling pathway [122, 241], and the tyrosinase gene plays a critical role in the melanin production [18]. In TRPM3 *lacZ* transgenic mice, the tyrosinase gene is mutated (G²⁹¹→T²⁹¹). Therefore, to study the roles of mTRPM3 in the visual system (*e.g.*, eye pigment cells) and the melanocytes, it was necessary to remove these mutations.

In order to obtain mice heterozygous for the TRPM3 null allele, we mated two heterozygotes (TRPM3^{+/-}) with each other to produce an F₁ generation. Theoretically, the F₁ population will follow the principles of Mendelian segregation, resulting in 1/4 homozygous mutants (TRPM3^{-/-}), 2/4 heterozygotes (TRPM3^{+/-}), and 1/4 homozygous wild-type (TRPM3^{+/+}). For genotyping and genetic background isogenization, touchdown PCR was applied (Sections: 2.2.8.2 and 2.2.8.2). The homozygous TRPM3 knock-out mice (m/m) were identified by using primer pairs against the gene trap insertion (P_{Neo}), and primer pairs against wild-type allele (P_{Wt})⁵ (Figure: 3.31A, lane IV). Furthermore, Western blots confirmed that the knockout mice lack TRPM3 protein expression (Section: 3.3.2.2). Homozygous Agouti mice (A/A) were selected from the homozygous TRPM3 knockout mice using primer pairs against the non-Agouti (a) sequence (Figure: 3.31B, lane III). Among the homozygous Agouti TRPM3 knockout mice (A/A; m/m), the homozygous non-albino

⁵Four primer pairs (not shown) against different positions in wild-type allele were used to ensure a homologous genotype of TRPM3 knockout mouse.

3.4. Phenotypic analysis of a *TRPM3*^{-/-} mouse model

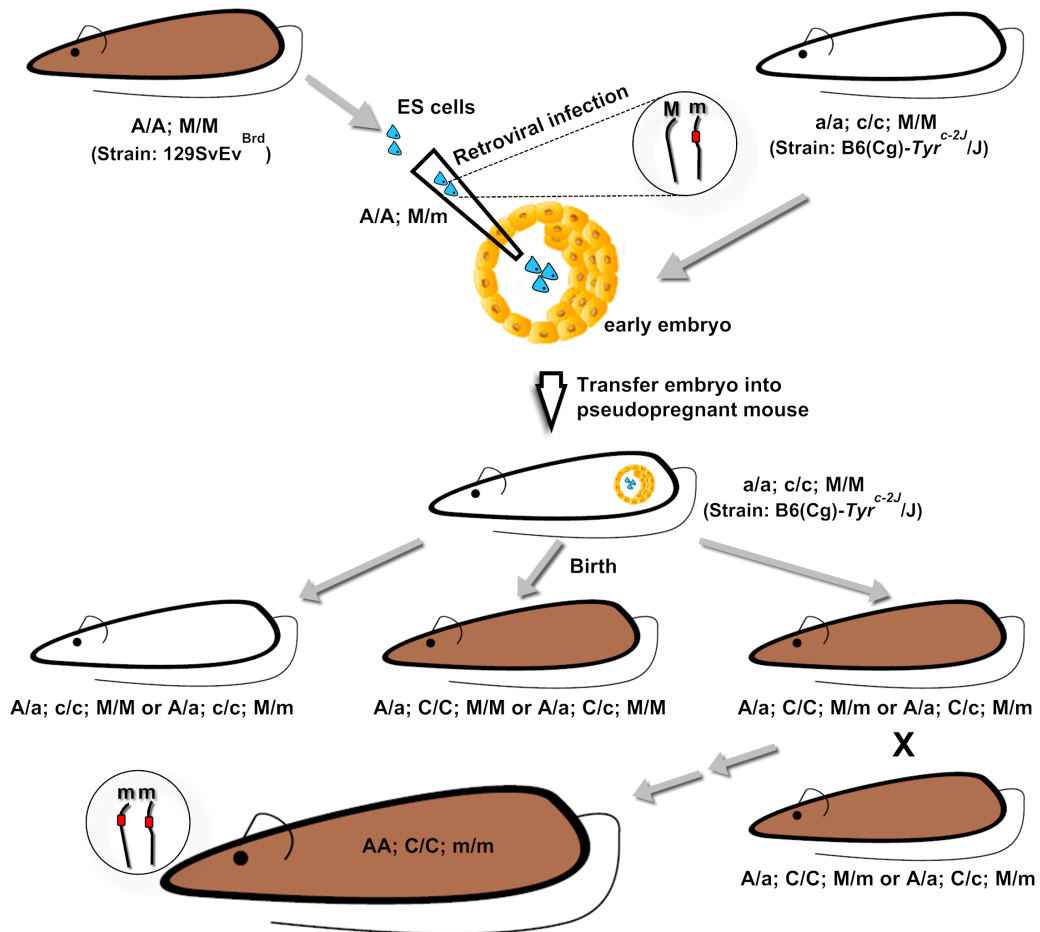


Figure 3.30: Generation of homozygous *Agouti* and non-albino *TRPM3*^{-/-} mouse
 The *TRPM3* mutant allele (*M/m*) introduced by gene trapping is retrovirally infected into the strain 129S5Ev^{Brd}-derived ES cells (*A/A; M/M*). After the ES cells have been injected into the early embryos, the embryos are intermediately transferred to the recipient female mice (strain B6(Cg)-*Tyr*^{c-2J}/J (*a/a; c/c; M/M*)). The progeny mice which are heterozygous for the *TRPM3* mutation were mated with each other to produce homozygous *Agouti* and non-albino *TRPM3*^{-/-} mice

mice (*C/C*) was identified through DNA amplification and sequencing, by which the non-mutated tyrosinase sequence shows only one distinct peak at position 540 (Figure: 3.31C, bottom). Once the homozygous *Agouti* and non-albino *TRPM3*^{-/-} mice (*A/A; C/C; m/m*) were generated, they were used for some phenotypic analyses, *e.g.*, the visual test.

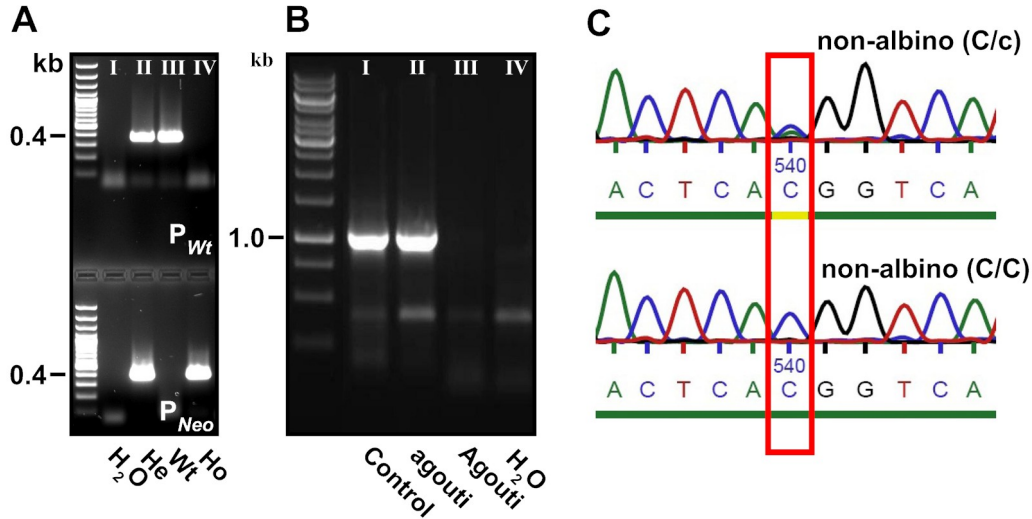


Figure 3.31: Generation of homozygous *Agouti* and *non-albino* *TRPM3*^{-/-} mice using genotyping and DNA sequencing

A: Primer pairs against the wild-type allele (P_{Wt}) and the gene trap insertion (P_{Neo}) were used to identify homozygous *TRPM3* knock-out mice (m/m). Compared to wild-type (lane III) and heterozygous (lane II) mice, homozygous *TRPM3* knock-out mice were identified using P_{Neo} primer pairs, but not by using P_{Wt} primer pairs (lane IV). **B:** Homozygous *Agouti* mice (A/A) were selected from homozygous *TRPM3* knockout mice by using primer pairs against non-*Agouti* (a) sequence. Thus, no signals of homozygous *Agouti* mice were observed in the DNA gel (lane III). H₂O (lane IV) and DNA sequence of an albino mouse (lane I) were used as negative and positive controls, respectively. **C:** The non-mutated tyrosinase sequence of homozygous non-albino mouse (C/C) was found through DNA amplification and sequencing. The sequence has only one peak at position 540 (bottom) in comparison with it in the heterozygous non-albino mouse (C/c, top). **Abbreviations:** P_{Wt} , primers against wild-type allele; P_{Neo} , primers against gene trap insertion; Ho, homozygous; He, heterozygous; Wt, wild-type.

3.4.2 The viability of *TRPM3*^{-/-} mice

To assess the role of *TRPM3* in normal development, *TRPM3*^{+/-} mice were bred with each other. From a total of 204 animals, we observed that homozygous *TRPM3*^{-/-} mice are viable and fertile. *TRPM3*^{+/-} mice have a normal Mendelian ratio of genotypes in the offspring (51:104:49 for *TRPM3* wild-type:heterozygous:homozygous mutant mice), with no gender bias (99:105 for male:female). Thus, although *TRPM3* is highly conserved among the members of *TRPM* subfamily, its loss does not affect its survival.

3.4.3 Morphological observations on *TRPM3*^{-/-} mice

To assess their general health, we monitored the physical appearance of the mice. Both *TRPM3* knock-out male and female mice are indistinguishable from their wild-type and heterozygous littermates by gross observations. The *TRPM3* wild-type, heterozygous and knock-out mice routinely engage in grooming behavior. No differences in coat color (white-bellied agouti) and whisker thickness of mice were observed. The ear pinnae and footpads are pink colored – a sign of good health. The body size and weight of adult mutant mice and their littermate controls were recorded weekly, but no difference was found (data not shown). No abnormalities in posture and gait of *TRPM3*^{-/-} were detected during a 5-minute session in an open field (Figure: 3.32A). No distinct morphological differences between *TRPM3* wild-type and knockout mice were observed at E9, 9.5, 11.5, 13, 14 (Section: 3.3.3.2). In summary, no gross morphological changes were detectable between *TRPM3*^{+/+}, *TRPM3*^{+/-}, *TRPM3*^{-/-} mice. The *TRPM3*^{-/-} mouse is apparently healthy.

3.4.4 Behavioral analyses of the visual ability of *TRPM3*^{-/-} mice

As described above, *TRPM3* is mainly found in nervous and sensory tissues (Section: 3.20). Because behavioral analyses of visual ability can be used to test the neuronal and sensory functions of mice, some basic tests of mouse visual ability such as the visual placing test and visual cliff test were performed.

The visual placing test showed that *TRPM3*^{-/-} mice (n=8) extended their forepaws for landing when they were slowly lowered towards the table surface (Section: 2.2.8.3). This result indicates that the *TRPM3*^{-/-} mouse is not blind. In the visual cliff test, 11 *TRPM3*^{-/-} mice (m*TRPM3*-KO) and 12 *TRPM3*^{+/+} mice (m*TRPM3*-WT) were evaluated for their gross visual ability in a visual cliff apparatus (Figure: 2.9). Each mouse was tested for 10 consecutive trials. Figure 3.32B demonstrates that the mean percent correct was 78.2% (SE ± 4%) for the m*TRPM3*-KO mice and 85.8% (SE ± 2.3%) for the m*TRPM3*-WT mice ($P = 0.11$). These data imply that the *TRPM3*^{-/-} mice show normal visual behavior and have gross visual ability.

In summary, although *TRPM3* is highly conserved, the phenotype of its mutation in the *TRPM3* is minor. The *TRPM3*^{-/-} mouse is viable, fertile and healthy. So far, we can conclude that the *TRPM3*^{-/-} mouse has normal visual ability, motor behavior (*e.g.*, posture and gait) and general appearance (*e.g.*, grooming behavior, coat color, body size and weight).

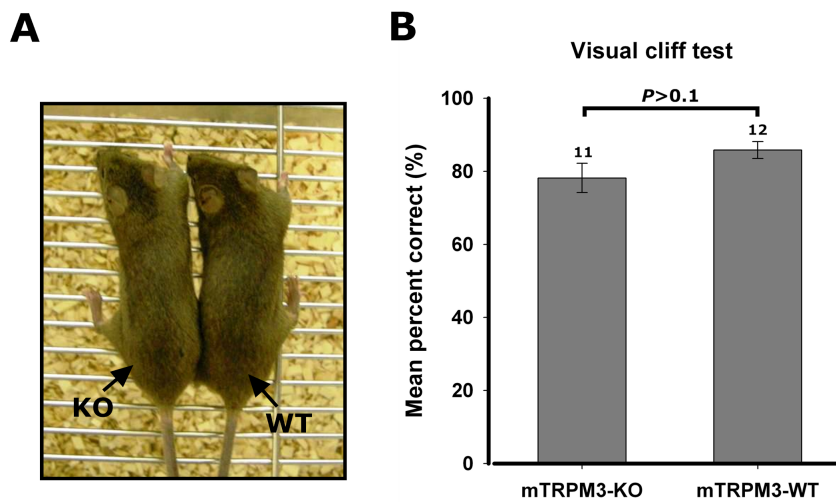


Figure 3.32: Phenotype of *TRPM3*^{-/-} mice and visual testing

A: No distinct differences in general appearance (*e.g.*, coat color) or activity were observed between *TRPM3* knock-out and wild-type mouse (male, 16 weeks). **B:** *TRPM3*^{-/-} mice showed intact gross visual ability as compared to *TRPM3*^{+/+} mice. The percentage of time the mice spent moving on the horizontal plane (“safe” side) was recorded. Values indicate the group means \pm SEM. Unpaired Student’s t-test was used for statistics. The total number of tested mice was shown as numbers above the bars.

Discussion

TRPM3 is a prototypical melastatin channel in the chordate. Several publications concerning its mRNA sequences, splicing variants, function, and expression pattern have been published before and during this work. In many regards, the findings show disagreements, even between mouse and human species. Therefore, there is still considerable need for additional studies to address TRPM3's biological role at the cellular and whole animal level.

We cloned two new TRPM3 splice variants from mouse kidney: mouse TRPM3₁₇₁₉ (mM3₁₇₁₉) and mouse TRPM3₁₃₃₇ (mM3₁₃₃₇). Both variants were functionally expressed in heterologous expression systems. Heterologously expressed mM3₁₇₁₉ and mM3₁₃₃₇ form Ca²⁺-permeable channels that are constitutively active. The molecular structure and channel properties of mM3₁₇₁₉ were analyzed by using different molecular biological approaches. The tissue expression profile of mTRPM3 was established down to the cellular level by means of a *lacZ* TRPM3^{-/-} mouse. Despite TRPM3's high level of conservation and its broad expression, the TRPM3^{-/-} mouse is viable and has similar general appearance to the wild-type mouse.

4.1 Molecular cloning and functional analysis of mM3₁₇₁₉ and mM3₁₃₃₇

4.1.1 Cloning and characterization of mM3₁₇₁₉ and mM3₁₃₃₇

Using 5'-RACE and PCR, mM3₁₇₁₉ and mM3₁₃₃₇ were cloned from mouse kidney. The sequences were analyzed by DNA sequencing and the *ClustalW2* software. The general

structural features of the mM3₁₇₁₉ and mM3₁₃₃₇ sequences include: 1) the first coding exon corresponds to the exons known for human TRPM3₁₃₂₅ and a human full-length TRPM3 splice variant (unpublished data of our group); 2) N-termini contain a large homology region; 3) both variants have conserved pore helices, selectivity loops, and pore structures. The pore lacks a short amino acid stretch (additional 13 amino acid residues) found in previously published splice variants [157]; 4) mM3₁₃₃₇ is 382 amino acid residues shorter than mM3₁₇₁₉ in the C-terminus (Figure: 4.1).

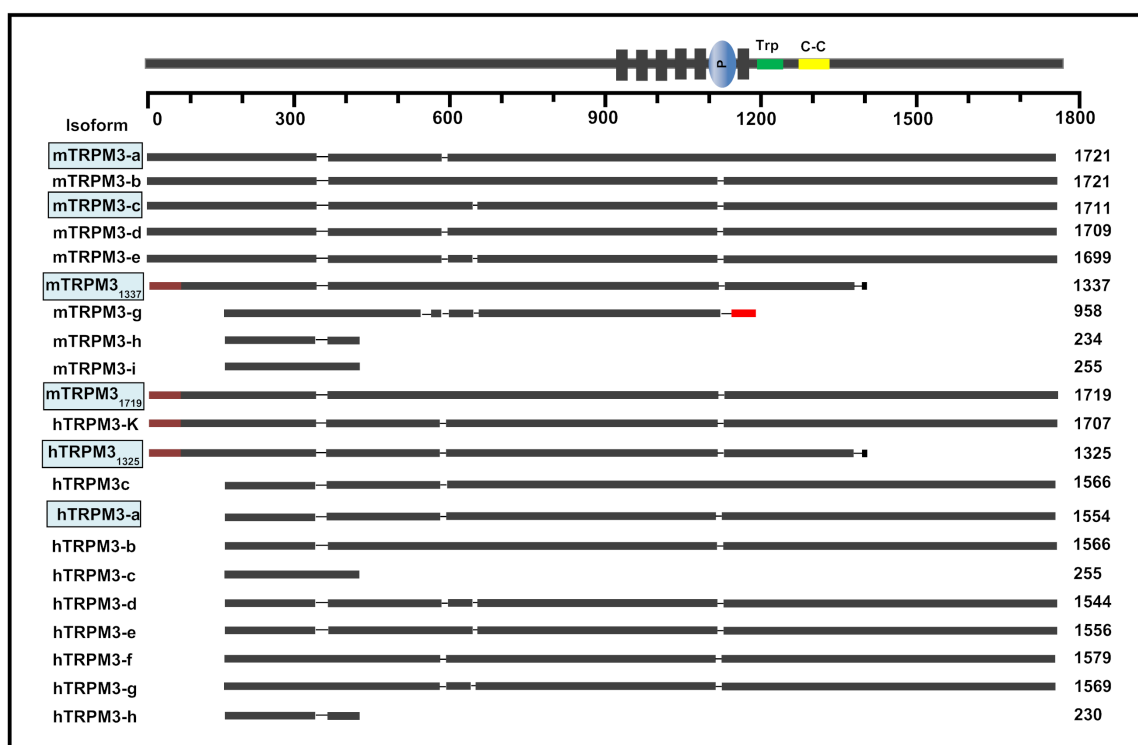


Figure 4.1: TRPM3 protein isoforms

The TRPM3 protein isoforms are basically distinguished by their different N-, and/or C-terminus architectures resulting from alternative splicing. The different amino acid residue sequences are labeled with different colors. The TRPM3 isoforms with channel activity are highlighted with blue bars. Modified from Oberwinkler *et al.* [2005].

To further investigate the functional properties, both variants were subcloned into the pcDNA-3.1 expression vector, and their protein expression tested after heterologous expression in HEK-293 cells. Western blots showed that mM3₁₇₁₉ and mM3₁₃₃₇ had strong protein expression levels in HEK-293 cells. The subcellular localization of mM3₁₇₁₉ and mM3₁₃₃₇ were mainly detected in the intracellular compartments by immuno-staining, although they

were also occasionally found at the plasma membrane. Because this intracellular localization pattern may not reflect the physiological pattern for mTRPM3 expressed *in vivo* [155, 156], and TRPM3 has also been suggested to be involved in the functions of epithelial cells [68, 70], we used MDCK cells as a cell model to study the mM3₁₇₁₉ expression pattern in a differentiated epithelium. Because the differentiated MDCK cells are largely untransfectable and because mM3₁₇₁₉ expression in undifferentiated MDCK cells was also observed to be in the intracellular compartment, we generated a stable MDCK cell line which inducibly expressed HA-tagged mM3₁₇₁₉ (M3^{pGene} cells) to study the subcellular localization of mTRPM3 in the epithelia. When M3^{pGene} cells were grown on a semi-permeable filter to form differentiated cells, protein expression of mM3₁₇₁₉ was exclusively detected in the basolateral plasma membrane.

Many regulatory pathways or agents have been considered to be involved in the regulation of the TRPM3 channel activities. We used aequorin- and/or fura-2-based methods to measure $[Ca^{2+}]_i$ changes in HEK-293 cells expressing mM3₁₇₁₉ and mM3₁₃₃₇, upon the extracellular applications of thapsigargin (1 μ M), hypo-osmolality, D-erythro-sphingosine (20 μ M), Ca²⁺ (10 mM) or PS (50 μ M). In agreement with the studies reported by Grimm *et al.* [2003] and Oberwinkler *et al.* [2005], mM3₁₇₁₉ and mM3₁₃₃₇ are constitutively active and Ca²⁺-permeable. Ca²⁺ steps resulted in the increase in $[Ca^{2+}]_i$. Although mM3₁₇₁₉ and mM3₁₃₃₇ can be activated by PS, which was also observed by Wagner *et al.* [2008] using another TRPM3 isoform, the PS concentration needed for activation (in the micromolar range) is unlikely to be physiologically important for TRPM3. The possibility that similar substances work at lower concentration is further investigation needed. In contrast to the studies published by Grimm *et al.* [2005], Harteneck *et al.* [2007] and Lee *et al.* [2003], D-erythro-sphingosine, hypo-osmolality and thapsigargin did not result in the increased $[Ca^{2+}]_i$ in mM3₁₇₁₉ and mM3₁₃₃₇ expressing cells compared to controls. These differences may be due to different TRPM3 splice variants used in the experiments. Our results indicate that mM3₁₇₁₉ and mM3₁₃₃₇ are not SOC, osmolality-regulated and lipid-activated channels, but are constitutively active Ca²⁺-permeable channels.

We found that TRPM3 is a constitutively active Ca²⁺-permeable channel. Therefore, we wanted to find ions which block Ca²⁺ influx through TRPM3. Based on a close phylogenetic relationship to TRPM7 in which the trace divalent ions play an important role, we tested Cd²⁺, Co²⁺, Cu²⁺, Mg²⁺, Mn²⁺, Ni²⁺, Sr²⁺ and Zn²⁺ to investigate whether they have effects on Ca²⁺ permeation through mM3₁₇₁₉. With the exception of Mg²⁺, other ions

noted above (1 mM) reduced Ca²⁺ influx through mM3₁₇₁₉ (Figure: 3.5). Furthermore, we tested a series of Ni²⁺ and estimated the IC₅₀ value for Ni²⁺ inhibition of Ca²⁺ entry through mM3₁₇₁₉ (Figure: 3.4). However, at high concentrations divalent metal ions (≥ 1 mM) may be toxic to cells in the cell culture [86]. Thus, we conclude that divalent ions probably affect the Ca²⁺ permeation through mM3₁₇₁₉, and Mg²⁺ does not inhibit mM3₁₇₁₉ Ca²⁺ entry at the physiological concentration.

4.1.2 Mutagenesis analysis of the pore

Our experimental results show that mM3₁₇₁₉ is permeable to Ca²⁺. Therefore, we tested whether the pore plays a role in cation permeation through mM3₁₇₁₉. The function of the pore was analyzed using site-directed mutagenesis method.

According to published work on TRP channels and sequence homology to the bacterial K⁺ channel (KcsA channel), the proposed structural basis of the TRPM3 pore region contains a hydrophobic pore helix and a hydrophilic selectivity loop [149, 161, 215, 244]. In TRPM3, the putative pore helix and selectivity loop are proposed to be formed by amino acid residues Pro¹⁰⁶⁰ to Tyr¹⁰⁶⁵ and Ala¹⁰⁷⁰ to Arg¹⁰⁷⁵, respectively [149, 244]. For a visual presentation, a model for mM3₁₇₁₉ pore structure was generated using *ClustalW2* and Swiss Model Workspace software (Section: 1.3.1.2). In this model, the TM5 domain faces the lipid membrane, whereas the TM6 domain lines the pore region. Four TM5–pore–TM6 subunits are thought to form a putative cation–permeable channel (Figure: 4.2) [9, 42, 61, 191, 228, 249].

Based on various studies with TRPM4, TRPM6 and TRPM7, Pro¹⁰⁶⁰, Gly¹⁰⁶⁶, and Asp¹⁰⁷⁴ were replaced by Arg¹⁰⁶⁰, Val¹⁰⁶⁶, and Ala¹⁰⁷⁴, respectively (Section: 3.2.1.1). The functional data for these mutants were obtained from an aequorin–based intracellular Ca²⁺ assay. The experimental findings show that Pro¹⁰⁶⁰ within the pore helix and Gly¹⁰⁶⁶ within the linker between the pore helix and selectivity loop are essential for the mM3₁₇₁₉ channel activity: 1) Pro¹⁰⁶⁰ and Gly¹⁰⁶⁶ are highly conserved among the members of TRPM subfamily; 2) *P1060R* and *G1066V* mutations resulted in a loss of channel function (Section: 3.6); 3) because the Pro¹⁰⁶⁰–induced helix kink may expose of carbonyl oxygens which are in turn capable of binding cations [186], the mutation of Pro¹⁰⁶⁰ may influence the cation binding in mM3₁₇₁₉; 4) because glycine confers a high conformational flexibility on the protein chain and probably plays a role in the loop formation [100, 229], a change in the conformation of the loop of mM3₁₇₁₉ could be induced by the Gly¹⁰⁶⁶ mutation.

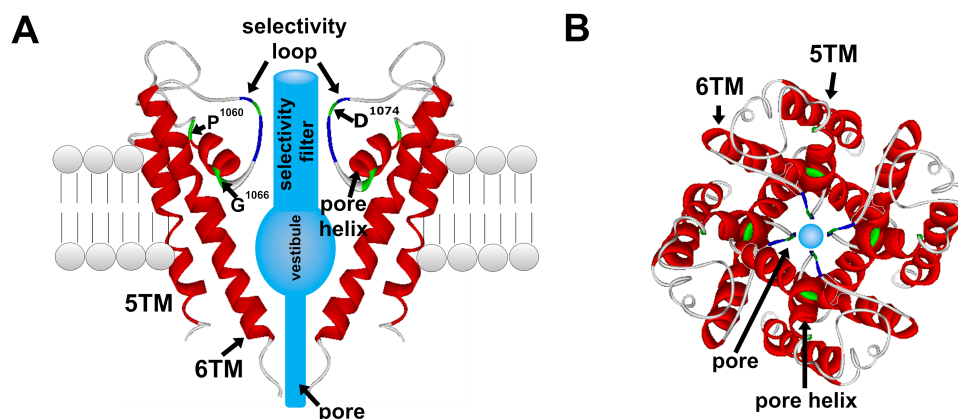


Figure 4.2: Pore model of mM3₁₇₁₉ using KcsA channel as template

A pore model for mM3₁₇₁₉ was generated by using *ClustalW2* software and Swiss Model Workspace [9, 42, 61, 191, 228, 249]. The side (**A**) and top (**B**) views of the mM3₁₇₁₉ pore structure are shown. **A**: The TM5 domain faces the lipid membrane, while the TM6 domain lines the pore region. The amino acid residues in TM5 and TM6 are colored in red. The pore helix, selectivity loop, and amino acids to be mutated (*P1060R*, *G1066V*, *D1074A*) in the pore region are indicated in red, blue, and green, respectively. **B**: A putative cation-permeable channel is formed by 4× the TM5-pore-TM6 domains from four subunits.

The ion selectivity of the channel depends on the structure of the selectivity filter. In the bacterial K⁺ channel, carbonyl oxygens line the walls of the selectivity filter and form transient binding sites for dehydrated K⁺ ions [42]. The selectivity loop of mM3₁₇₁₉ has two acidic residues (Asp¹⁰⁷¹ and Asp¹⁰⁷⁴) which could provide carbonyl oxygen atoms [42] or amino acid side chains [228] to line the pore structure. Nilius and colleagues found that mutation of Asp⁹⁸⁴ within the TRPM4 selectivity loop¹ yielded a non-functional channel with a dominant negative phenotype [149]. However, this result was not observed in the experiment with mM3₁₇₁₉, in which the Asp¹⁰⁷⁴ was substituted by an alanine. In spite of this, Ca²⁺ influx through mM3₁₇₁₉ was decreased as a result of the neutralization of Asp¹⁰⁷⁴ (Section: 3.2.1.1). This observation indicates that Asp¹⁰⁷⁴ may be involved in the formation of the selectivity filter, but is not the ion interaction site *per se*. Thus, Asp¹⁰⁷⁴ seems not to be an important determinant for mM3₁₇₁₉ Ca²⁺ permeation. The possible structural elements (*e.g.*, critical amino acid residues and pore diameter) that determine the selectivity filter function of mM3₁₇₁₉ need further investigation.

In addition, all mM3-RYW, mM3-VEV, and mM3-AP mutants were co-expressed with

¹Asp⁹⁸⁴ in TRPM4 is correspondent to Asp¹⁰⁷⁴ in mM3₁₇₁₉.

wild-type mM3₁₇₁₉. No dominant negative effects of them were observed by means of an aequorin-based intracellular Ca²⁺ assay (Figures: 3.6 and 3.7). We interpret these findings as an indication, that all or at least the majority of these residues have to be mutant within a multimeric pore in order to disrupt Ca²⁺ entry.

In summary, the two murine cDNAs we identified are strictly homologous to the one we have identified in human brain. In contrast to the latter, they are expressible in heterologous cell models and encode constitutively active Ca²⁺-permeable ion channels.

4.2 Molecular structure and functional relevance of the C-terminus

Because the N-terminus is highly conserved throughout the TRPM subfamily and the structure and function of the C-terminus are unknown, we focused on analyzing the functional components of the C-terminus of mM3₁₇₁₉. Apart from TRP and Coiled-Coil (C-C) domains, no other functional elements have been reported in the C-terminus of mTRPM3. To elucidate its molecular structure and functional relevance, the C-terminus of mM3₁₇₁₉ was studied using different methods including molecular cloning, immuno-staining, FRET, confocal microscopy, site-directed mutagenesis, and the yeast two hybrid system (Y2H) (Section: 3.2.1.2).

4.2.1 C-terminus of mM3₁₇₁₉ and palmitoylation

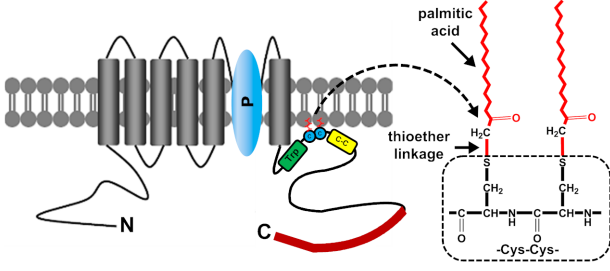
The cDNA sequence of the mM3₁₇₁₉ C-terminus (M3TC, amino acid residues 1166–1719) was amplified by PCR and cloned into the pcDNA3.1/V5-His-TOPO[®] vector. A YFP tag was added to its isolated C-terminus by means of in-frame fusion. The immunofluorescence signal of the YFP-tagged M3TC was found to be exclusively localized at the plasma membrane of the HEK 293 cells.



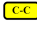

Attachment of soluble protein to the cytosolic plasma membrane could be due to: 1) a covalently attached lipid anchor such as isoprenoid, palmitoyl or myristoyl groups (Section: 3.2.1.2); 2) non-covalent interactions (*e.g.*, electrostatic interactions and hydrophobic bonds) with other membrane proteins; 3) lipid-binding motifs (*e.g.*, pleckstrin homology (PH) domain). Using different ligands activating signaling pathways ultimately resulting in PLC stimulation, phospholipid binding domains (*e.g.*, PH domain) were found to

be unlikely. Subsequently, *N*-myristoylation (Section: 3.2.1.2) was ruled out, because *N*-myristoylation is a stable co-translational lipid modification process and the typical recognition motif (Met-Gly-X-X-X-Ser/Thr) is not present in the C-terminus of mM3₁₇₁₉. Farnesylation (Section: 3.2.1.2) and palmitoylation of cysteine residues provide the other covalent modification mechanism. Hence, to study whether farnesylation and/or palmitoylation are involved in the mM3₁₇₁₉ C-terminus membrane attachment, all of the cysteine residues in the C-terminus were mutated. The cysteine residues of the mM3₁₇₁₉ C-terminus were step-wise replaced by serine residue (Section:3.2.1.2). The results indicate that the amino acid residues Cys¹¹⁷⁴-Cys¹¹⁷⁵ are involved in the protein-membrane attachment. Furthermore, this finding also implies that palmitoylation is probably responsible for the C-terminus membrane attachment, because 1) the cysteine residue for farnesylation is located four residues from the protein's C-terminus, but the Cys¹¹⁷⁴-Cys¹¹⁷⁵ residues are found to be much more N-terminal, and 2) palmitoylation is most common protein-lipid modification among the integral and peripheral membrane proteins [224]. In order to study the functional implication of palmitoylation in mM3₁₇₁₉ membrane attachment, we applied 2-bromopalmitate (2-BP) (a palmitoylation inhibitor), and generated a mM3₁₇₁₉-SS mutant of the whole channel cDNA (Cys¹¹⁷⁴-Cys¹¹⁷⁵ to Ser¹¹⁷⁴-Ser¹¹⁷⁵ mutations). The results imply that: 1) palmitoylation probably mediates Cys¹¹⁷⁴-Cys¹¹⁷⁵ membrane attachment; 2) palmitoylation of the C-terminus exerts influence on the mM3₁₇₁₉ channel function, although it does not change the mM3₁₇₁₉ expression pattern in HEK-293 cells; 3) besides the C-terminus, palmitoylation could also occur in the N-terminus or transmembrane domains of mM3₁₇₁₉, because Ca²⁺ influx through mM3₁₇₁₉-SS mutant with 2-BP treatment is much less than Ca²⁺ influx through mM3₁₇₁₉-SS mutant without 2-BP treatment (Figure: 3.10E-F).

Although the mechanisms by which the membrane-bound Cys¹¹⁷⁴-Cys¹¹⁷⁵ influence mM3₁₇₁₉ channel activity are not understood, it can be assumed that 1) palmitoylation targets mM3₁₇₁₉ to some specialized lipid microdomains on the cytosolic face of the plasma membrane where mM3₁₇₁₉ function as a cation channel [45]; 2) palmitoylation may affect the interaction of mM3₁₇₁₉ with other ion channels or signal molecules; 3) palmitoylation may be a basolateral localization signal for mM3₁₇₁₉; 4) attachment of Cys¹¹⁷⁴-Cys¹¹⁷⁵ to the membrane possibly stabilizes the functional homomer structure of mM3₁₇₁₉.

According to the sequence alignments, both Cys¹¹⁷⁴ and Cys¹¹⁷⁵ are highly conserved among the TRPM3 isoforms, but are not present in the other members of TRPM subfamily

Table 4.1: Domain composition of mM3₁₇₁₉


Domain	Putative biological role	Ref.
 TRP domain	—	—
 palmitoylation site	subcellular trafficking	—
 Coiled-Coil domain	multimer assembly	[218]
 PKIG binding site	PKA signaling	—

(data not shown). However, other cysteine residues might fulfill their function in other TRP channels. For example, palmitoylation of a stathmin-2 domain in the N-terminus of TRPC5 is involved in the loading of TRPC5 in transport packets directed into growth cones [57]. Thus, the modification of Cys¹¹⁷⁴ and Cys¹¹⁷⁵ of mM3₁₇₁₉ by palmitoylation may be unique for TRPM3 in the TRPM subfamily.

4.2.2 C-terminus of mM3₁₇₁₉ and homomultimerization

Because all TRP channels are thought to form tetramers as functional units [95, 187], it is likely that mM3₁₇₁₉ is expressed as a multimer to form a functional pore structure. Supporting the possibility of homomultimerization, the interactions between mM3₁₇₁₉ subunits were confirmed by using Co-IP and FRET techniques (Figures: 3.12 and 3.11). Additionally, the results from Co-IP and Y2H show that the interaction site for mM3₁₇₁₉ homomultimerization may lie in the C-terminus in a region from the amino acid residues 1133 to 1337 (Section: 3.2.2). This finding is consistent with previously reported studies in which the Coiled-Coil (C-C) domain was suggested to be responsible for the self-tetramerization of TRPM3 [218]. The contribution of the C-terminus in the self-association of channels is also found in other TRP channels. For example, the interaction sites of TRPV1 subunits [54] and TRPM8 subunits [48] are located in the TRP domain and Coiled-Coil (C-C) domain, respectively. In the case of TRPM3, we found that the protein sequence required for channel multimerization resides in the C-terminus sequence of both new splice variants,

and, therefore, might also be the TRP domain or C-C domain.

4.2.3 C-terminus of mM3₁₇₁₉ and its putative interaction partners

Many membrane proteins such as ion channels regulate cell function by forming molecular complexes with binding partners [7]. Therefore, to understand the physiological role of mM3₁₇₁₉, it is important to identify other proteins with which it interacts. To minimize the identification of false positive protein interactions (Section: 2.2.4.1), a GAL4-based yeast two hybrid (Y2H) screening was conducted because the AH109 yeast strain of this Y2H system contains four reporter genes which are under the control of three completely heterologous Gal4-responsive UAS and promoter elements–GAL1, GAL2, and MEL1 [87]. Because no functional elements in the C-terminus of mM3₁₇₁₉ have been described, the M3₁₇₁₉ C-terminus (M3CT, residues 1133–1719) was chosen as a “bait” to screen a human kidney cDNA library to identify potential binding partners for M3₁₇₁₉ (Section: 3.2.3).

A list of confirmed hits was obtained by using either high or medium stringency selection procedures (Tables: 3.1 and 3.2). The majority of these would not be necessarily involved in channel function and will require a more detailed analysis. We investigated one example, cAMP-dependent protein kinase inhibitor gamma (PKIG), in more detail, because Ca²⁺ influx through mM3₁₇₁₉ was increased when the cells expressing mM3₁₇₁₉ were pre-incubated with db-cAMP. The evidence for a protein–protein interaction between the C-terminus of mM3₁₇₁₉ and PIKG were verified by Y2H. The binding site for PKIG may be located between or involve the amino acid residues 1338–1719 of the mM3₁₇₁₉ C-terminus, because no interaction between the C-terminus of mM3₁₃₃₇ and PKIG was observed by Y2H (Figure: 3.14). However, no effects of PIKG on the mM3₁₇₁₉ channel activity was found in the experiment using aequorin. Therefore, whether PKA signaling plays a role in the mTRPM3 function needs to be investigated further.

Crystallin-alpha B (CRYAB) and eukaryotic translation elongation factor 1 alpha 1 (EEF1A1) are also proteins of interest. Crystallin-alpha (alpha A and alpha B) are basic structural proteins of the vertebrate lens. Compared to crystallin-alpha A which is mainly found in the lens, CRYAB is widely expressed in different tissues such as lens, brain and kidney. Accumulation of CRYAB in the brain is associated with some neurodegenerative diseases such as multiple sclerosis (MS) and Alzheimer disease [205, 222]. Mutation of CRYAB might lead to cataract formation because crystallin has a major contribution to the refractive power and translucency of the lens [17]. Combined with the findings noted

in Section 4.3.1, the hypothesis could be proposed that the interaction of mM3₁₇₁₉ with CRYAB in the lens epithelium might be involved in the lens ion-homeostasis underlying the regulation of mM3₁₇₁₉. EEF1A1 transfers each aminoacyl-tRNA molecule onto the ribosome. Because EEF1A1 is bound to GTP, it raises the possibility that the C-terminus of mM3₁₇₁₉ may contain a specific GTP interacting site (*e.g.*, GTP kinase domain). Hence, mM3₁₇₁₉ might be involved in G-protein regulated signal cascade. However, all such assumptions need to be confirmed by different biological and biochemical approaches.

4.3 Expression pattern of mouse TRPM3

4.3.1 Expression analysis of TRPM3 in mouse tissues using Northern blot, antibodies and *lacZ* staining

It was hitherto believed that TRPM3 gene expression was restricted to a limited number of tissues. For example, human TRPM3 (hTRPM3) is highly expressed in the kidney, while mouse TRPM3 (mTRPM3) is primarily detected in the brain, but not in the kidney [58, 106, 155, 157].

To investigate mTRPM3 expression, we initially carried out Northern blot analysis. Except for brain and eyes, no mRNA transcripts were detected in other tissues including the kidney (Figure: 3.3.1). These data are in line with the results reported by other research groups [58, 106, 157]. For the detection of TRPM3 protein, commercially available and own antibodies were used and characterized by Western blot and immunostainings. However, the commercially available antibodies were distinctly unspecific for mTRPM3 in both immunofluorescence staining and in Western blots (data not shown). Our peptide antibodies displayed strong background staining in cryosection, although they worked well in the immunocytochemical staining in overexpression models. Our peptide antibody was also used to detect TRPM3 protein expression in native mouse tissue (eyes). In agreement with the Northern blot, TRPM3 protein expression was found in the eyes of TRPM3 wild-type mouse (but not in the TRPM3 knockout mouse). The molecular mass (>170 kDa) was consistent with the calculated molecular mass of mM3₁₇₁₉ (ca. 190 kDa) and with the molecular mass seen in HEK-293 cells expressing mM3₁₇₁₉. These results indicate that the long isoforms, like mM3₁₇₁₉, are the major cDNAs expressed in the mouse eye.

The Northern blot has a high specificity so that the false positive results are unlikely. However, it has a low sensitivity, and thus signals resulting from weak gene expression may

be missed [206]. Application of specific antibodies is another conventional experimental method to study gene expression. Nevertheless, the antibodies against TRPM3 applied in the immunohistochemical staining (cryosection) had a strong background signal. Therefore, to investigate the expression pattern of TRPM3 more precisely, we purchased a TRPM3 knockout mouse whose TRPM3 gene was disrupted by *Gene Trapping* using a *lacZ* reporter gene construct (Figure: 2.8). The β -galactosidase encoded by *lacZ* gene was detected by X-Gal staining. Compared to immunostaining, *lacZ* staining is highly sensitive at the single cell level [46] and has very low background [28].

Whereas no *lacZ* signals were observed in vascular tissues, smooth muscles of the gut, and most of the viscera, we could detect isolated signals in testis, kidney glomerulus, and pancreatic islet. The latter is in line with a recent report by Wagner *et al.* [231], which reports that TRPM3 is detectable in pancreatic islets. Whereas the *lacZ* signals were rather rare in those organs of mesodermal origin that were studied by Northern blot, TRPM3 signals were most abundant in neuronal/ectodermal tissues. According to the *lacZ* staining, mTRPM3 expression is primarily found in the cerebral cortex (layers I, IV, V and VI), cerebellum (Purkinje and granule cell layers), dentate gyrus (granule cell layer), hippocampus proper CA1-CA3 (pyramidal cell layer), neural layers of retina (ganglionic and inner nuclear layers) and myenteric (Auerbach's) plexus. All of these tissues are of neuroectodermal origin. Other noteworthy expression signals were seen in the embryonic ear bubble, olfactory epithelia and dorsal root ganglion.

In summary, our expression studies showed a predominant expression of mTRPM3 in sensory and neuronal cells of ectodermal origin.

4.3.2 Mouse TRPM3 and subcellular localization

Epithelial cells and neurons, two types of polarized cells, exhibit functional as well morphological polarity, *i.e.* different functions are associated with two distinct morphologic surface domains: apical/axonal and basolateral/somatodendritic domains [3, 179, 204]. For example, the somatodendritic domain receives and processes signal information, while the axonal domain is responsible for the rapid transmission of electrical impulses [20, 134]. To generate this cell-surface polarity and be able to perform their physiological function, cells need to target newly synthesized proteins (*e.g.*, ion channels) and lipids to the appropriate domains of cell membranes [138, 252].

As far as we know, regulation of $[Ca^{2+}]_i$ by TRP channels is often restricted to some

specific microdomains in polarized cells [19, 135, 170]. For example, the TRPV4 channel is localized basolaterally in the epithelial cells of kidney where it responds to osmolality changes and triggers Ca^{2+} influx [68, 112, 212]. The TRPV4 channel is also observed in the apical membrane of the ciliated epithelia where it functions as a mechano- and thermosensor in the regulation of ciliary beat and cell volume [68, 102, 111]. Mouse TRPM3 was localized basolaterally in the $\text{M3}^{p\text{Gene}}$ MDCK cell line (Section: 3.1.2). This result indicates that mTRPM3 is localized in the basolateral domain of epithelial cells and thus, probably resides in the somatodendritic compartment, rather than the axon, in neurons.

4.3.3 Mouse TRPM3 expression and its biological roles

Since mTRPM3 is primarily expressed in nervous and sensory tissues, the discussions of suggestive biological roles of mTRPM3 are focused on the hippocampal formation, choroid plexus epithelium and eye (retina and lens) where the most *lacZ* staining was observed.

The mammalian choroid plexus (CP) is a highly ramified vascular structure composed of a layer of cuboid epithelial cells derived from ependymal cells which surround a core of capillaries and loose connective tissue. The CP produces cerebrospinal fluid (CSF) which nourishes the brain and protects the developing and mature brain from trauma. CSF secretion involves ion movement across the epithelium from the blood to the ventricles and is achieved by the asymmetrical distribution of ion transporters and channels in the apical or basolateral domain of the CP epithelial cells. The ion movement gives rise to an osmotic gradient which drives H_2O secretion isosmotically [23]. In the TRP superfamily, TRPV4 is expressed in modified ependymal cells of CP and may act as a mechano- and thermosensitive sensor for epithelial homeostasis [68, 129]. Because mTRPM3 is strongly expressed in the modified ependymal cells lining the CP and because mTRPM3 is localized in the basolateral domain of the epithelium, it could be hypothesized that mTRPM3 may be involved in the generation of an electrical gradient for ion transport (*e.g.*, Ca^{2+}) via unknown pathways. TRPM3 has also been reported to be responsive to extracellular hypo-osmolality [68, 70]. However, we could not reproduce the functional data published by Harteneck *et al.* [68, 70]. Thus, TRPM3 should not be considered as an osmo-sensor in the CP.

The most important function of the hippocampal formation is in learning and memory. Ca^{2+} plays a pivotal role in the molecular mechanisms underlying the formation of memories, especially long-term synaptic potentiation (LTP) and depression (LTD). Depolarization of the post-synaptic neuron (*e.g.*, somata or dendritic spines) leads to Ca^{2+} entry

which in turn triggers LTP [143]. TRPC5 [57], TRPC6 [160], TRPV1 [55], TRPM2 [69, 116] and TRPM7 [245] have been reported to be expressed and play an important role in the mouse hippocampal formation (*e.g.*, TRPC5 may be involved in the regulation of hippocampal neuron development [57]). Because mTRPM3 is highly expressed in the hippocampal formation (especially the granule cell layer of dentate gyrus and the pyramidal cell layer of hippocampus proper (CA1-CA3)), it may play a role in learning and memory formation and its underlying mechanisms. To evaluate learning and memory abilities in TRPM3^{-/-} mice, behavioral experiments should be applied in future studies to clarify these questions.

We found mTRPM3 in several sensory organs, but focused on the eye. The observation that considerable mTRPM3 expression is detected in the retina (pigment epithelium, ganglion cell and inner nuclear layers) and lens (epithelium and fibres) raises the possibility that mTRPM3 plays a role in visual function. Therefore, visual ability tests such as visual placing and cliff tests were performed with TRPM3^{-/-} mice. However, the TRPM3^{-/-} mice were found to be not blind and their overall visual ability (*e.g.*, depth perception) remained intact (Section: 3.4.4). Though mTRPM3 might, for instance, multimerize with other ion channels in retinal cells, the main conclusion now is that mTRPM3 does not play a major role in the primary sensory processes. However, mTRPM3 might still contribute to more subtle aspects of visual processing at the level of retina. Some studies also suggested that mTRPM3 could be a candidate gene for “early-onset pulverent cataract” (CAAR) [106, 147]. CAAR is an autosomal recessive form of hereditary cataract caused by mutations in the alpha-A crystallin gene [74]. The alpha-A and alpha-B crystallins are two subunits of alpha crystallins which together with beta and gamma crystallins constitute ca. 90% of the soluble protein of the vertebrate eye lens. The alpha-B crystallin is considered to be involved in the formation of dominant congenital posterior polar cataract in human [17]. Y2H assay showed that mTRPM3 interacts with alpha-B crystallin (Table: 3.2). Thus, mTRPM3 may play a role in the regulation of protein solubility and cataract formation in the lens via alpha-B crystallin.

4.4 Phenotype of the TRPM3 knockout mice

We obtained TRPM3 knockout mice offered by *Lexion genetics*. Before the phenotypic analysis, the mouse was genotyped and its genetic backgrounds were isogenized for skin coloration markers (Agouti (A), tyrosinase (C)). The absence of mTRPM3 protein expression in the TRPM3^{-/-} mouse was confirmed by Western blot. Two heterozygotes (TRPM3^{+/-})

were mated with each other to produce an F₁ generation. The results from the phenotyping of the F₁ generation showed that the TRPM3^{-/-} mouse is viable with a normal Mendelian offspring ratio. Compared to the TRPM3 wild-type mouse, no differences of general appearance such as grooming behaviors and coat color were observed. Body size and weight are normal compared to the TRPM3^{+/+} mouse. Its motor behavior such as posture and gait are normal, and no evidence for ataxia was found. Based on the high expression of mTRPM3 in retina, we performed initial studies on vision. However, the TRPM3^{-/-} mouse's overall visual ability is intact. Although TRPM3 is highly conserved in the TRPM family, the mutation in the TRPM3 gene did not appear to exert a major influence on its phenotype.

In summary, we found that mTRPM3 is highly Ca²⁺ permeable and, to a considerable extent, constitutively active, like a number of TRP channels (*e.g.*, TRPM6 and TRPM7). Besides TRP and C-C domains, palmitoylated Cys¹¹⁷⁴-Cys¹¹⁷⁵ residues and a putative binding position for channel homomultimerization were detected in the TRPM3 C-terminus. While TRPM1 expression is restricted to a few tissues (*e.g.*, pigmented cells), TRPM3 is widely expressed in variety of cells and tissues, and is especially strong in the nervous and sensory systems. Unlike the TRPM6^{-/-} mouse [232], the TRPM3^{-/-} mouse is viable and not embryonically lethal. The phenotypic analysis showed that the TRPM3^{-/-} mouse lacks morphological and behavioural defects, and its overall visual ability is intact.

Conclusions

TRPM3 is a highly conserved melastatin-like transient receptor potential (TRP) gene with direct orthologs in all chordates and close homologs in all bilateral animals. So far, little is known about its biological role, activation mechanism, expression pattern and the functional role of its domains. The aim of this work was to clone a cDNA of mouse TRPM3, to express it in *in vitro* overexpression models and evaluate its function, to raise antisera against TRPM3 in order to determine its cellular expression profile in the mouse and, finally, to obtain a knock-out allele in the mouse in order to assess its biological role.

1. In this work, we cloned two cDNAs of mTRPM3, both starting with the unique starting exon we had identified in a 5'-RACE study. One variant is 1337 amino acids long and has a shorter C-terminal domain than the other, which has 1719 amino acid residues. Both splice variants are readily expressible in HEK-293 cells. Plasma membrane localization was greatly augmented by stable inducible expression in differentiated, polarized MDCK cells, where mTRPM3₁₇₁₉ resided in the basolateral compartment. When overexpressed in HEK-293 cells, TRPM3 was unresponsive to hypo- or hyperosmolar stimuli, *D-erythro*-sphingosine and protocols used to elicit store-operated calcium entry. Instead, we observed a robust constitutive calcium entry through TRPM3, which was seen with both splice variants and abolished by point mutations in the pore domain.
2. We confirmed by means of fluorescence resonance energy transfer (FRET) and co-immunoprecipitation that TRPM3, like other TRP channels, forms multimeric channel complexes. The C-terminus of TRPM3 was found to attach to the plasma membrane through a palmitoylation of a dual-cysteine motif, a modification that

quantitatively affected calcium entry through TRPM3. In a systematic yeast two hybrid screen of a kidney library against the C-terminus of TRPM3, we identified a number of candidate interaction partners of TRPM3, including alpha-B crystallin and protein kinase inhibitor gamma (PKIG).

3. We investigated the TRPM3 expression pattern by a combination of Northern blots, Western blots and lacZ stainings in a mouse model based on the *GeneTrap* approach. We found TRPM3 to be mainly enriched in eye and brain tissues, but, unlike human TRPM3, very low levels in kidney. Using lacZ staining of cryostat sections, TRPM3 was detected mainly in sensory tissues like the bipolar and ganglion cell layers of the eye, the embryonic ear bubble and dorsal root ganglia. In the brain, a considerable enrichment of TRPM3 gene activity was seen, among others, in various neuron populations of the hippocampus formation (dentate gyrus, CA1, CA3), the Purkinje cells layer, and the neocortex. Thus, TRPM3 is mainly expressed in cells of ectodermal origin.
4. We characterized a mouse model in which TRPM3 had been targeted by a gene trap insertion. We confirmed the gene trap insertion by means of PCR, we confirmed the absence of the protein in eye tissues by means of a Western blot using a newly made peptide rabbit antiserum, and we isogenized the genetical background for skin coloration markers using Mendelian crosses. A basic study of TRPM3's phenotype showed the absence of morphological and overall behavioural defects and complete viability of the mutant. Further assays addressing the visual abilities of the TRPM3^{-/-} mouse showed no signs of blindness.

In summary, we cloned cDNAs of TRPM3, expressed them *in vitro* and found that TRPM3 is calcium-permeable and constitutively active. TRPM3 is palmitoylated on its C-terminus and interacts with a variety of proteins we identified by a yeast two hybrid approach, many of them novel in this regard. TRPM3 is highly enriched in sensory and central nervous tissues. The TRPM3^{-/-} mouse is viable without any major neurological or sensory defect as far as tested. Further investigation on tissues which will have to address the specific function of TRPM3 where it is enriched.

References

- [1] Elie Abed, Dominique Labelle, Corine Martineau, Andrew Loghin, and Robert Moreau. Expression of transient receptor potential (trp) channels in human and murine osteoblast-like cells. *Mol Membr Biol*, 26(3):146–158, Apr 2009. [93](#)
- [2] Benjamin Adams, Thomas Fitch, Stephen Chaney, and Robert Gerlai. Altered performance characteristics in cognitive tasks: comparison of the albino icr and cd1 mouse strains. *Behavioural Brain Research*, 133(2):351 – 361, 2002. [51](#)
- [3] Bruce Alberts, Alexander Johnson, and Julian Lewis. Molecular Biology of THE CELL. *Taylor & Francis*, 5th., 2008. [111](#)
- [4] Julio Alvarez, Alain Coulombe, Olivier Cazorla, Mehmet Ugur, Jean-Michel Rauzier, Janos Magyar, Eve-Lyne Mathieu, Guylain Boulay, Rafael Souto, Patrice Bideaux, Guillermo Salazar, Francois Rassendren, Alain Lacampagne, Jeremy Fauconnier, and Guy Vassort. ATP/UTP activate cation-permeable channels with TRPC3/7 properties in rat cardiomyocytes. *Am J Physiol Heart Circ Physiol*, 295(1):H21–28, 2008. [65](#)
- [5] Indu S. Ambudkar. Ca²⁺ signaling microdomains:platforms for the assembly and regulation of TRPC channels. *Trends in Pharmacological Sciences*, 27(1):25–32, 2006. [2](#)
- [6] Hemasse Amiri, Gunter Schultz, and Michael Schaefer. Fret-based analysis of TRPC subunit stoichiometry. *Cell Calcium*, 33(5-6):463, 2003. [33](#), [70](#)
- [7] Naohiko ANZAI, Hiroki MIYAZAKI, and Shinichi SAKAMOTO. Identification of intracellular regulatory protein for ion channel using yeast two-hybrid system. *Folia Pharmacologica Japonica*, 122(4):331–337, 2003. [109](#)
- [8] Maite Arniges, Jose M. Fernandez-Fernandez, Nadine Albrecht, Michael Schaefer, and Miguel A. Valverde. Human TRPV4 Channel Splice Variants Revealed a Key Role of Ankyrin Domains in Multimerization and Trafficking. *J. Biol. Chem.*, 281(3):1580–1586, 2006. [5](#), [70](#)

REFERENCES

- [9] Konstantin Arnold, Lorenza Bordoli, Jürgen Kopp, and Torsten Schwede. The swiss-model workspace: a web-based environment for protein structure homology modelling. *Bioinformatics*, 22:195–201, Jan 2006. [104](#), [105](#)
- [10] Frederick M. Ausubel. Current Protocols in Molecular Biology. *John Wiley & Sons Inc*, 2001. [21](#), [26](#), [29](#), [42](#)
- [11] Odmara L Barreto-Chang and Ricardo E Dolmetsch. Calcium Imaging of Cortical Neurons using Fura-2 AM. *Journal of Visualized Experiments*, 23, 2009. [45](#)
- [12] Valerie Baubet, Herve Le Mouellic, Anthony K. Campbell, Estelle Lucas-Meunier, Philippe Fossier, and Philippe Brulet. Chimeric green fluorescent protein-aequorin as bioluminescent Ca²⁺ reporters at the single-cell level. *Proc Natl Acad Sci U S A*, 97(13):7260–7265, 2000. [46](#), [47](#)
- [13] EE Baulieu. Contragestion and other clinical applications of RU 486, an antiprogestosterone at the receptor. *Science*, 245(4924):1351–1357, 1989. [40](#)
- [14] Benjamin Beck, Alexander Zholos, Vadym Sydorenko, Morad Roudbaraki, V'yacheslav Lehen'kyi, Pascal Bordat, Natalia Prevarskaya, and Roman Skryma. Trpc7 is a receptor-operated DAG-activated channel in human keratinocytes. *J Invest Dermatol*, 126(9):1982–1993, 2006. [2](#)
- [15] C. Bendixen, S. Gangloff, and R. Rothstein. A yeast mating-selection scheme for detection of protein-protein interactions. *Nucleic Acids Res*, 22:1778–1779, May 1994. [33](#)
- [16] Michael J. Berridge, Peter Lipp, and Martin D. Bootman. The versatility and universality of calcium signalling. *Nat Rev Mol Cell Biol*, 1(1):11–21, 2000. [1](#)
- [17] V. Berry, P. Francis, M. A. Reddy, D. Collyer, E. Vithana, I. MacKay, G. Dawson, A. H. Carey, A. Moore, S. S. Bhattacharya, and R. A. Quinlan. Alpha-b crystallin gene (cryab) mutation causes dominant congenital posterior polar cataract in humans. *Am J Hum Genet*, 69(5):1141–1145, Nov 2001. [109](#), [113](#)
- [18] R. E. Boissy and J. J. Nordlund. Molecular basis of congenital hypopigmentary disorders in humans: a review. *Pigment Cell Res*, 10(1-2):12–24, Feb/Apr 1997. [96](#)
- [19] Martin D. Bootman, Peter Lipp, and Michael J. Berridge. The organisation and functions of local Ca²⁺ signals. *J Cell Sci*, 114(12):2213–2222, 2001. [112](#)
- [20] F. Bradke and C. G. Dotti. Membrane traffic in polarized neurons. *Biochim Biophys Acta*, 1404(1-2):245–258, Aug 1998. [111](#)

REFERENCES

- [21] R. Brent and M. Ptashne. A eukaryotic transcriptional activator bearing the DNA specificity of a prokaryotic repressor. *Cell*, 43:729–736, Dec 1985. [33](#)
- [22] M Brini. Calcium-sensitive photoproteins. *Methods*, 46(3):160–6, 2008. [57](#)
- [23] P.D. Brown, S.L. Davies, T. Speake, and I.D. Millar. Molecular mechanisms of cerebrospinal fluid production. *Neuroscience*, 129(4):955 – 968, 2004. Brain Water Homeostasis. [112](#)
- [24] K. E. Hammond-Kosack J. Jones M. R. Knight E. Johannes C. Moyen. Systemin triggers an increase of cytoplasmic calcium in tomato mesophyll cells: Ca^{2+} mobilization from intra- and extracellular compartments. *Plant, Cell & Environment*, 21(11):1101–1111, 1998. [48](#)
- [25] M. J. Caplan, J. L. Stow, A. P. Newman, J. Madri, H. C. Anderson, M. G. Farquhar, G. E. Palade, and J. D. Jamieson. Dependence on pH of polarized sorting of secreted proteins. *Nature*, 329:632–635, Oct 1987. [54](#)
- [26] William A. Catterall. From ionic currents to molecular mechanisms: The structure and function of voltage-gated sodium channels. *Neuron*, 26(1):13 – 25, 2000. [5](#)
- [27] C. T. Chien, P. L. Bartel, R. Sternglanz, and S. Fields. The two-hybrid system: a method to identify and clone genes for proteins that interact with a protein of interest. *Proc Natl Acad Sci U S A*, 88:9578–9582, Nov 1991. [33](#)
- [28] Hemin R. Chin and Steven O. Moldin. Studing brain development and wiring using a modified gene trap approach. *Methods in genomic neuroscience*, page 106, 2001. [111](#)
- [29] V. Chubanov, M. Mederos y Schnitzler, J. Wäring, A. Plank, and T. Gudermann. Emerging roles of TRPM6/TRPM7 channel kinase signal transduction complexes. *Naunyn Schmiedeberts Arch Pharmacol*, 371:334–341, Apr 2005. [7](#)
- [30] Vladimir Chubanov, Karl P. Schlingmann, Janine Waring, Jolanta Heinzinger, Silke Kaske, Siegfried Waldegger, Michael Mederos y Schnitzler, and Thomas Gudermann. Hypomagnesemia with secondary hypocalcemia due to a missense mutation in the putative pore-forming region of trpm6. *J. Biol. Chem.*, 282(10):7656–7667, 2007. [11](#), [62](#)
- [31] Vladimir Chubanov, Siegfried Waldegger, Michael Mederos y Schnitzler, Helga Vitzthum, Martin C. Sassen, Hannsjrg W. Seyberth, Martin Konrad, and Thomas Gudermann. Disruption of TRPM6/TRPM7 complex formation by a mutation in the TRPM6 gene causes hypomagnesemia with secondary hypocalcemia. *Proceedings of the National Academy of Sciences of the United States of America*, 101(9):2894–2899, 2004. [5](#), [6](#), [7](#)
- [32] David E. Clapham. Trp channels as cellular sensors. *Nature*, 426(6966):517–524, 2003. [1](#), [4](#), [6](#)

REFERENCES

- [33] David E. Clapham, Craig Montell, Guenter Schultz, and David Julius. International Union of Pharmacology. XLIII. Compendium of Voltage-Gated Ion Channels: Transient Receptor Potential Channels. *Pharmacol Rev*, 55(4):591–596, 2003. [4](#)
- [34] David E. Clapham, Loren W. Runnels, and Carsten Strubing. The trp ion channel family. *Nat Rev Neurosci*, 2(6):387–396, 2001. [6](#)
- [35] Robert M Clegg. Fluorescence resonance energy transfer. *Current Opinion in Biotechnology*, 6(1):103 – 110, 1995. [32](#)
- [36] Sean P. Collins and Michael D. Uhler. Characterization of PKIgamma , a Novel Isoform of the Protein Kinase Inhibitor of cAMP-dependent Protein Kinase. *J. Biol. Chem.*, 272(29):18169–18178, 1997. [77](#)
- [37] Emmanuelle Cordat. Unraveling trafficking of the kidney anion exchanger 1 in polarized MDCK epithelial cells. *Biochemistry and Cell Biology*, 84(6):949–959, 2006. [55](#)
- [38] D. J. Cosens and Aubrey Manning. Abnormal electroretinogram from a drosophila mutant. *Nature*, 224(5216):285–287, 1969. [3](#)
- [39] Jacqueline N. Crawley. What’s Wrong With My Mouse?: Behavioral Phenotyping of Transgenic and Knockout Mice, 2nd Edition. *New York: Wiley-Liss*, pages 90–94, 2007. [50](#), [51](#)
- [40] Richard N. Day. Visualization of Pit-1 Transcription Factor Interactions in the Living Cell Nucleus by Fluorescence Resonance Energy Transfer Microscopy. *Mol Endocrinol*, 12(9):1410–1419, 1998. [32](#)
- [41] Federica Di Palma, Inna A. Belyantseva, Hung J. Kim, Thomas F. Vogt, Bechara Kachar, and Konrad Noben-Trauth. Mutations in Mcoln3 associated with deafness and pigmentation defects in varitint-waddler (Va) mice. *Proceedings of the National Academy of Sciences of the United States of America*, 99(23):14994–14999, 2002. [6](#)
- [42] Declan A. Doyle, João Morais Cabral, Richard A. Pfuetzner, Anling Kuo, Jacqueline M. Gulbis, Steven L. Cohen, Brian T. Chait, and Roderick MacKinnon. The Structure of the Potassium Channel: Molecular Basis of K⁺ Conduction and Selectivity. *Science*, 280(5360):69–77, 1998. [4](#), [5](#), [104](#), [105](#)
- [43] Lyn M. Duncan, James Deeds, Frank E. Cronin, Michael Donovan, Arthur J. Sober, Michael Kauffman, and Jeanette J. McCarthy. Melastatin Expression and Prognosis in Cutaneous Malignant Melanoma. *J Clin Oncol*, 19(2):568–576, 2001. [9](#)
- [44] Lyn M. Duncan, Jim Deeds, John Hunter, Jing Shao, Lisa M. Holmgren, Elizabeth A. Woolf, Robert I. Tepper, and Andrew W. Shyjan. Down-Regulation of the Novel Gene Melastatin Correlates with Potential for Melanoma Metastasis. *Cancer Res*, 58(7):1515–1520, 1998. [9](#)

REFERENCES

- [45] Alaa El-Din El-Husseini and David S. Bredt. Protein palmitoylation: a regulator of neuronal development and function. *Nat Rev Neurosci*, 3(10):791–802, 2002. [107](#)
- [46] Chaeles P. Emerson and H. lee Sweeney. Methods in muscle biology. *Methods in cell biology*, 52:398, 1997. [111](#)
- [47] Michael Engelke, Olaf Friedrich, Petra Budde, Christina Schfer, Ursula Niemann, Christof Zitt, Eberhard Jngling, Oliver Rocks, Andreas Lckhoff, and Jrgen Frey. Structural domains required for channel function of the mouse transient receptor potential protein homologue TRP1 β . *FEBS Letters*, 523(1-3):193 – 199, 2002. [7](#)
- [48] Isabell Erler, Dalia M. M. Al-Ansary, Ulrich Wissenbach, Thomas F. J. Wagner, Veit Flockerzi, and Barbara A. Niemeyer. Trafficking and Assembly of the Cold-sensitive TRPM8 Channel. *J. Biol. Chem.*, 281(50):38396–38404, 2006. [7](#), [108](#)
- [49] Isabell Erler, Daniela Hirnet, Ulrich Wissenbach, Veit Flockerzi, and Barbara A. Niemeyer. Ca²⁺-selective Transient Receptor Potential V Channel Architecture and Function Require a Specific Ankyrin Repeat. *J. Biol. Chem.*, 279(33):34456–34463, 2004. [5](#), [6](#)
- [50] Mark Estacion, Su Li, William G. Sinkins, Martin Gosling, Parmjit Bahra, Chris Poll, John Westwick, and William P. Schilling. Activation of Human TRPC6 Channels by Receptor Stimulation. *J. Biol. Chem.*, 279(21):22047–22056, 2004. [65](#)
- [51] S. Fields and O. Song. A novel genetic system to detect protein-protein interactions. *Nature*, 340:245–246, Jul 1989. [33](#)
- [52] M.W. Fox. The visual cliff test for the study of visual depth perception in the mouse. *Animal Behaviour*, 13(2-3):232 – 233, 1965. [51](#)
- [53] Lidia M. Futey, Quintus G. Medley, Graham P. Ct, and Thomas T. Egelhoff. Structural Analysis of Myosin Heavy Chain Kinase A from Dictyostelium. *J. Biol. Chem.*, 270(2):523–529, 1995. [7](#)
- [54] Nuria Garcia-Sanz, Asia Fernandez-Carvajal, Cruz Morenilla-Palao, Rosa Planells-Cases, Emmanuel Fajardo-Sanchez, Gregorio Fernandez-Ballester, and Antonio Ferrer-Montiel. Identification of a Tetramerization Domain in the C Terminus of the Vanilloid Receptor. *J. Neurosci.*, 24(23):5307–5314, 2004. [5](#), [108](#)
- [55] Helen E. Gibson, Jeffrey G. Edwards, Rachel S. Page, Matthew J. Van Hook, and Julie A. Kauer. Trpv1 channels mediate long-term depression at synapses on hippocampal interneurons. *Neuron*, 57(5):746–759, Mar 2008. [113](#)

REFERENCES

- [56] Monu Goel, William G. Sinkins, and William P. Schilling. Selective Association of TRPC Channel Subunits in Rat Brain Synaptosomes. *J. Biol. Chem.*, 277(50):48303–48310, 2002. [5](#)
- [57] Anna Greka, Betsy Navarro, Elena Oancea, Anne Duggan, and David E. Clapham. TRPC5 is a regulator of hippocampal neurite length and growth cone morphology. *Nat Neurosci*, 6(8):837–845, 2003. [6](#), [108](#), [113](#)
- [58] Christian Grimm, Robert Kraft, Sophie Sauerbruch, Gunter Schultz, and Christian Harteneck. Molecular and Functional Characterization of the Melastatin-related Cation Channel TRPM3. *J. Biol. Chem.*, 278(24):21493–21501, 2003. [9](#), [10](#), [11](#), [12](#), [13](#), [56](#), [57](#), [110](#)
- [59] Christian Grimm, Robert Kraft, Gunter Schultz, and Christian Harteneck. Activation of the Melastatin-Related Cation Channel TRPM3 by D-erythro-Sphingosine. *Mol Pharmacol*, 67(3):798–805, 2005. [11](#), [12](#), [52](#), [57](#)
- [60] G Grynkiewicz, M Poenie, and RY Tsien. A new generation of Ca²⁺ indicators with greatly improved fluorescence properties. *J. Biol. Chem.*, 260(6):3440–3450, 1985. [45](#)
- [61] N. Guex and M. C. Peitsch. Swiss-model and the swiss-pdbviewer: an environment for comparative protein modeling. *Electrophoresis*, 18:2714–2723, Dec 1997. [104](#), [105](#)
- [62] Didem Gz, Keith Studholme, Douglas A. Lappi, Mark D. Rollag, Ignacio Provencio, and Lawrence P. Morin. Targeted Destruction of Photosensitive Retinal Ganglion Cells with a Saporin Conjugate Alters the Effects of Light on Mouse Circadian Rhythms. *PLoS ONE*, 3(9):e3153, 09 2008. [51](#)
- [63] Richard Hallworth, Benjamin Currall, Michael G. Nichols, Xudong Wu, and Jian Zuo. Studying inner ear protein-protein interactions using fret and flim. *Brain Research*, 1091(1):122 – 131, 2006. [32](#), [33](#)
- [64] RW Hammerton, KA Krzeminski, RW Mays, TA Ryan, DA Wollner, and WJ Nelson. Mechanism for regulating cell surface distribution of Na⁺,K(+)-ATPase in polarized epithelial cells. *Science*, 254(5033):847–850, 1991. [54](#)
- [65] Yuji Hara, Minoru Wakamori, Masakazu Ishii, Emi Maeno, Motohiro Nishida, Takashi Yoshida, Hisanobu Yamada, Shunichi Shimizu, Emiko Mori, Jun Kudoh, Nobuyoshi Shimizu, Hitoshi Kurose, Yasunobu Okada, Keiji Imoto, and Yasuo Mori. LTRPC2 Ca²⁺-permeable channel activated by changes in redox status confers susceptibility to cell death. *Mol Cell*, 9:163–173, Jan 2002. [8](#)
- [66] Roger C. Hardie. Trp channels and lipids: from drosophila to mammalian physiology. *J Physiol*, 578(1):9–24, 2007. [3](#), [8](#)

REFERENCES

- [67] Roger C. Hardie and Baruch Minke. The *trp* gene is essential for a light-activated Ca^{2+} channel in drosophila photoreceptors. *Neuron*, 8(4):643 – 651, 1992. [3](#)
- [68] C. Harteneck and B. Reiter. Trp channels activated by extracellular hypo-osmoticity in epithelia. *Biochemical Society Transactions*, 035(1):91–95, 2007. [12](#), [57](#), [103](#), [112](#)
- [69] Christian Harteneck. Function and pharmacology of TRPM cation channels. *Naunyn-Schmiedeberg's Archives of Pharmacology*, 371(4):307–314, 2005. [113](#)
- [70] Christian Harteneck and Guenter Schultz. TRPV4 and TRPM3 as Volume-Regulated Cation Channels. *TRP Ion Channel Function in Sensory Transduction and Cellular Signaling Cascades*, Crc Pr Inc, 2006. [57](#), [103](#), [112](#)
- [71] Megumi Hatori, Hiep Le, Christopher Vollmers, Sheena Racheal Keding, Nobushige Tanaka, Christian Schmedt, Timothy Jegla, and Satchidananda Panda. Inducible Ablation of Melanopsin-Expressing Retinal Ganglion Cells Reveals Their Central Role in Non-Image Forming Visual Responses. *PLoS ONE*, 3(6):e2451, 06 2008. [51](#)
- [72] Inka Heiner, Jrg Eisfeld, Christian R Halaszovich, Edith Wehage, Eberhard Jngling, Christof Zitt, and Andreas Lckhoff. Expression profile of the transient receptor potential (TRP) family in neutrophil granulocytes: evidence for currents through long TRP channel 2 induced by ADP-ribose and NAD. *Biochem. J.*, 371(3):1045–1053, 2003. [8](#)
- [73] Nicole Hellwig, Nadine Albrecht, Christian Harteneck, Gunter Schultz, and Michael Schaefer. Homo- and heteromeric assembly of TRPV channel subunits. *J Cell Sci*, 118(5):917–928, 2005. [70](#)
- [74] E. Héon, A. D. Paterson, M. Fraser, G. Billingsley, M. Priston, A. Balmer, D. F. Schorderet, A. Verner, T. J. Hudson, and F. L. Munier. A progressive autosomal recessive cataract locus maps to chromosome 9q13-q22. *Am J Hum Genet*, 68(3):772–777, Mar 2001. [113](#)
- [75] Charles J. Heyser, Kelly Moc, and George F. Koob. Effects of Naltrexone Alone and In Combination With Acamprosate on the Alcohol Deprivation Effect in Rats. *Neuropsychopharmacology*, 28(8):1463–1471, 2003. [50](#)
- [76] Thomas Hofmann, Vladimir Chubanov, Thomas Gudermann, and Craig Montell. TRPM5 Is a Voltage-Modulated and Ca^{2+} -Activated Monovalent Selective Cation Channel. *Current Biology*, 13(13):1153–1158, 2003. [8](#)
- [77] Thomas Hofmann, Alexander G. Obukhov, Michael Schaefer, Christian Harteneck, Thomas Gudermann, and Gunter Schultz. Direct activation of human TRPC6 and TRPC3 channels by diacylglycerol. *Nature*, 397(6716):259–263, 1999. [2](#)

REFERENCES

- [78] Thomas Hofmann, Michael Schaefer, Gunter Schultz, and Thomas Gudermann. Subunit composition of mammalian transient receptor potential channels in living cells. *Proc Natl Acad Sci U S A*, 99(11):7461–7466, 2002. [33](#), [70](#)
- [79] John R. Hofstetter, Aiwu Zhang, Aimee R. Mayeda, Tim Guscar, John I. Nurnberger, and Debomoy K. Lahiri. Genomic dna from mice: A comparison of recovery methods and tissue sources. *Biochemical and Molecular Medicine*, 62(2):197–202, 1997. [49](#)
- [80] I. A. Hope and K. Struhl. Functional dissection of a eukaryotic transcriptional activator protein, GCN4 of yeast. *Cell*, 46:885–894, Sep 1986. [33](#)
- [81] J. J. Hunter, J. Shao, J. S. Smutko, B. J. Dussault, D. L. Nagle, E. A. Woolf, L. M. Holmgren, K. J. Moore, and A. W. Shyjan. Chromosomal localization and genomic characterization of the mouse melastatin gene (Mln1). *Genomics*, 54:116–123, Nov 1998. [9](#)
- [82] Jessica A. Hurt, Stacey A. Thibodeau, Andrew S. Hirsh, Carl O. Pabo, and J. Keith Joung. Highly specific zinc finger proteins obtained by directed domain shuffling and cell-based selection. *Proc Natl Acad Sci USA*, 100:12271–12276, Oct 2003. [33](#)
- [83] Daniel Huson, Daniel Richter, Christian Rausch, Tobias DeZulian, Markus Franz, and Regula Rupp. Dendroscope: An interactive viewer for large phylogenetic trees. *BMC Bioinformatics*, 8(1):460, 2007. [3](#), [7](#)
- [84] Hiroaki Inoue, Hiroshi Nojima, and Hiroto Okayama. High efficiency transformation of escherichia coli with plasmids. *Gene*, 96(1):23–28, 1990. [22](#)
- [85] R.F. Irvine. 'quantal' Ca^{2+} release and the control of Ca^{2+} entry by inositol phosphates: a possible mechanism. *FEBS Lett.*, 263:5–9, 1990. [2](#)
- [86] Paul Jackson, Wendy Anderson, Jane DeWitt, Huei-Yang Ke, Cheryl Kuske, Robyn Moncrief, and Gary Rayson. Accumulation of toxic metal ions on cell walls of *Datura innoxia* suspension cell cultures. *In Vitro Cellular & Developmental Biology - Plant*, 29(4):220–226, 1993. [104](#)
- [87] P. James, J. Halladay, and E. A. Craig. Genomic Libraries and a Host Strain Designed for Highly Efficient Two-Hybrid Selection in Yeast. *Genetics*, 144(4):1425–1436, 1996. [109](#)
- [88] Marc Jenke, Araceli Snchez, Francisco Monje, Walter Sthmer, Rdiger M. Weseloh, and Pardo Luis A. C-terminal domains implicated in the functional surface expression of potassium channels. *The EMBO Journal*, 22:395–403, 2003. [7](#)
- [89] Jianmin Jiang, Mingjiang Li, and Lixia Yue. Potentiation of TRPM7 Inward Currents by Protons. *J. Gen. Physiol.*, 126(2):137–150, 2005. [9](#)

REFERENCES

- [90] Yunju Jin, Dong Kwan Kim, Lee-Yong Khil, Uhtaek Oh, Jun Kim, and Jiyeon Kwak. Thimerosal decreases TRPV1 activity by oxidation of extracellular sulfhydryl residues. *Neuroscience Letters*, 369(3):250–255, 2004. [4](#)
- [91] J. K. Joung, E. I. Ramm, and C. O. Pabo. A bacterial two-hybrid selection system for studying protein-DNA and protein-protein interactions. *Proc Natl Acad Sci U S A*, 97:7382–7387, Jun 2000. [43](#)
- [92] Marianthi Karali, Ivana Peluso, Valeria Marigo, and Sandro Banfi. Identification and Characterization of MicroRNAs Expressed in the Mouse Eye. *Invest. Ophthalmol. Vis. Sci.*, 48(2):509–515, 2007. [93](#)
- [93] Matthew H. Kaufman. The atlas of mouse development. *Academic Press*, 2, 1992. [93](#)
- [94] U. Benjamin Kaupp and Reinhard Seifert. Cyclic Nucleotide-Gated Ion Channels. *Physiol. Rev.*, 82(3):769–824, 2002. [5](#)
- [95] Noemi Kedei, Tamas Szabo, Jack D. Lile, James J. Treanor, Zoltan Olah, Michael J. Iadarola, and Peter M. Blumberg. Analysis of the Native Quaternary Structure of Vanilloid Receptor 1. *J. Biol. Chem.*, 276(30):28613–28619, 2001. [4](#), [108](#)
- [96] Anne K. Kenworthy. Imaging protein-protein interactions using fluorescence resonance energy transfer microscopy. *Methods*, 24(3):289 – 296, 2001. [32](#)
- [97] Michael-Christopher Keogh, Jung-Ae Kim, Michael Downey, Jeffrey Fillingham, Dipanjan Chowdhury, Jacob C. Harrison, Megumi Onishi, Nira Datta, Sarah Galicia, Andrew Emili, Judy Lieberman, Xuotong Shen, Stephen Buratowski, James E. Haber, Daniel Durocher, Jack F. Greenblatt, and Nevan J. Krogan. A phosphatase complex that dephosphorylates gammaH2AX regulates DNA damage checkpoint recovery. *Nature*, 439(7075):497–501, 2006. [38](#)
- [98] Hubert H. Kerschbaum, J. Ashot Kozak, and Michael D. Cahalan. Polyvalent cations as permeant probes of MIC and TRPM7 pores. *Biophys J*, 84:2293–2305, Apr 2003. [9](#)
- [99] W Klement and J O Arndt. The role of nociceptors of cutaneous veins in the mediation of cold pain in man. *J Physiol*, 449(1):73–83, 1992. [9](#)
- [100] Florian Krieger, Andreas Mglich, and Thomas Kiefhaber. Effect of proline and glycine residues on dynamics and barriers of loop formation in polypeptide chains. *J Am Chem Soc*, 127(10):3346–3352, Mar 2005. [104](#)
- [101] Vidhyasankar Krishnamoorthy, Varsha Jain, Pitchaiah Cherukuri, Sonia Baloni, and Narendar K. Dhingra. Intravitreal Injection of Fluorochrome-Conjugated Peanut Agglutinin Results

REFERENCES

- in Specific and Reversible Labeling of Mammalian Cones In Vivo. *Invest. Ophthalmol. Vis. Sci.*, 49(6):2643–2650, 2008. [51](#)
- [102] Michael Kttgen, Bjorn Buchholz, Miguel A. Garcia-Gonzalez, Fruzsina Kotsis, Xiao Fu, Mara Doerken, Christopher Boehlke, Daniel Steffl, Robert Tauber, Tomasz Wegierski, Roland Nitschke, Makoto Suzuki, Albrecht Kramer-Zucker, Gregory G. Germino, Terry Watnick, Jean Prenen, Bernd Nilius, E. Wolfgang Kuehn, and Gerd Walz. TRPP2 and TRPV4 form a poly-modal sensory channel complex. *J. Cell Biol.*, 182(3):437–447, 2008. [112](#)
- [103] F. Lang and M. Paulmichl. Properties and regulation of ion channels in MDCK cells. *Kidney Int*, 48:1200–1205, Oct 1995. [55](#)
- [104] Pierre Launay, Andrea Fleig, Anne-Laure Perraud, Andrew M. Scharenberg, Reinhold Penner, and Jean-Pierre Kinet. TRPM4 Is a Ca^{2+} -Activated Nonselective Cation Channel Mediating Cell Membrane Depolarization. *Cell*, 109(3):397 – 407, 2002. [6](#), [8](#)
- [105] Jung-Ha Lee, Juan Carlos Gomora, Leanne L. Cribbs, and Edward Perez-Reyes. Nickel block of three cloned t-type calcium channels: Low concentrations selectively block $[\alpha]1\text{h}$. *Biophysical Journal*, 77(6):3034 – 3042, 1999. [59](#)
- [106] Ning Lee, Jian Chen, Lucy Sun, Shujian Wu, Kevin R. Gray, Adam Rich, Minxue Huang, Jun-Hsiang Lin, John N. Feder, Evan B. Janovitz, Paul C. Levesque, and Michael A. Blannar. Expression and Characterization of Human Transient Receptor Potential Melastatin 3 (hTRPM3). *J. Biol. Chem.*, 278(23):20890–20897, 2003. [8](#), [9](#), [10](#), [11](#), [12](#), [13](#), [56](#), [57](#), [83](#), [110](#), [113](#)
- [107] Wai Fook Leong, Tielin Zhou, Gek Liang Lim, and Baojie Li. Protein Palmitoylation Regulates Osteoblast Differentiation through BMP-Induced Osterix Expression. *PLoS ONE*, 4(1):e4135, 01 2009. [69](#)
- [108] Chaohong Li and Qingbo Xu. Mechanical stress-initiated signal transductions in vascular smooth muscle cells. *Cellular Signalling*, 12(7):435 – 445, 2000. [1](#)
- [109] Mingjiang Li, Jianmin Jiang, and Lixia Yue. Functional Characterization of Homo- and Heteromeric Channel Kinases TRPM6 and TRPM7. *J. Gen. Physiol.*, 127(5):525–537, 2006. [6](#), [8](#), [69](#)
- [110] Dan Liu and Emily R. Liman. Intracellular Ca^{2+} and the phospholipid PIP2 regulate the taste transduction ion channel TRPM5. *Proceedings of the National Academy of Sciences of the United States of America*, 100(25):15160–15165, 2003. [6](#), [8](#)

REFERENCES

- [111] Ivan M. Lorenzo, Wolfgang Liedtke, Michael J. Sanderson, and Miguel A. Valverde. TRPV4 channel participates in receptor-operated calcium entry and ciliary beat frequency regulation in mouse airway epithelial cells. *Proc Natl Acad Sci U S A*, 105(34):12611–12616, 2008. [112](#)
- [112] G. Malnic, R. W. Berliner, and G. Giebisch. Flow dependence of K^+ secretion in cortical distal tubules of the rat. *Am J Physiol Renal Physiol*, 256(5):F932–941, 1989. [112](#)
- [113] Pam Massulloa, Adriana Sumoza-Toledoa, Harivadan Bhagata, and Santiago Partida-Sánchez. TRPM channels, calcium and redox sensors during innate immune responses. *Seminars in cell & developmental biology*, 17(6):654–666, 2006. [6](#)
- [114] Stuart P. McElroy, Alison M. Gurney, and Robert M. Drummond. Pharmacological profile of store-operated Ca^{2+} entry in intrapulmonary artery smooth muscle cells. *European Journal of Pharmacology*, 584(1):10 – 20, 2008. [59](#)
- [115] David D. McKemy, Werner M. Neuhauser, and David Julius. Identification of a cold receptor reveals a general role for TRP channels in thermosensation. *Nature*, 416:52–58, Mar 2002. [9](#)
- [116] S. McNulty and E. Fonfria. The role of TRPM channels in cell death. *Pflgers Arch*, 451:235–242, Oct 2005. [113](#)
- [117] Michael Mederos y Schnitzler, Janine Waring, Thomas Gudermann, and Vladimir Chubanov. Evolutionary determinants of divergent calcium selectivity of TRPM channels. *FASEB J.*, 22(5):1540–1551, 2008. [7](#), [9](#), [11](#), [62](#)
- [118] Zhu-Zhong Mei, Rong Xia, David J. Beech, and Lin-Hua Jiang. Intracellular Coiled-coil Domain Engaged in Subunit Interaction and Assembly of Melastatin-related Transient Receptor Potential Channel 2. *J. Biol. Chem.*, 281(50):38748–38756, 2006. [7](#)
- [119] Andrew L. Miller, Eric Karplus, and Lionel F. Jaffe. Imaging $[Ca^{+2}]_i$ with aequorin using a photon imaging detector. In Richard Nuccitelli, editor, *A Practical Guide to the Study of Calcium in Living Cells*, volume 40 of *Methods in Cell Biology*, pages 305 – 338. Academic Press, 1994. [47](#)
- [120] Arlo J. Miller, Jinyan Du, Sheldon Rowan, Christine L. Hershey, Hans R. Widlund, and David E. Fisher. Transcriptional Regulation of the Melanoma Prognostic Marker Melastatin (TRPM1) by MITF in Melanocytes and Melanoma. *Cancer Res*, 64(2):509–516, 2004. [9](#)
- [121] B. A. Miller. The Role of TRP Channels in Oxidative Stress-induced Cell Death. *Journal of Membrane Biology*, 209(1):31–41, 2006. [8](#)
- [122] Rosalynn J. Miltenberger, Randall L. Mynatt, J. Erby Wilkinson, and Richard P. Woychik. The Role of the agouti Gene in the Yellow Obese Syndrome. *J. Nutr.*, 127(9):1902S–, 1997. [96](#)

REFERENCES

- [123] Baruch Minke and Boaz Cook. TRP Channel Proteins and Signal Transduction. *Physiol. Rev.*, 82(2):429–472, 2002. [3](#)
- [124] Baruch Minke and Zvi Selinger. Role of Drosophila TRP in inositide-mediated Ca^{2+} entry. *Molecular Neurobiology*, 12(2):163–180, 1996. [3](#)
- [125] Baruch Minke and Zvi Selinger. The roles of trp and calcium in regulating photoreceptor function in drosophila. *Current Opinion in Neurobiology*, 6(4):459 – 466, 1996. [3](#)
- [126] Baruch Minke, Chun-Fang Wu, and William L. Pak. Induction of photoreceptor voltage noise in the dark in drosophila mutant. *Nature*, 258(5530):84–87, 1975. [3](#)
- [127] Axel Mithfer and Christian Mazars. Aequorin-based measurements of intracellular Ca^{2+} -signatures in plant cells. *Biol. Proced. Online*, 9(4):105–118, 2002. [47](#)
- [128] Atsushi Miyawaki. Fluorescence imaging of physiological activity in complex systems using GFP-based probes. *Current Opinion in Neurobiology*, 13(5):591 – 596, 2003. [47](#)
- [129] Atsuko Mizuno, Naoko Matsumoto, Masashi Imai, and Makoto Suzuki. Impaired osmotic sensation in mice lacking TRPV4. *Am J Physiol Cell Physiol*, 285(1):C96–101, 2003. [112](#)
- [130] Mahealani K. Monteilh-Zoller, Meredith C. Hermosura, Monica J.S. Nadler, Andrew M. Scharenberg, Reinhold Penner, and Andrea Fleig. TRPM7 Provides an Ion Channel Mechanism for Cellular Entry of Trace Metal Ions. *J. Gen. Physiol.*, 121(1):49–60, 2002. [8](#), [59](#), [61](#)
- [131] C Montell, K Jones, E Hafen, and G Rubin. Rescue of the Drosophila phototransduction mutation trp by germline transformation. *Science*, 230(4729):1040–1043, 1985. [3](#)
- [132] Craig Montell. The trp superfamily of cation channels. *Sci. STKE*, 2005(272):re3–, 2005. [3](#), [5](#), [6](#), [69](#)
- [133] Craig Montell, Lutz Birnbaumer, and Veit Flockerzi. The trp channels, a remarkably functional family. *Cell*, 108(5):595–598, 2002. [6](#)
- [134] Bryan D. Moyer and Bruce A. Stanton. Confocal Imaging of GFP-Labeled Ion Channels. *Ion Channel Localization*, pages 187–214, 2001. [111](#)
- [135] S. Muallem and T. M. Wilkie. G protein-dependent Ca^{2+} signaling complexes in polarized cells. *Cell Calcium*, 26(5):173 – 180, 1999. [112](#)
- [136] Stuart J. Mundell, Robert P. Loudon, and Jeffrey L. Benovic. Characterization of G Protein-Coupled Receptor Regulation in Antisense mRNA-Expressing Cells with Reduced Arrestin Levels. *Biochemistry*, 38(27):8723, 1999. [65](#)

REFERENCES

- [137] Manabu Murakami, Feng Xua, Ichiro Miyoshib, Eisaku Satoa, Kyoichi Onoa, and Toshihiko Iijima. Identification and characterization of the murine TRPM4 channel. *Biochemical and Biophysical Research Communications*, 307(3):522–528, 2003. [8](#), [69](#)
- [138] Theodore R. Muth and Michael J. Caplan. Transport protein trafficking in polarized cells. *Annual Review of Cell and Developmental Biology*, 19(1):333–366, 2003. [111](#)
- [139] Monica J. S. Nadler, Meredith C. Hermosura, Kazunori Inabe, Anne-Laure Perraud, Qiqin Zhu, Alexander J. Stokes, Tomohiro Kurosaki, Jean-Pierre Kinet, Reinhold Penner, Andrew M. Scharenberg, and Andrea Fleig. LTRPC7 is a Mg-ATP-regulated divalent cation channel required for cell viability. *Nature*, 411(6837):590–595, 2001. [7](#), [9](#)
- [140] K. Nagamine, J. Kudoh, S. Minoshima, K. Kawasaki, S. Asakawa, F. Ito, and N. Shimizu. Molecular cloning of a novel putative Ca^{2+} channel protein (TRPC7) highly expressed in brain. *Genomics*, 54:124–131, Nov 1998. [8](#)
- [141] J Naylor, CJ Milligan, F Zeng, C Jones, and DJ Beech. Production of a specific extracellular inhibitor of trpm3 channels. *Br J Pharmacol*, 155(4):567–73, 2008. [12](#)
- [142] Michele L. Nealen, Michael S. Gold, Paul D. Thut, and Michael J. Caterina. TRPM8 mRNA Is Expressed in a Subset of Cold-Responsive Trigeminal Neurons From Rat. *J Neurophysiol*, 90(1):515–520, 2003. [9](#)
- [143] Roger A. Nicoll. Expression mechanisms underlying long-term potentiation: a postsynaptic view. *Philosophical Transactions of the Royal Society of London. Series B: Biological Sciences*, 358(1432):721–726, 2003. [113](#)
- [144] Bernd Nilius. From TRPs to SCOs, CCEs, and CRACs: consensus and controversies. *Cell Calcium*, 33:293–298, 2003. [2](#)
- [145] Bernd Nilius, Frank Mahieu, Jean Prenen, Annelies Janssens, Grzegorz Owsianik, Rudi Vennekens, and Thomas Voets. The Ca^{2+} -activated cation channel TRPM4 is regulated by phosphatidylinositol 4,5-biphosphate. *EMBO J*, 25:467–478, Feb 2006. [4](#), [8](#), [65](#)
- [146] Bernd Nilius, Grzegorz Owsianik, Thomas Voets, and John A. Peters. Transient receptor potential cation channels in disease. *Physiol Rev*, 87:165–217, Jan 2007. [13](#)
- [147] Bernd Nilius, Grzegorz Owsianik, Thomas Voets, and John A. Peters. Transient Receptor Potential Cation Channels in Disease. *Physiol. Rev.*, 87(1):165–217, 2007. [113](#)
- [148] Bernd Nilius, Jean Prenen, Guy Droogmans, Thomas Voets, Rudi Vennekens, Marc Freichel, Ulrich Wissenbach, and Veit Flockerzi. Voltage Dependence of the Ca^{2+} -activated Cation Channel TRPM4. *J. Biol. Chem.*, 278(33):30813–30820, 2003. [8](#)

REFERENCES

- [149] Bernd Nilius, Jean Prenen, Annelies Janssens, Grzegorz Owsianik, Chunbo Wang, Michael X. Zhu, and Thomas Voets. The Selectivity Filter of the Cation Channel TRPM4. *J. Biol. Chem.*, 280(24):22899–22906, 2005. [10](#), [11](#), [61](#), [62](#), [104](#), [105](#)
- [150] Bernd Nilius, Jean Prenen, Annelies Janssens, Grzegorz Owsianik, Chunbo Wang, Michael X. Zhu, and Thomas Voets. The selectivity filter of the cation channel TRPM4. *J. Biol. Chem.*, 280(24):22899–22906, 2005. [63](#)
- [151] Bernd Nilius, Jean Prenen, Jisen Tang, Chunbo Wang, Grzegorz Owsianik, Annelies Janssens, Thomas Voets, and Michael X. Zhu. Regulation of the Ca^{2+} Sensitivity of the Nonselective Cation Channel TRPM4. *J. Biol. Chem.*, 280(8):6423–6433, 2005. [8](#)
- [152] Bernd Nilius, Karel Talavera, Grzegorz Owsianik, Jean Prenen, Guy Droogmans, and Thomas Voets. Gating of TRP channels: a voltage connection? *J Physiol*, 567(1):35–44, 2005. [8](#)
- [153] Bernd Nilius, Thomas Voets, and John Peters. TRP Channels in Disease. *Sci. STKE*, 2005(295):re8–, 2005. [6](#)
- [154] Elena Oancea, Joshua T. Wolfe, and David E. Clapham. Functional TRPM7 Channels Accumulate at the Plasma Membrane in Response to Fluid Flow. *Circ Res*, 98(2):245–253, 2006. [9](#)
- [155] J. Oberwinkler. Trpm3, a biophysical enigma? *Biochemical Society Transactions*, 035(1):89–90, 2007. [103](#), [110](#)
- [156] J. Oberwinkler and S. E. Philipp. TRPM3. *Handb Exp Pharmacol*, pages 253–267, 2007. [8](#), [9](#), [10](#), [103](#)
- [157] Johannes Oberwinkler, Annette Lis, Klaus M. Giehl, Veit Flockerzi, and Stephan E. Philipp. Alternative Splicing Switches the Divalent Cation Selectivity of TRPM3 Channels. *J. Biol. Chem.*, 280(23):22540–22548, 2005. [9](#), [10](#), [11](#), [12](#), [52](#), [56](#), [83](#), [93](#), [102](#), [110](#)
- [158] Yoshihiro Ohmiya and Takashi Hirano. Shining the light: the mechanism of the bioluminescence reaction of calcium-binding photoproteins. *Chemistry & Biology*, 3(5):337 – 347, 1996. [46](#)
- [159] Benito Ordaz, Jisen Tang, Rui Xiao, Alfonso Salgado, Alicia Sampieri, Michael X. Zhu, and Luis Vaca. Calmodulin and Calcium Interplay in the Modulation of TRPC5 Channel Activity: IDENTIFICATION OF A NOVEL C-TERMINAL DOMAIN FOR CALCIUM/CALMODULIN-MEDIATED FACILITATION. *J. Biol. Chem.*, 280(35):30788–30796, 2005. [4](#)

REFERENCES

- [160] Yuji Otsuka, Hiroyuki Sakagami, Yuji Owada, and Hisatake Kondo. Differential Localization of mRNAs for Mammalian *trps*, *Presumptive Capacitative Calcium Entry Channels*, in the *Adult Mouse Brain*. *The Tohoku Journal of Experimental Medicine*, 185(2):139–146, 1998. [113](#)
- [161] Grzegorz Owsianik, Karel Talavera, Thomas Voets, and Bernd Nilius. PERMEATION AND SELECTIVITY OF TRP CHANNELS. *Annual Review of Physiology*, 68(1):685–717, 2006. [6](#), [10](#), [104](#)
- [162] Raghu Padinjat and Simon Andrews. TRP channels at a glance. *J Cell Sci*, 117(24):5707–5709, 2004. [5](#)
- [163] R. Madelaine Paredes, Julie C. Etzler, Lora Talley Watts, Wei Zheng, and James D. Lechleiter. Chemical calcium indicators. *Methods*, 46(3):143 – 151, 2008. Optical Methods in Calcium Signaling. [56](#)
- [164] Anant B. Parekh and Jr. Putney, James W. Store-Operated Calcium Channels. *Physiol. Rev.*, 85(2):757–810, 2005. [2](#), [12](#)
- [165] J. M. Parker and R. S. Hodges. Prediction of surface and interior regions in proteins—part i: Linear tripeptide sequences identify structural boundaries in proteins. *Pept Res*, 4(6):347–354, Nov/Dec 1991. [44](#)
- [166] J. M. Parker and R. S. Hodges. Prediction of surface and interior regions in proteins—part ii: Predicting secondary structure in regions bound by surface exposed regions. *Pept Res*, 4(6):355–363, Nov/Dec 1991. [44](#)
- [167] Andrea M. Peier, Aziz Moqrich, Anne C. Hergarden, Alison J. Reeve, David A. Andersson, Gina M. Story, Taryn J. Earley, Ilaria Dragoni, Peter McIntyre, Stuart Bevan, and Ardem Patapoutian. A TRP channel that senses cold stimuli and menthol. *Cell*, 108:705–715, Mar 2002. [9](#)
- [168] Cristian A. Pérez, Liquan Huang, Mingqing Rong, J. Ashot Kozak, Axel K. Preuss, Hailin Zhang, Marianna Max, and Robert F. Margolskee. A transient receptor potential channel expressed in taste receptor cells. *Nat Neurosci*, 5:1169–1176, Nov 2002. [8](#)
- [169] Anne-Laure Perraud, Andrea Fleig, Christopher A. Dunn, Leigh Ann Bagley, Pierre Launay, Carsten Schmitz, Alexander J. Stokes, Qiqin Zhu, Maurice J. Bessman, Reinhold Penner, Jean-Pierre Kinet, and Andrew M. Scharenberg. Adp-ribose gating of the calcium-permeable *ltrpc2* channel revealed by nudix motif homology. *Nature*, 411(6837):595–599, 2001. [7](#), [8](#)
- [170] Ole H. Petersen. Localization and regulation of Ca^{2+} entry and exit pathways in exocrine gland cells. *Cell Calcium*, 33(5-6):337 – 344, 2003. [112](#)

REFERENCES

- [171] Christopher B. Phelps and Rachel Gaudet. The Role of the N Terminus and Transmembrane Domain of TRPM8 in Channel Localization and Tetramerization. *J. Biol. Chem.*, 282(50):36474–36480, 2007. [6](#), [8](#)
- [172] S. C. Pingle, J. A. Matta, and G. P. Ahern. Capsaicin Receptor: TRPV1 A Promiscuous TRP Channel. *Handb Exp Pharmacol*, page 155171, 2007. [6](#)
- [173] Lawrence H. Pinto and Christina Enroth-Cugell. Tests of the mouse visual system. *Mammalian Genome*, 11(7):531–536, 2000. [50](#)
- [174] Dirk Prawitt, Thorsten Enklaar, Gabi Klemm, Barbara Gartner, Christian Spangenberg, Andreas Winterpacht, Michael Higgins, Jerry Pelletier, and Bernhard Zabel. Identification and characterization of MTR1, a novel gene with homology to melastatin (MLSN1) and the trp gene family located in the BWS-WT2 critical region on chromosome 11p15.5 and showing allele-specific expression. *Hum. Mol. Genet.*, 9(2):203–216, 2000. [8](#)
- [175] James W. Putney. Physiological mechanisms of TRPC activation. *Pflugers Arch*, 451:29–34, Oct 2005. [12](#)
- [176] Marilyn D. Resh. Fatty acylation of proteins: new insights into membrane targeting of myristoylated and palmitoylated proteins. *Biochimica et Biophysica Acta (BBA) - Molecular Cell Research*, 1451(1):1 – 16, 1999. [67](#)
- [177] A. Riccio, A.D. Medhurst, C. Mattei, R.E. Kelsell, A.R. Calver, A. D Randall, C.D. Benham, and M.N. Pangalos. mRNA distribution analysis of human TRPC family in CNS and peripheral tissues. *Brain Res Mol Brain Res*, 109(1-2):95–104, 2002. [5](#)
- [178] Tibor Rohcs, Coeli M B Lopes, Ioannis Michailidis, and Diomedes E Logothetis. PI(4,5)P₂ regulates the activation and desensitization of TRPM8 channels through the TRP domain. *Nature Neuroscience*, 8:626 – 634, 2005. [5](#), [6](#)
- [179] Michael H. Ross and Wojciech Pawlina. Histology: A Text and Atlas. *Lippincott Williams & Wilkins*, 5th., 2006. [111](#)
- [180] Rüdiger Rudolf, Marco Mongillo, Rosario Rizzuto, and Tullio Pozzan. Looking forward to seeing calcium. *Nature Reviews Molecular Cell Biology*, 4(7):579–586, 2003. [32](#)
- [181] Loren W. Runnels, Lixia Yue, and David E. Clapham. TRP-PLIK, a Bifunctional Protein with Kinase and Ion Channel Activities. *Science*, 291(5506):1043–1047, 2001. [7](#)
- [182] A. G. Ryazanov, K. S. Pavur, and M. V. Dorovkov. Alpha-kinases: a new class of protein kinases with a novel catalytic domain. *Curr Biol*, 9:R43–R45, Jan 1999. [7](#)

REFERENCES

- [183] Alexey G. Ryazanov, Michael D. Ward, Charmaine E. Mendola, Karen S. Pavur, Maxim V. Dorovkov, Martin Wiedmann, Hediye Erdjument-Bromage, Paul Tempst, Toni Gestone Parmer, C. Robert Prostko, F. Joseph Germino, and William N. Hait. Identification of a new class of protein kinases represented by eukaryotic elongation factor-2 kinase. *Proceedings of the National Academy of Sciences of the United States of America*, 94(10):4884–4889, 1997. [7](#)
- [184] Joseph Sambrook and David W. Russell. *Molecular Cloning: A Laboratory Manual*. Cold Spring Harbor Laboratory, (0003), 2000. [21](#), [26](#), [29](#), [39](#)
- [185] Yorikata Sano, Kohei Inamura, Akira Miyake, Shinobu Mochizuki, Hiromichi Yokoi, Hitoshi Matsushime, and Kiyoshi Furuichi. Immunocyte Ca^{2+} Influx System Mediated by LTRPC2. *Science*, 293(5533):1327–1330, 2001. [7](#), [8](#)
- [186] Mark S.P. Sansom. Proline residues in transmembrane helices of channel and transport proteins: a molecular modelling study. *Protein Eng.*, 5(1):53–60, 1992. [104](#)
- [187] Michael Schaefer. Homo- and heteromeric assembly of trp channel subunits. *Pflgers Archiv European Journal of Physiology*, 451(1):35–42, 2005. [5](#), [6](#), [69](#), [108](#)
- [188] Michael Schaefer, Tim D. Plant, Nicole Stresow, Nadine Albrecht, and Gunter Schultz. Functional Differences between TRPC4 Splice Variants. *J. Biol. Chem.*, 277(5):3752–3759, 2002. [70](#)
- [189] M Schmidt, C Nehls, U Rumenapp, and KH Jakobs. m3 Muscarinic receptor-induced and Gi-mediated heterologous potentiation of phospholipase C stimulation: role of phosphoinositide synthesis. *Mol Pharmacol*, 50(4):1038–1046, 1996. [65](#)
- [190] Carsten Schmitz, Anne-Laure Perraud, Catherine O. Johnson, Kazunori Inabe, Megan K. Smith, Reinhold Penner, Tomohiro Kurosaki, Andrea Fleig, and Andrew M. Scharenberg. Regulation of vertebrate cellular Mg^{2+} homeostasis by TRPM7. *Cell*, 114:191–200, Jul 2003. [7](#)
- [191] Torsten Schwede, Jürgen Kopp, Nicolas Guex, and Manuel C. Peitsch. Swiss-model: An automated protein homology-modeling server. *Nucleic Acids Res*, 31:3381–3385, Jul 2003. [104](#), [105](#)
- [192] Steven G. Sedgwick and Stephen J. Smerdon. The ankyrin repeat: a diversity of interactions on a common structural framework . *Current Pharmaceutical Design*, 24(8):311–316, 1999. [5](#)
- [193] Betty W. Shen, Anne-Laure Perraud, Andrew Scharenberg, and Barry L. Stoddard. The crystal structure and mutational analysis of human nudt9. *Journal of Molecular Biology*, 332(2):385 – 398, 2003. [7](#)

REFERENCES

- [194] O. Shimomura and F.H. Johnson. Regeneration of the photoprotein aequorin. *Nature*, 256(5514):236–238, 1975. [46](#)
- [195] O. Shimomura, F.H. Johnson, and Y. Saiga. Extraction, purification and properties of aequorin, a bioluminescent protein from the luminous hydromedusan, aequorea. *J Cell Comp Physiol.*, Jun(59):223–39, 1962. [46](#)
- [196] O. Shimomura, Y. Kishi, and S Inouye. The relative rate of aequorin regeneration from apoaequorin and coelenterazine analogues. *Biochem J.*, 296(Pt3):549–551, 1993. [46](#)
- [197] O. Shimomura, B. Musicki, and Y. Kishi. Semi-synthetic aequorin. an improved tool for the measurement of calcium ion concentration. *Biochem J.*, 251(2):405–410, Apr 1988. [46](#)
- [198] Qin Shu, Kwong Kwok Wong, Jack M. Su, Adekunle M. Adesina, Li Tian Yu, Yvonne T. M. Tsang, Barbara C. Antalfy, Patricia Baxter, Laszlo Perlaky, Jianhua Yang, Robert C. Dauser, Murali Chintagumpala, Susan M. Blaney, Ching C. Lau, and Xiao-Nan Li. Direct orthotopic transplantation of fresh surgical specimen preserves cd133⁺ tumor cells in clinically relevant mouse models of medulloblastoma and glioma. *Stem Cells*, 26(6):1414–1424, Jun 2008. [85](#)
- [199] Ramakrishnaiah Siddappa, Anton Martens, Joyce Doorn, Anouk Leusink, Cristina Olivo, Ruud Licht, Linda van Rijn, Claudia Gaspar, Riccardo Fodde, Frank Janssen, Clemens van Blitterswijk, and Jan de Boer. cAMP/PKA pathway activation in human mesenchymal stem cells in vitro results in robust bone formation in vivo. *Proceedings of the National Academy of Sciences*, 105(20):7281–7286, 2008. [79](#)
- [200] Samuel Sidi, Rainer W. Friedrich, and Teresa Nicolson. NompC TRP Channel Required for Vertebrate Sensory Hair Cell Mechanotransduction. *Science*, 301(5629):96–99, 2003. [3](#)
- [201] W. K. SILVERS. An experimental approach to action of genes at the agouti locus in the mouse. iii. transplants of newborn aw-, a-and at-skin to ay-, aw-, a-and aa hosts. *J Exp Zool*, 137:189–196, Feb 1958. [96](#)
- [202] T. Sivaraman, T.K.S. Kumar, G. Jayaraman, and C. Yu. The Mechanism of 2,2,2-Trichloroacetic Acid-Induced Protein Precipitation. *Journal of Protein Chemistry*, 16:291–297(7), 1997. [38](#)
- [203] Jessica E. Smotrys and Maurine E. Linder. Palmitoylation of intracellular signaling proteins: Regulation and function. *Annual Review of Biochemistry*, 73(1):559–587, 2004. [67](#)
- [204] Susan Standring. Gray’s anatomy: The anatomical basis of clinical practice. *Churchill Livingstone*, 39th., 2005. [111](#)

REFERENCES

- [205] L. Steinman. Multiple sclerosis. presenting an odd autoantigen. *Nature*, 375(6534):739–740, Jun 1995. [109](#)
- [206] Sylvia Streit, Christoph W. Michalski, Mert Erkan, Jörg Kleeff, and Helmut Friess. Northern blot analysis for detection and quantification of rna in pancreatic cancer cells and tissues. *Nat Protoc*, 4:37–43, 2009. [111](#)
- [207] Stephen A. Stricker and Toni L. Smythe. Endoplasmic reticulum reorganizations and Ca^{2+} signaling in maturing and fertilized oocytes of marine protostome worms: the roles of MAPKs and MPF. *Development*, 130(13):2867–2879, 2003. [1](#)
- [208] Akiyuki Takahashi, Patricia Camacho, James D. Lechleiter, and Brian Herman. Measurement of intracellular calcium. *Physiol. Rev.*, 79(4):1089–1125, 1999. [1](#), [47](#)
- [209] Ryuichi Takezawa, Carsten Schmitz, Philippe Demeuse, Andrew M. Scharenberg, Reinhold Penner, and Andrea Fleig. Receptor-mediated regulation of the TRPM7 channel through its endogenous protein kinase domain. *Proceedings of the National Academy of Sciences of the United States of America*, 101(16):6009–6014, 2004. [6](#), [7](#)
- [210] Jisen Tang, Yakang Lin, Zongming Zhang, Svetlana Tikunova, Lutz Birnbaumer, and Michael Xi Zhu. Identification of Common Binding Sites for Calmodulin and Inositol 1,4,5-Trisphosphate Receptors on the Carboxyl Termini of Trp Channels. *J. Biol. Chem.*, 276(24):21303–21310, 2001. [4](#)
- [211] O. Thastrup, P. J. Cullen, B. K. Drøbak, M. R. Hanley, and A. P. Dawson. Thapsigargin, a tumor promoter, discharges intracellular ca^{2+} stores by specific inhibition of the endoplasmic reticulum ca^{2+} -atpase. *Proc Natl Acad Sci U S A*, 87(7):2466–2470, Apr 1990. [57](#)
- [212] Wei Tian, Michele Salanova, Hongshi Xu, Jessie N. Lindsley, Terry T. Oyama, Sharon Anderson, Sebastian Bachmann, and David M. Cohen. Renal expression of osmotically responsive cation channel TRPV4 is restricted to water-impermeant nephron segments. *Am J Physiol Renal Physiol*, 287(1):F17–24, 2004. [112](#)
- [213] D. Werry Tim, I. Christie Mark, A. Dainty Ian, F. Wilkinson Graeme, and B. Willars Gary. Ca^{2+} signalling by recombinant human CXCR2 chemokine receptors is potentiated by P2Y nucleotide receptors in HEK cells. *British Journal of Pharmacology*, 135(5):1199–1208, 2002. [10.1038/sj.bjp.0704566](#). [65](#)
- [214] Kazuya Togashi, Yuji Hara, Tomoko Tominaga, Tomohiro Higashi, Yasunobu Konishi, Yasuo Mori, and Makoto Tominaga. TRPM2 activation by cyclic ADP-ribose at body temperature is involved in insulin secretion. *EMBO J*, 25:1804–1815, May 2006. [8](#)

REFERENCES

- [215] Catalin N. Topala, Wouter Tiel Groenestege, Stéphanie Thébault, Dennis van den Berg, Bernd Nilius, Joost G. Hoenderop, and René J. Bindels. Molecular determinants of permeation through the cation channel TRPM6. *Cell Calcium*, 41:513–523, Jun 2007. [10](#), [104](#)
- [216] D A Towler, J I Gordon, S P Adams, and L Glaser. The biology and enzymology of eukaryotic protein acylation. *Annual Review of Biochemistry*, 57(1):69–97, 1988. [65](#)
- [217] Larisa Tsavaler, Michael H. Shapero, Stan Morkowski, and Reiner Laus. Trp-p8, a Novel Prostate-specific Gene, Is Up-Regulated in Prostate Cancer and Other Malignancies and Shares High Homology with Transient Receptor Potential Calcium Channel Proteins. *Cancer Res*, 61(9):3760–3769, 2001. [9](#)
- [218] Pamela R. Tsuruda, David Julius, and Jr Daniel L. Minor. Coiled coils direct assembly of a cold-activated trp channel. *Neuron*, 51(2):201–212, 2006. [7](#), [108](#)
- [219] Marc H.V. Van Regenmortel. Which structural features determine protein antigenicity? *Trends in Biochemical Sciences*, 11(1):36–39, 1986. [45](#)
- [220] Jacco van Rheenen, Michiel Langeslag, and Kees Jalink. Correcting Confocal Acquisition to Optimize Imaging of Fluorescence Resonance Energy Transfer by Sensitized Emission. *Biophys. J.*, 86(4):2517–2529, 2004. [32](#)
- [221] Damian B. van Rossum, Randen L. Patterson, Sumit Sharma, Roxanne K. Barrow, Michael Kornberg, Donald L. Gill, and Solomon H. Snyder. Phospholipase Cgamma1 controls surface expression of TRPC3 through an intermolecular PH domain. *Nature*, 434:99–104, Mar 2005. [4](#)
- [222] T. van Veen, L. van Winsen, J. B. A. Crusius, N. F. Kalkers, F. Barkhof, A. S. Peña, C. H. Polman, and B. M. J. Uitdehaag. [alpha]b-crystallin genotype has impact on the multiple sclerosis phenotype. *Neurology*, 61(9):1245–1249, Nov 2003. [109](#)
- [223] Elisabetta Vegeto, George F. Allan, William T. Schrader, Ming-Jer Tsai, Donald P. McDonnell, and Bert W. O'Malley. The mechanism of ru486 antagonism is dependent on the conformation of the carboxy-terminal tail of the human progesterone receptor. *Cell*, 69(4):703 – 713, 1992. [40](#)
- [224] M Veit, E Ponimaskin, and MF Schmidt. Analysis of s-acylation of proteins. *Methods Mol Biol*, 446:163–82, 2008. [107](#)
- [225] Kartik Venkatachalam, Thomas Hofmann, and Craig Montell. Lysosomal localization of trpm13 depends on trpm12 and the mucopolidosis-associated protein trpm11. *J. Biol. Chem.*, 281(25):17517–17527, 2006. [70](#)

REFERENCES

- [226] Kartik Venkatachalam and Craig Montell. Trp channels. *Annual Review of Biochemistry*, 76(1):387–417, 2007. [5](#)
- [227] Thomas Voets, Guy Droogmans, Ulrich Wissenbach, Annelies Janssens, Veit Flockerzi, and Bernd Nilius. The principle of temperature-dependent gating in cold- and heat-sensitive TRP channels. *Nature*, 430:748–754, Aug 2004. [9](#)
- [228] Thomas Voets, Annelies Janssens, Guy Droogmans, and Bernd Nilius. Outer Pore Architecture of a Ca²⁺-selective TRP Channel. *J. Biol. Chem.*, 279(15):15223–15230, 2004. [104](#), [105](#)
- [229] Thomas Voets and Bernd Nilius. The pore of trp channels: trivial or neglected? *Cell Calcium*, 33(5-6):299 – 302, 2003. TRP channels: facts, fictions, challenges. [104](#)
- [230] Thomas Voets, Bernd Nilius, Susan Hoefs, Annemiete W. C. M. van der Kemp, Guy Droogmans, Rene J. M. Bindels, and Joost G. J. Hoenderop. TRPM6 Forms the Mg²⁺ Influx Channel Involved in Intestinal and Renal Mg²⁺ Absorption. *J. Biol. Chem.*, 279(1):19–25, 2004. [8](#), [59](#)
- [231] Thomas F. J. Wagner, Sabine Loch, Sachar Lambert, Isabelle Straub, Stefanie Mannebach, Ilka Mathar, Martina Dufer, Annette Lis, Veit Flockerzi, Stephan E. Philipp, and Johannes Oberwinkler. Transient receptor potential M3 channels are ionotropic steroid receptors in pancreatic β cells. *Nat Cell Biol*, 10(12):1421–1430, 2008. [13](#), [57](#), [111](#)
- [232] Roxanne Y. Walder, Baoli Yang, John B. Stokes, Patricia A. Kirby, Xiao Cao, Peijun Shi, Charles C. Searby, Russell F. Husted, and Val C. Sheffield. Mice defective in Trpm6 show embryonic mortality and neural tube defects. *Hum. Mol. Genet.*, page ddp392, 2009. [114](#)
- [233] Richard G. Walker, Aarron T. Willingham, and Charles S. Zuker. A Drosophila Mechanosensory Transduction Channel. *Science*, 287(5461):2229–2234, 2000. [3](#)
- [234] Y Wang, B W O'Malley, S Y Tsai, and B W O'Malley. A regulatory system for use in gene transfer. *Proceedings of the National Academy of Sciences of the United States of America*, 91(17):8180–8184, 1994. [40](#)
- [235] W. W. Ward and M. J. Cormier. Extraction of Renilla-type luciferin from the calcium-activated photoproteins aequorin, mnemiopsin, and berovin. *Proc Natl Acad Sci U S A*, 27(7):2530–2534, 1975. [47](#)
- [236] W. W. Ward and M. J. Cormier. An energy transfer protein in coelenterate bioluminescence. Characterization of the Renilla green-fluorescent protein. *J. Biol. Chem.*, 254(3):781–788, 1979. [47](#)

REFERENCES

- [237] Sarah E. Webb and Andrew L. Miller. Calcium signalling during embryonic development. *Nat Rev Mol Cell Biol*, 4(7):539–551, 2003. [1](#)
- [238] Martin Weber, Leonid Motin, Simon Gaul, Friederike Beker, Rainer H. A. Fink, and David J. Adams. Intravenous anaesthetics inhibit nicotinic acetylcholine receptor-mediated currents and Ca^{2+} transients in rat intracardiac ganglion neurons. *Br J Pharmacol*, 144(1):98–107, 2004. [45](#)
- [239] Barbara J. Wedel, Guillermo Vazquez, Richard R. McKay, Gary St. J. Bird, and Jr. Putney, James W. A Calmodulin/Inositol 1,4,5-Trisphosphate (IP_3) Receptor-binding Region Targets TRPC3 to the Plasma Membrane in a Calmodulin/ IP_3 Receptor-independent Process. *J. Biol. Chem.*, 278(28):25758–25765, 2003. [4](#)
- [240] Edith Wehage, Jorg Eisfeld, Inka Heiner, Eberhard Jungling, Christof Zitt, and Andreas Luckhoff. Activation of the Cation Channel Long Transient Receptor Potential Channel 2 (LTRPC2) by Hydrogen Peroxide. A SPLICE VARIANT REVEALS A MODE OF ACTIVATION INDEPENDENT OF ADP-RIBOSE. *J. Biol. Chem.*, 277(26):23150–23156, 2002. [8](#)
- [241] B. D. Wilson, M. M. Ollmann, L. Kang, M. Stoffel, G. I. Bell, and G. S. Barsh. Structure and function of asp, the human homolog of the mouse agouti gene. *Hum Mol Genet*, 4:223–230, Feb 1995. [96](#)
- [242] Fred S. Wouters and Philippe I. H. Bastiaens. Fluorescence lifetime imaging of receptor tyrosine kinase activity in cells. *Current Biology*, 9(19):1127 – 1132, 1999. [32](#)
- [243] P. G. Wu and L. Brand. Resonance energy transfer: Methods and applications. *Analytical Biochemistry*, 218(1):1 – 13, 1994. [32](#)
- [244] Rong Xia, Zhu-Zhong Mei, Hong-Ju Mao, Wei Yang, Li Dong, Helen Bradley, David J. Beech, and Lin-Hua Jiang. Identification of Pore Residues Engaged in Determining Divalent Cationic Permeation in Transient Receptor Potential Melastatin Subtype Channel 2. *J. Biol. Chem.*, 283(41):27426–27432, 2008. [10](#), [61](#), [104](#)
- [245] Z.-G. Xiong, W.-Y. Lu, and J. F. MacDonald. Extracellular calcium sensed by a novel cation channel in hippocampal neurons. *Proceedings of the National Academy of Sciences of the United States of America*, 94(13):7012–7017, 1997. [113](#)
- [246] Shang-Zhong Xu, Fanning Zeng, Guylain Boulay, Christian Grimm, Christian Harteneck, and David J. Beech. Block of TRPC5 channels by 2-aminoethoxydiphenyl borate: a differential, extracellular and voltage-dependent effect. *Br J Pharmacol*, 145:405–414, Jun 2005. [11](#), [12](#)

REFERENCES

- [247] X.-Z. Shawn Xu, Fabian Moebius, Donald L. Gill, and Craig Montell. Regulation of melastatin, a TRP-related protein, through interaction with a cytoplasmic isoform. *Proceedings of the National Academy of Sciences of the United States of America*, 98(19):10692–10697, 2001. [8](#)
- [248] James D. Mills Ammasi Periasamy Ye Chen. Protein localization in living cells and tissues using fret and flim. *Differentiation*, 71(9-10):528–541, 2003. [32](#)
- [249] Gary Yellen. The voltage-gated potassium channels and their relatives. *Nature*, 419-(6902):35–42, 2002. [4](#), [104](#), [105](#)
- [250] KH Young. Yeast two-hybrid: so many interactions, (in) so little time.. *Biol Reprod*, 58(2):302–311, 1998. [33](#)
- [251] Joseph P. Yuan, Kirill Kiselyov, Dong Ming Shin, Jin Chen, Nikolay Shcheynikov, Shin H. Kang, Marlin H. Dehoff, Martin K. Schwarz, Peter H. Seeburg, Shmuel Muallem, and Paul F. Worley. Homer Binds TRPC Family Channels and Is Required for Gating of TRPC1 by IP3 Receptors. *Cell*, 114(6):777–789, 2003. [4](#)
- [252] M. M. Zegers and D. Hoekstra. Mechanisms and functional features of polarized membrane traffic in epithelial and hepatic cells. *Biochem. J.*, 336(2):257–269, 1998. [111](#)
- [253] Lian Zhang, Karyn Foster, Qiuju Li, and Jeffrey R. Martens. S-acylation regulates Kv1.5 channel surface expression. *Am J Physiol Cell Physiol*, 293(1):C152–161, 2007. [67](#)
- [254] Yifeng Zhang, Mark A. Hoon, Jayaram Chandrashekar, Ken L. Mueller, Boaz Cook, Dianqing Wu, Charles S. Zuker, and Nicholas J.P. Ryba. Coding of Sweet, Bitter, and Umami Tastes: Different Receptor Cells Sharing Similar Signaling Pathways. *Cell*, 112(3):293 – 301, 2003. [8](#)
- [255] Jieqing Zhu, Bing-Hao Luo, Patrick Barth, Jack Schonbrun, David Baker, and Timothy A. Springer. The structure of a receptor with two associating transmembrane domains on the cell surface: Integrin α _v β ₃. *Molecular Cell*, 34(2):234 – 249, 2009. [69](#)

Curriculum Vitae

Personal Details

Gender: Male

Date of birth: 6th of May, 1973

Marital status: Married

Place of birth: Shanghai, China

Present Citizenship: Chinese

Education

- Since 10/2006 **Ph.D. candidate** in the Institute of Pharmacology and Toxicology of the Philipps University, Marburg, Germany
Project title: *Localization and Functional Analysis of the Calcium Permeable Melastatin-like Channel TRPM3*
- 10/2001–09/2006 **Master study** in Human Biology at the Philipps University, Marburg, Germany. Major in neuroscience
Project title: *Analysis of the High-Mobility-Group A1 Protein as a Putative Novel Binding Partner for Fibroblast Growth Factor Binding Protein-1*
- 09/1991–07/1996 **Study of clinical medicine** in the Shanghai Medical College of Fudan University (Former: Shanghai Medical University), Shanghai, China
- 09/1988–07/1991 **High school** in Tongji middle school, Shanghai, China

Publications and Award

Publications

1. Phenotypical divergence between mice and humans carrying loss-of-function alleles of TRPM6. Chubanov V., Storch U., **Chen X.**, Schnitzler M.Y., Hofmann T., Gudermann T. *NAUNYN-SCHMIEDEBERGS ARCHIVES OF PHARMACOLOGY*, 379:32, 2009. (abstract)
2. Neuronal and Sensory Expression of Mouse TRPM3. **Chen X.**, Chubanov V., Dietz A.S., Hofmann T. (*manuscript in preparation*)
3. Magnesium-dependent suppression of larval anabolism and pupation arrest in *Drosophila trpm*. Hofmann T., **Chen X.**, Dietz A.S., Chubanov V., Gudermann T., Montell C. (*manuscript in preparation*)

Award

Project title: *Bio-Plastics Engineering*

Tianzhong Zheng, Caidong Liu, **Xiaodi Chen**, Keming Zhu

Shanghai Science and Technology Progress Award (2001, third prize)

Declaration

I herewith declare that this thesis entitled "Localization and Functional Analysis of the Calcium Permeable Melastatin-like Channel TRPM3" was done independently and under use of the aforementioned assistance and sources. The doctoral thesis has not been submitted in the current or similar form at other universities.

The thesis work was conducted from Oct.1, 2006 to Sep.30, 2009 under the supervision of Dr. Hofmann and Prof. Dr. Tim Plant at the Department of Pharmacology and Toxicology of Philipps University Marburg.

Ehrenwörtliche Erklärung

Ich erkläre ehrenwörtlich, da ich die dem Fachbereich Medizin Marburg zur Promotion-sprfung eingereichte Arbeit mit dem Titel "Localization and Functional Analysis of the Calcium Permeable Melastatin-like Channel TRPM3" im Institut für Pharmakologie und Toxikologie unter Leitung von Prof. Dr. Frank Czubayko mit Unterstützung durch Dr. Thomas Hofmann and Prof. Dr. Tim Plant ohne sonstige Hilfe selbst durchgeführt und bei der Abfassung der Arbeit keine anderen als die in der Dissertation aufgeführten Hilfsmittel benutzt habe. Ich habe bisher an keinem in- oder ausländischen Medizinischen Fachbereich ein Gesuch um Zulassung zur Promotion eingereicht, noch die vorliegende oder eine andere Arbeit als Dissertation vorgelegt.

Vorliegende Arbeit wurde (oder wird) in folgenden Publikationsorganen (siehe Abschnitt 8) veröffentlicht.

Marburg, December 11, 2009

List of academic teachers

My academic teachers were women/men in Marburg:

Aigner, Aumüller, Boeckhoff, Büch, Chubanov, Cubayko, Daut, Dietrich, Eilers, Elsässer, Gudermann, Hasilik, Hofmann, Kirchner, Koolmann, Lill, Liss, Löffler, Lohoff, Müller, Plant, Renz, Röhm, Röper, Schäfer, Seitz, Suske, Voigt, Weihe